NUMERICAL INVESTIGATION ON THE EFFECTIVENESS OF SEISMIC RETROFITTING OF A HISTORICAL MASONRY MOSQUE

Master of Science Thesis

Abide AŞIKOĞLU

Eskişehir, 2018

NUMERICAL INVESTIGATION ON THE EFFECTIVENESS OF SEISMIC RETROFITTING OF A HISTORICAL MASONRY MOSQUE

Abide AŞIKOĞLU

MASTER OF SCIENCE THESIS

Program in Mechanics, Department of Civil Engineering
Supervisor: Assoc. Prof. Dr. Özgür AVŞAR

Eskişehir
Anadolu University
Graduate School of Sciences
June 2018

FINAL APPROVAL FOR THESIS

This thesis titled "Numerical Investigation on The Effectiveness of Seismic Retrofitting of a Historical Masonry Mosque" has been prepared and submitted by Abide AŞIKOĞLU in partial fulfillment of the requirements in "Anadolu University Directive on Graduate Education and Examination" for the Degree of Master of Science in Civil Engineering Department has been examined and approved on 28/06/2018.

Committee Members	**Title Name Surname**	**Signature**
Member (Supervisor)	: Assoc. Prof. Dr. Özgür AVŞAR	.....
Member	: Prof. Dr. Murat Altuğ ERBERİK	.....
Member	: Assoc. Prof. Dr. İlker KAZAZ	.....

Prof. Dr. Ersin YÜCEL
Director of Graduate School of Sciences

ABSTRACT

NUMERICAL INVESTIGATION ON THE EFFECTIVENESS OF SEISMIC RETROFITTING OF A HISTORICAL MASONRY MOSQUE

Abide AŞIKOĞLU

Department of Civil Engineering
Program in Mechanics

Anadolu University, Graduate School of Sciences, June 2018

Supervisor: Assoc. Prof. Dr. Özgür AVŞAR

Earthquake effects have been always a great challenge for the structures, specially heritage ones. Historical masonry structures were constructed based on the self-weight loading and consequently have high compressive strength. On the contrary, masonry material is vulnerable against any seismic actions due to its quasi-brittle behaviour. These complex structures require special care and multidisciplinary approach while performing seismic assessment. In the present thesis, a case study of historical Kütahya Kurşunlu Mosque was conducted. Firstly, site investigations were carried out to identify the structural condition and severe damage on the mosque was reported. Therefore, the historical masonry mosque has undergone several interventions and retrofitting actions in order to improve the seismic performance and structural integrity. The main objective of the thesis is to study the effectiveness of the seismic retrofitting on the mosque by using finite element method. Two representative structural schemes, non-retrofitted and retrofitted, were generated as three-dimensional finite element model. Ambient Vibration Measurements and Operational Modal Analysis was performed in order to characterize the dynamic properties of the mosque. Thus, the finite element models were calibrated according to the experimental modal analysis. In order to evaluate the seismic behaviour of the mosque, nonlinear pushover and dynamic analyses were performed. Finally, seismic response of the two models were studied in terms of peak displacements, absolute accelerations and damage patterns. A positive contribution of the retrofitting to the structural behaviour was observed. The numerical damage pattern allowed to validate the adopted nonlinear behaviour of the structure by comparing with the real damage.

Keywords: Historical masonry structure, Finite element analysis, Nonlinear analysis, Seismic performance, Retrofitting.

ÖZET

TARİHİ YIĞMA BİR YAPIDA UYGULANAN GÜÇLENDİRMENİN DEPREM PERFORMANSINA ETKİSİNİN SAYISAL YÖNTEMLE İNCELENMESİ

Abide AŞIKOĞLU

İnşaat Mühendisliği Anabilim Dalı
Mekanik Bilim Dalı

Anadolu Üniversitesi, Fen Bilimleri Enstitüsü, Haziran 2018

Danışman: Doç. Dr. Özgür AVŞAR

Deprem etkileri özellikle tarihi yapılar için her zaman büyük bir meydan okuma olmuştur. Yığma yapılar, geçmişte düşey yükler dikkate alınarak inşa edilmesi sebebiyle basınç gerilmelerine karşı oldukça dayanıklı olan yapılardır. Fakat, yığma malzemenin yarı kırılgan davranışı sebebiyle deprem etkilerine karşı hasar görebilirliği oldukça fazladır. Tarihi yapıların sismik değerlendirmesi yapılırken özellikle dikkat edilmeli ve çok disiplinli bir yaklaşım sergilenmelidir. Tez kapsamında, tarihi Kurşunlu Cami incelenmiştir. Yapılan saha gözlem çalışmaları sonucunda camide geçmiş depremlerde meydana geldiği düşünülen ciddi hasarlar gözlemlenmiştir. Bu sebeple, sismik performansını geliştirmek ve yapısal bütünlüğü sağlaması adına tarihi yığma camide güçlendirme çalışmaları yapılmıştır. Bu tez çalışmasının temel amacı, sonlu elemanlar yöntemi kullanarak camiye uygulanan sismik güçlendirmenin etkinliğini ortaya koymaktır. Güçlendirmesiz ve güçlendirmeli olmak üzere iki adet temsili yapının 3 boyutlu sonlu elemanlar modeli hazırlanmıştır. Caminin dinamik özelliklerini belirlemek için Çevresel Titreşim Ölçümleri alınmış ve Operasyonal Modal Analiz gerçekleştirilmiştir. Böylelikle, elde edilen deneysel modal analiz sonuçlarına göre camiye ait sonlu elemanlar modeli kalibre edilmiştir. Tarihi caminin sismik davranışını değerlendirmek için doğrusal olmayan itme ve dinamik analizler gerçekleştirilmiştir. Tez kapsamında son olarak ise her iki modelin sismik tepkileri yer değiştirme, mutlak ivme ve hasar dağılımlarına dayanarak incelenmiştir. Uygulanan güçlendirmenin yapısal davranışa olumlu katkısı olduğu gözlemlenmiştir. Numerik hasar dağılımı, tespit edilen gerçek hasar ile karşılaştırıldığında yapı için tanımlanan doğrusal olmayan davranış modelinin kabul edilebilir olduğunu ortaya koymaktadır.

Anahtar Sözcükler: Tarihi yığma yapı, Sonlu elemanlar analizi, Doğrusal olmayan analiz, Sismik performans, Güçlendirme.

ACKNOWLEDGEMENTS

First and foremost, I would like to express my deepest gratitude to my supervisor Associate Professor Dr. Özgür Avşar, for his guidance, patience, continuous encouragement, constructive criticism and full availability. His dedication and keen interest to educate has inspired me to seek a career in academia. Thanks for believing in me and providing all the support.

I would like to show my sincere gratitude to Professor Dr. Paulo B. Lourenço for giving me an opportunity to work with his team at University of Minho, his guidance, expertise, discussions, shared advices, making the time in his heavy schedule and giving me an access to the research facilities, particularly licensed versions of TNO DIANA and ARTeMIS.

I would like to express my appreciation to PhD student Luís Carlos Silva for his aspiring guidance during my study. I am thankful for his invaluable knowledge shared, friendly advices, interest, motivation and availability. *Muito obrigada!*

I would also like to thank PhD student Giorgos Karanikoloudis for introducing me the software ARTeMIS, helping me to perform Operational Modal Analysis and his companion in the library during my mobility at University of Minho. *Σε ευχαριστώ πάρα πολύ!*

Moreover, I would like to thank to Research Assistant Dr. Onur Kaplan for his experimental campaign, Ambient Vibration Measurements of the Kütahya Kurşunlu Mosque, and to Research Assistant Dr. Onur Tunaboyu for his interest during this academic period.

I also would like to thank to Turkish Republic of Northern Cyprus Government for the financial support during my master education as a MSc. scholar.

Additionally, I would like to thank to my course colleagues Esengül, İsmail, Şenol for their friendship and to my childhood friend İnci and my family in Guimarães Derya, for their support and friendship.

Last but not least, I am extremely grateful to my parents, Mehmet and Selcan, and to my brothers, Yılmaz and Fahri. Thanks for the trust and support that I feel wherever I go and whatever I do. A special thanks to my brother Fahri for all the cheering me up, and Yılmaz who donated his brand-new laptop that made all computational efforts possible during this study. Thanks for being great brothers!

Abide AŞIKOĞLU

28/06/2018

STATEMENT OF COMPLIANCE WITH ETHICAL PRINCIPLES AND RULES

I hereby truthfully declare that this thesis is an original work prepared by me; that I have behaved in accordance with the scientific ethical principles and rules throughout the stages of preparation, data collection, analysis and presentation of my work; that I have cited the sources of all the data and information that could be obtained within the scope of this study, and included these sources in the references section; and that this study has been scanned for plagiarism with "scientific plagiarism detection program" used by Anadolu University, and that "it does not have any plagiarism" whatsoever. I also declare that, if a case contrary to my declaration is detected in my work at any time, I hereby express my consent to all the ethical and legal consequences that are involved.

Abide AŞIKOĞLU

TABLE OF CONTENT

Page

TITLE PAGE i

FINAL APPROVAL FOR THESIS ii

ABSTRACT iii

ÖZET iv

ACKNOWLEDGEMENTS v

STATEMENT OF COMPLIANCE WITH ETHICAL PRINCIPLES AND RULES vi

TABLE OF CONTENT vii

INDEX OF TABLES ix

INDEX OF FIGURES xi

INDEX OF ABBREVIATION AND SYMBOLS xvii

1. INTRODUCTION 1

1.1 Motivation 5

1.2 General Overview 12

1.3 Previous Studies 16

1.4 Scope of the Study 22

1.5 Outline of the Thesis 23

2. CASE STUDY: KÜTAHYA KURŞUNLU MOSQUE 24

2.1 Brief Description of the Mosque 25

2.2 In-situ Observation and Repair Works 28

2.3 Steel Girder Retrofitting 35

3. NUMERICAL MODELING 40

3.1 Generation of Finite Element Model 42

3.1.1 Geometry description 42

3.1.2 Mesh generation 47

3.1.3 Boundary conditions 48

3.2 Constitutive Material Model and Nonlinear Material Properties 49

4. IDENTIFICATION OF MODAL PARAMETERS 53

4.1 Ambient Vibration Measurements 55

4.2 Operational Modal Analysis 57

4.3 Calibration of the Numerical Model 61

4.4 Eigenvalue Analysis 63

Page

5. SEISMIC ASSESSMENT BY NONLINEAR STATIC ANALYSIS 68
5.1 Nonlinear Pushover Analysis 68
5.1.1 Direction +X 69
5.1.2 Direction -X 73
5.1.3 Direction +Y 73
5.1.4 Direction -Y 76
5.2 Final Remarks 77
6. SEISMIC ASSESSMENT BY NONLINEAR DYNAMIC ANALYSIS 78
6.1. Real Acceleration as Ground Motion 78
6.2. Damping of the Structural System 83
6.3. Nonlinear Time History Analysis Results 84
6.3.1. Change in the displacement response 85
6.3.2 Change in the out-of-plane displacement 90
6.3.3 Change in relative out-of-plane displacement at the dome supporting walls 96
6.3.4 Change in the in-plane displacements 98
6.3.5 Change in the absolute acceleration response 101
6.3.6 Change in the strain distribution 103
6.3.7 Change in the hysteretic response 105
6.3.8 Correlation of cracks on the non-retrofitted mosque 110
6.4 Final Remarks 115
7. CONCLUSIONS 117
REFERENCES 120
APPENDICES 126
APPENDIX - 1 : ARCHITECTURAL DRAWINGS 126
APPENDIX - 2 : DAMAGE ASSESSMENT 133
CURRICULUM VITAE 149

INDEX OF TABLES

Page

Table 1.1. Presented case studies, cause for loss and intervention decisions (Silva, 2013) 5

Table 1.2. List of some of the catastrophic earthquakes happened in Turkey (KOERI) 7

Table 1.3. List of UNESCO World Heritage Sites in Turkey (Http-6) 9

Table 1.4. Number of immovable cultural property in Turkey and selected cities in Turkey 10

Table 2.1. Past events with high intensity in Kütahya (KOERI; Yılmaz and Avşar (2013)) 28

Table 3.1. Physical properties of the shell elements 46

Table 3.2. Linear elastic properties of the materials 47

Table 3.3. Densities and reference mechanical properties of different types of coarse masonry with poor mortar (Angelillo, Lourenço, and Milani, 2014; translated from Italian Code, 2009) 51

Table 3.4. Nonlinear properties of the materials 52

Table 4.1. Comparison between SSI-UPC and EFDD results using MAC 60

Table 4.2. Comparison of the experimental and calibrated numerical modal frequencies 62

Table 4.3. Calibrated Modulus of Elasticity values for masonry materials 62

Table 4.4. Frequencies, periods and cumulative mass participation ratios of the retrofitted model for the first 100 modes in each direction 65

Table 4.5. Frequencies, periods and mass participation ratios of non-retrofitted model for the first 100 modes in each direction 67

Table 6.1 Seismological properties of selected ground motions (TR-NSMN) 79

Table 6.2. Selected modes to calculate Rayleigh damping parameters 84

Table 6.3. Response on each control node in terms of peak displacement in the transversal (X) direction, Erzincan Earthquake 86

Table 6.4. Response on each control node in terms of peak displacement in the transversal (X) direction, Düzce - Bolu Earthquake 86

Page

Table 6.5. Response on each control node in terms of peak displacement in the transversal (X) direction, Bingöl Earthquake 86

Table 6.6. Response on each control node in terms of peak displacement in the longitudinal (Y) direction, Erzincan Earthquake 86

Table 6.7. Response on each control node in terms of peak displacement in the longitudinal (Y) direction, Düzce - Bolu Earthquake 87

Table 6.8. Response on each control node in terms of peak displacement in the longitudinal (Y) direction, Bingöl Earthquake 87

INDEX OF FIGURES

Page

Figure 1.1. Heritage structures in Famagusta after restoration works....4

Figure 1.2. Seismic Hazard map of Turkey (AFAD, 2018)....6

Figure 1.3. The westward migrating earthquake sequence along the North Anatolian Fault starting from 1939 (Akyüz et al., 2002)....7

Figure 1.4. UNESCO World Heritage Sites in Turkey (Http-5)....10

Figure 1.5. The elements of the structural analysis of historical constructions, (adapted from Roca, 2005)....13

Figure 1.6. Deformation and typical damage on the load bearing walls (Tomaževič, 1999)....14

Figure 1.7. Typical failure modes of masonry load bearing walls subjected to in-plane seismic load (Tomaževič, 1999)....14

Figure 1.8. Types of structural analysis for historical constructions, (adopted from TYDRYK, 2017)....15

Figure 2.1. Kütahya Kurşunlu Mosque after interventions, January 2017....25

Figure 2.2. Location of the historical mosque....26

Figure 2.3. Architectural plan of the mosque (in cm)....26

Figure 2.4. Kütahya Kurşunlu Mosque before intervention started in 2013....27

Figure 2.5. Seismicity map of Kütahya province (AFAD, 2018)....28

Figure 2.6. Connected wooden tie beams on the arch elements of portico....28

Figure 2.7. Arch response on the different arch systems....29

Figure 2.8. Visual observations on the South Wall....30

Figure 2.9. Vertical cracks....31

Figure 2.10. Damage observed on the West Wall....31

Figure 2.11. Damage observed on the dome....32

Figure 2.12. Damage observed on the octagonal drum....33

Figure 2.13. Grout injection....34

Page

Figure 2.14. Application of stitching technique on the extrados 34

Figure 2.15. Stainless steel girder application plan.....36

Figure 2.16. Loss of wooden beam elements at the bottom part of the drum.....37

Figure 2.17. Steel girder application steps.....37

Figure 2.18. Single bar U160 steel girder at the top section of the drum and anchorage connection.....38

Figure 2.19. Application of double steel girder (2U160) on the load bearing walls.....39

Figure 2.20. Lead covering after steel girder retrofitting 39

Figure 3.1. Modeling techniques defined in (TYDRYK, 2017) 41

Figure 3.2. Modeling strategies for masonry structures (Lourenço, 2002) 42

Figure 3.3. Configuration of the structural components.....43

Figure 3.4. Geometry simplification of the pendentives 44

Figure 3.5. Steel girder configuration.....44

Figure 3.6. Adopted linear elastic timber elements (colored as yellow) 45

Figure 3.7. Adopted corrections on the geometry of the large openings (Lourenço et al., 2007) 45

Figure 3.8. Identification of the different materials 46

Figure 3.9. The beam element L13BE, with a total thirteen degree-of-freedom (TNO DIANA, 2017).....47

Figure 3.10. The shell element T15SH, with a total fifteen degrees-of-freedom 48

Figure 3.11. The solid element TE12L, with a total twelve degrees-of-freedom 48

Figure 3.12. Top view of boundary constrains at the supports.....49

Figure 3.13. Adopted behavior for masonry materials.....49

Figure 3.14. Nonlinear material property of the adopted steel 52

Figure 4.1. Dynamic-based assessment of the structure, (adapted from Gentile and Saisi, 2007) 55

Page

Figure 4.2. Station layout and sensor directions 56

Figure 4.3. Test equipment; Left: Base station and 1st station, Right top: 4th station, Right bottom: accelerometer at the base station.....57

Figure 4.4. Singular values of spectral densities of all setups, EFDD method.....58

Figure 4.5. Selection and linking process of modes across all test setups, SSI-UPC method.....59

Figure 4.6. First 4 mode shapes derived by SSI method, ARTeMIS Modal.....60

Figure 4.7. Experimental and calibrated numerical modes of vibrations.....62

Figure 4.8. Several mode shapes of retrofitted model, FX+ for DIANA.....64

Figure 4.9. Several mode shapes of non-retrofitted model, FX+ for DIANA.....66

Figure 5.1. Global coordinate system and defined control nodes.....69

Figure 5.2. The pushover curves in the positive transversal direction.....70

Figure 5.3. The non-retrofitted numerical and real damage on the south wall, maximum principal strain distribution at load factor 0.27g in +X direction.....71

Figure 5.4. The non-retrofitted numerical and real damage on the west façade, maximum principal strain distribution at load factor 0.27g in +X direction.....71

Figure 5.5. The non-retrofitted numerical and real damage on the east façade, maximum principal strain distribution at load factor 0.27g in +X direction.....72

Figure 5.6. The non-retrofitted numerical and real damage on the dome, maximum principal strain distribution at load factor 0.27g.....72

Figure 5.7. The pushover curves in the negative transversal direction.....73

Figure 5.8. The pushover curves in the positive longitudinal direction.....74

Figure 5.9. Comparison of the non-retrofitted numerical and real damage on the West Wall, maximum principal strain distribution at load factor 0.3g.....75

Figure 5.10. Comparison of the non-retrofitted numerical and real damage on the Dome, maximum principal strain distribution at load factor 0.3g.....75

Figure 5.11. The pushover curves in the negative longitudinal direction.....76

Page

Figure 5.12. Numerical damage on the south façade, maximum principal tensile strain distribution at the load factor 0.4g 76

Figure 6.1. Epicenter of earthquakes marked with red.....78

Figure 6.2. Acceleration-time series of each record (TR-NSMN).....81

Figure 6.3. Elastic response spectra of input records and design spectrum as per TEC (2007) for Z3 soil condition 81

Figure 6.4. Arias Intensity of the selected accelerograms 82

Figure 6.5. Rayleigh damping (Chopra, 2012) 83

Figure 6.6. Directions and locations of control points on the model 85

Figure 6.7. Pushover curve, inter-story drift ratio limits suggested by the Turkish guideline for historical structures (TYDRYK, 2017) 88

Figure 6.8. Comparison of drift ratio demands on each structural component regarding to (TYDRYK, 2017) 89

Figure 6.9. Displacement-time series of control nodes of East and West Walls for 3 ground motions in X direction 90

Figure 6.10. Displacement-time series of control nodes of North Wall, South Wall and Portico for 3 ground motions in Y direction.....91

Figure 6.11. Change in response of control points on South Wall, North Wall and Portico due to retrofitting in terms of out-of-plane displacement 92

Figure 6.12. Change in response of control points on East Wall and West Wall due to retrofitting in terms of out-of-plane displacement 93

Figure 6.13. Change in out-of-plane behavior at time step when South Wall has peak displacement.....94

Figure 6.14. Change in out-of-plane behavior at time step when North Wall has peak displacement.....94

Figure 6.15. Change in out-of-plane behavior in terms of absolute displacement at time step when West Wall has peak displacement 95

Figure 6.16. Change in out-of-plane behavior in terms of absolute displacement at time step when East Wall has peak displacement.....96

Page

Figure 6.17. Schematic representation of the residual displacements on the dome supporting walls.....97

Figure 6.18. Change in out-of-plane displacement relative to the west wall.....98

Figure 6.19. Change in out-of-plane displacement relative to the south wall 98

Figure 6.20. Displacement-time series of control nodes of East and West Walls for 3 ground motions.....99

Figure 6.21. Displacement-time series of control nodes of the north wall, south wall and portico for 3 ground motions.....99

Figure 6.22. Change in response of control points on the east wall and west wall due to retrofitting in terms of in-plane displacement.....100

Figure 6.23. Change in response of control points on South Wall, North Wall and Portico due to retrofitting in terms of in-plane displacement.....101

Figure 6.24. Change in absolute acceleration demand in transverse direction.....102

Figure 6.25. Change in absolute acceleration demand in longitudinal direction.....102

Figure 6.26. Principal tensile strains of South-West façade resulted by Bolu record, deformed shape scale factor:5 103

Figure 6.27. Principal tensile strains of North-East façade resulted by Bolu record, deformed shape scale factor:5 103

Figure 6.28. Change in the hysteretic response in the transversal direction.....106

Figure 6.29. Change in the hysteretic response in the longitudinal direction.....107

Figure 6.30. Change in the hysteretic response in the X direction, detailed 108

Figure 6.31. Change in the hysteretic response in the Y direction, detailed 109

Figure 6.32. Correlation of cracks observed in-situ and numerical model on the south façade.....110

Figure 6.33. Correlation of the vertical crack observed in the numerical model and in-situ 112

Figure 6.34. Correlation of the vertical crack observed on the east façade in the numerical model and in-situ 113

Figure 6.35. Correlation of the crack observed on the dome interior face in the numerical model and in- situ 114

Page

Figure 6.36. Variation in the average relative residual displacement with respect to each ground motion.....116

INDEX OF ABBREVIATION AND SYMBOLS

A	:	Area
AG	:	Aegean graben
B	:	Damping reduction factor
c	:	Damping ratio
$\bar{C}$	:	Damping matrix
E	:	Modulus of Elasticity
EAF	:	East Anatolian Fault
EFDD	:	Enhanced Frequency Domain Decomposition
f	:	Frequency of the vibration mode
f_c	:	Compressive strength
FEA	:	Finite Element Analysis
FEM	:	Finite Element Model
f_{exp}	:	Frequency of the experimental vibration mode
F_h	:	Horizontal force
f_{num}	:	Frequency of the numerical vibration mode
FRF	:	Frequency Response Functions
f_t	:	Tensile strength
F_v	:	Vertical force
g	:	Gravitational acceleration
G	:	Shear stiffness
G_c	:	Compressive fracture energy
GCI	:	Getty Conservation Institute

G^{Cr}	:	Cracked shear stiffness
G_t	:	Tensile fracture energy
h	:	Crack bandwidth
ICCROM	:	International Centre for the Study of the Preservation and Restoration of Cultural Property
ICOMOS	:	International Council on Monuments and Sites
ISCARSAH	:	International Scientific Committee on the Analysis and Restoration of Structures of Architectural Heritage
$\overline{K}$	:	Stiffness matrix
KOREI	:	Kandilli Observatory and Earthquake Research Institute
L_f	:	Load factor
$\overline{M}$	:	Mass matrix
MAC	:	Modal Assurance Criterion
M_w	:	Moment magnitude
NAF	:	North Anatolian Fault
OMA	:	Operational Modal Analysis
PGA	:	Peak Ground Acceleration
PGD	:	Peak Ground Displacement
PGV	:	Peak Ground Velocity
SSI-UPC	:	Stochastic Subspace Identification-Unweighted Principal Components
T	:	Period
t	:	Time
TEC	:	Turkish Earthquake Code
TYDRYK	:	Tarihi Yapılar için Deprem Risklerinin Yönetimi Kılavuzu
UNDP-PFF	:	The United Nations of Development Programme-Partnership for the Future

UNESCO	:	The United Nations Educational, Scientific and Cultural Organisation
WMF	:	World Monuments Fund
α	:	Viscous damping coefficient
β	:	Viscous damping coefficient
γ	:	Unit weight
μ	:	Shear retention factor
τ_s	:	Shear strength
υ	:	Poisson ratio
φ_{aj}	:	Analytical mode vector
φ_{ej}	:	Experimental mode vector
ω_η	:	Natural frequency

1. INTRODUCTION

Throughout the history, tangible and intangible cultural heritage is admitted as national and cultural identity of a society. Architectural heritage, defined as tangible heritage, has been physical manifestation of the history and material evidence of the past generations, craftmanship, technique, and cultural context (Orbaşlı, 2007). Therefore, preservation of built heritage plays an important role in order to maintain and promote national identity and cultural diversity from generations to generations. Moreover, historic areas have been catalyst for the regeneration of their environment and contribute to the economy of cities (Orbaşlı, 2007). Despite the fact that heritage defines identity to the community it belongs, the legacy shares a particular creative quality, a uniqueness, originality and authenticity which make it the common universal heritage of humankind (Jokilehto, 1999). In fact, the Nara Document (1994) emphasizes the spirit of conservation and preservation of any kind of heritage with the following words;

> "The diversity of cultures and heritage in our world is an irreplaceable source of spiritual and intellectual richness for all humankind. The protection and enhancement of cultural heritage and heritage diversity in our world should be actively promoted as an essential aspect of human development (the Nara Document, 1994)."

The history of architectural conservation dates back to late eighteenth century. Since then, the principles and ethics of conservation have been formed by several influences. In eighteenth century, ancient structures had been reutilized different than its former purpose. For instance, Roman temples and basilicas had been used as churches in Italy namely the church of San Lorenzo, former Roman temple of Antoninus and Faustina. Reusing of the building materials and parts of buildings was very common by the Venetians. In nineteenth century, reordering and reconstruction of the monuments was admitted as restoration works. At the end of nineteenth century, preservation and presentation of important monuments had been considered as clearing their environment from clustered urban fabric and displaying them with more sophisticated landscape planning by constructing large gardens. In addition, 'anti-restoration' movement was started in the second half of the nineteenth century. The main objective was to search for authenticity and to protect heritage structures when it was necessary. The practices and debates of the nineteenth century originated the twentieth century's and today's principles of conservations. In the twentieth century, two World Wars and economic value associated with cultural tourism formed a new approach to the conservation practice. In

aftermath, national or ethnic identity prioritized and considered during the conservation of buildings. During this period, rebuilding of symbolic architecture was preferred due to the fact that the national identity of an ancient structure was more significant than strict adherence to conservation theory. Therefore, rebuilding had to be accepted within the principles of conservation due to its symbolic meaning (Orbaşlı, 2007). Even so, The Convention for the Protection of Cultural Property in the Event of Armed Conflict, which is also known as Hague Convention, was held by The United Nations Educational, Scientific and Cultural Organisation (UNESCO) in 1954. The major objective of the convention is to ensure the respect to the cultural heritage in times of armed conflict (UNESCO, 1954).

Due to its long-life span, it is possible to identify particular cultures by studying the architectural structure. The ancient structure does not only influence its environment but also it is influenced by different cultures. For instance, materials, structural systems and forms of ornaments are related with only particular cultures (Jokilehto, 1999). Ancient structures have undergone several modifications that belong to different periods of time. Therefore, a multi-disciplinary approach has to be taken in order to understand the necessities of a such structure so as to perform restoration and conservation works. In this sense, international meetings have been held with the participation of different professions. In 1931, first international meeting was held by International Museum Office at Athens Conference. The first international document outlining resolutions for the conservation of historical monuments, which is also known as Athens Charter, was drafted. In 1964, the Second International Congress of Architects and Technicians of Historic Monuments was held in Venice. The first adopted resolution was the International Charter for the Conservation and Restoration of Monuments and Sites, also known as the Venice Charter. The second resolution was the establishment of International Council on Monuments and Sites (ICOMOS) by UNESCO. In Venice Charter, it is addressed that the principles of preservation and restoration of ancient buildings should be agreed in an international basis and each country should adopt its own plan by considering its own culture. Besides, several charters have been adopted by ICOMOS in national and international basis up to the present. For instance, The Burra Charter (2013) (first adopted in 1979 and periodically updated) and ICOMOS Turkey Architectural Heritage Conservation Charter (2013) are only the two of the national charters. Furthermore, The International Scientific Committee on the Analysis and

Restoration of Structures of Architectural Heritage (ISCARSAH) was founded by ICOMOS in 1996 as the technical committee of the council. In the present time, conservation and preservation of historical structures should be conducted according to the principle of minimum intervention (ICOMOS-TR, 2013). Current guideline, namely Recommendations for the Analysis, Conservation and Structural Restoration of Architectural Heritage, was published in 2003 by ISCARSAH. Guideline addresses that structural conservation plan requires both qualitative and quantitative approach. Qualitative data is reported with respect to historical research, in-situ observations like structural damage, material decay etc. Quantitative data is obtained by using analytical and scientific methods, for instance testing, calculations, experiments and mathematical modelling. This holistic approach makes adoption and application of the rules and codes on historical structures very complicated and difficult. Therefore, the guideline discourages application of design codes for modern structures on the heritage structures.

Convention Concerning the Protection of the World Cultural and Natural Heritage was adopted by UNESCO as a part of the 17th General Conference held in Paris on November 16, 1972. Resolutions adopted in the convention was within the framework of action as: (i) to promote the cultural and natural possessions as the common heritage of all humankind, (ii) to raise awareness on the conservation and protection of universal heritage, and, (iii) to provide necessary cooperation with state parties to ensure protection, conservation and presentation of the cultural and natural heritage which are subjected to decay (UNESCO, 1972). By the year 2017, a number of 1073 properties have been officially recorded as outstanding universal heritage in the World Heritage List by UNESCO. The 832 of these properties are cultural, the 206 of them are natural and the 35 of the properties are defined as mixed, both cultural and natural. Moreover, UNESCO has defined tentative list of properties that have high potential of universal heritage which state parties are encouraged to prepare their tentative list and to be nominated for the World Heritage List. By the year 2017, the 1706 properties and 54 properties from all around the world are defined in the Tentative List and List of World Heritage in Danger, respectively (Http-1).

Moreover, there are several non-profit organizations, foundations and universities aiming at protection and conservation of the heritage structures. For instance, The International Centre for the Study of the Preservation and Restoration of Cultural Property (ICCROM), World Monuments Fund (WMF), The Getty Conservation Institute (GCI),

in national basis Technical Committee on Cultural Heritage of the United Nations Development Programme Partnership for the Future (UNDP PFF) – Cyprus are only some of them. Many universities and institutions are not only conducting scientific research studies to put forward new technologies and methodologies but also consulting and cooperating with private sectors and state parties so as to protect universal heritage. Specifically, Technical Committee on Cultural Heritage of UNDP – Cyprus serves as a model of two different communities working on common heritage that has outstanding universal value. Turkish and Greek Cypriots are working together in order to protect and promote their common cultural and built heritage in Cyprus. One of the most important intervention plan is in progress in the Walled City of Famagusta which is funded by European Union. The technical committee is aware of the universal value of the cultural heritage regardless from its ethnic or religious difference. It is a solid example of how heritage shapes the respect between communities. In Figure 1.1, two examples of heritage structures after restoration works adopted by Technical Committee of Cultural Heritage UNDP - Cyprus are given. It is believed that Othello Castle is the castle which William Shakespeare was inspired by while writing his famous play '*The Tragedy of Othello*' and consequently it enriches universal value of the ancient structure (Figure 1.1(a)). Furthermore, old town Famagusta is surrounded by ancient masonry walls which give the name to the city 'Walled City of Famagusta' (Figure 1.1(b)). It is obvious that the city will definitely lose its identity without these ancient walls.

(a) Othello Castle / Citadel *(b) Part of the Famagusta Walls (Http-2)*

Figure 1.1. *Heritage structures in Famagusta after restoration works*

There are several reasons for sudden losses of built heritage and generally occurs in human origin - war conflicts, terrorism, vandalism, lack of conservation and protection, inappropriate applications, and in natural origin – natural disasters like earthquakes, floods, fire and long term effect of permanent load. Silva (2013) presented several case

examples of built heritage that suffered sudden collapse associated with war conflicts and terrorism, earthquake, fire and long-term effects due to high permanent load. Presented case examples and their intervention decisions are given in Table 1.1.

Table 1.1. *Presented case studies, cause for loss and intervention decisions (Silva, 2013)*

Example Case	Cause for loss	Intervention
Mostar bridge Our Lady Church in Dresden Historic centre of Warsaw	War	Reconstruction (1)
Bamian Buddha's	War with religious contents	None, so far
Temples of Mali		Rebuilt *
Twin Towers	Terrorism	Rebuilt (2)
City of Lisbon in 1755	Earthquake	City rebuilt (2)
Chiado in 1989	Fire	Reconstruction (3)
Civic Tower of Pavia	Creep / Long term effect of permanent loads	None

(1) Reconstruction of the ancient buildings
(2) The rebuilt of the city/building altered the built heritage aesthetics'
(3) Reconstruction maintained, when possible, the ancient buildings façades
* Rebuilt in 2015 (Http-3)

1.1 Motivation

As addressed previously, there are several reasons for sudden losses of built heritage. The source of motivation in the present study is the sudden losses of heritage structures due to dynamic loading, namely earthquakes. Although heritage structures stand for ages, they become vulnerable against any action day by day. In fact, those structures have already experienced degradation due to natural actions or human actions. Therefore, conservation of the heritage buildings, which are especially located in the high seismic prone zones on the Earth, should be provided. Accordingly, Turkey is one of the countries that was subjected to destructive earthquakes in the past. Turkey is located in the second most active seismic zones on the Earth, namely Alpine-Himalayan Belt. The major faults are the North Anatolian Fault (NAF), East Anatolian Fault (EAF) and Aegean Graben (AG) and additionally, there are several local faults in the country. A great majority of the country (96%) is under seismic risk. Approximately 70% of the population, 74% of country's industry and 75% of power stations are situated in the high

seismic prone zone (Figure 1.2). In Figure 1.2, contour distribution of Peak Ground Acceleration (PGA) is given in terms of the probability of exceedance of the earthquake within a period of 50 years in 10%. The red color indicates the highest seismicity nearly up to 0.8g while the white color depicts the lowest seismic activity in the region and black lines represent the faults.

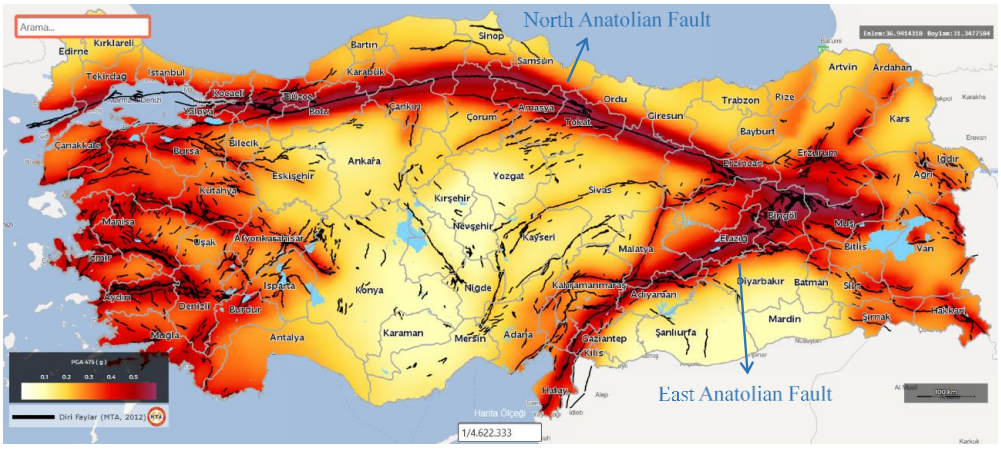

Figure 1.2. *Seismic Hazard map of Turkey (AFAD, 2018)*

Throughout the history, many destructive earthquakes occurred in Turkey. North Anatolian Fault is experiencing a westward migrating earthquake sequence as shown in Figure 1.3. The sequence has begun with 1939 Erzincan Earthquake resulting 360 km-length surface rupture and right-lateral displacements up to 10 m. Following events happened in 1942 (M7.1, with 50 km rupture), 1943 (M7.7, with 280 km rupture), 1944 (M7.4, 165 km rupture), 1951 (M6.8, 30 km rupture), 1957 (M7, rupture ranging between 30 – 50 km), 1967 (M7.2, 80 km rupture), and finally two earthquakes happened in 1999 (M7.5, 130 km rupture and M7.1, with 50 km of rupture). Consequently, approximate 1,000 km fault unzipped starting from Erzincan nearly to Marmara Sea (Rockwell, 2013). Rockwell (2013) states that similar earthquake sequence happened a century ago was concluded regarding to the paleo-seismic site works and it is found that the current sequence, which has started in 1939, has not completed yet. Therefore, another destructive earthquake is expected in the Marmara Sea next to İstanbul, the most populated city in the country with 15 million people. In addition to İstanbul, western part of the country is expected to be affected. On the other hand, NAF is not the only fault that can create catastrophic earthquakes. Several major earthquakes occurred along the East Anatolian Fault and in Aegean Graben as well. In Table 1.2 list of the catastrophic

earthquakes occurred in westward migrating earthquake sequence along the NAF and several events in EAF and AG are given. The number of fatalities in the selected events is astonishing, and it is not acceptable in a developed country. Almost 33,000 death tolls after 1936 Erzincan Earthquake, nearly 18,000 of casualties after 1999 Kocaeli Earthquake officially recorded only for those events.

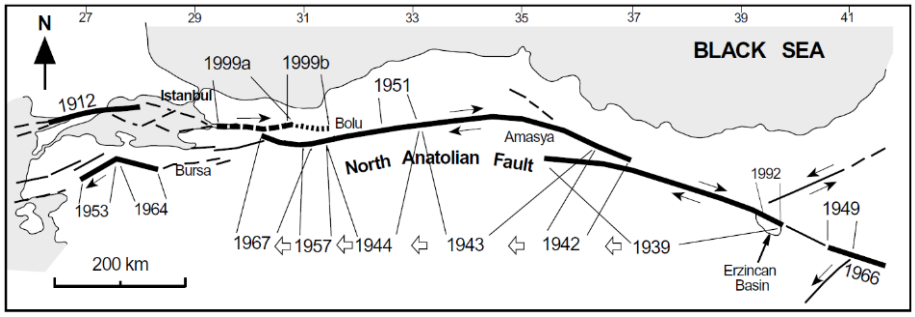

Figure 1.3. *The westward migrating earthquake sequence along the North Anatolian Fault starting from 1939 (Akyüz et al., 2002)*

Table 1.2. *List of some of the catastrophic earthquakes happened in Turkey (KOERI)*

Date	Time (Local Time)	Location	Mercalli Intensity	Ms	Death Tolls	No. Damaged Buildings	Fault Line
27.12.1939	1:57	Erzincan	X-XI	7.9	32968	116720	NAF
20.12.1942	16:03	Tokat	IX	7	3000	32000	NAF
27.11.1943	0:20	Samsun	IX-X	7.2	4000	40000	NAF
1.2.1944	5:22	Bolu	IX-X	7.2	3959	20865	NAF
13.8.1951	20:33	Çankırı	IX	6.9	50	3354	NAF
26.5.1957	8:33	Bolu	IX	7.1	52	5200	NAF
22.7.1967	18:56	Adapazarı	IX	6.8	89	7116	NAF
17.8.1999	3:01	Kocaeli	X	7.8	17480	73342	NAF
12.11.1999	18:57	Düzce	IX	7.5	763	35519	NAF
13.3.1992	19:08	Erzincan	VIII	6.8	653	8057	NAF
19.8.1966	14:22	Muş	IX	6.9	2396	20007	EAF
6.9.1975	12:20	Diyarbakır	VIII	6.6	2385	8149	EAF
23.10.2011	13:41	Van	VIII	7.2	644	17005	EAF
1.5.2003	3:27	Bingöl	VIII	6.4	176	6000	EAF
9.8.1912	3:29	Tekirdağ	X	7.3	216	5540	
18.3.1953	21:06	Çanakkale	IX	7.2	265	6750	
6.10.1964	16:31	Balıkesir	IX	7	23	5398	AG
28.3.1970	23:02	Kütahya	IX	7.2	1086	19291	AG
19.5.2011	23:15	Kütahya	VI	5.9	3	-	AG

Table 1.2 also gives official records of number of buildings that were damaged during each earthquake. Those numbers show that the building stock of the country consist of considerable amount of buildings vulnerable against to earthquake motions. At the time of a such event, the loss of property did create a state of chaos for people and brought security, economic and social concerns. The severe consequences of such events increased the awareness of earthquake disaster preservation plans for public and constructing earthquake resistant structures. By this time, there have been made very important developments in the field of structural and earthquake engineering. For instance, specifications for the buildings to be constructured in disaster areas are periodically updated, concrete quality has been increased by adopting ready-mixed concrete plants and application of the new technologies have begun such as seismic isolators, dampers, retrofitting, strengthening techniques and reconstruction of buildings regarding to earthquake resistant building code. As structural engineers, providing security for human life is the priority. Furthermore, it is also crucial to minimize the effects of earthquakes on the structures in order to ensure social and economic concerns of the country. However, protection of heritage structures still requires significant developments and collapse or severe damage of any structure which promotes a value for the society should be prevented against earthquake actions. Turkey has been home to many civilizations throughout the history and consequently, the culture of the country has been influenced and shaped by those periods of time. Therefore, there are wide range of cultural and built heritage belonging to different eras of time which forms Turkey's outstanding legacy of heritage. Turkey has 17 properties inscribed on the UNESCO World Heritage List as given in Table 1.3 and shown in Figure 1.4. Moreover, the 71 sites have been nominated in the Tentative List of UNESCO World Heritage. On the other hand, according to General Directorate of Cultural Heritage and Museums of Republic of Turkey Ministry of Culture and Tourism, there are approximately 107,000 immovable cultural property that has to be preserved and protected all around the Turkey as given in Table 1.4 (Http-4). Immovable cultural properties are defined according to their service. Types of the built heritage has been specified as sample of civil architecture, religious, cultural, governmental, military, industrial, commercial structures, cemeteries, ruins, memorials and monuments and protected streets. In Table 1.4, some of the cities with high number of immovable built heritage are also given. The vast majority of the built heritage has been recorded in İstanbul, with nearly 31,000 cultural buildings. İzmir,

Bursa, Balıkesir, Antalya, capital city Ankara, Kütahya and Eskişehir also has a great amount of cultural property that should be conserved (Http-5). It is important to mention that the selected cities are in the regions with high seismic activity. Regarding to the seismic map of Turkey, it is obvious that the most majority of the architectural heritage is under seismic risk. In this context, essential developments have begun to mitigate seismic risk on the historical structures. In the current and upcoming provision TEC 2007 and TEC 2019, there are requirements and restrictions on the performance assessment of existing reinforced concrete and masonry structures but there is no regulation about seismic assessment of the historical structures. It is worth to mention that historical structures are not abstract beings so that implementation of structural engineering in a conventional way as in modern structures is not feasible (Roca, 2006). These structures have complex geometries, diverse materials and they are imposed to several repair works or transformation due to long-time effects or severe damage. Therefore, more general and flexible applications of structural engineering is suggested (Roca, 2006). However, lack of detailed guidance for those special structures has been arisen an essential need for a such technical document rather than regulations.

Table 1.3. *List of UNESCO World Heritage Sites in Turkey (Http-6)*

UNESCO World Heritage Sites	Date of Inscription
Historic Areas of İstanbul	1985
Göreme National Park and the Rock Sites of Cappadocia	1985
Great Mosque and Hospital of Divriği	1985
Hattusha: the Hittite Capital	1986
Nemrut Mountain	1987
Xanthos-Letoon	1988
Hierapolis-Pamukkale	1988
City of Safranbolu	1994
Archaeological Site of Troy	1998
Selimiye Mosque and its Social Complex	2011
Neolithic Site of Çatalhöyük	2012
Pergamon and its Multi-Layered Cultural Landscape	2014
Bursa and Cumalıkızık: the Birth of the Ottoman Empire	2014
Diyarbakır Fortress and Hevsel Gardens Cultural Landscape	2015
Ephesus	2015
Archaeological Site of Ani	2016
Aphrodisias	2017

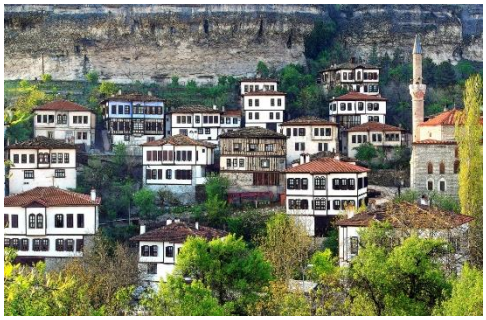

(a) City of Safranbolu

(b) Selimiye Mosque and its Social Complex

(c) Ephesus

(d) Historic areas of İstanbul

Figure 1.4. *UNESCO World Heritage Sites in Turkey (Http-7)*

Table 1.4. *Number of immovable cultural property in Turkey and selected cities in Turkey*

Type	**Number of immovable cultural properties need to be conserved**								
	Turkey	İstanbul	İzmir	Bursa	Balıkesir	Antalya	Ankara	Kütahya	Eskişehir
Samples of civil architecture	68114	25026	4623	3164	2488	1506	1215	1056	1078
Religious structures	9876	1232	435	420	179	181	228	223	138
Cultural structures	12118	2308	587	308	183	477	199	174	97
Govermental structures	2889	521	227	86	89	32	187	29	60
Military structures	1225	107	27	49	14	88	9	2	16
Industrial and commercial structures	3992	532	708	49	74	79	90	27	155
Cemeteries	5168	690	174	167	83	186	146	54	32
Memorials and monuments	356	74	28	13	12	13	34	6	3
Ruins	2552	691	94	72	28	278	19	13	4
Protected streets	69	10	6	1	2	3	-	-	-
Total	**106359**	31191	6909	4329	3152	2843	2127	1584	1583

Recently, a guideline on management of earthquake risk for historical structures has been published by Directorate General of Foundations (TYDRYK, 2017). The main purpose of the guideline is to provide technical document about principles of seismic assessment and strengthening and retrofitting applications on the historical structures. It is stressed that the recommendations in the guideline should not be applied without any critics. The Turkish guideline for earthquake management of historical constructions has eight main chapters as follows (TYDRYK, 2017);

Chapter 1: Objective and scope

The main objective of the recommendation is to identify seismic performance of the structure before an event, to define survey and research studies, specify main calculation principles under vertical and horizontal loading, develop interventions and take remedial measures before an earthquake. It also encourages to apply urgent intervention, ensure safety to damaged cultural heritage, prevent total collapse during any repair work after an earthquake.

Chapter 2: Basic definitions and concepts

Description of the basic technical terms related with conservation of the architectural heritage, disasters and structural engineering are given in this section.

Chapter 3: Research, information gathering

In this section, several explanations are made to proceed qualitative and quantitative approach. Historical research, site investigations, laboratory and in-situ experiments and structural monitoring have been described.

Chapter 4: Construction materials and damage on historical structures

Properties of construction materials and their damage causes are explained in detail. Natural stone, adobe, brick, mortar, timber, iron(steel), concrete and reinforced concrete are investigated.

Chapter 5: Structural components of the historical constructions and their construction practice

Construction practice of the components are explained briefly. Rock carving, masonry, timber, steel and early concrete structures are described.

Chapter 6: Structural modelling and assessment

In this section, types of loads subjected on the structure are defined. Mechanical properties for different types of masonry are suggested according to Italian Code.

Structural configuration, load path, connections between components are discussed. Different modelling techniques are suggested such as diagonal strut model, equivalent frame model and finite element model. Furthermore, analysis methods are described, namely linear pushover and dynamic analysis, nonlinear pushover and dynamic analysis, self-weight analysis and kinematic analysis. Performance limit states due to excitation are suggested and assessment in terms of performance limit states are encouraged.

Chapter 7: Intervention methods

Basic descriptions are made about intervention methods on masonry structures and strategies adopting on the foundation, load bearing walls, connections, columns or piers, slabs, vaults or dome and also timber roof, minarets towers and adobe structures are discussed in detail.

Chapter 8: Earthquake-based disaster management

Disaster management on historical structures are explained in this section. Shoring templates and operating procedures to support buildings damaged by earthquake is given extensively. In addition, a template of quick diagnosis of damage/condition evaluation form for historical structures after an earthquake are presented.

1.2 General Overview

In order to study historical structures, a set of activities should be considered. These activities are inspection and identification of the current state of the structure by means of visual in-situ observations and non-destructive tests, historical research, monitoring and structural modelling and analysis (Figure 1.5) (Roca, 2005). Conclusions on the condition of the building can be drawn by the combination of qualitative (inspection, historical research) and quantitative (monitoring, structural analysis) data. Quantitative analysis requires a structural model which is constituted from a set of hypotheses on the mechanical response of the structure, material properties, internal morphology and structural configuration (Roca, 2006). Validation of the adopted hypothesis should be provided by calibration of the model by using empirical evidence. By calibrating the model, the representative structural scheme can be used to study response of the building under different types of loading. However, it should be noted that having a realistic structural scheme with a precise description of the historical structure is not possible even though too much effort carried out during the visual inspection and experimental descriptions (Roca, 2006).

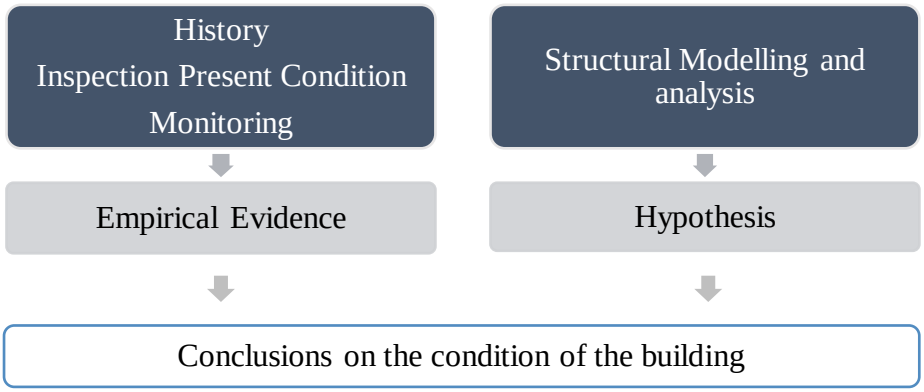

Figure 1.5. *The elements of the structural analysis of historical constructions, (adapted from Roca, 2005)*

A vast majority of the historical structures is constituted from masonry buildings. Ancient masonry structures are known with their very complex nature based on heterogeneous material distribution, sophisticated geometrical features, limited information on the connections between structural and non-structural components, building condition after long period of time and stiffness of the horizontal elements (Lourenço *et al.*, 2011). This complexity is the main concern on the seismic vulnerability of a such historical structure. These historical structures have very high capacity under compression behavior while they are quite vulnerable against any horizontal action due to very low tensile and shear strengths and quasi-brittle behavior of the masonry. Load bearing walls of the building have considerably high stiffness in-plane direction than its out-of-plane direction. Hence, direction of the horizontal load influences the seismic behavior (Lourenço *et al.*, 2011). Different types of damage pattern are observed regarding to the direction of seismic loading as illustrated in Figure 1.6. When structural walls are subjected to seismic motion along their lower inertial direction, out-of-plane bending is observed causing vertical cracks at the corners and in the middle portion of the walls. Once the seismic motion is in the plane of the walls, horizontal cracks due to bending and diagonal cracks due to shear is resulted (Tomaževič, 1999).

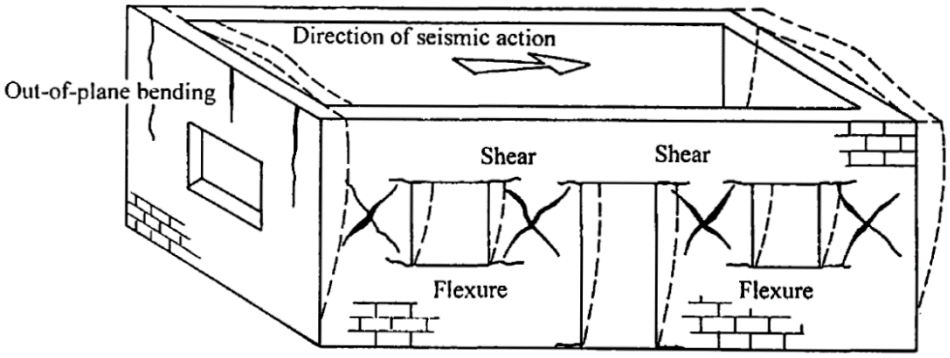

Figure 1.6. *Deformation and typical damage on the load bearing walls (Tomaževič, 1999)*

Tomaževič (1999) defines three types of failure mechanisms for structural masonry walls subjected to in-plane seismic loads as shown in Figure 1.7. The mechanisms depend on several factors, namely the geometry of the wall (height/width ratio), quality of materials, boundary restrains and loads (vertical and horizontal) acting on the walls. Sliding shear failure is observed when the vertical load is very low, and quality of the mortar is poor. In case of sliding shear failure, horizontal crack on one of the horizontal mortar joints is observed because of the fact that seismic load causes shearing the wall into two parts and sliding the upper part. Shear failure occurs when the principal tensile stresses higher than the tensile strength of the masonry and it is identified by diagonal cracks develop in the wall. The diagonal cracks can propagate along the mortar joints and/or pass through the masonry units. The flexural mode of failure, which is indicated by crushing at the ends of the wall because of the compressed regions, is observed due to the improved shear resistance and high moment/shear ratio.

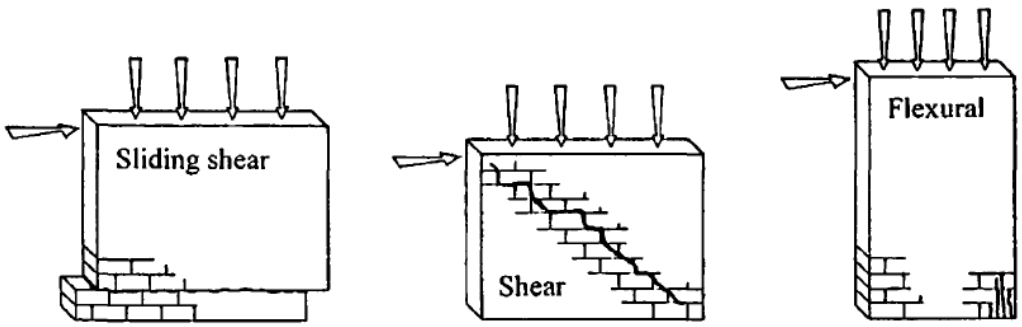

Figure 1.7. *Typical failure modes of masonry load bearing walls subjected to in-plane seismic load (Tomaževič, 1999)*

Generally, seismic performance of a historical structure is related to its ability to redistribute the seismic loads between the elements which is mainly depend on the connection between orthogonal walls, the flexibility of the horizontal diaphragms and their connection to the load bearing walls. Thus, structural integrity is provided by diaphragmatic action, known as 'box behavior' (Lourenço *et al.*, 2011). In the Guideline for Earthquake Risk Management for Historical Structures of Turkey (TYDRYK), different types of structural analysis methods are defined to perform seismic assessment for historical constructions (Figure 1.8). Linear elastic analysis assumes only the elastic properties of the material and it is the easiest tool due to low computational effort and low number of input parameters for material. Its application to the masonry structures is not suggested in case of studying structural safety and capacity (Roca *et al.*, 2010; Lourenço, 2002). Limit analysis is used to calculate the ultimate structural load and failure mechanism of the structure by assuming zero tensile strength for the masonry (Lourenço, 2002). The purpose of the nonlinear pushover analysis is to perform nonlinear analysis in order to obtain structural capacity by considering nonlinear mechanical properties of the materials. In this type of analysis, horizontal loads are generated as 1st mode proportional, mass proportional or mode superposition method. Incremental equivalent lateral force is applied monotonically until the structure experiences failure. Response spectrum analysis considers linear elastic material property and seismic input is adopted by a given response spectrum. Nonlinear dynamic analysis in time domain is the profound analysis type which simulates nonlinear response of the existing structure within the accepted limitations and assumptions. Complete nonlinear mechanical properties of the materials have to be defined. Real accelerograms or artificial accelerograms are considered as dynamic input.

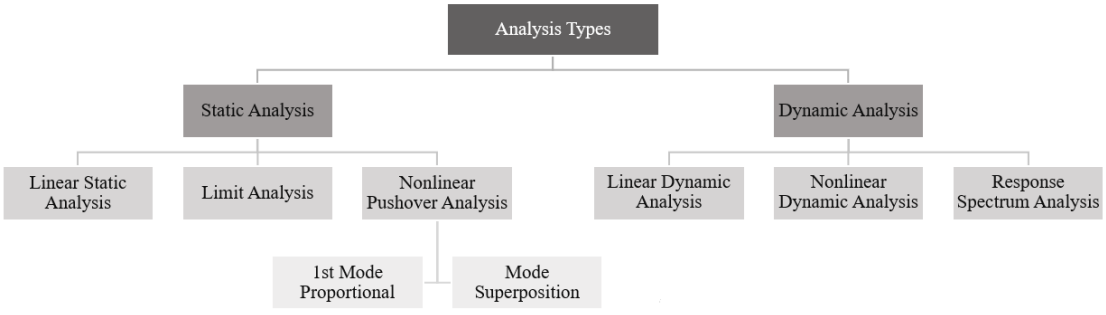

Figure 1.8. *Types of structural analysis for historical constructions, (adapted from TYDRYK, 2017)*

1.3 Previous Studies

Seismic performance and assessment of historical masonry structures has been a subject to various study. Several studies are explained briefly in this section.

Karanikoloudis and Lourenço (2018) investigated an ancient adobe structure called Church of Kuño Tumbo located in Peru. The structural assessment and seismic safety of the church was carried out by conducting nonlinear static and dynamic analysis, and macro-block limit analysis. Current condition of the church was put forward by site investigations in which sonic testing and damage mapping were involved. Additionally, the modal properties of the structure were executed by ambient vibration tests. Material properties were defined by considering the experimental tests, onsite testing and literature. In order to study the structure, finite element method was conducted, and macro-modeling approach was considered whereas the total strain rotating crack model was defined as constitutive material model. Finite element model was constructed by using solid elements in software Midas FX+ for DIANA. Two groups of numerical models were prepared. In the first group material properties were defined according to the literature review and the second group considers the in-site material tests. In each group, two different models were identified with respect to the presence of ties which are located in the transversal direction and connects the longitudinal parallel walls. In the modeling stage, soil-structure interaction was also considered by introducing translational springs in three directions. Moreover, the existing damage was modeled by using interface elements having linear elastic properties. However, the existing damage was only considered during the Eigenvalue analysis and it is stated that the undamaged model of the structure was taken into account for the structural analyses. The main objective is to construct a model which produces and verifies the existing damage and in aftermath, study the safety of the repaired structure. According to the eigenvalue analysis, it is found that the presence of tie elements changes the global behavior of the nave in the transverse direction by providing lateral restraint and confinement. In fact, numerical models without tie elements were considered only during the structural analyses. It is due to the fact that the presence of the ties does not allow uniform transversal behavior. The adopted pushover analysis considers lateral loading proportional to the mass of the structure applied in all directions. The results showed that the model defined according to in-situ material testing has higher lateral load capacity. The investigation was carried out by studying several load steps within the post-peak behavior and total principal strain

distribution relation with the existing damage pattern. For the nonlinear dynamic analyses, two artificial accelerograms were used compatible with the design response spectrum defined in Eurocode 8 produced by software LNEC-SPA and these dynamic inputs were applied in the principal horizontal directions. The results of the nonlinear dynamic analysis have high consistency with the damage observed in-situ and tensile crack patterns from the pushover analysis.

Ciocci, Sharma and Lourenço (2018) performed a study of seismic safety assessment of Ica Cathedral which is located in Peru. The cathedral experienced severe damage and total collapse of the components because of the recent earthquakes occurred in 2007 and 2009. The structure is constituted from timber substructure and masonry envelope. A linear analysis was performed for the timber substructure, which is constructed by SAP2000, and the compliance of the capacity with Eurocode 5 was studied. Two individual three-dimensional numerical models were prepared for the timber substructure and masonry envelope by using FX+ for DIANA. Linear elastic analysis was also performed for the numerical model of timber substructure. Finite element model of the masonry envelope was constructed by using solid elements and the model was calibrated according to the Operational Modal Analysis. Nonlinear static and dynamic analyses were performed for the masonry substructure and the complete model (combination of timber and masonry envelope). The nonlinear pushover analyses were carried out by considering mass proportional seismic loads. For the dynamic analyses, two artificial accelerograms generated regarding to the design spectrum defined in Eurocode 8 were used. The timber substructure was defined as linear elastic material whereas nonlinear material properties were assigned for the masonry substructure. The change in seismic response was studied by comparing the individual masonry envelope and complete model of the timber and masonry substructures. Introducing timber substructure to the masonry envelope increased the seismic capacity nearly 25% in both principal direction. A maximum value of 3% drift ratio was observed for the model with masonry envelope only. Additionally, total principal strain distributions were given, and similar damage pattern was observed with the critical cracking in-situ and cracks resulted by pushover analyses.

Kazaz and Kocaman (2018) investigated Erzurum Lala Paşa Mosque which is one of the cultural heritage located in Erzurum, Turkey. The seismic response of the mosque was studied by conducting finite element analysis. A representative numerical model was

prepared by using SolidWorks and analyzed in ANSYS APDL. Structural components were constructed by using solid elements. Material properties of the masonry were defined by conducting non-destructive test, namely Schmidt Hardness test. Additionally, modulus of elasticity and compressive strength of the masonry walls were defined according to the literature review. Willam-Warnke Model was assumed as constitutive material model. Eigenvalue analysis, nonlinear self-weight analysis and nonlinear dynamic analysis were performed. For dynamic analysis, a real accelerogram record from an earthquake occurred in Erzincan in 1992 was used. According to the results, lateral load capacity of the wall is based on axial force, boundary conditions and overturning behavior.

Silva (2013) studied seismic performance of Christchurch Catholic Basilica which which is one of the heritage constructions located in New Zealand. The structure experienced severe damage as a result of a set of earthquakes happened in 2011. A finite element model of the basilica was prepared by using macro-modeling approach. The numerical model was constructed by using TNO DIANA and nonlinear pushover analyses were conducted in order to perform seismic assessment of the basilica. Different types of numerical models were prepared considering different mesh generation, different types of materials and consideration of the existing damage. A set of beam, shell and solid elements were used, and nonlinear material properties were defined for masonry and concrete material. The representative model was calibrated according to the dynamic identification tests. Total strain fixed crack model was assumed for the nonlinear behaviour of the material. Softening of the tension and compression is given by exponential and parabolic stress-strain relation, respectively. Nonlinear pushover analyses were carried out in both principal directions. The capacity curves of the structure are given for several control points and the maximum lateral load capacity is 0.2g and 0.3g in transversal and longitudinal direction, respectively. It is noted that several in-plane and out-of-plane failure mechanisms were observed.

Mangia *et al.* (2016) performed nonlinear static analysis in order to investigate the nonlinear behavior of Elti Hatun Mosque which is located in Tunceli, Turkey. The finite element model of the mosque was prepared by using solid elements in DIANA software. The nonlinear property of the masonry elements was adopted from literature review and total strain rotation crack model was used as constitutive material model. Masonry elements were constructed by using macro modeling strategy. In the study, pushover

analysis was conducted proportional to the total mass of the mosque in the horizontal orthogonal directions. The maximum load capacity of the mosque is found as 0.65g and 0.32g in longitudinal and transversal directions, respectively.

Şeker *et al.* (2015) performed a study on the structural behavior of Lala Pasha Mosque located in Erzurum by means of linear static and dynamic analysis. 3D finite element model was defined by using ANSYS software and minaret of the mosque was disregarded during the finite element modelling. Material properties were assumed as linear elastic and mechanical properties of the material were chosen from the literature. Consequently, it is found that stresses resulted by static analysis are in acceptable range. However, dynamic analysis showed that high tensile stresses above the limit value were observed at the supports of the piers and corners of the windows. The most critical parts of the mosque were concluded as portico, supports of the main dome and corners of the window and door openings.

Dogangun *et al.* (2008) studied effect of minaret height on the seismic response. Three different minaret models having 20 m, 25 m and 30 m height were used. In all numerical models, structural material, geometry of the base of the minaret and transition zone on the minaret are the same. Moreover, stairs were modelled in the finite element model. Modulus of elasticity of uncracked section was used for the materials and linear elastic material was assigned. Higher mode effects were observed in the modal analysis. Regarding to dynamic analysis, inter-story drift ratio responses were compared with the TEC 2007 requirements which indicates that inter-story drift ratio should be less than 2%. The minaret model with 30 m height has inter-story drift ratio higher than 2%. Furthermore, maximum tensile stresses were compared with the limit values suggested in the literature and the results have been found that they exceed limit values. According to the study, longer minarets are subjected to more deformation comparing to the shorter ones and high stresses were concentrated at the base and transition zone of the minaret.

Şeker, Doğangün, and Çakır (2013) analyzed structural performance of the Kara Mustafa Pasha Mosque by means of finite element method. Structural assessment was performed under static and dynamic loading. Finite element model of the mosque was prepared by using solid elements and material properties of the structure is the same for all structural components except the dome. Finite element analysis was performed in ANSYS. Tensile and compressive stresses due to static loading are below the limit values and maximum displacement was reported at the top point of the dome. Mode

superposition method was used to perform dynamic analysis and the first thirty modes were considered. Portico and upper part of the entrance wall were subjected to high stresses. In addition, dynamic analysis in time domain was performed by conducting horizontal components of the İzmit Earthquake. Several conclusions were made regarding to the analysis. The mosque is safe under static loading and there are stress concentrations on the portico and upper part of the wall under dynamic loading. However, magnitude of these stresses is found as lower than the limit values.

Doğangün *et al.* (2006) presented damage and failure mechanisms on the minarets resulted by earthquake and wind loading. Furthermore, a case study of dynamic response of the 25 m height minaret of Rızvaniye Mosque was carried out. Finite element analysis was performed by using SAP2000. The walls, square-planned base and stairs of the minaret were modelled by using solid elements while shell elements were considered on the Ottoman cone and baluster of the balcony. Only one material property was assigned. Eigenvalue analysis was performed and frequency of the first mode of vibration was computed as 0.72 s. Considering the mode shape, square minaret stool is very rigid comparing to the polygonal body of the minaret and it is concluded that minaret stool provides fixed support to the polygonal body. During the dynamic analysis, North-South component of the Kocaeli Earthquake and West-East component of the Düzce Earthquake were acted in x direction. The minaret experienced tensile stresses higher than the limit values and these stresses concentrated on the transition zone, which is geometric form between square minaret stool and polygonal body. Maximum displacement at the top was observed as 0.13 m and 0.3 m due to Kocaeli and Düzce Earthquake ground motion, respectively. The minaret showed undesired response regarding to the analysis results and damage was observed.

Can, Kubin and Ünay (2012) examined historical masonry structure with an irregular geometric plan, namely Küçük Mustafa Pasha Bath, under static and dynamic loading. The finite element was made of shell elements and material properties of the components were admitted regarding to literature review and provisions. Same material properties were used for brick, dome and pendentives while different material type was assigned for stone walls. Macro model was assumed for the walls. Dynamic analyses were performed by defining G+EQx and G+EQy loadings. Maximum displacement was observed at the top point of the dome for both horizontal directions. The peak drift ratio was found to be less than 2% which is restrained by TEC 2007. Even though tensile stress

concentration was observed at the lower sections of the walls and corners of the openings, structural components of the building values of those stresses are within the limit values that are suggested for masonry structures by the code.

Almac *et al.* (2016) studied Macedonian Tower which is located in Edirne, Turkey and its origin dates back to Roman Empire. Experimental modal analysis was performed in order to identify the modal properties of the tower. Laser scanning, which provides 3D point cloud data, were employed to model geometric properties of the tower more accurately. The Finite element model was constructed in ABAQUS and only one material was defined. Material of the model was admitted as distributed homogenously and presents linear elastic property. Linear static and dynamic analysis were performed. In linear static analysis, stress was concentrated in the main entrance, but it is found that the magnitude of the stress does not represent any damage. Seismic response of the tower under earthquake excitation was investigated by means of spectrum analysis. As per TEC 2007, the response spectrum was defined for 10% probability of exceedance in 50 years-475 years return period. Within the framework of the earthquake scenario, historical masonry tower is over protected.

Ertuğrul (2015) studied the seismic performance of a Byzantine Basilica located in Cyprus. In the study, several non-destructive tests were carried out, namely rock hammer, ultrasonic pulse velocity, infrared thermography, ground penetrating radar test aiming at identifying the mechanical properties of the structure. Static analysis was performed for horizontal and vertical directions of the structure and dynamic analysis was conducted by response spectrum and time history analyses.

Cagnan (2012) investigated seismic performance of a historical masonry structure known as St. Nicholas Cathedral. The cathedral is situated in Cyprus and the history of the structure dates back to 1300s. During the Ottoman Empire, a minaret was added to the cathedral and transformed to a mosque. Calcarenite is the main construction material throughout the building. Several material tests were performed to identify the material properties of the main walls. In the study, three different 3D finite element models were prepared in SAP2000. Shell elements were used for structural components in the first two models. The only difference between the models is the inclusion of minaret and stairs to the second model to investigate the effect of the minaret on the seismic response of the structure. In the third model, the west peripheral wall and piers located in the building were modeled as solid elements. Environmental effects were also considered by defining

two different moduli of elasticity, tensile and compressive strengths. Nonlinear behavior was assigned to the construction materials. Analytical model was calibrated regarding to the conducted ambient vibration measurements. Modal analysis was performed for all cases and it is found that minaret and stairs do not contribute to the elastic response of the structure. Dynamic analysis was performed by means of response spectrum analysis and time history analysis by using six different records. First model was used for the dynamic analysis due to the highest mass participation ratio. Analytical results showed that the structure would experience high tensile stresses observed on the buttresses and several rehabilitation applications were recommended.

1.4 Scope of the Study

Within the light of presented state-of-art, Kütahya Kurşunlu Mosque, which is located in the seismic prone zone in Turkey, was studied in the present thesis. Case-based interventions were applied in terms of restoration and retrofitting works of the mosque. In the present study, current condition of the mosque and effectiveness of the adopted seismic retrofitting was discussed. The study was performed by using Finite Element Method. A three-dimensional finite element model of the mosque with seismic retrofitting and without retrofitting was prepared. Furthermore, dynamic properties of the current condition of the mosque was identified by performing Ambient Vibration Measurements and Operational Modal Analysis. In order to have representative structural scheme of the historical masonry mosque, numerical model was calibrated according to the Operational Modal Analysis results. Nonlinear properties of the masonry material were assumed according to the literature. Seismic performance of the historical masonry mosque was studied by conducting nonlinear static (pushover) analysis and nonlinear dynamic analysis in the time domain. Nonlinear pushover analysis was performed in all directions of the mosque, both in positive and negative. Nonlinear dynamic analysis was conducted in time domain by using three-real accelerograms recorded in Turkey. Two horizontal components of the earthquakes were applied as bi-directional time history analysis.

1.5 Outline of the Thesis

The present thesis is composed of seven chapters with the contents given briefly as follows;

Chapter 1: General overview of the conservation principles throughout centuries and reflection of built heritage on societies. Emphasizing the seismicity of Turkey and architectural heritage under seismic risk. Literature review on the seismic assessment of historical constructions and previous studies.

Chapter 2: Description of the historical content, location and main features of Kütahya Kurşunlu Mosque. Investigation of the damage observed in situ and presentation of adopted intervention and retrofitting techniques.

Chapter 3: Preparation of 3D finite element model for numerical analysis of non-retrofitted and retrofitted Kütahya Kurşunlu Mosque. Presentation of nonlinear properties of the materials and adopted constitutive law.

Chapter 4: Identification of the dynamic properties of the historical mosque by conducting ambient vibration measurements and operational modal analysis. Calibration of the finite element model regarding to the experimental modal analysis. Presentation of modal properties from experimental and numerical modal analysis.

Chapter 5: Presentation and comparison of the response from nonlinear pushover analysis. Generation of capacity curves for the mosque. Presentation and validation of numerical damage patterns.

Chapter 6: Selection of ground motions for nonlinear dynamic analysis. Presentation and comparison of response from nonlinear dynamic analysis for non-retrofitted and retrofitted models. Comparison of crack propagation due to retrofitting. Correlation of crack patterns between numerical and real behavior of the non-retrofitted case.

Chapter 7: A brief summary and conclusions are given, and further steps are recommended for future studies.

2. CASE STUDY: KÜTAHYA KURŞUNLU MOSQUE

As addressed previously, historical masonry structures are quite vulnerable under seismic actions, and it is crucial to examine the dynamic response of these structures and take necessary precautions before they experience total collapse or severe damage. Efficient and cost-effective strengthening and retrofitting techniques are required for protecting architectural heritage. Each ancient structure is an abstract being that has unique architectural, material and structural properties. Therefore, case-based solutions need to be developed for conservation, strengthening and retrofitting of each historical masonry structure. Within this framework, Kütahya Kurşunlu Mosque was investigated in the present study (Figure 2.1). Construction of Kütahya Kurşunlu Mosque dates back to 1377-1378. As per restitution report approved by Kütahya Regional Directorate of Conservation of Cultural Assets, it is noted that the mosque was constructed by using ruins of a building, in the late 1370s and it was undergone several conservation processes between the 13th and 19th centuries. Five different eras were identified with respect to adopted interventions on the historical mosque. Accordingly, the first period was defined as before the construction of the mosque in 1377-1378, the second period was from 1377/78 to 1520 or 1697/98, the third was between 16th / 17th century and 1950, from 1950 to 1975 is the 4th period of time and the fifth was identified between 1975 and 1990. In 2013, restoration works of the mosque was started again regarding to the architectural and structural concerns of the Directorate General of Foundations. Restoration and seismic retrofitting interventions are still in progress during this thesis. Repair work on the severe damage and steel girder retrofitting was completed. Afterwards, steel tensioning elements will be adopted along the load bearing walls in order to ensure safety for severe damage.

(a) North-East façade *(b) South façade*

Figure 2.1. *Kütahya Kurşunlu Mosque after interventions, January 2017*

2.1 Brief Description of the Mosque

Historical masonry mosque, namely Kütahya Kurşunlu mosque, is located in the southern part of central Kütahya province in Western Turkey (Figure 2.2). The mosque is situated in the residential area of the city and north, east and south of the building land surrounded by streets while a residential building is located in the western side of the mosque. In fact, Kütahya Kurşunlu Mosque is not attached with the residential building on the west façade so that the structure is isolated from the buildings in all directions. The mosque has rectangular plan with a length of 13 m and width of 9.3 m (Figure 2.3). The highest element of the mosque is the minaret with 28 m and it has rectangular minaret stool with a polygonal transition section to a circular body. The height of the load bearing walls and the top point of the dome is 7.8 m and 11 m, respectively (See Appendix 1). The construction material of the mosque is cut stone and brick. Load bearing walls were constructed as three-leaf masonry. The outer layer of the walls was made of cut stone whereas rubble stone was used for the inner layer and core of the load bearing walls. The dome, which was restrained by octagonal drum, the vaults, pendentives and octagonal drum was constructed by using brick. The minaret stool and circular body was constituted with cut stone and brick, respectively.

Figure 2.2. *Location of the historical mosque*

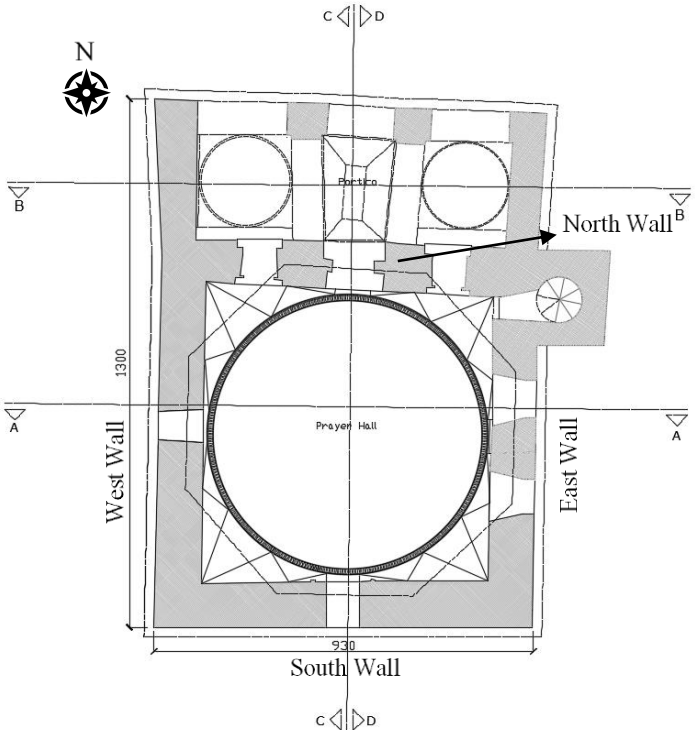

Figure 2.3. *Architectural plan of the mosque (in cm)*

Although the mosque is standing for centuries, it is obvious that a such structure experienced human origin and natural origin damage during its life span and today the current condition of the structure differs from its original design due to adopted interventions. In Figure 2.4, the condition of the Kütahya Kurşunlu Mosque before restoration and retrofitting works started in 2013 is shown. It is possible to say that the last conservation works was done without considering principle of minimum intervention (admitted by ICOMOS) and used without any respect to the heritage building. The plastering and blue wall painting was applied on the masonry walls and additional brick walls and rooms were added. Consequently, the heritage structure was far behind its cultural and historical legacy and it was almost impossible to identify as an ancient building due to its appearance.

(a) North-East façade (Http-8)

(b) South façade (Http-9)

Figure 2.4. *Kütahya Kurşunlu Mosque before intervention started in 2013*

The main objective of the present study is to investigate the seismic performance of the historical masonry mosque since the mosque is located in Kütahya province having high seismic activity in the region as shown in Figure 2.5. As per AFAD (2018), PGA value ranges from nearly 0.22g to 0.53g for Kütahya. Three earthquakes with high intensities happened in Kütahya province in March and April 1970 and May 2011 (Table 2.1). Accordingly, the structure has already experienced high seismic loads which were combined with long term effects on the structure. Therefore, current condition of the historical mosque and effectiveness of the retrofitting technique has to be studied to ensure safety for the future events.

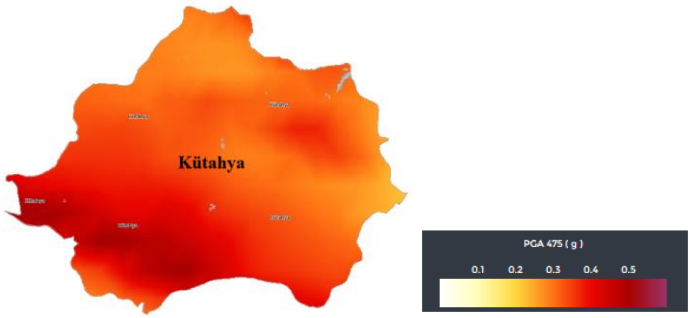

Figure 2.5. *Seismicity map of Kütahya province (AFAD, 2018)*

Table 2.1. *Past events with high intensity in Kütahya (KOERI; Yılmaz and Avşar, 2013)*

Date	Time (Local Time)	Location	Marcelli Intensity	Ms	Death Tolls	No. Damaged Buildings	Distance between the epicentre & the mosque (km)
28.03.1970	23:02	Gediz-Kütahya	IX	7.2	1086	19291	≈ 70
19.04.1970	15:29	Gediz-Kütahya	VIII	5.8		1360	≈ 70
19.05.2011	23:15	Simav-Kütahya	VI	5.9	3	1500	≈ 90

2.2 In-situ Observation and Repair Works

In-situ visual observations were carried out before any improvements implemented to the historical structure so as to understand the behavior. Observed damage patterns and adopted repair works are listed as follows;

i. At the time of in-situ inspection, restoration works were completed for the minaret. Therefore, no damage is reported on the minaret.

ii. Some of the wooden tie beams, which were used as tension tie to overcome tensile stresses developed on the arch elements, were removed. On the other hand, material decay is observed on the existing wooden tie beams (Figure 2.6).

(a) Removed wooden tie beam

(b) Material decay on the wooden tie beam

Figure 2.6. *Connected wooden tie beams on the arch elements of portico*

Scientific committee of the restoration and retrofitting of Kütahya Kurşunlu Mosque suggested to replace those tie beam elements with steel tie rods. It is worth to mention that these tie beam elements contribute to the response of the arch system. Especially, it is much important when the arch element is composed of masonry material because masonry is known with its low tensile capacity. A representative example of an arch system was conducted by using SAP2000. When an arch is affected under gravity loads only, the variation in moment, shear and axial load in the arch was displayed for two extreme support conditions in Figure 2.7. Change in arch response was investigated when the tie beams are provided to the system as shown in Figure 2.7.

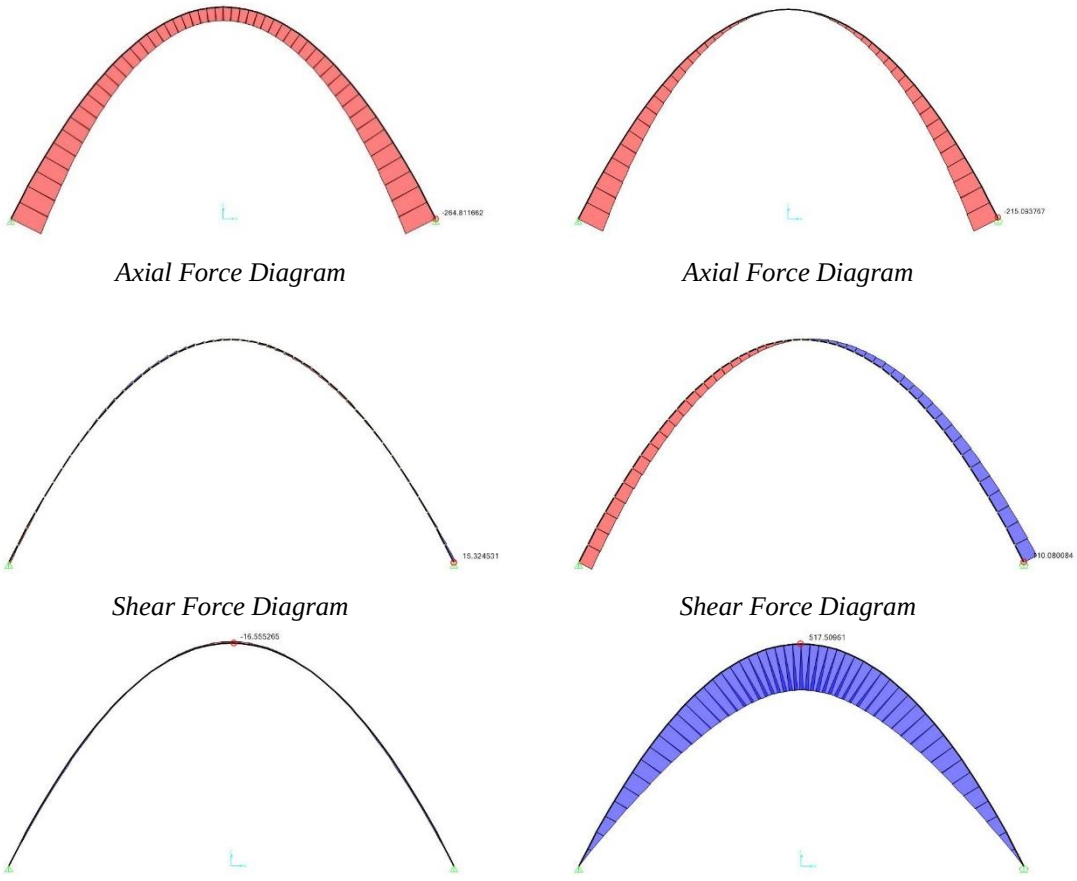

Axial Force Diagram *Axial Force Diagram*

Shear Force Diagram *Shear Force Diagram*

Moment Diagram *Moment Diagram*

(a) Pin-Pin support system (representing the presence of tie beams) *(b) Pin-Roller support system*

Figure 2.7. *Arch response on the different arch systems*

Single span arch system was modelled with two different support systems in order to represent existence of the tie beams. In the first case, Figure 2.7(a), the arch support system is expected to be pin-pin support when a tie beam is provided. On the other hand,

if the tie beam is absent or one of the arch supports do not fulfill translational constraint, the arch system becomes pin-roller support system as illustrated in Figure 2.7(b). Change in internal forces are presented and a significant difference is observed on the diagrams. The first arch system (pin-pin support) behaves as a thrust element. Shear force and bending moment demands are quite low which seem to be in the accepted limits for masonry. In contrast, the latter requires high tensile capacity to overcome high shear forces and bending moments which are unfavorable for masonry systems.

iii. Severe damage was observed on the South Wall. The crack initiated vertically from the top level of the wall façade and the width of the crack below the window opening was reached up to centimeters as shown in Figure 2.8(a). Additionally, loss of wooden beams located along the South Wall was reported. Wooden beams were in charge of compensating low tensile strength of the masonry elements in the load bearing wall cross sections (Figure 2.8(b)).

(a) Vertical cracks

(b) Material decay on the wooden beam located in the South Wall

Figure 2.8. *Visual observations on the South Wall*

iv. Vertical cracks, which are indicators of out-of-plane bending, were observed on the load bearing walls of the prayer hall. These cracks were initiated around the window openings. A decrease was observed in the crack size of the wall along the height (Figure 2.9).

(a) West Wall *(b) East façade*

Figure 2.9. *Vertical cracks*

v. On the West façade of the mosque, a distinct vertical crack was noted. The location of the vertical crack corresponds to the intersection of the two perpendicular walls, North and West Prayer Hall Walls, and West Portico Wall (outer leave, Figure 2.10(a)). The damage can be related with the lack of connection between structural elements. Another vertical crack was observed in the middle of the West Portico Wall (inner layer). The crack propagates along the height of the wall as given in Figure 2.10(b).

(a) Intersection of the Prayer Hall and Portico *(b) Crack on the West Portico Wall, inner layer*

Figure 2.10. *Damage observed on the West Wall*

vi. Extensive damage is reported not only at the intrados but also at the extrados when lead surface cover of the dome was removed. It is possible to say that the stability of the dome is debatable for the future events due to the existing crack propagation (Figure 2.11).

(a) Crack observed on the extrados

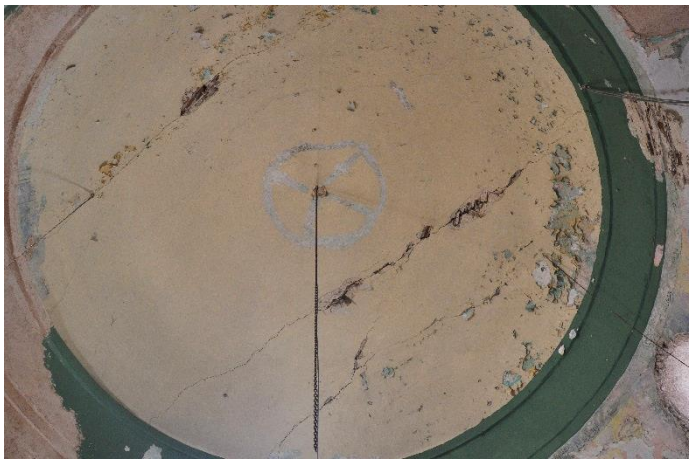

(b) Crack observed on the intrados

Figure 2.11. *Damage observed on the dome*

vii. Additionally, vertical cracks were noticed on the octagonal drum, both interior and exterior surfaces (Figure 2.12). It is believed that the structural walls exhibited out-of-plane movement so that opening of the octagonal drum, support of the dome, can be concluded. In fact, lack of integral behavior of the mosque contributed to the cracks observed on the octagonal drum which followed the crack propagation on the dome.

(a) Exterior crack on the octagonal drum

(b) Interior crack on the octagonal drum

Figure 2.12. *Damage observed on the octagonal drum*

In this context, different repair works were carried out. High strength grout injection was applied to the load bearing walls so as to provide integration between masonry units through the crack openings (Figure 2.13). The latter, the stitching technique was implemented to the damage observed on the dome. Stainless steel elements were used to prevent the widening of existing cracks (Figure 2.14).

(a) Before *(b) After*

Figure 2.13. *Grout injection*

Firstly, the old material beside the crack line at the extrados was removed. Stainless steel elements were fixed in the perpendicular direction of the crack line, after high strength grout injection was applied to the crack openings. Finally, steel elements were covered by masonry material which were compatible with the old material (Figure 2.14). In case of high tensile stresses, the stress distribution is expected on the masonry units with low tensile capacity where the steel elements are fixed. Additional cracks are expected due to change in high tensile stress distribution. Therefore, additional improvements are necessary in order to overcome the crack opening and ensure structural safety.

(a) Removing the old material *(b) Stainless steel elements along the crack*

Figure 2.14. *Application of stitching technique on the extrados*

(c) Stainless steel elements fixed along the crack

(e) Covering the steel elements

Figure 2.14 (continued) *Application of stitching technique on the extrados*

2.3 Steel Girder Retrofitting

The historical mosque was undergone restoration as mentioned previously, however seismic retrofitting is crucial to a such building with severe damage. Therefore, steel girder retrofitting was implemented to the ancient mosque by considering the principle of minimum interventions and reversibility. Within the scope of the present thesis, the effectiveness of the steel girder retrofitting was investigated by using numerical method. The configuration of the steel girder retrofitting is depicted in Figure 2.15. U-section stainless steel elements were used. Steel girder retrofitting was decided based on two issues; (i) damage observed in the dome, (ii) damage observed on the structural walls. In old construction techniques, wooden beam elements were used for masonry mosques at the bottom level of the dome in order to compensate tensile stresses. In this sense, old brick material was removed from the bottom level of the drum to check the condition of wooden beams. Hence, total loss of wooden beams was reported (Figure 2.16). The loss of those tension elements would probably have contributed to the damage observed. Therefore, single U160 stainless steel elements were placed not only at the base (empty)

section of the drum (Figure 2.17(a)) but also at the top of the drum walls (Figure 2.18). Each steel element was welded to each other (Figure 2.17(b)). Following that, space between steel elements and masonry material was filled with hydraulic lime-based mortar (Figure 2.17(c)). Finally, steel elements were covered by masonry units which are compatible with the old material (Figure 2.17(d)). It is expected that these elements provide additional support system to the dome and limit the expansion of existing cracks in case of any action.

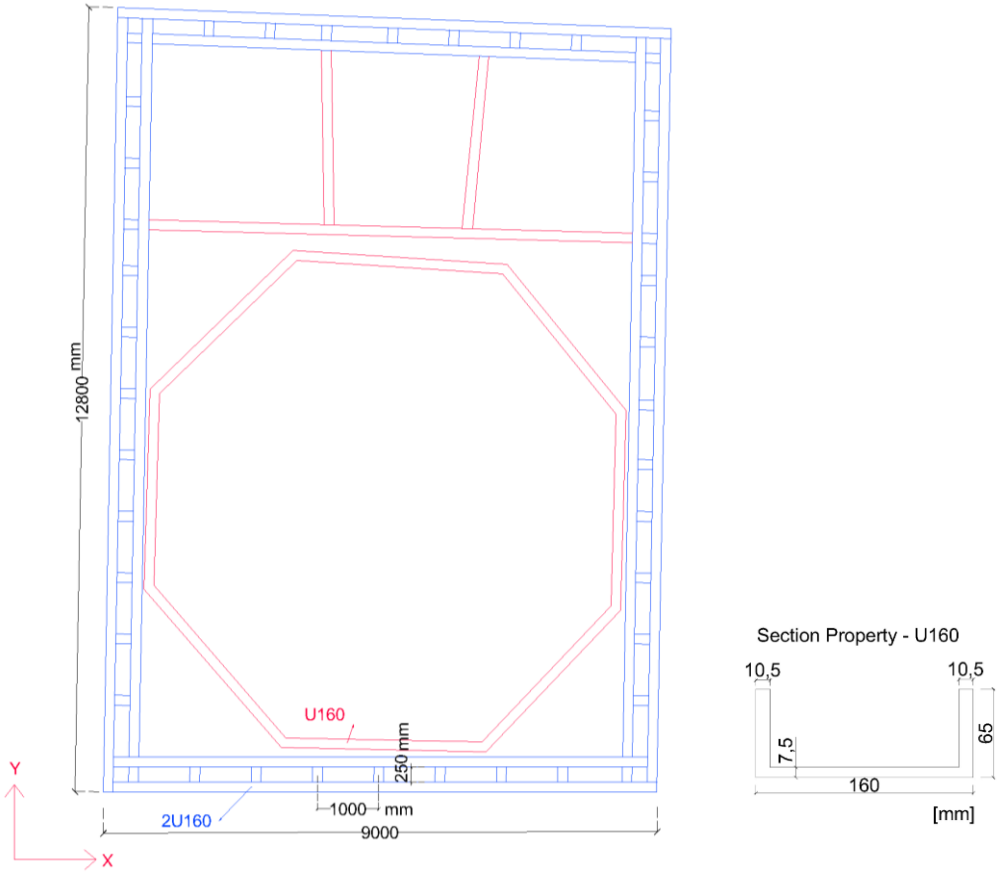

Figure 2.15. *Stainless steel girder application plan*

(a) Part of the octagonal drum

(b) Loss of wooden beam

Figure 2.16. *Loss of wooden beam elements at the bottom part of the drum*

(a) Steel girder at the bottom section of the drum

(b) Welded connection

(c) Hydraulic lime based mortar injection and covering

(d) Covering the girders with new masonry material

Figure 2.17. *Steel girder application steps*

Figure 2.18. *Single bar U160 steel girder at the top section of the drum and anchorage connection*

Furthermore, steel girder elements were anchored at the top level of the load bearing walls aiming at structural integrity of the mosque (Figure 2.19). On the North Wall, single U160 steel girders were anchored whereas double U160 steel elements were implemented to the rest of the load bearing walls (See Figure 2.15). All steel elements were fixed to the walls by using steel anchors after hydraulic lime-based injection was applied to the anchor holes. The connection between elements on the main prayer hall walls and portico walls was provided by single U160 steel elements (Figure 2.19(d)). Additionally, parallel

double steel profiles were connected to each other by using U160 in every 1 meter (Figure 2.19(a) and Figure 2.19(b)). Finally, steel girders were covered with horasan mortar and the dome, top surface of the walls and portico was coated with lead cover as shown in Figure 2.20.

(a) West Wall

(b) Portico Wall

(c) Connection of the members

(d) Connection between members

Figure 2.19. *Application of double steel girder (2U160) on the load bearing walls*

Figure 2.20. *Lead covering after steel girder retrofitting*

3. NUMERICAL MODELING

Seismic assessment of historical masonry structures can be carried out by considering different methods. Several approaches are available to model and analyze the structure depending on the level of complexity, time requirement to perform an assessment, sources that practitioner have and financial issues (Lourenço, 2001). Today, it is possible to perform structural analysis of historical masonry construction from simplified methods, which considers hand calculations, to very complex numerical computations, which adopt nonlinear equations (Lourenço, 2001).

TYDRYK (2017) defines different strategies to model masonry structures, such as simplified wall model, strut model, equivalent frame model and finite element model (Figure 3.1). Simplified wall model considers each structural wall independent from each other in a regular-planed building. Generally, it is assumed that the horizontal load is distributed by means of rigid diaphragm action. Vertical loads result normal stresses whereas seismic loads cause shear stresses in-plane direction of the walls. In case of eccentricity between mass center and rigidity center, torsional moment results additional shear forces on the walls which are not parallel to the horizontal loading (Figure 3.1(a)). Strut model is more common in modeling masonry infill walls in reinforced concrete buildings. However, TYDRYK (2017) also suggests this method for a masonry building which has horizontal and vertical lintels in its structural system (Figure 3.1(b)). Equivalent frame model considers 2D beam elements to represent structural system of the masonry buildings (Figure 3.1(c)). In finite element model (FEM), stress-strain relations and boundary conditions of the system play an important role when static and dynamic analyses are performed. FEM is constructed by using 1-dimensional (line), 2-dimensional (shell; linear or curved) and 3-dimensional (solid) elements which are shown in Figure 3.1(d). This method requires more time on modeling in order to have accurate numerical representative scheme of the real structure. Nevertheless, FEM is preferred by many researchers because it is the most profound strategy to perform seismic assessment of an existing masonry structure. However, there are major difficulties in the numerical modeling, particularly for ancient masonry structures. For instance, missing geometrical data, sophisticated architectural features and variability in mechanical properties of the material and the structural system are some of the drawbacks. Therefore, a set of major simplifications have to be admitted whereas Lourenço (2001) phrases ‘Prefer simplicity

over complexity'. Modeling of every detail of the structure should be avoided, and simplified versions of the geometry should be considered.

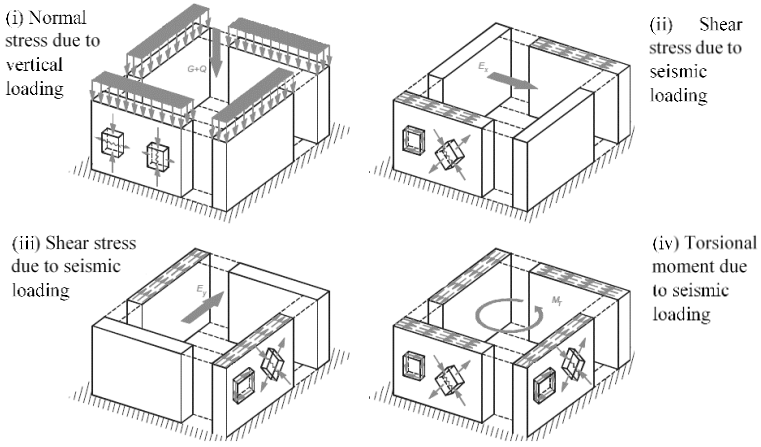

(a) Simplified wall model

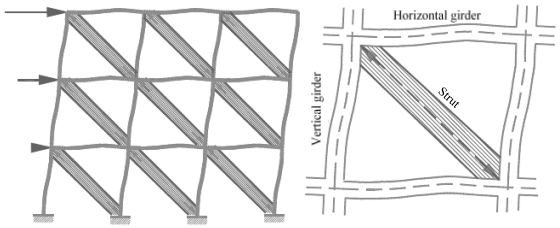

(b) Strut model

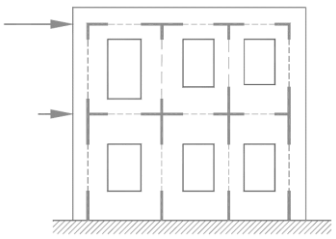

(c) Equivalent frame model

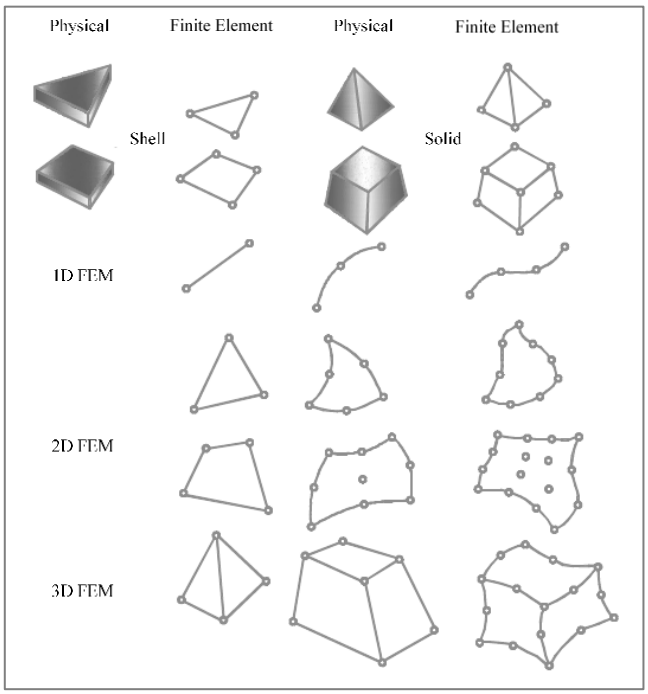

(d) Finite element model

Figure 3.1. *Modeling techniques defined in (TYDRYK, 2017)*

Masonry structures are represented in FEM by considering two different modeling approaches, namely micro-modeling and macro-modeling as shown in Figure 3.2 (Lourenço, 2002). Micro-modeling considers masonry units, mortar and unit-mortar interface separately (Figure 3.2(a)) or expanded units with an average interface by lumping interface and mortar (Figure 3.2(b)). Micro-models are applicable for a structural component when local behavior is required. Macro-models assume homogenous material property for continuous model as shown in Figure 3.2(c) (Lourenço, 2002).

In the present case study, FEM is selected as the analysis tool and a numerical model of the historical mosque was prepared using the software FX+ for DIANA. Homogenous material behavior was assumed for the masonry, therefore macro-modeling strategy was adopted. In this chapter, the finite element model generation of the Kütahya Kurşunlu Mosque is presented. Pre-processing stage is detailed with geometric description of the representative scheme, mesh generation of the numerical model, adopted constitutive material model, nonlinear material properties and boundary conditions.

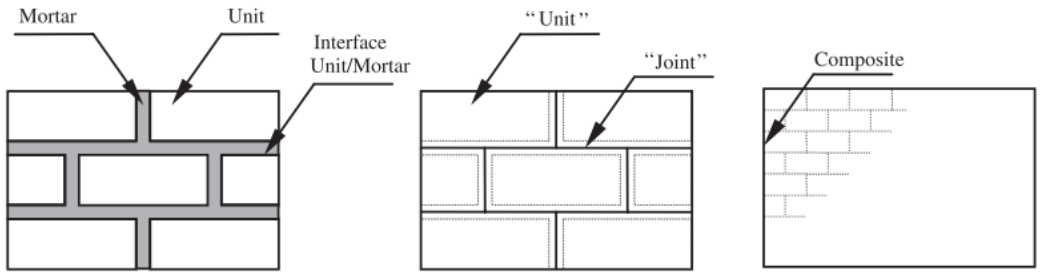

(a) Detailed micro-modeling *(b) Simplified micro-modeling* *(d) Macro-modeling*

Figure 3.2. *Modeling strategies for masonry structures (Lourenço, 2002)*

3.1 Generation of Finite Element Model

It is possible to adopt different finite element modeling strategies for masonry structures and there is no strict adherence to a specific modeling way. However, it is almost impossible to have an exact model of the existing structure. Even so, modeling techniques, which calculate accurate results, should be preferred to define the geometry and the numerical model.

3.1.1 Geometry description

In order to construct a representative model of a structure, different methodologies can be adopted, such as using additional 3D modeling software or selected finite element

analysis software itself. In the present study, geometric modeling of the mosque was carried out by using AutoCAD 2016. After 3D geometry was constructed, it was imported to FX+ for DIANA for the pre-processing stage. A simplified geometry of the mosque was considered in the modelling.

Within the scope of the study, the vast majority of the structural volume was modelled. Since no damage was reported on the minaret, it was not included in the numerical model. To represent retrofitted Kütahya Kurşunlu Mosque, structural scheme was constructed by using beam, shell and solid elements. A set of beam elements were used to represent the steel girder elements on the retrofitted mosque. Shell elements constituted the load bearing walls, arcades, piers, dome and drum. In addition, the simplified geometry considers the pendentives above the portico as slab which was also modelled by shell elements. The shell elements represent the middle plane of the structural elements. Therefore, a necessity for different arrangements from the reality was arisen. For instance, the connection between the dome, octagonal drum and load bearing walls were provided by pendentives which results different arrangement of middle planes of the components in reality (Figure 3.3). However, the numerical model assumes that the octagonal drum and walls were located in the same middle plane (Figure 3.3(b)). A set of solid elements were used to model pendentives instead of shell elements. The pendentives have volume which is difficult to be simplified and be representative in terms of stiffness by using shell elements (Figure 3.4). Moreover, the location of the steel girder elements differ from the reality due to the limitations of the shell elements adopted for the walls in the numerical model (See Figure 2.15 and Figure 3.5).

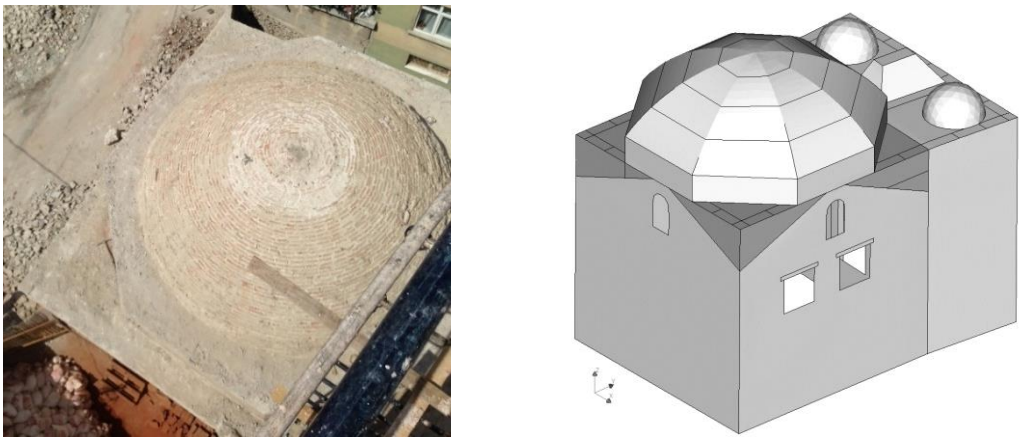

(a) In-situ *(b) 3D geometry model*

Figure 3.3. *Configuration of the structural components*

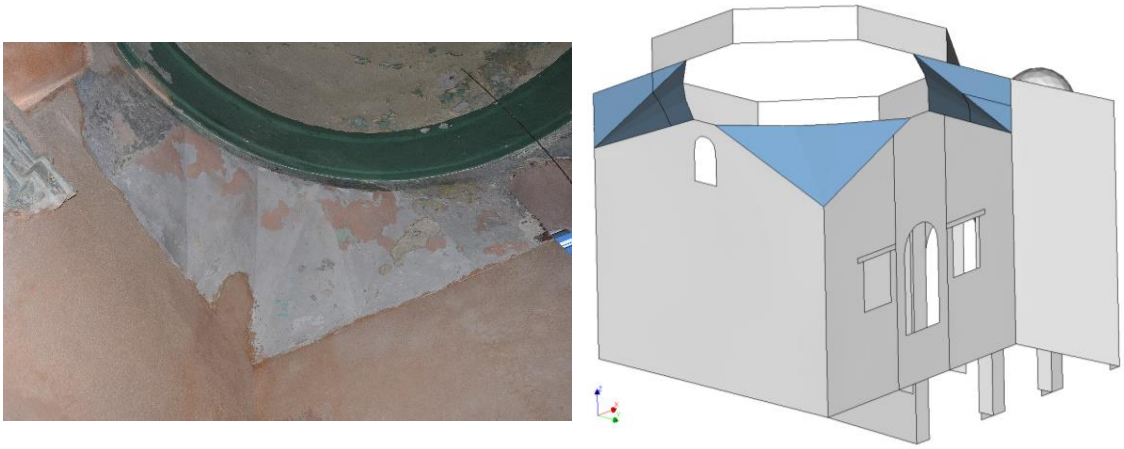

(a) Pendentive *(b) Solid element model of the pendentives*

Figure 3.4. *Geometry simplification of the pendentives*

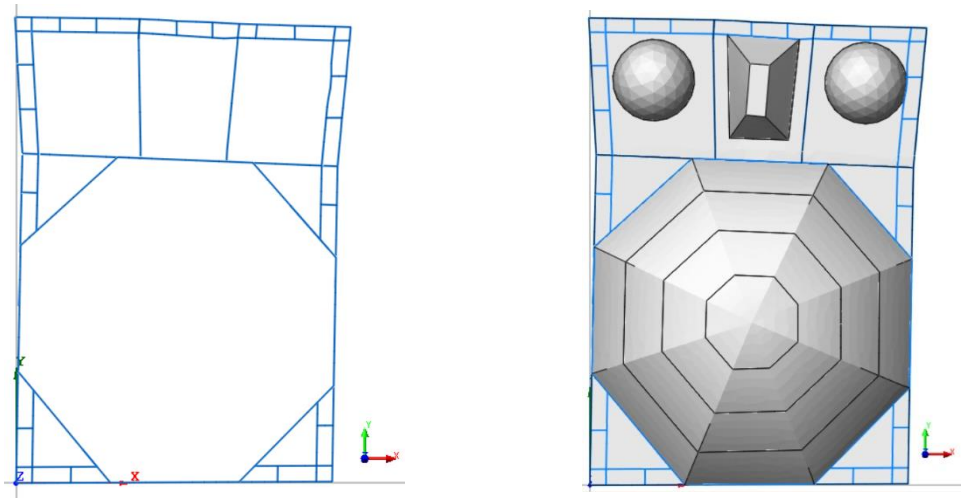

(a) Top view

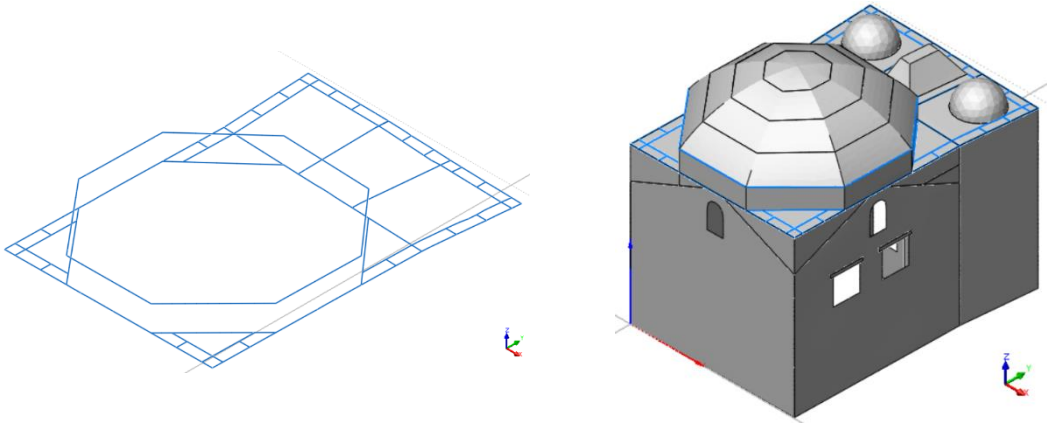

(b) Side view

Figure 3.5. *Steel girder configuration*

In the numerical model of the mosque, door and window openings were also considered. Additional element set was introduced above the square-shaped window openings and were modeled as linear elastic materials (See Figure 3.6). The main reason of such consideration is based on Lourenço *et al.* (2007) where they indicated that the large openings with flat headings result high tensile stress concentrations, which are not realistic, under self-weight loading. In order to have better representation, the geometry of the large opening is changed as shown in Figure 3.7 and a considerable reduction in the tensile stress in the reshaped area is concluded.

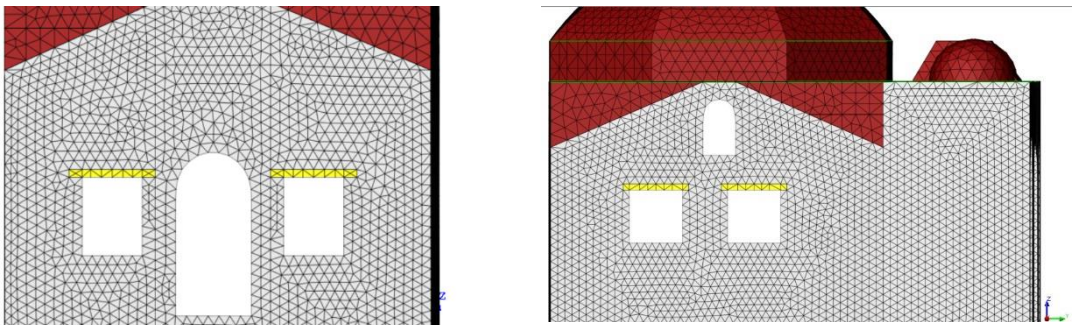

(a) North façade *(b) East façade*

Figure 3.6. *Adopted linear elastic timber elements (colored as yellow)*

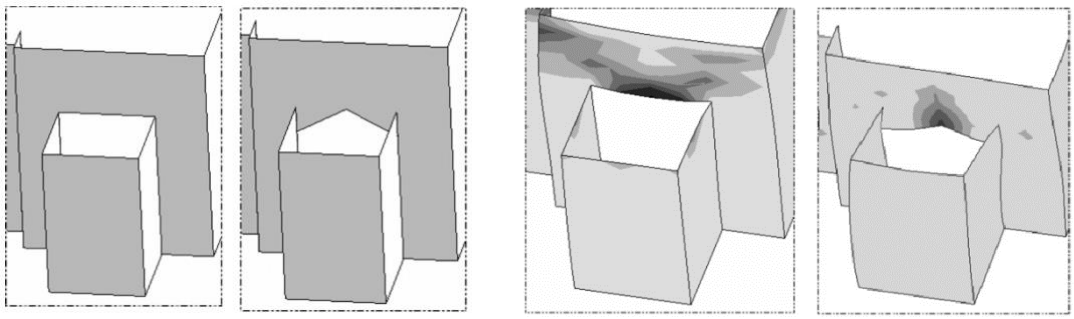

(a) Geometric description *(b) Tensile stress concentration*

Figure 3.7. *Adopted corrections on the geometry of the large openings (Lourenço et al., 2007)*

At last, the geometric description of the numerical model was completed by defining the cross-section and thickness of the beam and shell elements, respectively. In contrast, solid elements already provide geometric information due to its volumetric feature. The cross-section of the beam elements is already given in Figure 2.15 and the thickness of the shell elements is provided in Table 3.1. Additionally, adopted material properties for the shell elements are given in Table 3.1 and Figure 3.8 depicts different types of materials defined for all types of element sets on the numerical model. It is

important to mention that different thickness values were defined for the dome as different layers to have better representation of the geometry. Besides, a constant thickness was defined for the slab above the portico as 600 mm in order to prevent high deformation due to bending.

Table 3.1. *Physical properties of the shell elements*

Elements	Thickness (mm)	Material
South wall	1000	Cut stone
East wall	1000	Cut stone
West wall	1000	Cut stone
North wall	1200	Cut stone
Dome_0.5m	500	Brick
Dome_0.4m	400	Brick
Dome_0.3m	300	Brick
Dome_0.2m	200	Brick
Drum	800	Brick
Portico walls	1000	Cut Stone
Interior west arcade	700	Cut Stone
Interior east arcade	700	Cut Stone
Exterior arcades	800	Cut Stone
Piers	900	Cut Stone
East Lintel	1000	Timber
West Lintel	1200	Timber
Vaults	200	Brick
Portico Slab	600	Brick

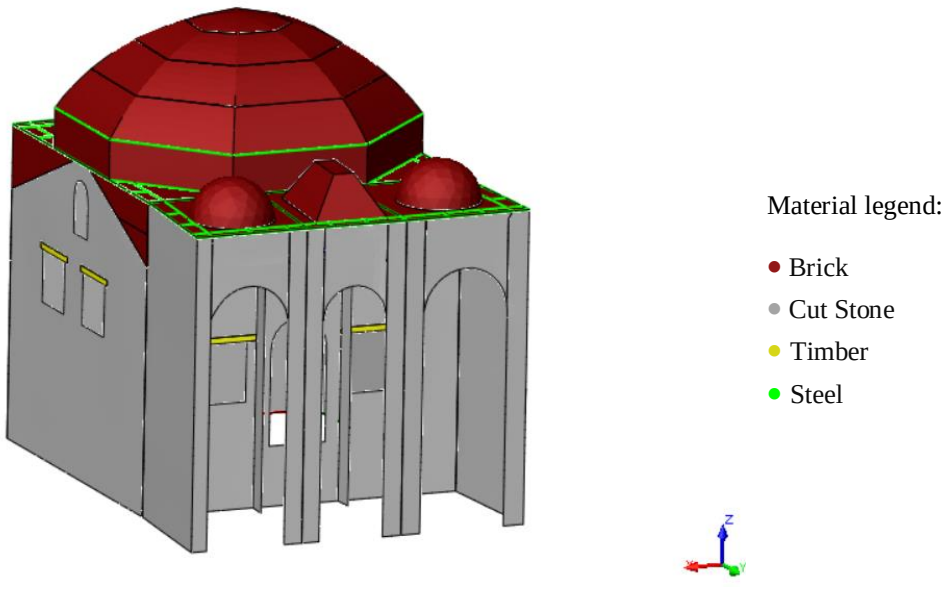

Figure 3.8. *Identification of the different materials*

As already stated, masonry material was modeled by considering macro-modeling approach which means that homogeneous and isotropic material behavior was admitted in the present work. Elastic material parameters of the Mosque are given in Table 3.2. The Young's Modulus for the brick and cut stone are given according to the calibration process carried out on the finite element model which is explained in detail in Section 4.

Table 3.2. *Linear elastic properties of the materials*

Material	γ (t/m3)	E (Mpa)	υ (Poisson ratio)
Cut Stone	2.1	1500*	0.2
Brick	2	2500*	0.2
Timber	0.7	11000	0.3
Steel	7.85	235000	0.3

*Calibrated parameters

3.1.2 Mesh generation

The adopted structural element types are presented in this section. Beam, shell and solid elements were selected from DIANA's library as L13BE, T15SH and TE12L, respectively. The beam element type is a two-node three-dimensional beam which has six degrees-of-freedom (DOF) per each node, namely three translations and three rotations as shown in Figure 3.9 and an additional variable in elongation Δu_x along the member which makes thirteen degrees-of-freedom in total. The formulation of the adopted beam element considers Bernoulli Theory in which the cross-section remains plane and perpendicular to the slope of the beam axis. L13BE is Class-II element which is compatible to perform linear and geometric and physical nonlinear analysis (TNO DIANA, 2017).

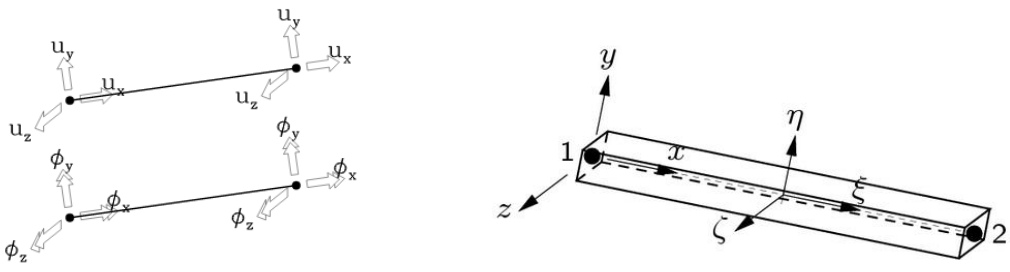

(a) DOF's per each node *(b) Straight 3D beam element*

Figure 3.9. *The beam element L13BE, with a total thirteen degree-of-freedom (TNO DIANA, 2017)*

For shell elements, a three-node triangular isoparametric curve elements were used (Figure 3.10). The shell elements have five DOF's per each node and the formulation of the element is based on linear interpolation (TNO DIANA, 2017). For solid elements, four-node and three side isoparametric solid tetrahedron elements were adopted. Solid elements have three translational degrees of freedom per node as shown in Figure 3.11. Mesh generation was performed by an automatic meshing strategy which uses triangular elements. The size of the mesh elements was adopted as 200 mm for the load bearing walls and arcades in order to mitigate convergence problems during the nonlinear analysis. In fact, mesh size and mesh distortions cause non-convergence. More coarse mesh size of 300 mm was conducted for the dome, drum, pendentives and vaults. Finally, the numerical model of the retrofitted mosque was constructed having 27,250 elements and 12,892 nodes in which 428 are beam elements, 22,987 are triangular shell elements and 3,844 are tetrahedral solid elements. There are 74,294 degrees of freedom in total.

(a) DOF's per each node *(b) Triangular curved shell element (TNO DIANA, 2017)*

Figure 3.10. *The shell element T15SH, with a total fifteen degrees-of-freedom*

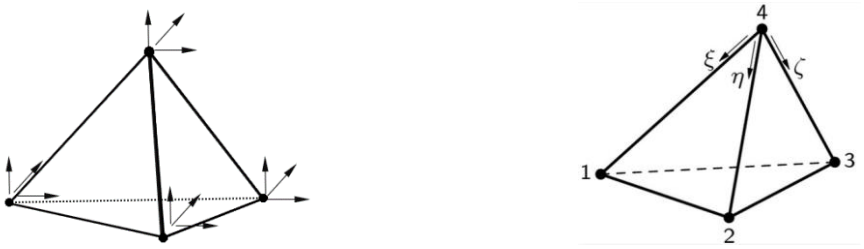

(a) DOF's per each node *(b) Tetrahedron solid element (TNO DIANA, 2017)*

Figure 3.11. *The solid element TE12L, with a total twelve degrees-of-freedom*

3.1.3 Boundary conditions

The final step of the numerical modeling corresponds to the defining of the boundary conditions of the system. Since there is no experimental soil test available, the foundation of the system was assumed as fully fixed. All degrees of freedom at the base of the structural components were restrained as shown in Figure 3.12.

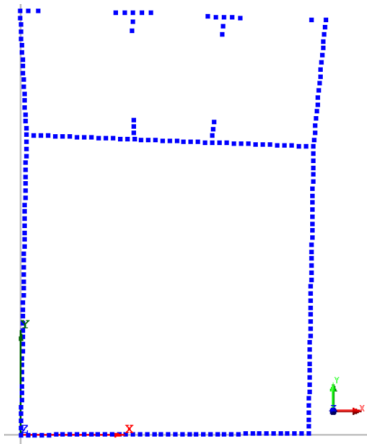

Figure 3.12. *Top view of boundary constrains at the supports*

3.2 Constitutive Material Model and Nonlinear Material Properties

Nonlinear behavior is provided by constitutive material models in the finite element method. In the present study, physical nonlinear behavior was defined by the total strain fixed crack model approach which is provided in DIANA. This constitutive material model allows nonlinear response for tensile, compressive and shear behavior in a finite element model. Within this scope, a stress-strain relation for tensile, compressive and shear behavior is defined and presented in Figure 3.13. The tensile behavior of the masonry is defined by adopting exponential stress-strain relation whereas the compressive behavior is adopted as presenting parabolic hardening and softening relation (Figure 3.13(a) and Figure 3.13(b)).

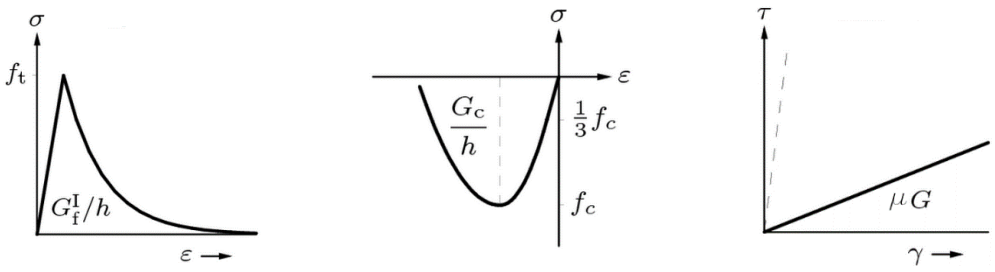

(a) Tension *(b) Compression* *(c) Shear*

Figure 3.13. *Adopted behavior for masonry materials*

Both tension and compression softening curves are based on fracture energy and its relationship with the crack bandwidth (h) of the element. The crack bandwidth is related with the area of the element and computed as follows (TNO DIANA, 2017):

$$h = \sqrt{A} \tag{3.1}$$

The total strain fixed crack model requires the modeling of shear behavior. The shear behavior is represented as it has linear stress-strain relationship (See Figure 3.13(c)). When the cracking is observed, the shear stiffness (G) is reduced by shear retention factor (μ) according to relationship given in Eq. 3.2 (TNO DIANA, 2017). The shear retention factor ranges from zero to one and, therefore, the default value of 0.01 is considered in the present study.

$$G^{Cr} = \mu . G \tag{3.2}$$

After adopting the material behavior, nonlinear material properties of the masonry material, namely cut stone and brick, has to be defined. However, no experimental material test was carried out in order to characterize the nonlinear mechanical properties of the masonry material used in the Mosque. Therefore, literature recommendations were taken into account. Compressive strength was decided according to the Italian Code 2009 recommendations. In the Italian Code, densities and reference mechanical properties are suggested for different types of masonry with poor mortar as given in Table 3.3. As already stated, modulus of elasticities of masonry materials were obtained from calibration process and they are in a good agreement with the recommended values by the Italian Code 2009. In the Italian Code (2009), compressive strength, which corresponds to calibrated Young's Modulus presented in Table 3.2, for cut stone masonry is suggested within the range of 2.6 MPa – 3.8 MPa while the range varies from 6 MPa to 8 MPa for masonry of squared stone blocks (Table 3.3). Moreover, Tomaževič (1999) recommends a range of tensile strength values for existing stone-masonry and brick masonry according to different research studies. Therefore, a value of 0.1 MPa was admitted for the tensile strength of both materials, cut stone and brick masonry. Next, the fracture energy of the masonry is defined. For the tensile fracture energy of masonry, a value of 0.012 N/mm is recommended (Angelillo, Lourenço, and Milani, 2014). For the compressive fracture energy (G_c), an average ductility index in compression (ratio between fracture energy and strength) is defined and different limit values are obtained from Model Code 90 (CEB-FIP, 1993) for different range of compressive strengths. A value of 1.6 mm is recommended for the ductility index in compression in which f_c values lower than 12 N/mm^2 (Angelillo, Lourenço, and Milani, 2014). Therefore, the relation given in Eq. 3.3 was assumed to estimate the compressive fracture energy in the present

study. Finally, the adopted nonlinear material properties for masonry and steel are summarized and presented in Table 3.3 and Figure 3.14.

$$G_c = 1.6 \times f_c \qquad for\ f_c < 12\ MPa \tag{3.3}$$

Table 3.3. *Densities and reference mechanical properties of different types of coarse masonry with poor mortar (Angelillo, Lourenço, and Milani, 2014; translated from Italian Code, 2009)*

Masonry Type	$\mathbf{f_c}\left(\frac{\mathbf{N}}{\mathbf{mm^2}}\right)$	$\boldsymbol{\tau_s}\left(\frac{\mathbf{N}}{\mathbf{mm^2}}\right)$	$\mathbf{E}\left(\frac{\mathbf{N}}{\mathbf{mm^2}}\right)$	$\gamma\left(\frac{\mathbf{Kg}}{\mathbf{m^3}}\right)$
Disarranged masonry of cobbles/boulders	1.0-1.8	0.020-0.032	690-1050	1900
Masonry of roughhewed stones	2.0-3.0	0.035-0.051	1020-1440	2000
Masonry of cut stones	2.6-3.8	0.056-0.074	1500-1980	2100
Masonry of soft stones	1.4-2.4	0.028-0.042	900-1260	1600
Masonry of squared stone blocks	6.0-8.0	0.090-0.120	2400-3200	2200
Brickwork of solid bloks and lime mortar	2.4-4.0	0.060-0.092	1200-1800	1800
Brickwork of semisolid blocks and cem. mortar	5.0-8.0	0.240-0.320	3500-5600	1500
Brickwork of air bricks (45 %)	4.0-6.0	0.300-0.400	3600-5400	1200
Brickwork of air bricks (<45 %)	3.0-4.0	0.100-0.130	2700-3600	1100
Masonry of concrete air-blocks (45-65 %)	3.0-4.4	0.180-0.240	2400-3520	1400
Masonry of concrete air-blocks (<45 %)	1.5-2.0	0.095-0.125	1200-1600	1200

Table 3.4. *Nonlinear properties of the materials*

Material	Compressive strength (f_c) [MPa]	Tensile strength (f_t) [MPa]	Compressive fracture energy (G_c) [N/mm]	Tensile fracture energy (G_t) [N/mm]
Cut stone	2.4	0.1	4.16	0.012
Brick	6	0.1	9.6	0.012

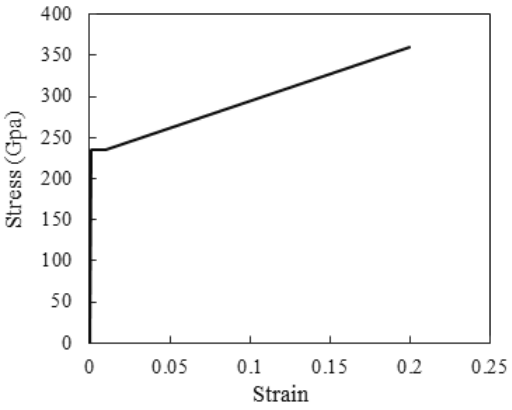

Figure 3.14. *Nonlinear material property of the adopted steel*

4. IDENTIFICATION OF MODAL PARAMETERS

Creating a representative numerical model for an ancient structure is a challenging task. Particular attention should be paid while working with historical structures. Geometrical features, material properties and boundary conditions of the real structure should be studied. According to the conservation and preservation principles, original structure shall be respected, and minimum interventions shall be applied (ICOMOS, 1964). Therefore, structural diagnosis should be performed within this framework. In this sense, non-destructive tests are preferred to identify existing properties and conditions of the structure. There are several experimental methods which are used to identify local or global properties of these structures. Experimental modal identification tests are one of the most common and effective methods that are used to identify dynamic properties of the existing structure in a more global basis. This method has an extensive application among the engineering fields, such as mechanical engineering, aerospace engineering and structural engineering (Farrar and Worden, 2007). In the early 1980s, application of the experimental modal analysis tests has been started in the civil engineering community (Farrar and Worden, 2007). Modal testing is defined as "the process involved in testing components or structures with the objective of obtaining a mathematical description of their dynamic or vibration behavior (Ewins, 2000) ". These experimental outputs are generally used for mathematical model calibration purposes, structural health monitoring by comparing several experimental tests, damage detection and so on.

Numerous studies have been done by using experimental modal identification tests on the historical structures. Gentile and Saisi (2007) performed ambient vibration measurements to identify modal responses on a masonry tower. By using ambient-vibration based investigations, numerical model has been updated with a good correlation and five vibration modes of the tower have been identified. Aguilar *et al.* (2012) has performed Operational Modal Analysis (OMA) tests on a Peruvian Historical Building and first two translational modes and subsequent seven local modes of the building have been identified clearly. Also, different modal identification methodologies have been used to characterize the modal properties of the building in the study. Nohutcu *et al.* (2015) has conducted Operational Modal Analysis to calibrate representative numerical model of a historical mosque. The average differences between frequencies of the first 5 vibration modes that have been found by experimental test and numerical analysis are

less than 1%. Sevim *et al.* (2011) have applied experimental modal testing to a historical masonry arch bridge in order to calibrate finite element model and perform nonlinear seismic performance by using calibrated numerical model. Frequencies of 4 modes have been correlated with up to 2% error. Lourenço *et al.* (2012) has performed a study of seismic performance and safety level of masonry ruins. Modal testing has been carried by using environmental noise as excitation source in order to update finite element model and have a representative structural scheme. Accordingly, a methodology based on operational modal analysis is feasible and effective to identify damage on masonry-like structures rapidly (Ramos *et al.*, 2010).

Experimental modal analysis can be performed by using two different techniques namely the Input-Output and the Output-Only techniques. In the Input-Output technique, a set of Frequency Response Functions (FRFs) is estimated by relating an applied force to the corresponding response at several points along the structure. Different types of equipment are used such as impulse hammer, impulse excitation device, electrodynamic shaker and eccentric mass vibrator. The main drawback of performing forced vibration tests is the difficulty to excite the structure with enough energy and control excitation on the structures to estimate modes of vibration in a low range of frequency (Cunha and Caetano, 2005). The Output-Only methods are based on considering ambient vibrations as source of excitation. The response of the structure resulted by any activity in the environment is measured. However, contribution of noise signals from undesired source is also included to the response which means the measurements represent modal contribution of the ambient forces and the structural system. Therefore, identification methods must have the ability to separate ambient influence from the structural response (Ramos, Aguilar and Lourenço, 2010). Doebling, Farrar and Cornwell (1997) states that interest in application of ambient excitation on civil engineering structures has been started in the late 1990s.

In this thesis, Output-Only technique, which is also known as Operational Modal Analysis, was applied to identify dynamic characteristics of the historical mosque. Operational Modal Analysis is one of the main steps to assess the condition of the structure (Gentile and Saisi, 2007). Dynamic-based assessment includes theoretical and experimental modal analysis as shown in Figure 4.1.

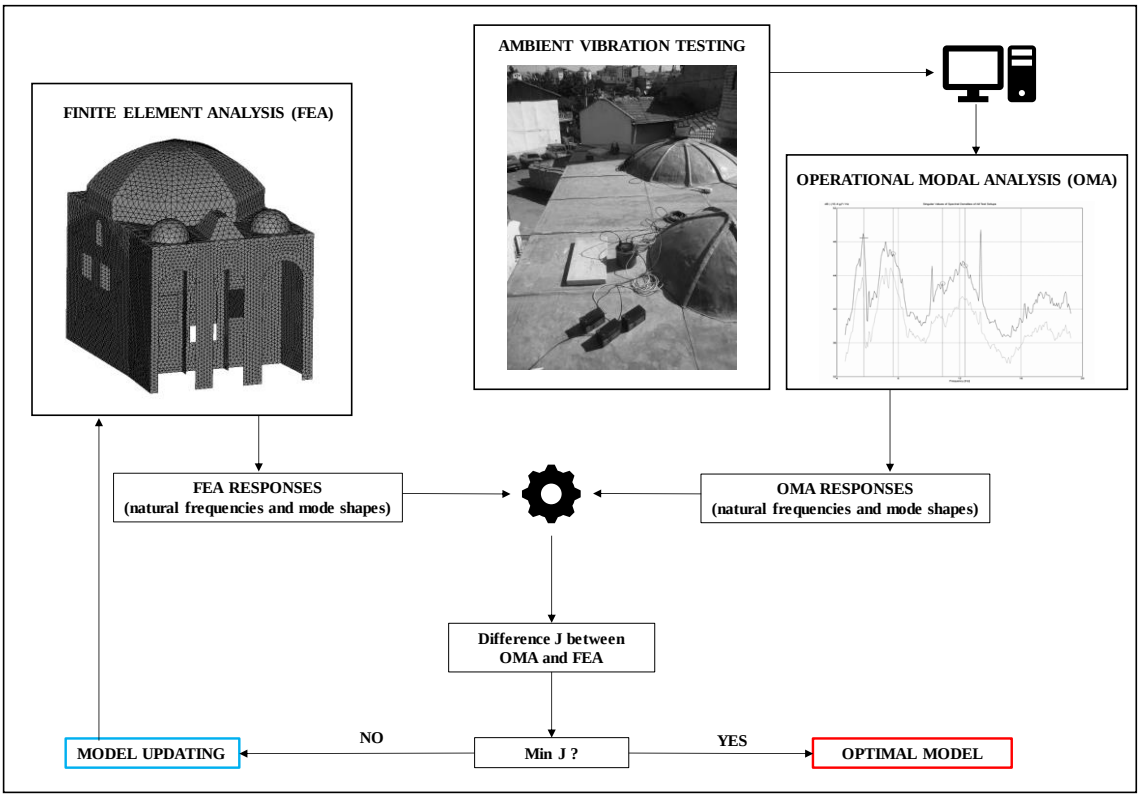

Figure 4.1. *Dynamic-based assessment of the structure, (adapted from Gentile and Saisi, 2007)*

In Figure 4.1, experimental modal analysis is carried by using natural vibrations as a source of excitation. Experimental results are used to perform Operational Modal Analysis by different methodologies and following that experimental modal parameters are extracted. After defining a preliminary finite element model of the structure, dynamic response of the numerical model is compared with the experimental results. Difference between Operational Modal Analysis and Finite Element Analysis is defined as "J" which can be calculated regarding to trial and error or parametric approaches. Uncertain structural parameters of the structure are identified by minimizing the difference between theoretical and experimental modal analysis.

4.1 Ambient Vibration Measurements

Ambient vibration test was performed on the historical Kurşunlu Mosque aiming at characterizing the modal characteristics of the mosque in the elastic range. Number of accelerometers was limited and only two accelerometers were available. For this reason, reference-based ambient vibration test was conducted. One of the accelerometer was fixed to a certain point, which was named as reference station, while the other

accelerometer was placed to 7 different locations on the mosque. In total, there are 8 stations, including reference station. Reference station was operated during the measurement while approximately 20 minutes spend at each station. The test was performed considering seven measurement setups. Location of each station on the Mosque and test equipment during the real application are shown in Figure 4.2 and Figure 4.3, respectively. Locations of the stations was decided regarding to the modal response of the preliminary numerical model. The selected points seem to be the most convenient locations based on identifying in-plane and out-of-plane movement of the components.

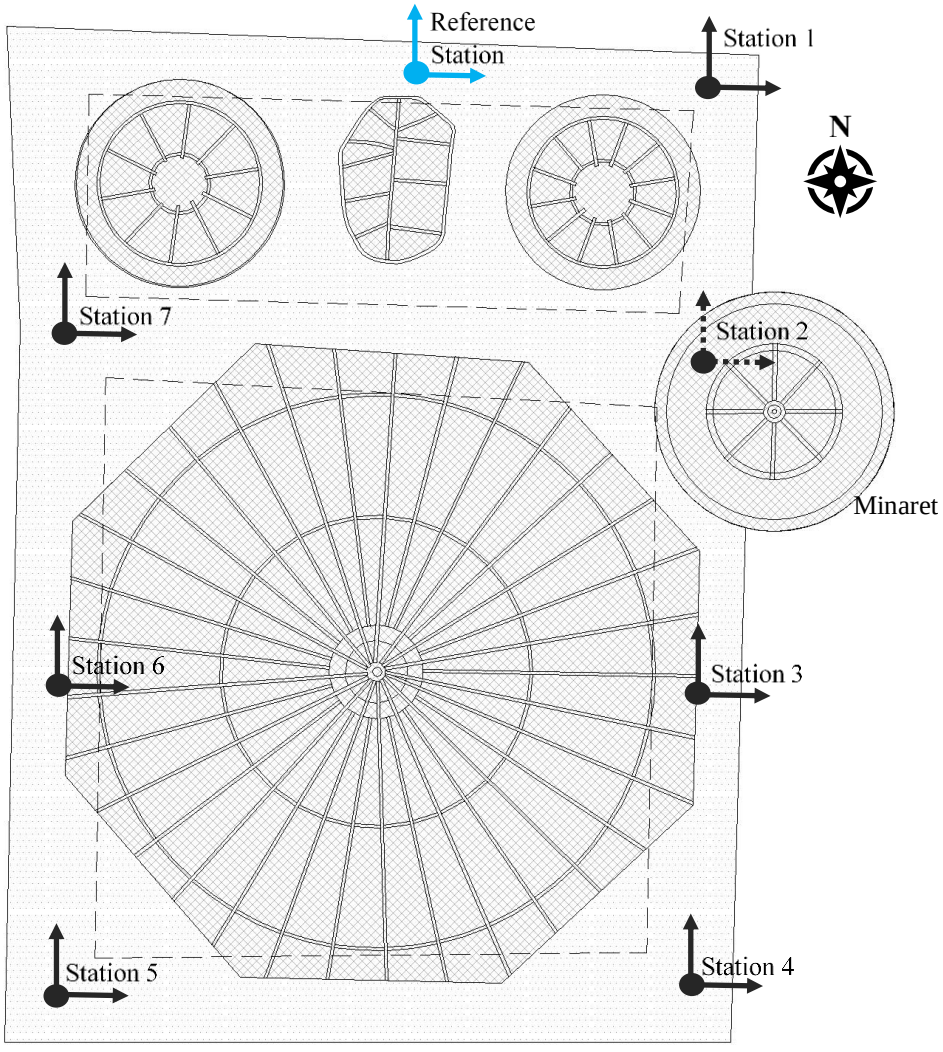

Figure 4.2. *Station layout and sensor directions*

Figure 4.3. *Test equipment; Left: Base station and 1st station, Right top: 4th station, Right bottom: accelerometer at the base station*

In order to perform ambient vibration tests, two digital triaxial accelerometers, namely Güralp 5TCDE, were used. The accelerometers have a frequency range of DC-100 Hz with sensitivity range from ±0.1 to ±4.0g and 10 V/g of resolution. Additionally, a data acquisition system with 24 bits resolution was used together.

4.2 Operational Modal Analysis

Operational Modal Analysis was performed by processing the Output-Only modal identification data obtained from ambient vibration test using ARTeMIS Modal software. The modal identification process was carried out by using two different signal processing methodologies namely Enhanced Frequency Domain Decomposition (EFDD) and the Stochastic Subspace Identification (SSI-data) methods. EFDD is defined as non-parametric which is mostly developed in frequency domain while SSI-data is parametric method that is originated in the time domain. Frequency domain methods are known as having very limited frequency resolution resulting from Fast Fourier Transform (FFT). Therefore, this method identifies close frequency values with limited precision. Parametric methods are robust and provide high frequency resolution on modal parameter

estimation due to the time-series processing (Ramos, 2007). It is important to mention that none of these methods are recommended one to another because the reliability of the results depend on the environmental noise, structural components, quality of measurement of the system and experience of the experimental campaign (Aguilar *et al.*, 2012). However, Ramos, Aguilar and Lourenço (2010) state that results of the non-parametric methods depend on the quality of the environmental noise and this drawback can be overcome by using parametric methods. Within this context, both methods were performed and compared with each other by calculating Modal Assurance Criterion (MAC). The process of the EFDD and SSI methods are shown in Figure 4.4 and Figure 4.5, respectively. First 4 modes of vibrations were identified. The frequency domain results (Figure 4.4) show that there are several sharp peaks within the range of 4 Hz- 15 Hz. However, only circled peaks were selected as modes of vibrations. The main reason is that when the other peaks have been selected, the response is very local that only such points, which sensors were located, vibrate. This is due to the fact that undesired source of vibrations might have high influence on the results.

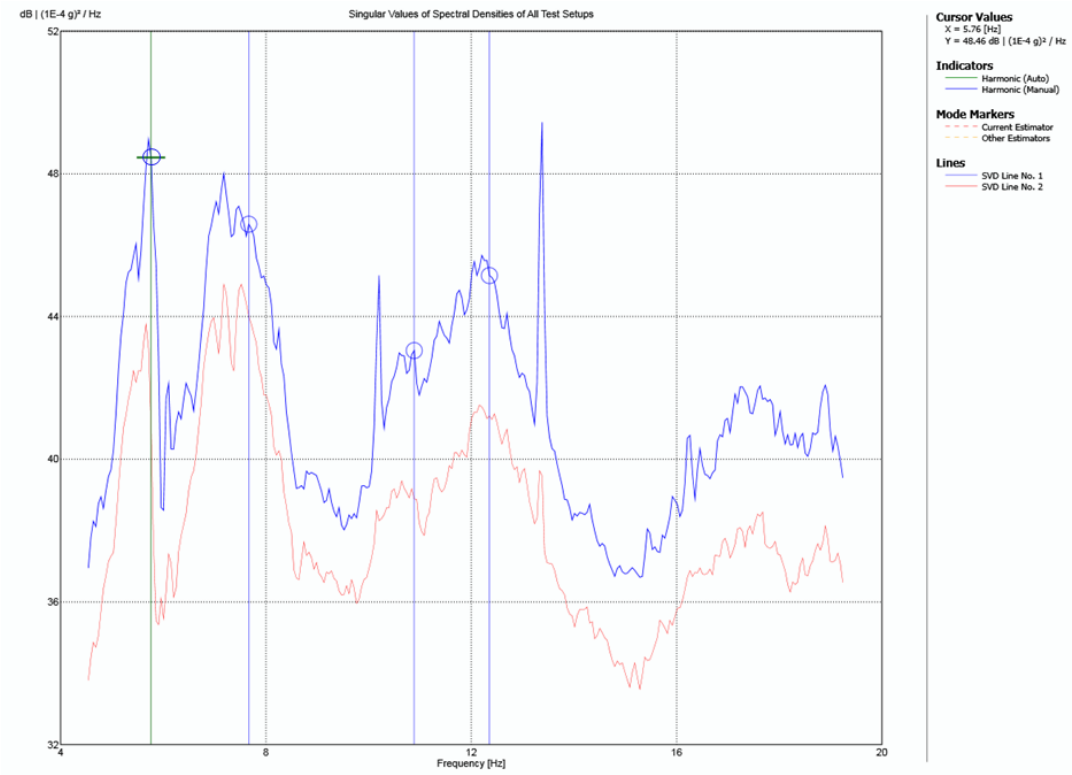

Figure 4.4. *Singular values of spectral densities of all setups, EFDD method*

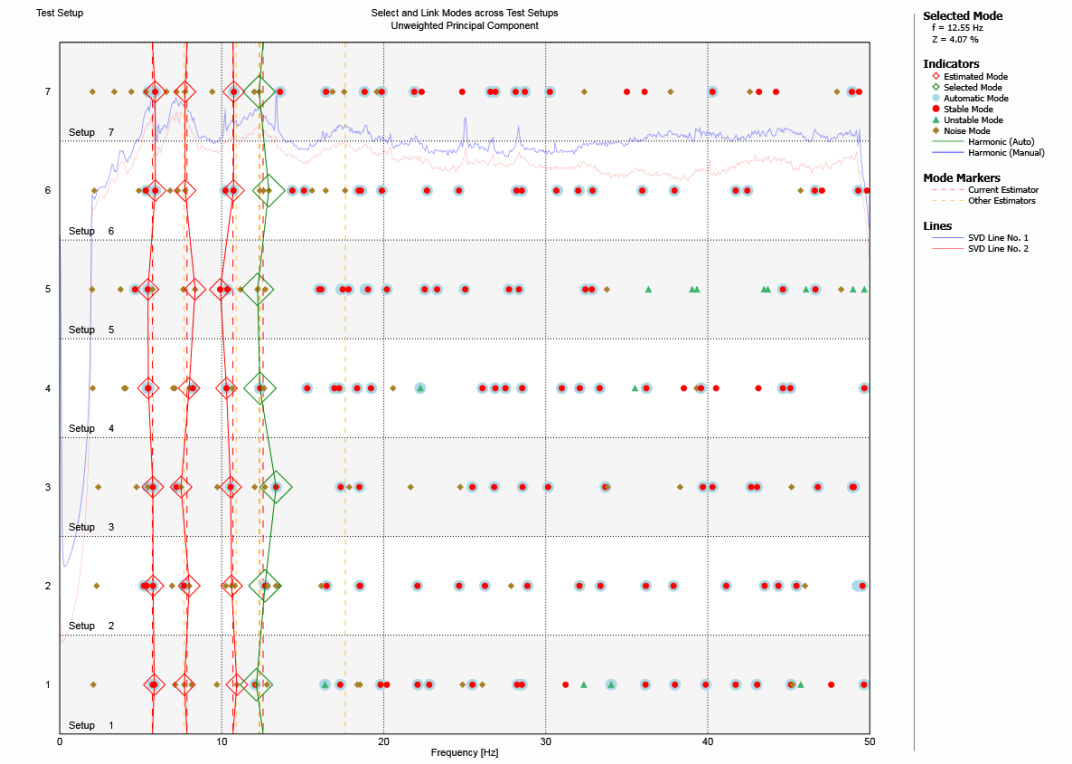

Figure 4.5. *Selection and linking process of modes across all test setups, SSI-UPC method*

In the SSI method, columns of stable poles were selected, and each setup has been linked with each other to identify the modes of vibrations. During the selection process, frequency and mode shapes of each pole were considered. Modal frequencies obtained from each method ranges from 5.7 Hz to 12.5 Hz. Following that, Modal Assurance Criterion (MAC) was calculated in order to compare the results of two methods. MAC is used to estimate the correlation between the mode shapes derived from experimental and analytical models (Friswell and Mottershead, 1995). It is also used to compare experimental results derived by different methods in ARTeMIS Modal. The MAC between analytical mode φ_{aj} and experimental mode φ_{ej} is defined as;

$$MAC_{jk} = \frac{|\varphi_{ej}{}^{T}.\varphi_{ak}|^{2}}{(\varphi_{ak}{}^{T}.\varphi_{ak}).(\varphi_{ej}{}^{T}.\varphi_{ej})} \tag{4.1}$$

The MAC value varies between 0 and 1. The value 1 means that mode vectors are multiple of each other while the value 0 represents that both mode vectors are orthogonal vectors. Calculated MAC values are given for SSI and EFDD method in Table 4.1. In the case where the value gets closer to 1, the correlation is assumed as satisfactory. The computed MAC values are ranging from 0.66 to 0.87 which are acceptable for the first 4 global modes of vibrations within this framework.

Table 4.1. *Comparison between SSI-UPC and EFDD results using MAC*

			SSI-UPC			
	***f* (Hz)**		**Mode 1**	**Mode 2**	**Mode 3**	**Mode 4**
			5.718	**7.852**	**10.688**	**12.547**
EFDD	**Mode 1**	**5.762**	**0.87**	0.129	0.117	0.019
	Mode 2	**7.666**	0.158	**0.728**	0.313	0.216
	Mode 3	**10.889**	0.112	0.009	**0.661**	0.489
	Mode 4	**12.354**	0.005	0.059	0.107	**0.783**

In this thesis, the mode shapes of vibrations of the mosque derived by SSI method were accepted as the experimental mode shapes of the structure in order to overcome the effects of undesired environmental noise (See Figure 4.6). Figure 4.6(a) illustrates that the first mode shape is the combination of torsional and translational mode in transverse direction of the building. This is due to the fact that North portion of the mosque includes window and door openings on the North Wall and as well as piers in the portico part. Therefore, North portion of the mosque is more flexible than the South wall in the transverse direction. The second mode shape is global translational mode in longitudinal direction Figure 4.6(b). The third and fourth modes of vibrations show that there is a lack of connection between perpendicular walls so that desired integrated behavior of the walls is not provided on the mosque (Figure 4.6(c) and Figure 4.6(d)).

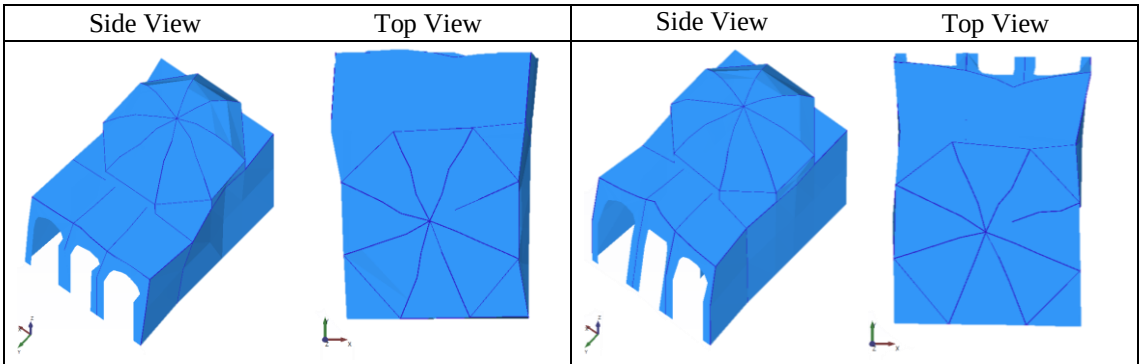

(a) 1st Mode *(b) 2nd Mode*

Figure 4.6. *First 4 mode shapes derived by SSI method, ARTeMIS Modal*

Side View	Top View	Side View	Top View
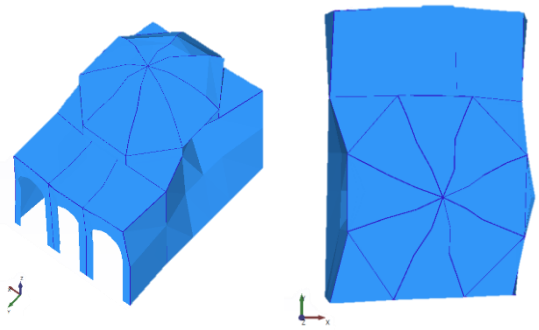		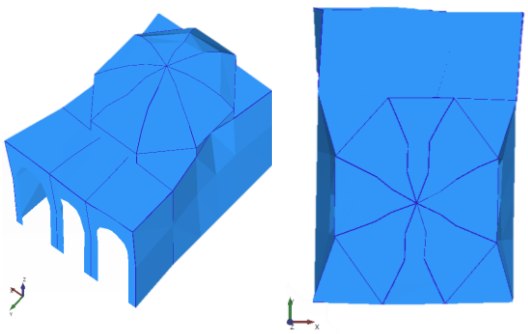	
f = 10.688 Hz		*f = 12.547 Hz*	
(c) 3rd Mode		*(d) 4th Mode*	

Figure 4.6 (continued) *First 4 mode shapes derived by SSI method, ARTeMIS Modal*

4.3 Calibration of the Numerical Model

Representative structural scheme of the mosque was improved by calibrating the finite element model regarding to the experimental modal analysis as explained previously. Calibration process of the numerical model was carried out by trial and error approach and two masonry materials on the mosque, namely cut stone and brick, were calibrated only. During the calibration process, retrofitted numerical model was used due to the fact that the Ambient Vibration Measurements, which was performed in 2017, represents the retrofitted mosque. Comparison between experimental and calibrated numerical frequencies are given in Table 4.2. Additionally, MAC values were calculated in order to compare mode vectors of the experimental and numerical results. Since the MAC values are low even after calibration, generally 0.8 and above MAC value is desirable, calibration process was done by minimizing the difference between the first four modal frequencies of the experimental and numerical modes of vibrations. The average error of the first four modes has been calculated as 4.9% which is quite reasonable within the framework of this study. Thus, calibrated elastic material properties of the masonry elements have been found as 1500 MPa for cut stone and 2500 MPa for brick, as given in Table 4.3. Furthermore, the experimental and numerical mode shapes are presented in Figure 4.7.

Table 4.2. *Comparison of the experimental and calibrated numerical modal frequencies*

Mode	f_{exp} (Hz)	f_{num} (Hz)	Error (%)	Average Error (%)	MAC
1	5.72	5.77	0.9	4.9	0.75
2	7.85	7.87	0.2		0.40
3	10.69	9.77	8.6		0.51
4	12.55	11.32	9.8		0.85

Table 4.3. *Calibrated Modulus of Elasticity values for masonry materials*

Type of Masonry	Modulus of Elasticity (MPa)
Cut Stone	1500
Brick	2500

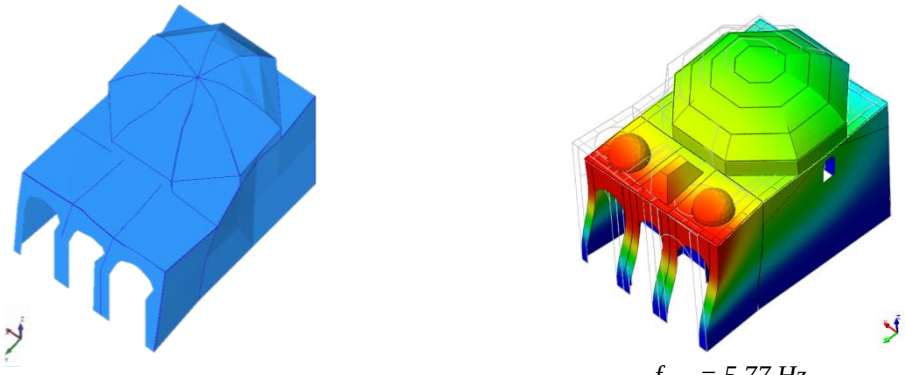

f_{exp} = 5.72 Hz f_{num} = 5.77 Hz

(a) 1st Mode

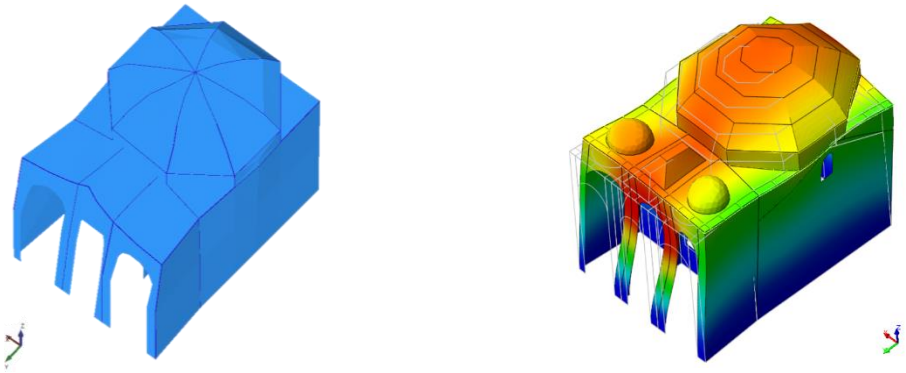

f_{exp} = 7.85 Hz f_{num} = 7.87 Hz

(b) 2nd Mode

Figure 4.7. *Experimental and calibrated numerical modes of vibrations*

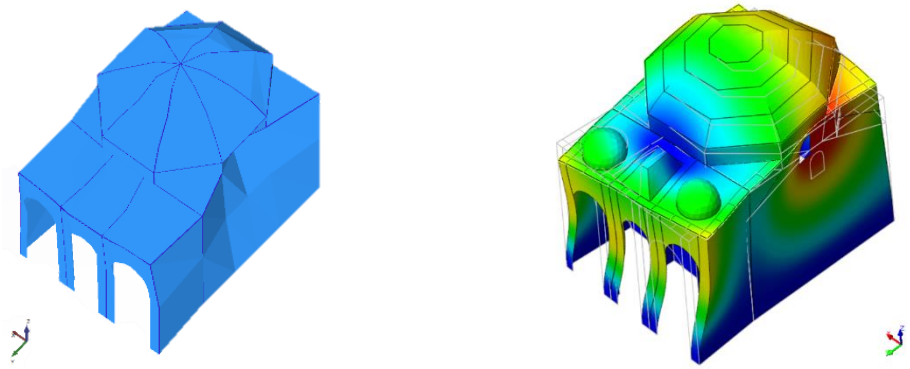

f_{exp} = 10.69 Hz f_{num} = 13.58 Hz

(c) 3rd Mode

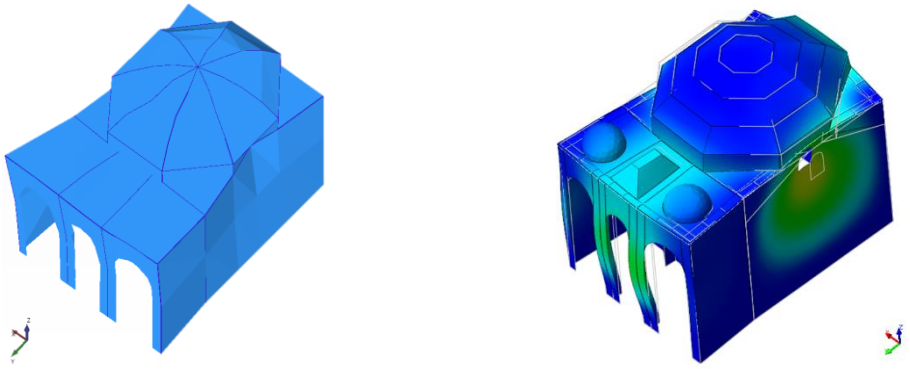

f_{exp} = 12.55 Hz f_{num} = 11.32 Hz

(d) 4th Mode

Figure 4.7. (continued) *Experimental and calibrated numerical modes of vibrations*

4.4 Eigenvalue Analysis

An eigenvalue analysis was performed to obtain mode shapes and frequencies of the retrofitted mosque. Several mode shapes of the retrofitted model for the first one hundred modes are presented in Figure 4.8. The first four global frequencies ranges from 5.75 Hz to 11.32 Hz. Moreover, the first four modes contribute to the cumulative mass participation ratio of 70.83% in the x direction and 67.28% in the y direction (Table 4.4). Considering one hundred modes, it is possible to obtain a cumulative mass participation ratio of 90.35% in the x direction, 89.84% y direction and 82.69% in the z direction. Accordingly, first four modes that have been obtained from experimental analysis is sufficient enough to characterize the dynamic behavior of the mosque with nearly 70% mass participation in x and y direction. As Chopra (2012) indicates that few first modes provide accurate results for a such N-DOF system. The first mode is global and translational in x direction and torsional effect is also observed due to the relatively high

modal displacements between South and North façades. Maximum modal displacements are presented on the portico while the structure experiences very limited modal displacement at the base. Comparing to the South Wall, North Wall and Portico is relatively flexible due to window and door openings and piers, respectively.

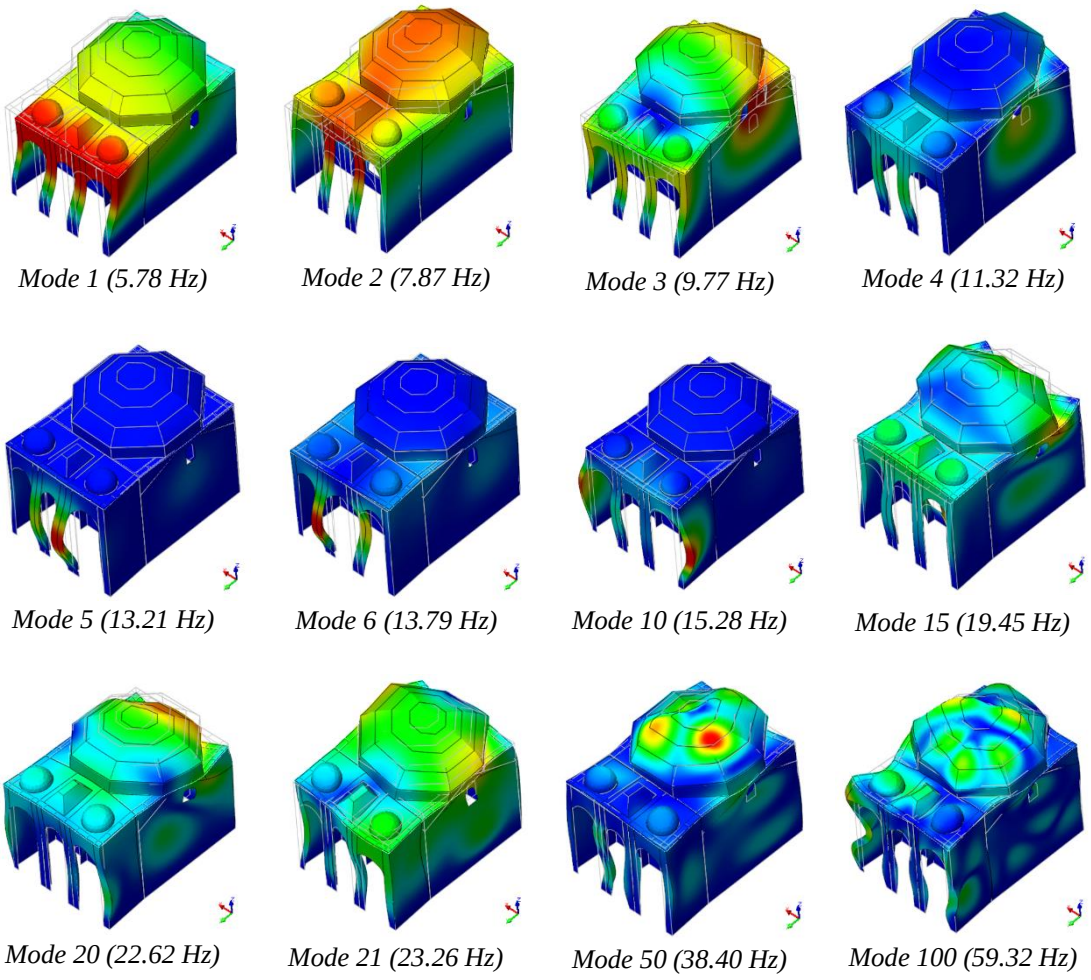

Figure 4.8. *Several mode shapes of retrofitted model, FX+ for DIANA*

Table 4.4. *Frequencies, periods and cumulative mass participation ratios of the retrofitted model for the first 100 modes in each direction*

Mode	*f* (Hz)	Period (s)	Cumulative Mass Participation (%)		
			X component	Y component	Z component
1	5.78	0.17	60.72	≈ 0.00	≈ 0.00
2	7.87	0.13	61.13	66.95	≈ 0.00
3	9.77	0.10	70.80	67.27	≈ 0.00
4	11.32	0.09	70.83	67.28	≈ 0.00
5	13.21	0.08	70.83	67.52	≈ 0.00
6	13.79	0.07	70.90	67.61	≈ 0.00
10	15.28	0.07	71.07	67.74	2.15
15	19.45	0.05	73.39	68.91	3.60
20	22.62	0.04	80.45	79.67	64.80
21	23.26	0.04	80.88	79.75	65.38
50	38.40	0.03	85.11	85.96	76.88
100	59.32	0.02	90.35	89.84	82.69

The second mode is translational mode which is dominated in longitudinal (Y) direction of the mosque. Maximum modal displacements are concentrated at the upper and middle section of the components along the longitudinal direction. Out-of-plane movement exists in the lower inertial direction of the load bearing walls, namely South Wall, North Wall and north façade of the Portico. The third mode is also translational mode in both x and y directions combined with torsional effect due to the out-of-plane movement of the West and South façade. The fourth mode is mostly dominated by the translational displacement in longitudinal direction. Moreover, the drum, which supports the dome, is subjected to out-of-plane movement. Besides, the structure vibrates more locally in the rest of the mode shapes. For instance, the fifth, sixth and seventh modes are concentrated on the Portico while the others experience higher modal displacements on the dome.

Experimental modal analysis was performed after steel girders were conducted to the mosque in 2017. Therefore, there is no mode shapes of the original structure without retrofitting. The main reason is that Anadolu University started to contribute in the scientific committee of restoration and seismic retrofitting works of the historical mosque in 2016 and the steel girder retrofitting has already been completed in that time. It is

believed that contribution of the steel girder retrofitting in elastic range is not effective to be observed due to the relatively low stiffness of the girders comparing to the very thick load bearing walls. Therefore, non-retrofitted numerical model was obtained by removing the steel girder retrofitting on the calibrated finite element model. It is important to mention that non-retrofitted model is exactly the same with the retrofitted model in terms of geometrical and material properties and the only difference is the existence of the steel girders on the retrofitted model. An eigenvalue analysis was performed for non-retrofitted model to see the difference in modal properties of the two models. In fact, frequencies, mode shapes and cumulative mass participation ratios of the non-retrofitted model are quite the similar with the retrofitted finite element model. Frequencies with very low variations (in a decimal point which can be accepted in a such complex structure) and mode shapes are given in Figure 4.9. Cumulative mass participation of the non-retrofitted model is also given in Table 4.5. There is no significant change in modal response. Therefore, non-retrofitted model was used in order to represent nonlinear response of the mosque before steel girder retrofitting.

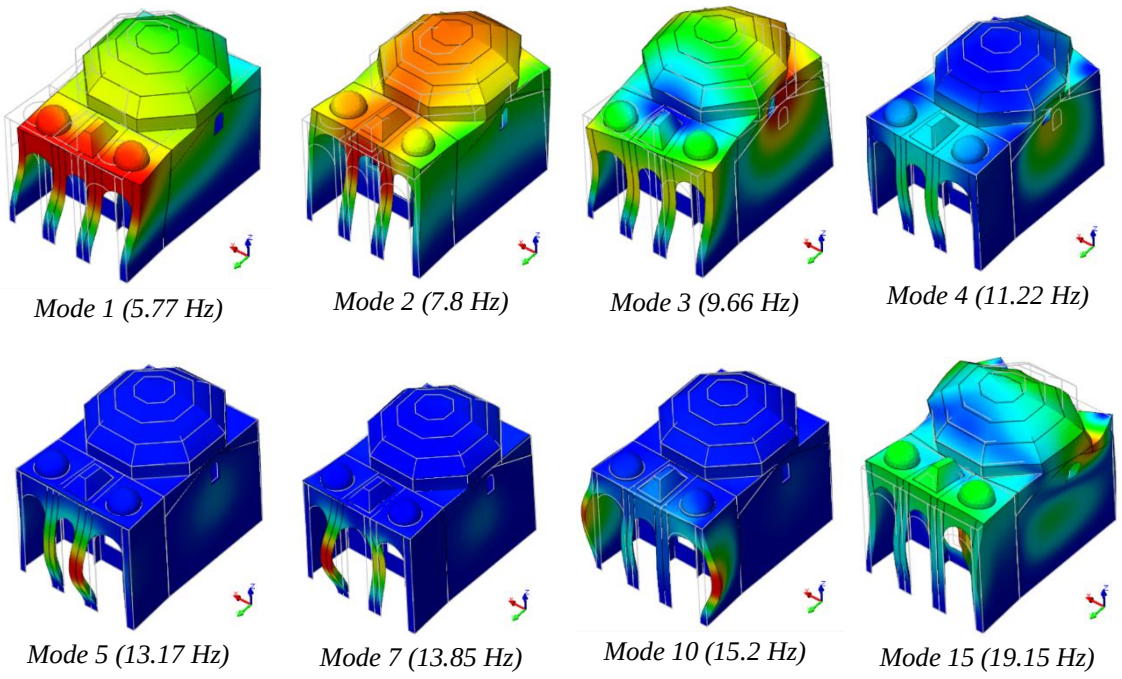

Figure 4.9. *Several mode shapes of non-retrofitted model, FX+ for DIANA*

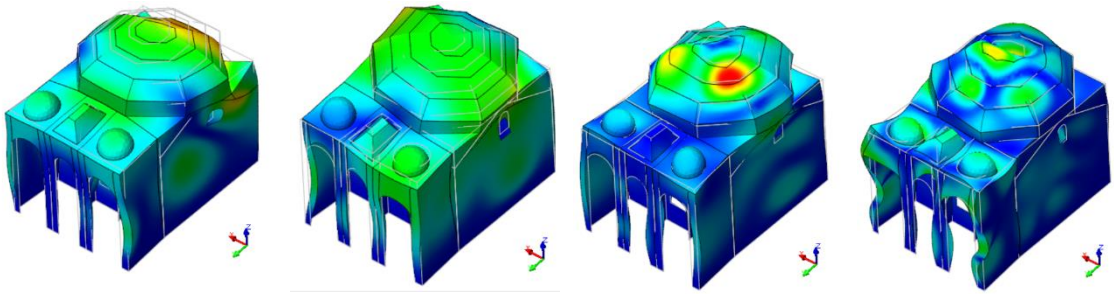

Mode 20 (22.39 Hz) *Mode 21 (23.1 Hz)* *Mode 50 (37.97 Hz)* *Mode 100 (58.6 Hz)*

Figure 4.9 (continued) *Several mode shapes of non-retrofitted model, FX+ for DIANA*

Table 4.5. *Frequencies, periods and mass participation ratios of non-retrofitted model for the first 100 modes in each direction*

Mode	*f* (Hz)	Period (s)	Cumulative Mass Participation (%)		
			X component	Y component	Z component
1	5.77	0.17	60.50	≈ 0.00	≈ 0.00
2	7.80	0.13	60.90	66.23	≈ 0.00
3	9.66	0.10	70.40	66.50	≈ 0.00
4	11.22	0.09	70.43	66.50	≈ 0.00
5	13.17	0.08	70.43	66.78	≈ 0.00
7	13.85	0.07	70.54	66.92	≈ 0.00
10	15.20	0.07	71.07	67.04	2.00
15	19.15	0.05	72.77	68.65	3.72
20	22.39	0.04	79.83	78.93	63.70
21	23.10	0.04	80.20	79.07	64.00
50	37.96	0.03	85.03	85.48	76.76
100	58.60	0.02	90.26	89.73	82.38

5. SEISMIC ASSESSMENT BY NONLINEAR STATIC ANALYSIS

The nonlinear static analyses are preferred to evaluate the seismic performance of a structure by spending less computational effort comparing to the dynamic analysis. In this chapter of the thesis, seismic assessment of the Kütahya Kurşunlu Mosque was carried out by conducting nonlinear pushover analyses. The analyses were performed by using TNO DIANA software. The iterative method of the analysis was selected as secant method and the arch length control method was used for the accurate numerical calculations closer to peak. Each equilibrium step was calculated according to the internal energy with a tolerance value of 0.001.

5.1 Nonlinear Pushover Analysis

The nonlinear pushover analysis is an effective tool to characterize the structural behavior of the building by estimating the capacity, damage distribution and failure mechanisms. In the present study, the seismic forces were represented as horizontal loading proportional to the mass of the structure to perform pushover analysis which is recommended for historical structures without box-behavior (Lourenço *et al.*, 2011). The adopted loading pattern was also considered by several research studies, for instance Braga (2014); Ciocci, Sharma, and Lourenço (2018); Karanikoloudis and Lourenço (2018); Lara (2016); Mangia *et al.* (2016); Silva (2013). After the structure was vertically loaded (self-weight of the structure), the seismic loads were applied by increasing monotonically. A unidirectional mass proportional seismic action, which is compatible with the global coordinate of the structural system, were implemented. The seismic performance was studied in both positive and negative transversal and longitudinal directions of the mosque. Several control points were defined in order to develop the pushover curves by relating base shear force and displacement. Thus, the base shear force is given in terms of load factor. The load factor is defined as the ratio between the sum of the acting horizontal forces to the sum of the vertical forces (self-weight), as given:

$$Lf = \frac{\sum F_H}{\sum F_V} \tag{5.1}$$

The selected control nodes are presented in Figure 5.1. The pushover analyses were computed for both numerical models with and without retrofitting and a comparison between the structural behavior is presented in this chapter. Furthermore, the maximum

principal tensile strains, which is a good damage indicator as seen in Mendes (2012); Ciocci, Sharma and Lourenço (2018); Karanikoloudis and Lourenço (2018), were investigated to compare the non-retrofitted model's damage pattern with the observed damage in-situ. It is important to mention that the final loading step of the presented pushover curves do not represent the global failure of the historical mosque. In fact, the principal tensile strain distribution at that point is in a good agreement with the reported damage on the mosque.

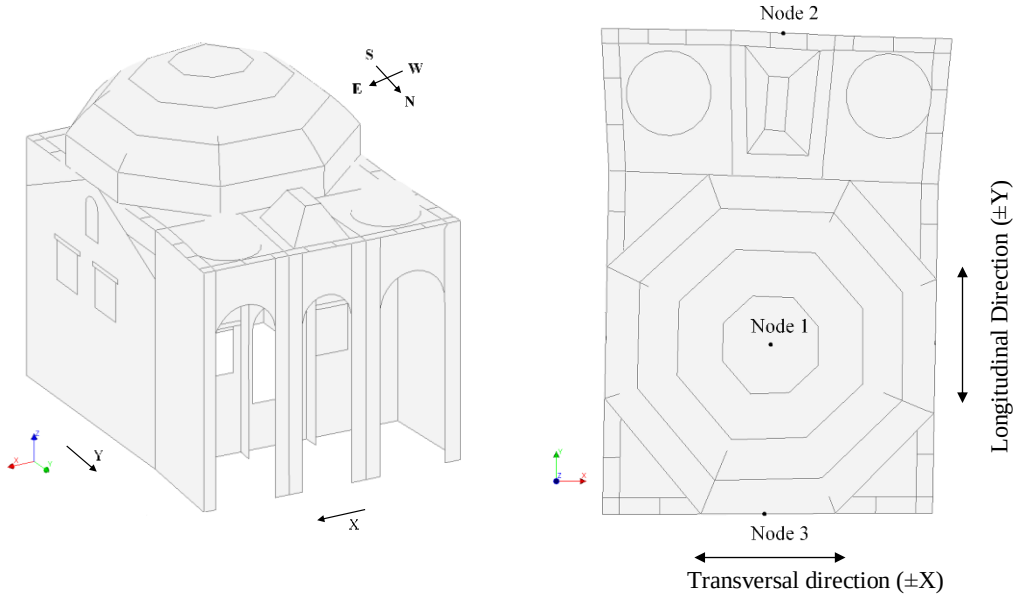

(a) Global axes *(b) Control Nodes*

Figure 5.1. *Global coordinate system and defined control nodes*

5.1.1 Direction +X

Firstly, a nonlinear pushover analysis was performed in the positive transversal direction of the historical structure. The capacity curve of the adopted analysis was computed by considering two different control points as given in Figure 5.2. The control points were located on the top point of the dome and the highest level of the portico, namely Node 1 and Node 2, respectively (See Figure 5.1). The pushover curves for both retrofitted and non-retrofitted model depict that the first crack initiates when a value of 0.18g horizontal load is acted on the structure. It is important to mention that the same value of linear capacity for both models is expected because, as already stated in the Section 4, the dynamic properties of the structure do not differ when the steel girder elements are introduced to the structure. The maximum lateral load in the positive X

direction is observed for non-retrofitted and retrofitted model as 0.38g and 0.4g, respectively. The control node at the portico (Node 2) experienced the highest displacement in both cases. The corresponding displacements at the Node 2 are 21 mm for the non-retrofitted case and 44 mm for the retrofitted case whereas the top of the dome (Node 1) was subjected to a value of 15 mm and 29 mm displacement, respectively. In the Figure 5.2, a considerable reduction in the lateral load capacity of the mosque is also observed for non-retrofitted model, from 0.38g to 0.27g.

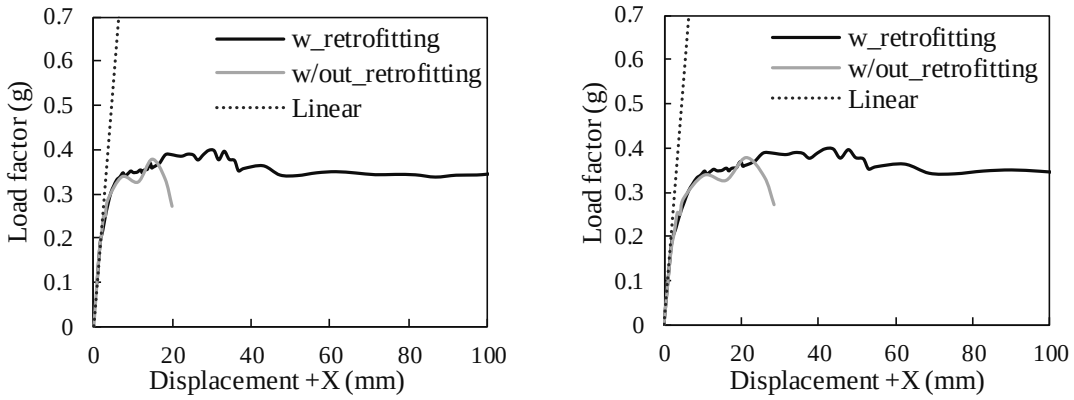

(a) Node 1 *(b) Node 2*

Figure 5.2. *The pushover curves in the positive transversal direction*

Next, the principal tensile strain distributions are presented in order to compare the numerical damage and the real damage pattern. It is worth to mention that nonlinear pushover analysis performed in +X direction presents a damage pattern which is in a good agreement with the damage observed in situ. It is possible to validate the consistency of the adopted nonlinear material properties of the calibrated numerical models. As already stated, the last load factor of the nonlinear pushover response of the model do not represent the total collapse. However, the strain distribution resulted by the last step loading factor presents damage pattern similar to the real damage observed. On the other hand, a severe diagonal crack on the north façade initiates on the numerical model of non-retrofitted mosque first but there is no evidence of diagonal crack on the north façade during the site investigations. Lateral loading in the positive transversal direction resulted diagonal crack on the south wall in which in-plane behavior was observed (Figure 5.3). In Figure 5.4, a vertical crack seems to be originated due to the lack of integrated behavior of the orthogonal structural components, namely west and north wall. On the east wall, diagonal cracks were also presented by the numerical model due to its in-plane movement

(Figure 5.5). At last, the dome experiences damage which seems to be originated because of the in-plane mechanism of the transversal walls and out-of-plane movement of longitudinal walls in +X direction (Figure 5.6).

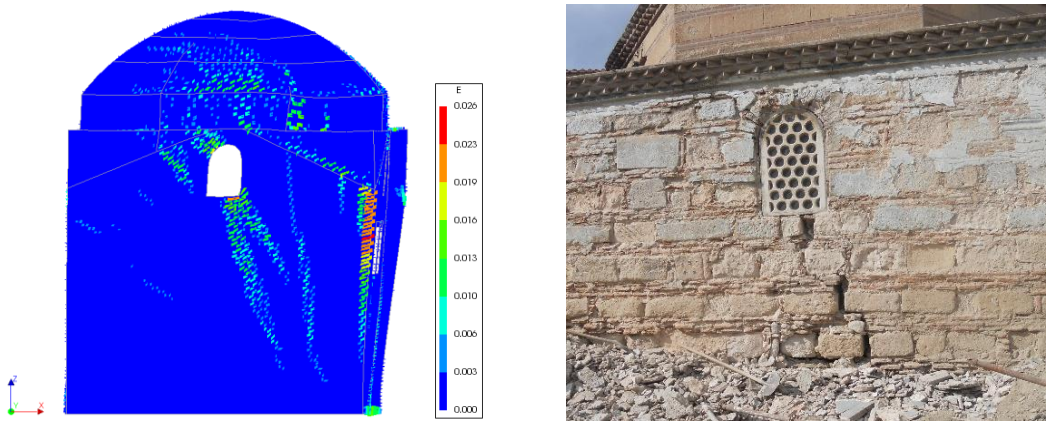

(a) Numerical damage *(b) Observed damage on the south façade*

Figure 5.3. *The non-retrofitted numerical and real damage on the south wall, maximum principal strain distribution at load factor 0.27g in +X direction*

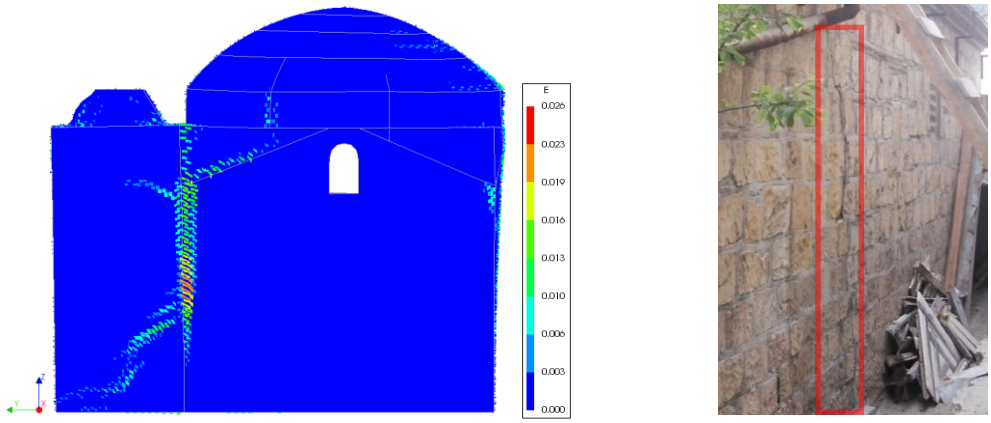

(b) Numerical damage on the west façade *(b) Observed damage on the west façade*

Figure 5.4. *The non-retrofitted numerical and real damage on the west façade, maximum principal strain distribution at load factor 0.27g in +X direction*

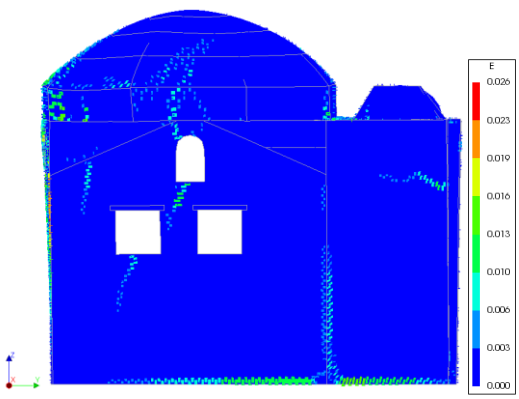

(a) Numerical damage on the east façade

(b) Cracks on the east façade

Figure 5.5. *The non-retrofitted numerical and real damage on the east façade, maximum principal strain distribution at load factor 0.27g in +X direction*

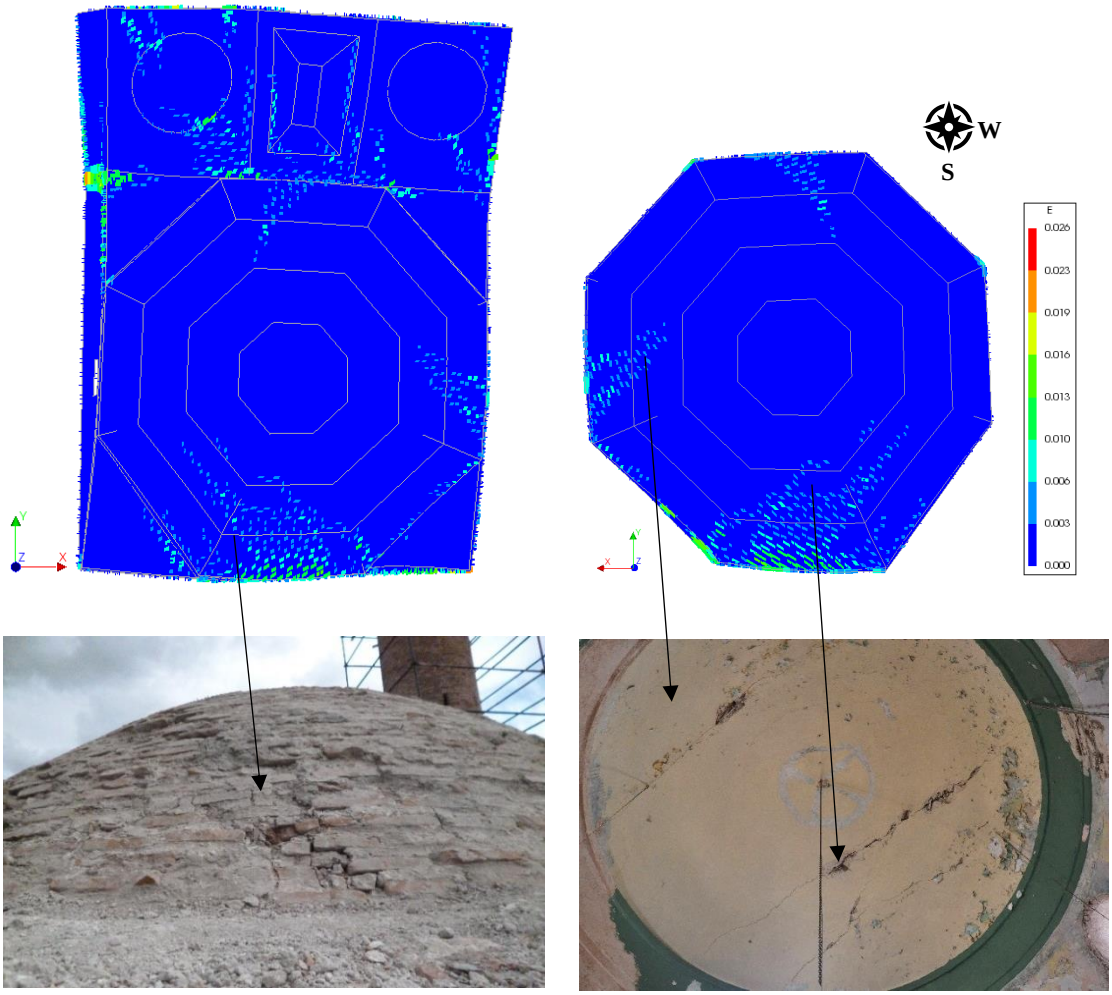

(a) Top view

(b) Bottom view (intrados)

Figure 5.6. *The non-retrofitted numerical and real damage on the dome, maximum principal strain distribution at load factor 0.27g*

5.1.2 Direction -X

In the negative transversal direction, the nonlinear behavior of the two models also initiate first crack when the seismic loads exceed 18% of the total weight of the structure as shown in Figure 5.7. In addition, the maximum lateral load capacity is almost the same with the observed ones in +X direction for both cases. However, the horizontal displacements are, when the peak load factor is observed, lower in the non-retrofitted case and higher in the retrofitted one in the +X direction. For Node 1, a value of 8 mm for non-retrofitted case and 37 mm for retrofitted case is noted. Displacements at Node 2 is 12 mm and 52 mm, respectively. The curves show that the load capacity of the model without retrofitting decreases slightly, from 0.37g to 0.33g.

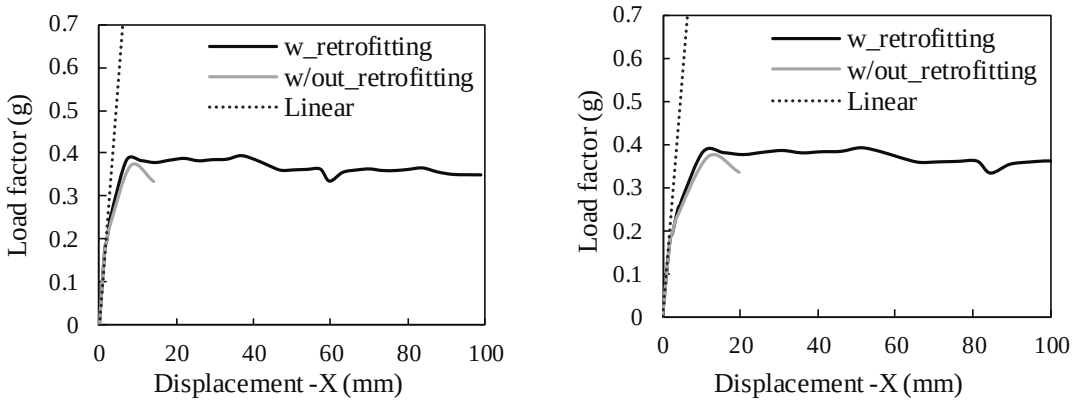

(a) Node 1 *(b) Node 2*

Figure 5.7. *The pushover curves in the negative transversal direction*

5.1.3 Direction +Y

In order to study pushover analysis in longitudinal (Y) direction of the structure, Node 3 was defined on the highest level of the south wall in which a severe damage was reported. Therefore, capacity curves represent the control points of Node 1 and Node 3 (See Figure 5.1(b)) as given in Figure 5.8. The initial cracking load in the positive longitudinal direction is found as 0.24g for the both numerical models. Higher linear behavior limit is expected in Y direction because of the fact that the structural components, namely bearing walls along the east and west façade, have higher stiffness in that direction. Furthermore, there is a significant difference on the maximum lateral load capacity in +Y direction between the two models. The model without steel elements has maximum lateral load capacity of 0.48g. In the post-peak behavior, nearly 10 mm

ultimate displacement is observed when the load factor decreases to 0.3g. On the other hand, the lateral load coefficient of the retrofitted numerical model reaches up to 0.56g. It is clear that both of the control points, Node 1 and Node 3, exhibit nonlinear behavior in each case.

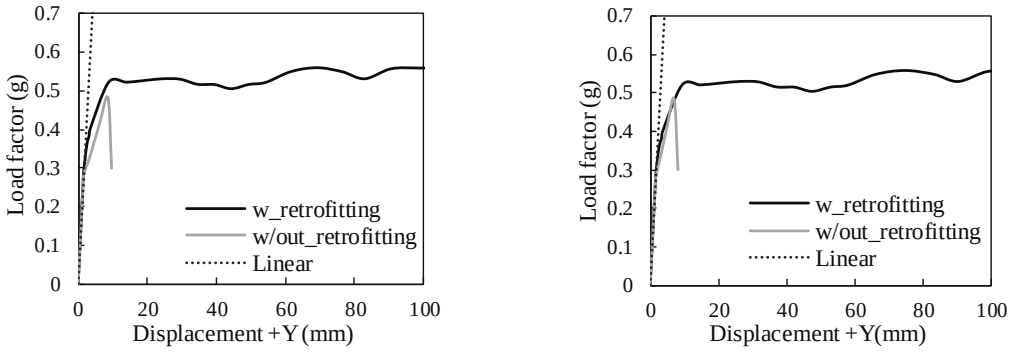

(a) Node 1 *(b) Node 3*

Figure 5.8. *The pushover curves in the positive longitudinal direction*

Figure 5.9 shows that the finite element model depicts vertical cracks on the west façade. A vertical crack is observed at the intersection of the orthogonal structural walls, north and west wall and also west façade of the portico (Figure 5.9(a)). In fact, each step of the pushover analysis was checked and the first crack initiates at the pendentive and followed by separation of the adjacent components (referring to vertical crack) due to the lack of connection of the members. Furthermore, the vertical crack on the west wall (Figure 5.4(b)), which starts just below the window opening, can be related to the damage observed on the non-retrofitted model due to the lateral load acted in positive y direction. On the other hand, the principal tensile strain distribution shows similar damage pattern observed on the outer and inner surfaces of the dome as shown in Figure 5.10 (See Figure 5.6 for the observed damage). The distribution and orientation of the strain propagation is also sharp and in a good agreement with the observed damage.

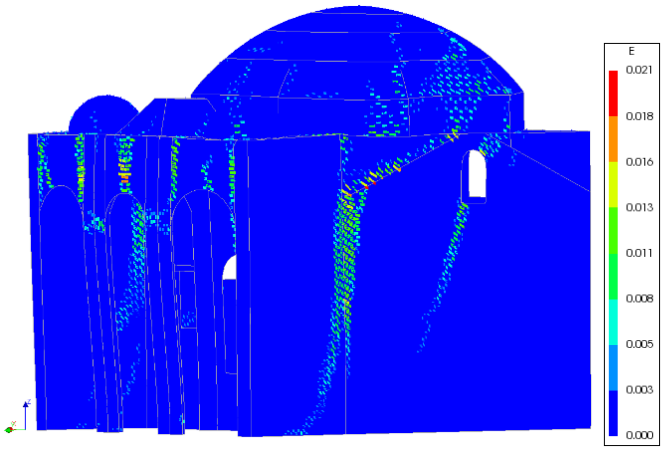

(a) West façade

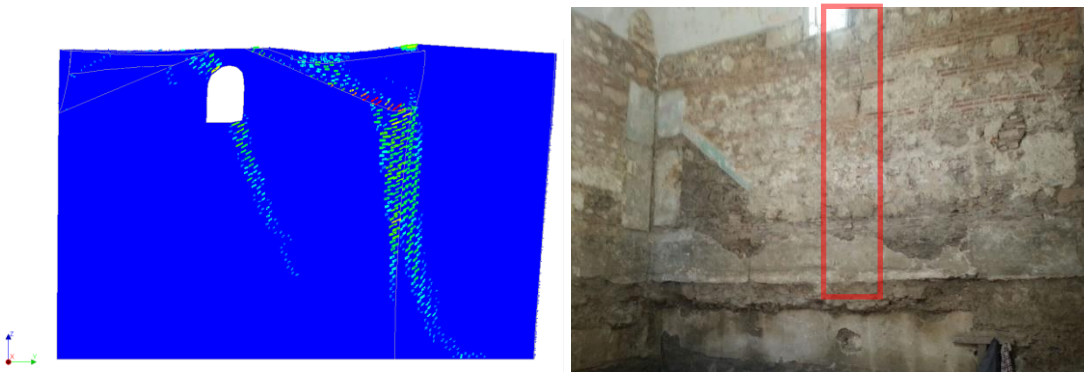

(b) West wall interior

Figure 5.9. *Comparison of the non-retrofitted numerical and real damage on the West Wall, maximum principal strain distribution at load factor 0.3g*

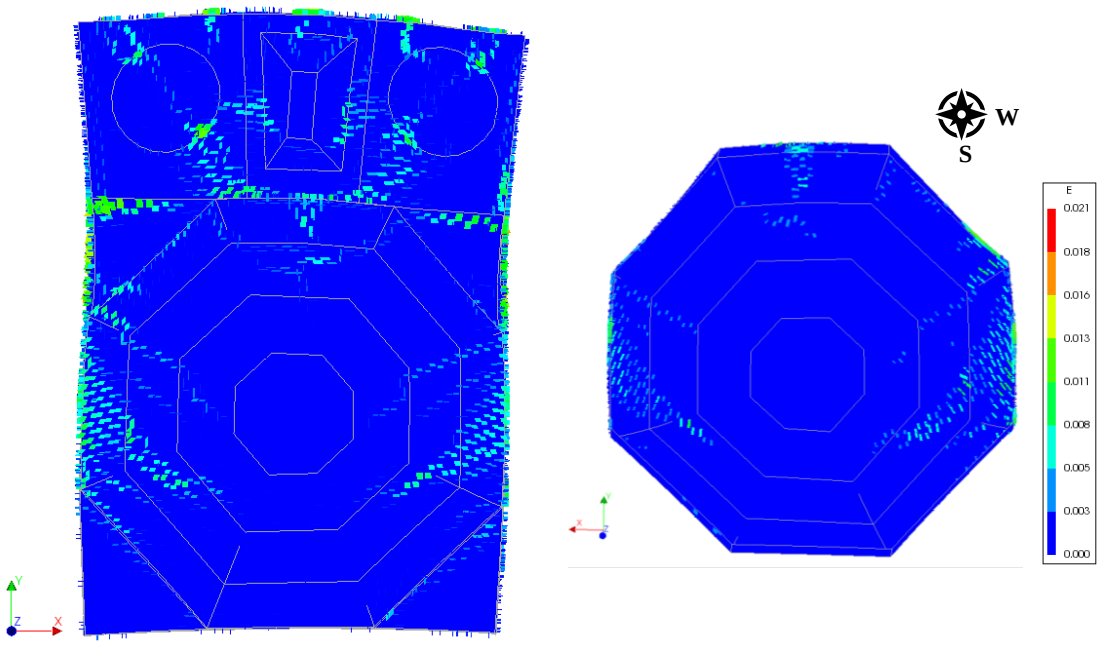

Figure 5.10. *Comparison of the non-retrofitted numerical and real damage on the Dome, maximum principal strain distribution at load factor 0.3g*

5.1.4 Direction -Y

In the negative longitudinal direction, the finite element models present higher elastic range comparing to the other directions, i.e. 28% of the total weight of the structure need to be applied as lateral force so that the structure exhibits nonlinear behavior (initiation of cracks). Figure 5.11 illustrates that the non-retrofitted representative scheme can resist lateral load up to half of its total weight. Besides, the capacity rises up to nearly 0.6g when the steel elements are introduced. Additionally, it is possible to state that the retrofitted model has higher capacity to dissipate energy, owing to its improved deformation capacity. Moreover, a minimum value of 0.1g reduction in the load capacity of the non-retrofitted model is noted in which the maximum displacement response is observed on the south wall (Node 3) as 15 mm (Figure 5.11(b)). Even so, the crack distribution of the non-retrofitted model (Figure 5.12), when the load coefficient reduces to 0.4g, depicts similar pattern of the severe damage observed on the south wall due to out-of-plane movement (Figure 5.3(b)).

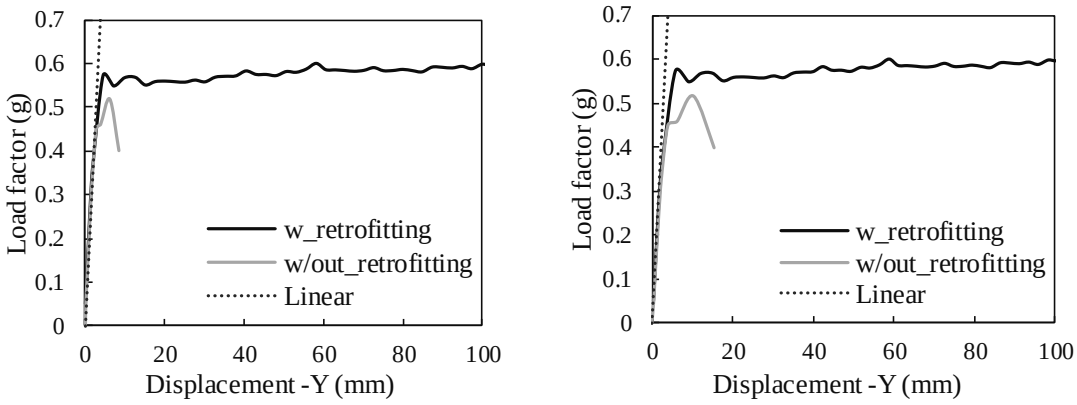

(a) Node 1 *(b) Node 3*

Figure 5.11. *The pushover curves in the negative longitudinal direction*

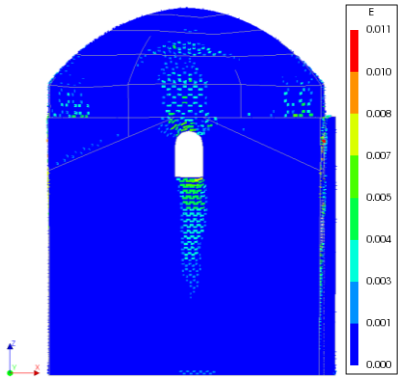

Figure 5.12. *Numerical damage on the south façade, maximum principal tensile strain distribution at the load factor 0.4g*

5.2 Final Remarks

In this chapter, seismic performance of the non-retrofitted and retrofitted Kütahya Kurşunlu Mosque was investigated by nonlinear pushover analysis and several conclusions are put forward. The elastic limit of the both models are the same as expected. However, the structures exhibit different elastic limit state in each orthogonal direction, 0.18g for transversal (X) and 0.24g for longitudinal (Y) direction. The stronger direction of the structure is longitudinal (Y) one in which the maximum applied lateral load is found as 0.6g and 0.5g for the retrofitted and non-retrofitted representative structural scheme, respectively. In the transversal direction, both models have slight difference and the lateral load capacity is nearly 40% of its total weight. Additionally, positive directions of each orthogonal component of the building is stiffer than its negative one because of the fact that the ancient mosque is not symmetric. A considerable decrease in the load capacity of the non-retrofitted model is concluded for all directions. In fact, non-retrofitted model still has the displacement capacity after it experiences a reduction in the capacity. However, the capacity curves were shortened at the load step when a considerable decrease was observed. On the other hand, it is possible to state the ductile behavior of the steel has a positive contribution to the global behavior. Last load steps of the curves do not represent the total collapse of the building, but the curves are sufficient enough to characterize and validate the local damage. Nevertheless, the retrofitted model has higher energy dissipation capacity in all directions. Furthermore, it is obvious that the principal tensile strain distribution depicts a numerical pattern on the non-retrofitted model which is compatible with the observed damage. Therefore, the adopted nonlinear behavior of the numerical model seems to be validated. In fact, pushover analysis conducted in +Y and +X direction has better representation of the observed damage.

6. SEISMIC ASSESSMENT BY NONLINEAR DYNAMIC ANALYSIS

Reproducing the dynamic behavior of a given structure, within an acceptable level accuracy, is a complex task. Uncertainties related with the geometrical, material and physical structural system contribute to increase such difficulty. In this context, the use of a dynamic analysis is, in theory, a better choice than the use of static or quasi-static approaches. In the present chapter, the seismic assessment of the historical masonry mosque is investigated by performing nonlinear time history analysis. The study was carried out for a set of three different earthquakes, in which only horizontal seismic components were considered. The vertical component of each input motion was disregarded.

6.1. Real Acceleration as Ground Motion

Real ground motions from past earthquakes occurred in Turkey was used to perform the nonlinear dynamic analysis. According to TEC (2007), a minimum of three ground motions are required to perform an analysis in the time domain. Furthermore, in case when three ground motions are considered, the results derived from the most severe one are assumed (TEC, 2007). In this context, three earthquakes were selected from the Strong Ground Motion Database of Turkey (TR-NSMN) operated by the Earthquake Department of Republic of Turkey Disaster and Emergency Management Authority. The location of the epicenter of each selected earthquake and its ground motions' seismological properties are given in Figure 6.1 and Table 6.1, respectively.

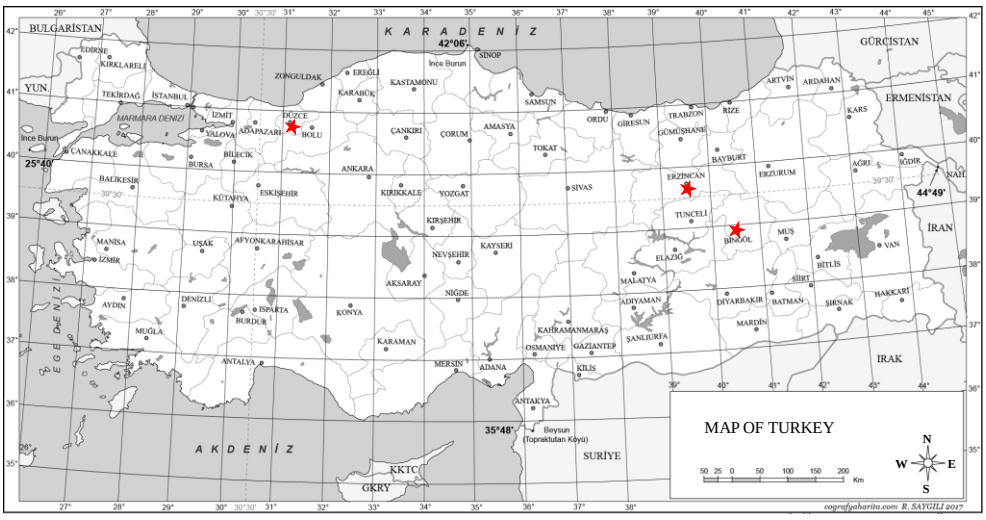

Figure 6.1. *Epicenter of earthquakes marked with red*

Table 6.1 *Seismological properties of selected ground motions (TR-NSMN)*

Earthquake	March 13,1992 Erzincan	November 12, 1999 Düzce	May 1, 2003 Bingöl
Station Location	Meteorology Building *Erzincan*	MPWR Building *Bolu*	MPWR Building *Bingöl*
Station ID	2402	1401	1201
Epicentre Coordinates	39.72ºN, 39.63ºE	40.79ºN, 31.217ºE	38.94ºN, 40.51ºE
Station Coordinates	39.752ºN, 39.487ºE	40.746ºN, 31.607ºE	38.897ºN,40.503ºE
Depth (km)	23	11	6
Mw	6.6	7.1	6.3
Site Conditions – Soil Type (Kalkan and Gülkan, 2004)	Soil	Soil	Stiff Soil
Longitudinal PGA (g)	0.413	0.754	0.556
Transverse PGA (g)	0.48	0.821	0.282
Longitudinal PGV (cm/s)	108	56.6	34.5
Transverse PGV (cm/s)	78.2	66.9	21.9
Longitudinal PGD (cm)	34.4	25.2	10.2
Transverse PGD (cm)	29.5	12.8	5.1

The selected accelerograms belong to the list of the more destructive earthquakes occurred in Turkey so far. Peak ground acceleration (PGA) values range from 0.28g to 0.82g. The peak ground velocity (PGV) is also considered during the ground motion selection because previous studies showed that, during a seismic assessment of certain types of structures, the PGV is an important intensity measure in addition to PGA. For instance, Avşar and Özdemir (2013) showed that the PGV has a good correlation with the dynamic response of seismic isolated bridges. Akkar, Sucuoğlu and Yakut (2005) investigated the dynamic response of reinforced concrete buildings, with different periods of vibration by considering different intensity measures. It has been also stated that PGV is a good intensity measure, particularly for vibration periods ranging 0.2s – 1.0s.

In Figure 6.2, the longitudinal and transversal components, of each accelerogram, are given. Linear baseline correction was done in SeismoSignal (Version 2016) to avoid unphysical velocities and displacements; the time series of ground velocity shall start and end with zero to have an efficient processing (Boore and Bommer, 2005). Figure 6.3

illustrates the response spectra of the input motions and the elastic response spectra defined in TEC 2007. As a damping coefficient of 3% was considered for the historical masonry structure, the response spectra of the input motions and the elastic response spectrum (TEC, 2007) are computed according to 3% viscous damping ratio. It is important to note that, once the current code admits a 5% damping ratio, a damping reduction factor (B) was used to be consistent with the studied structure. This damping reduction factor is calculated according to Eurocode 8 (EN 1998-2, 2005) and defined as:

$$B = \sqrt{\frac{0.05+c}{0.10}} \tag{6.1}$$

As already addressed, only the horizontal components of the earthquakes were used in the numerical analyses. The correct orientation of the two horizontal ground motion component, in respect to the structure, should account with the relative position of the accelerometer station which recorded the seismic signal. However, and as admitted in other studies (Kazaz and Kocaman, 2018; Ozturk, 2017; Ciocci, Sharma, and Lourenço, 2018; Braga, 2014), the orthogonal components of each input motions were applied orthogonally to the global coordinate axes of the mosque.

Orthogonal component of each input ground motion with higher spectral acceleration value were performed through the transversal direction which is the weak axis of the mosque. Spectral acceleration values were chosen regarding to the first vibration mode frequency, as shown in Figure 6.3. Thus, transverse components of Erzincan and Bolu records and longitudinal component of Bingöl record were performed in the transversal direction (+X) of the mosque. Other components of the input were acted in the longitudinal direction (+Y).

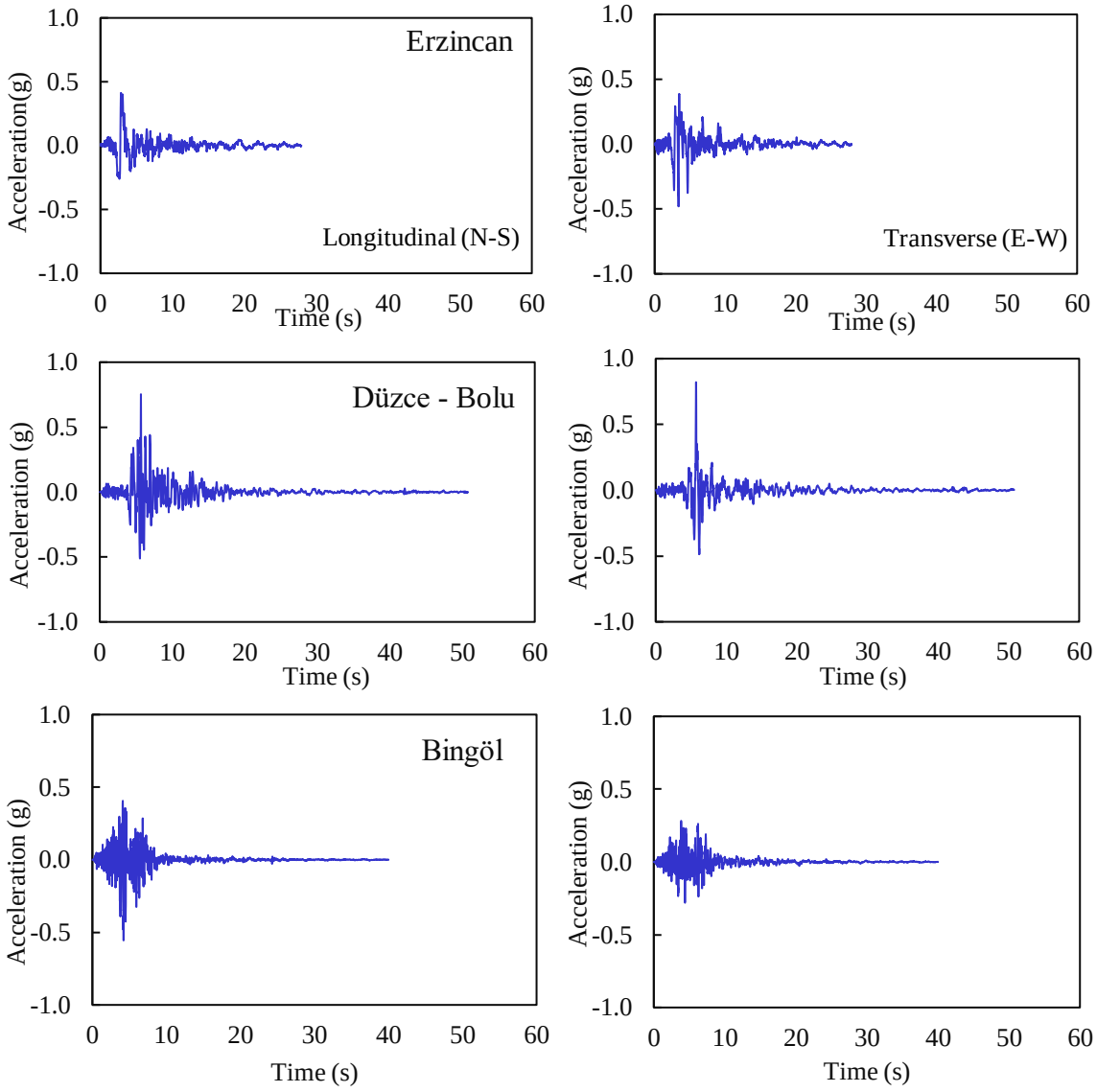

Figure 6.2. *Acceleration-time series of each record (TR-NSMN)*

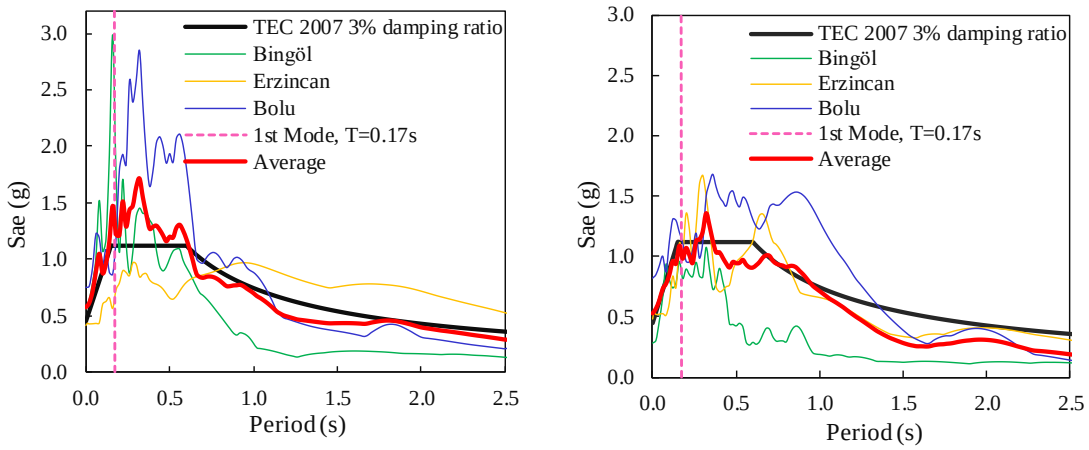

(a) Longitudinal components (N-S) *(b) Transverse components (E-W)*

Figure 6.3. *Elastic response spectra of input records and design spectrum as per TEC (2007) for Z3 soil condition*

Since nonlinear time history analyses require a high computational effort, only a part of strong ground motion was considered in this study aiming to speed-up the analyses. Thus, the duration of each record was shortened according to the cumulative energy duration that is proposed by Trifunac and Brady (1975), meaning that the time period under interest is in-between the 5% and 95% of the total arias intensity energy. Figure 6.4 depicts, for each accelerogram studied, the cumulative energy curve of the arias intensity which was computed using SeismoSignal (2016). It is clear that for the time instant of 20 s, the energy of the motion reaches almost 100% of the total and, therefore, only the first 20 s of each acceleration – time series were considered.

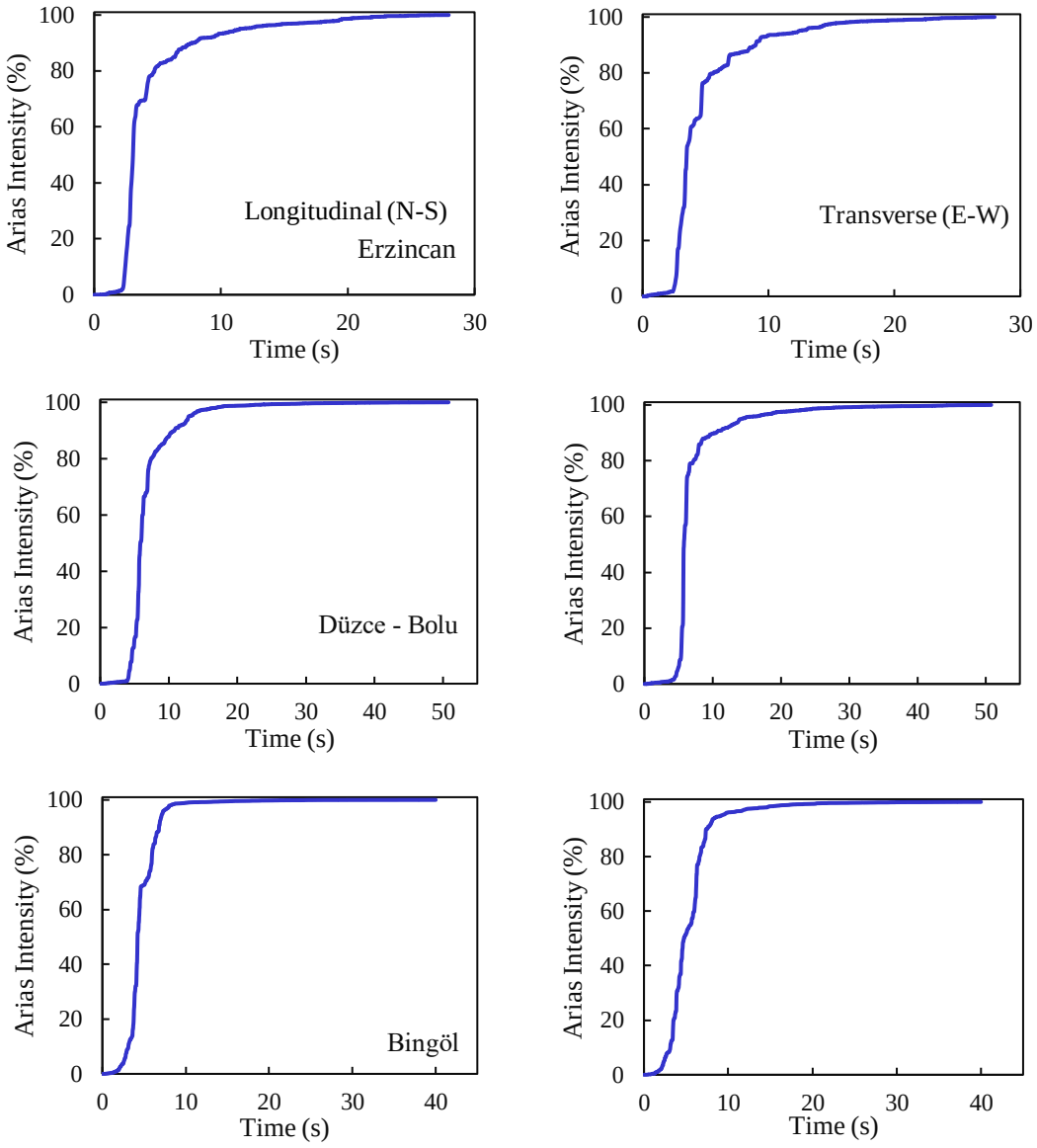

Figure 6.4. *Arias Intensity of the selected accelerograms*

6.2. Damping of the Structural System

Defining the damping properties of a given structure has always been a disputable task. Uncertainties of the structural systems lead to complexity in the numerical modelling, so several major assumptions were taken account before performing dynamic analysis. Within this context, a classical damping matrix is suggested to idealize the energy dissipation throughout the structure (Chopra, 2012). The viscous damping ratio of Kurşunlu Mosque was assumed as 3%, as admitted in other studies (Ciocci, Sharma and Lourenço, 2018; Kazaz and Kocaman, 2018) in which a Rayleigh damping strategy has been adopted during the nonlinear time history analyses:

$$\bar{C} = \alpha\bar{M} + \beta\bar{K} \tag{6.2}$$

In order to calculate Rayleigh viscous damping, α and β coefficients should be computed first. These parameters are found by defining the natural frequencies of two vibration modes that delimitate the range of interest. Equation 6.3 is used to determine Rayleigh coefficients from a specified damping ratio.

$$\zeta_\eta = \frac{\alpha}{2\omega_\eta} + \frac{\beta \cdot \omega_\eta}{2} \tag{6.3}$$

By considering same damping ratio for both i^{th} and j^{th} modes of the structure, Rayleigh damping coefficients can be determined as follows:

$$\alpha = \zeta \frac{2\omega_i\omega_j}{\omega_i+\omega_j} \qquad \beta = \zeta \frac{2}{\omega_i+\omega_j} \tag{6.4}$$

Figure 6.5 shows, in a graphical way, the definition of α and β parameters. The choice of proper i^{th} and j^{th} modes is of most importance, i.e. the specified modes should have a high contribution to the structures' response (Chopra, 2012).

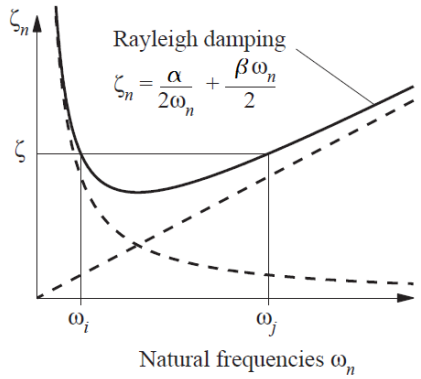

Figure 6.5. *Rayleigh damping (Chopra, 2012)*

To determine the Rayleigh damping coefficients of Kurşunlu Mosque, the selected i^{th} and j^{th} modes are given in Table 6.2. The selection of the modes relies on the contribution of the modes to the response. A minimum 80% of the participation of mass to response was taken account, as admitted in other study Ciocci, Sharma and Lourenço (2018). Table 6.2 gives that in the first 100 modes mass participates more than 80% in all directions. As a result of contribution of these modes, Rayleigh damping coefficients were calculated as $\alpha = 1.9854827$ and $\beta = 0.0001467$ with respect to 3% damping ratio.

Table 6.2. *Selected modes to calculate Rayleigh damping parameters*

Mode	f (Hz)	Cumulative Mass Participation (%)			ω_i (rad/s)
		X comp.	Y comp.	Z comp.	
1	5.78	60.7	0.2	0.0	36.32
100	59.3	90.4	89.8	82.7	372.59

6.3. Nonlinear Time History Analysis Results

The seismic performance of the retrofitted and non-retrofitted mosque is investigated in this section. Following to self-weight loading, dynamic loading was applied to the structure. Nonlinear time history analyses were carried out using the Hilber-Hughes-Taylor method which is also known as α-method. A secant method was selected to solve the nonlinear dynamic equilibrium solution. The convergence criterion for each iteration was defined in terms of internal energy with a tolerance value of 0.001. Bi-directional time history analyses were carried out by conducting two orthogonal components of each ground motion. It is important to mention that the response is more unfavorable when bi-directional dynamic analyses are performed than to the uni-axial ones. The seismic response improvement of the historical mosque, due to the retrofitting actions, was studied by examining different response parameters. Seismic response of the non-retrofitted and retrofitted historical mosque is investigated and presented regarding to change of in-plane and out-of-plane behavior. Effectiveness of the retrofitting were studied in terms of peak displacement, absolute acceleration response and principal tensile strain distribution on the structure. The damage occurs as a result of high relative displacements due to the low deformation capacity of the masonry materials. The principal tensile strains are good indicators of damage pattern on the structure. Figure 6.6 shows the location of control points aiming to understand the behavior of the structural components under dynamic loading. Selected control points are located at the top level of the wall, except the one at the dome.

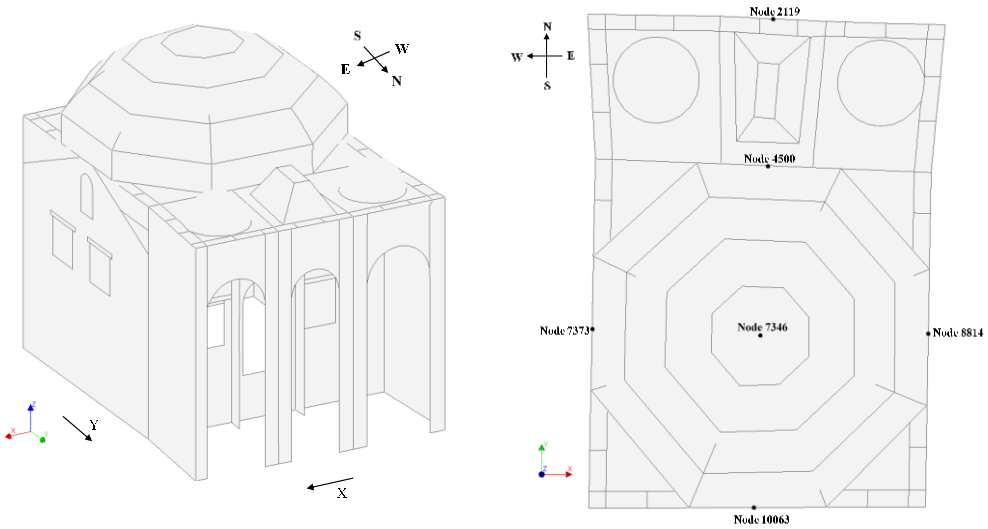

(a) Applied dynamic load directions *(b) Control nodes*

Figure 6.6. *Directions and locations of control points on the model*

6.3.1. Change in the displacement response

Peak displacement response was studied at different control points on both the non- and retrofitted models. Since there are many nodes on the given finite element model, considering few control points is not enough to generalize. Higher displacements are expected to occur at the top level of the walls therefore selected control points were located at this level (Figure 6.6(b)). At each control node, peak displacement values were selected from the time series of the response as given in Table 6.3-Table 6.8. The drift ratio at each control node was calculated to compare the serviceability of the structure by considering the reference values suggested in TYDRYK (2017) by Directorate General of Foundations. In the calculation of drift ratios, displacement values are divided by the maximum height of the bearing walls and the dome with respect to the base, which are 7.8 m and 11 m, respectively. When the load is applied in the transversal (X) direction, both East and West walls follow a predominant out-of-plane behavior whereas in the Portico, North and South walls have a predominant in-plane behavior. The contrary response occurs when the load is applied in the longitudinal direction (Y) (Figure 6.6). Results are given for both directions, X and Y, separately. Table 6.3, Table 6.4 and Table 6.5 give peak displacement values and variation of each in the transversal (X) direction and Table 6.6, Table 6.7 and Table 6.8 give the similar quantities for the longitudinal (Y) one.

Table 6.3. *Response on each control node in terms of peak displacement in the transversal (X) direction, Erzincan Earthquake*

Location	Behavior Mode	Node ID	*Model without Retrofitting*			*Model with Retrofitting*			Variation in Displacement (%)
			Peak Displacement (mm)	Corresponding Time (s)	Drift Ratio (%)	Peak Displacement (mm)	Corresponding Time (s)	Drift Ratio (%)	
South Wall	in-plane	10063	34	3.93	0.4	27	3.495	0.35	-20
East Wall	out-of-plane	8814	105	4.91	1.3	47	3.94	0.60	-55
West Wall	out-of-plane	7373	127	4.01	1.6	55	3.94	0.71	-56
Dome	-	7346	67	3.985	0.6	49	3.945	0.45	-27
North Wall	in-plane	4500	51	3.99	0.7	66	3.945	0.84	29
Portico	in-plane	2119	80	2.92	1.0	85	3.95	1.09	7

Table 6.4. *Response on each control node in terms of peak displacement in the transversal (X) direction, Düzce - Bolu Earthquake*

Location	Behavior Mode	Node ID	*Model without Retrofitting*			*Model with Retrofitting*			Variation in Displacement (%)
			Peak Displacement (mm)	Corresponding Time (s)	Drift Ratio (%)	Peak Displacement (mm)	Corresponding Time (s)	Drift Ratio (%)	
South Wall	in-plane	10063	93	6.06	1.2	100	6.03	1.28	7
East Wall	out-of-plane	8814	149	6.07	1.9	144	6.07	1.85	-3
West Wall	out-of-plane	7373	268	6.12	3.4	145	6.08	1.86	-46
Dome	-	7346	179	6.09	1.6	150	6.08	1.36	-16
North Wall	in-plane	4500	154	6.11	2.0	176	6.1	2.25	14
Portico	in-plane	2119	229	6.15	2.9	221	6.12	2.83	-4

Table 6.5. *Response on each control node in terms of peak displacement in the transversal (X) direction, Bingöl Earthquake*

Location	Behavior Mode	Node ID	*Model without Retrofitting*			*Model with Retrofitting*			Variation in Displacement (%)
			Peak Displacement (mm)	Corresponding Time (s)	Drift Ratio (%)	Peak Displacement (mm)	Corresponding Time (s)	Drift Ratio (%)	
South Wall	in-plane	10063	13	3.94	0.2	19	3.94	0.24	47
East Wall	out-of-plane	8814	65	3.99	0.8	37	3.96	0.48	-43
West Wall	out-of-plane	7373	48	7.45	0.6	33	3.95	0.42	-32
Dome	-	7346	41	3.96	0.4	33	3.95	0.30	-18
North Wall	in-plane	4500	41	3.96	0.5	43	3.96	0.56	6
Portico	in-plane	2119	62	3.98	0.8	55	3.97	0.70	-11

Table 6.6. *Response on each control node in terms of peak displacement in the longitudinal (Y) direction, Erzincan Earthquake*

Location	Behavior Mode	Node ID	*Model without Retrofitting*			*Model with Retrofitting*			Variation in Displacement (%)
			Peak Displacement (mm)	Corresponding Time (s)	Drift Ratio (%)	Peak Displacement (mm)	Corresponding Time (s)	Drift Ratio (%)	
South Wall	ouf-of-plane	10063	146	3.435	1.87	20	2.94	0.26	-86
East Wall	in-plane	8814	37	3.22	0.47	18	3.64	0.23	-50
West Wall	in-plane	7373	42	3.39	0.54	19	4.975	0.25	-54
Dome	-	7346	67	3.39	0.61	16	3.35	0.14	-76
North Wall	out-of-plane	4500	52	4.425	0.67	18	3.35	0.23	-66
Portico	out-of-plane	2119	69	4.445	0.89	17	3.35	0.22	-76

Table 6.7. *Response on each control node in terms of peak displacement in the longitudinal (Y) direction, Düzce - Bolu Earthquake*

Location	Behavior Mode	Node ID	*Model without Retrofitting*			*Model with Retrofitting*			Variation in Displacement (%)
			Peak Displacement (mm)	Corresponding Time (s)	Drift Ratio (%)	Peak Displacement (mm)	Corresponding Time (s)	Drift Ratio (%)	
South Wall	ouf-of-plane	10063	103	7.15	1.32	131	6.28	1.68	27
East Wall	in-plane	8814	73	6.26	0.93	148	6.26	1.90	104
West Wall	in-plane	7373	31	6.25	0.39	44	6.26	0.56	43
Dome	-	7346	83	6.3	0.75	111	6.27	1.01	35
North Wall	out-of-plane	4500	151	6.32	1.93	112	6.26	1.43	-26
Portico	out-of-plane	2119	195	6.34	2.49	118	6.25	1.51	-39

Table 6.8. *Response on each control node in terms of peak displacement in the longitudinal (Y) direction, Bingöl Earthquake*

Location	Behavior Mode	Node ID	*Model without Retrofitting*			*Model with Retrofitting*			Variation in Displacement (%)
			Peak Displacement (mm)	Corresponding Time (s)	Drift Ratio (%)	Peak Displacement (mm)	Corresponding Time (s)	Drift Ratio (%)	
South Wall	ouf-of-plane	10063	55	7.46	0.70	18	6.31	0.23	-67
East Wall	in-plane	8814	11	4.01	0.14	16	3.99	0.20	50
West Wall	in-plane	7373	6	7.39	0.08	16	6.17	0.21	166
Dome	-	7346	22	7.44	0.20	14	6.15	0.13	-33
North Wall	out-of-plane	4500	26	6.19	0.33	16	4.68	0.21	-38
Portico	out-of-plane	2119	28	6.2	0.36	17	6.14	0.21	-40

Generally, the introduction of the steel girders allowed to reduce the obtained out-of-plane peak displacements at the control points, as depicted in Table 6.3 - Table 6.8. Still, it is important to address that the peak displacement in the in-plane direction was increased, except the Erzincan ground motion case study (Table 6.6) wherein the in-plane peak displacements decrease for all the control points. According to the results, Bolu Earthquake induces, in both directions, the larger displacement response for the retrofitted and non-retrofitting models (Table 6.4 and Table 6.7). Although values reduce in terms of ratio, the magnitude of the displacements is, at some of the structural elements, high for the retrofitted model. These values can be an indication for severe damage of the masonry elements, because the material can hardly sustain large displacements due to its low tensile strength. In addition to structural components, peak displacement values at the top point of the dome was studied and it is possible to say that steel girders mitigate the displacement at that point.

A guideline for the seismic assessment of historical structures has been published by the Directorate General of Foundations of Republic of Turkey in 2017 (TYDRYK, 2017), wherein performance limit states for historical structures have been suggested and given in Figure 6.7. Results obtained from nonlinear dynamic analyses

were compared with the suggested drift ratio limits, see Figure 6.8. The charts depict drift ratio at the control points of each structural component on both retrofitted and non-retrofitted models, as a result of conducted ground motions. It is clear to say that, the response has, the most critical results for both orthogonal components and for both retrofitted and non-retrofitted structure when Bolu ground motion is considered. Although a reduction in peak displacement was observed between the models, the vast majority of the control nodes exceed the failure prevention limit in both models in both directions.

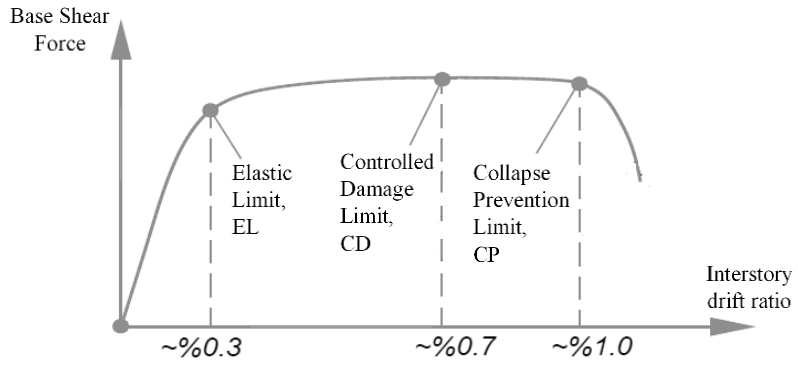

Figure 6.7. *Pushover curve, inter-story drift ratio limits suggested by the Turkish guideline for historical structures (TYDRYK, 2017)*

On the other hand and as expected, a reduction in the drift ratio was observed due to the application of the steel girder when the structure was subjected to the Erzincan and Bingöl earthquakes. Also, for all the control nodes of the retrofitted model and for the Erzincan earthquake, the response is below the elastic limit. Conversely, the non-retrofitted model lead to higher drift ratios which correspond to controlled damage and failure zones, see in Figure 6.8(b).

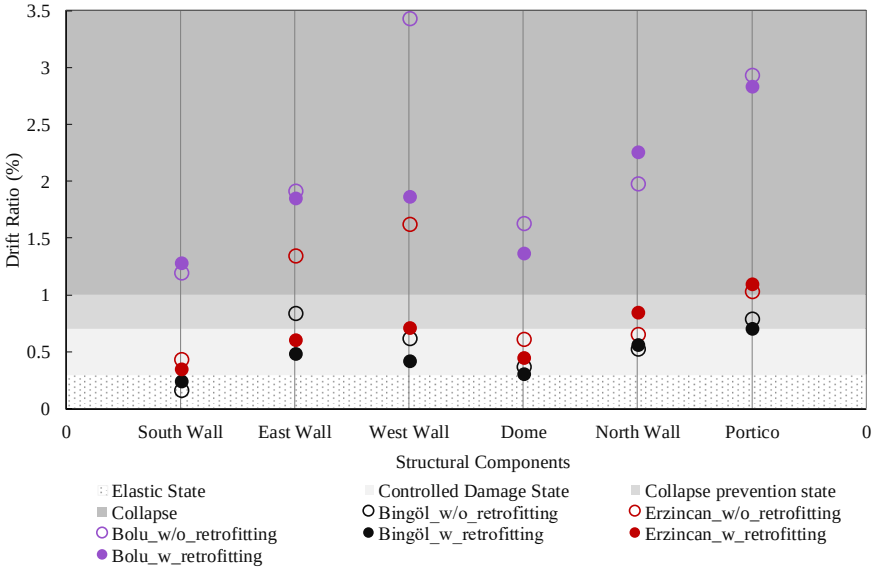

(a) Transversal (X) direction

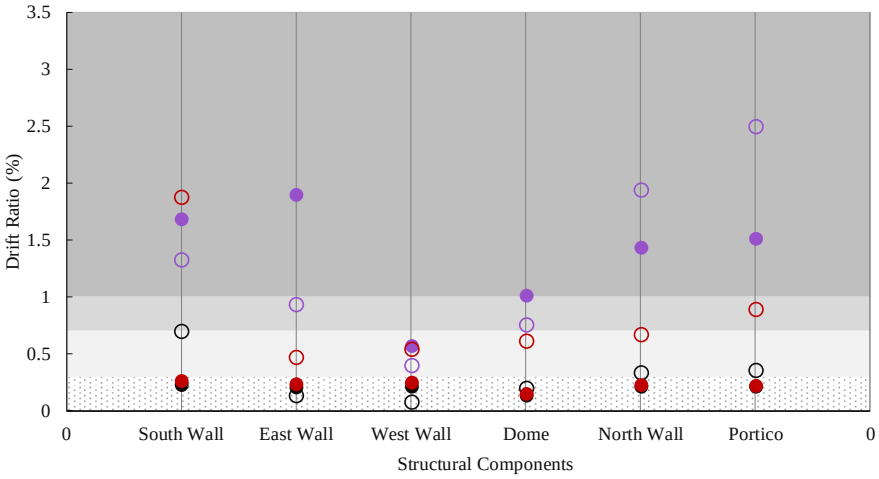

(b) Longitudinal (Y) direction

Figure 6.8. *Comparison of drift ratio demands on each structural component regarding to (TYDRYK, 2017)*

At last, it is important to mention that in the Turkish guideline, the performance limit states are only defined according to drift ratio values which are given as a specific value without taking account any parametric features. Dolatshahi, Nikoukalam, and Beyer (2018) states that empirical models are used to estimate in-plane deformation capacity in terms of drift capacity of the unreinforced masonry walls in the literature. Various empirical models are proposed by several codes by considering different parameters such as the failure mode, the aspect ratio, the axial load ratio, the normalized shear span, wall size and slenderness. In their study, sensitivity of the drift capacity has been studied by shear span, the aspect ratio, the axial load and the size of the wall in terms

of empirical relation. The study shows that drift capacity of the URM is influenced by different parameters (Dolatshahi, Nikoukalam, and Beyer, 2018).

6.3.2 Change in the out-of-plane displacement

The study of the out-of-plane dynamic behavior of masonry structures is still a challenge. Past events demonstrated that out-of-plane failure mechanisms tend to occur if a monolithic behavior of the structure is not assured, the so-called box behavior (Lourenço *et al.*, 2017). The out-of-plane displacement-time history at each control nodes are given in Figure 6.9 and Figure 6.10 for both x-(transversal) and y-(longitudinal) direction. These figures were plotted by considering parallel walls on the same plot to identify the change in response as a whole. Figure 6.9(a) shows that the response at the two control points has similar trend but both control nodes shift in the opposite direction from their origin. This may represent the expansion of the dome.

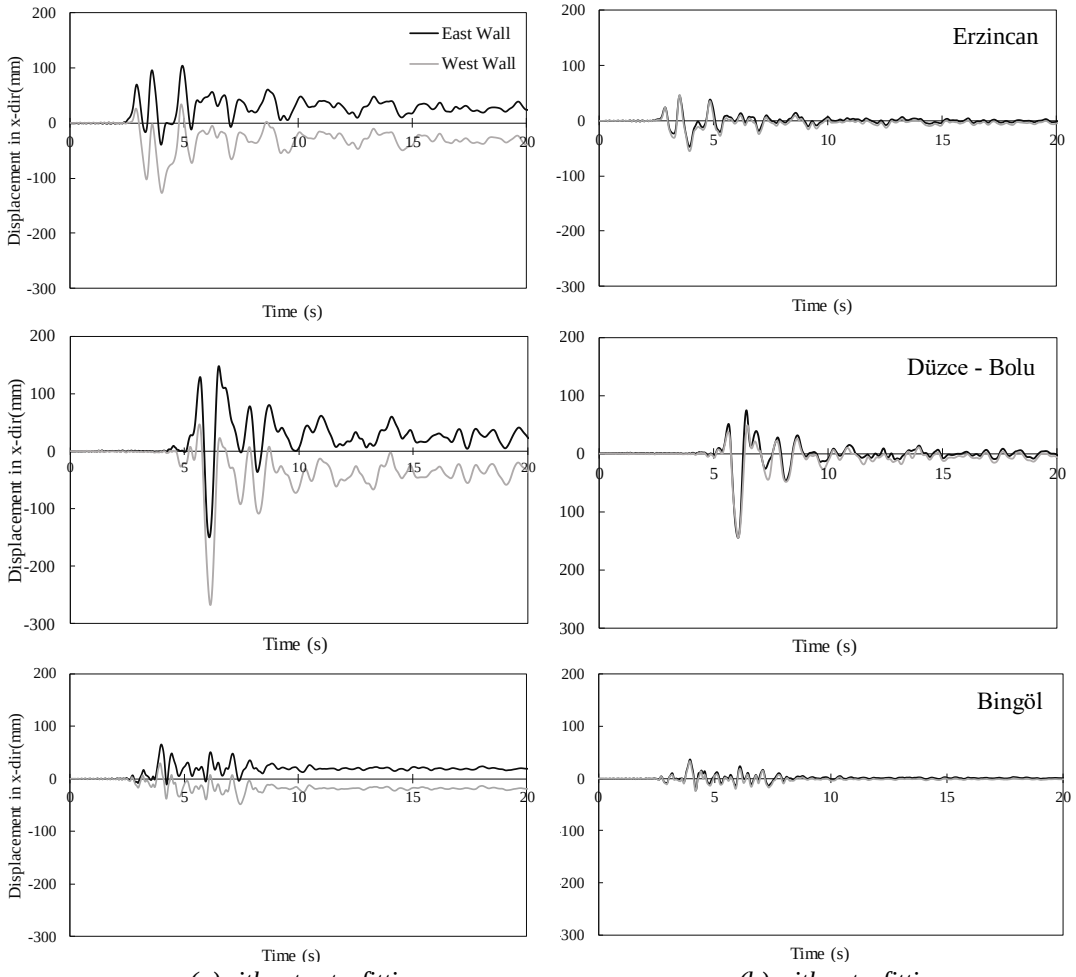

(a)without retrofitting *(b) with retrofitting*

Figure 6.9. *Displacement-time series of control nodes of East and West Walls for 3 ground motions in X direction*

More detailed investigation on this was done in the following subsection 6.3.3. In fact, residual displacements were observed on the non-retrofitted model in all dynamic cases (Figure 6.9(a) and Figure 6.10(a)). In Figure 6.9(b) and Figure 6.10(b), it is obvious that steel girder retrofitting mitigates residual displacements on the structure. The response of the nodes depicts similar trend with similar amplitudes and therefore integrated structural behavior can be concluded (Figure 6.9(b) and Figure 6.10(b)).

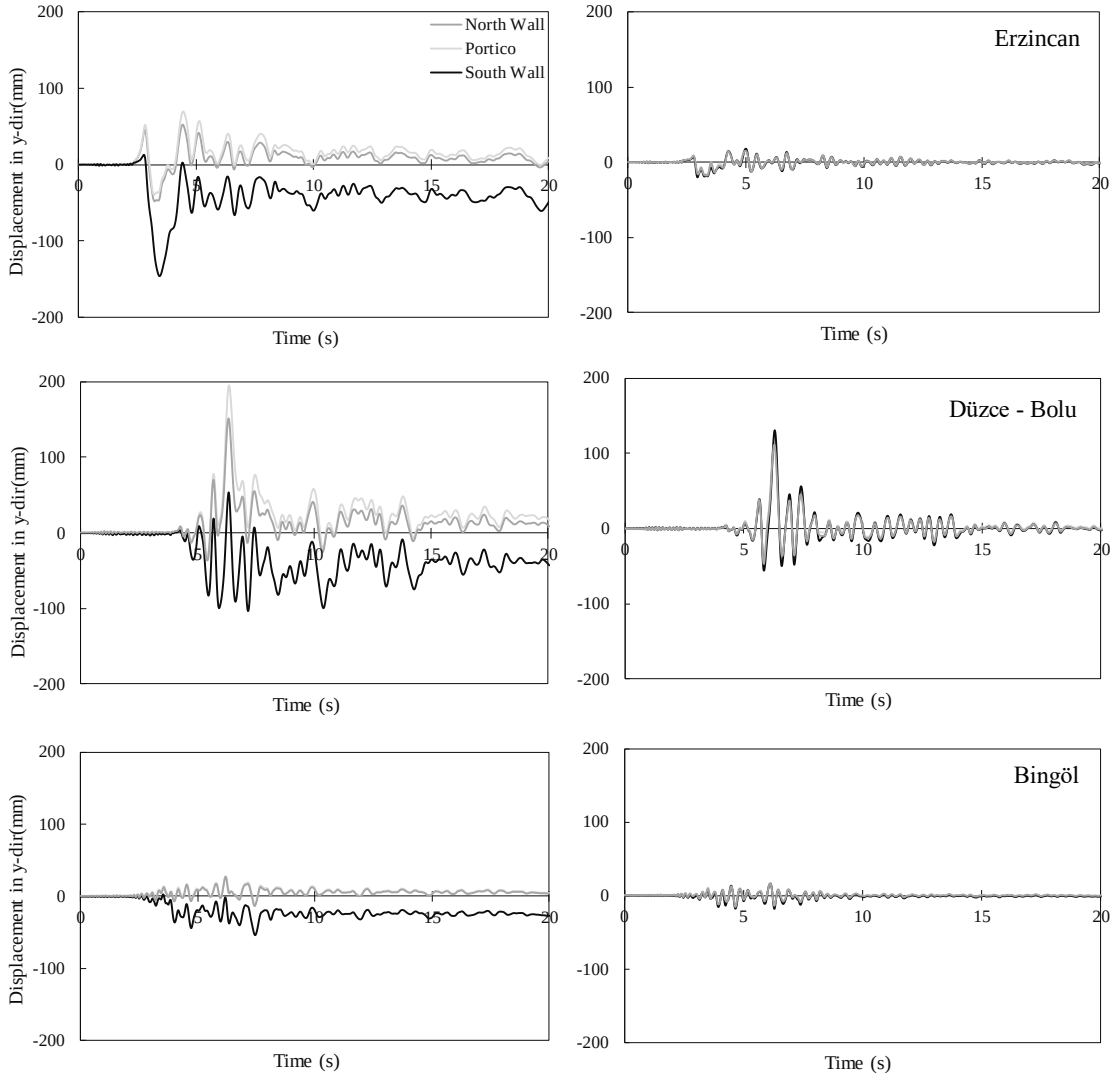

(a)without retrofitting *(b) with retrofitting*

Figure 6.10. *Displacement-time series of control nodes of North Wall, South Wall and Portico for 3 ground motions in Y direction*

Figure 6.11 and Figure 6.12 shows the effect of the steel girder retrofitting on the displacement-history. The response of each structural component considering three ground motions was investigated. In general and focusing on the imposed residual displacements, the steel girder retrofitting improved the structural behavior. A considerable decrease in peak displacement was observed in Erzincan case (Figure 6.11(a) and Figure 6.12(a)). Although the peak displacement was reduced in Figure 6.11 and Figure 6.12 with the applied retrofitting scheme, the imposed displacement responds are still high and can be an indication for structural damage.

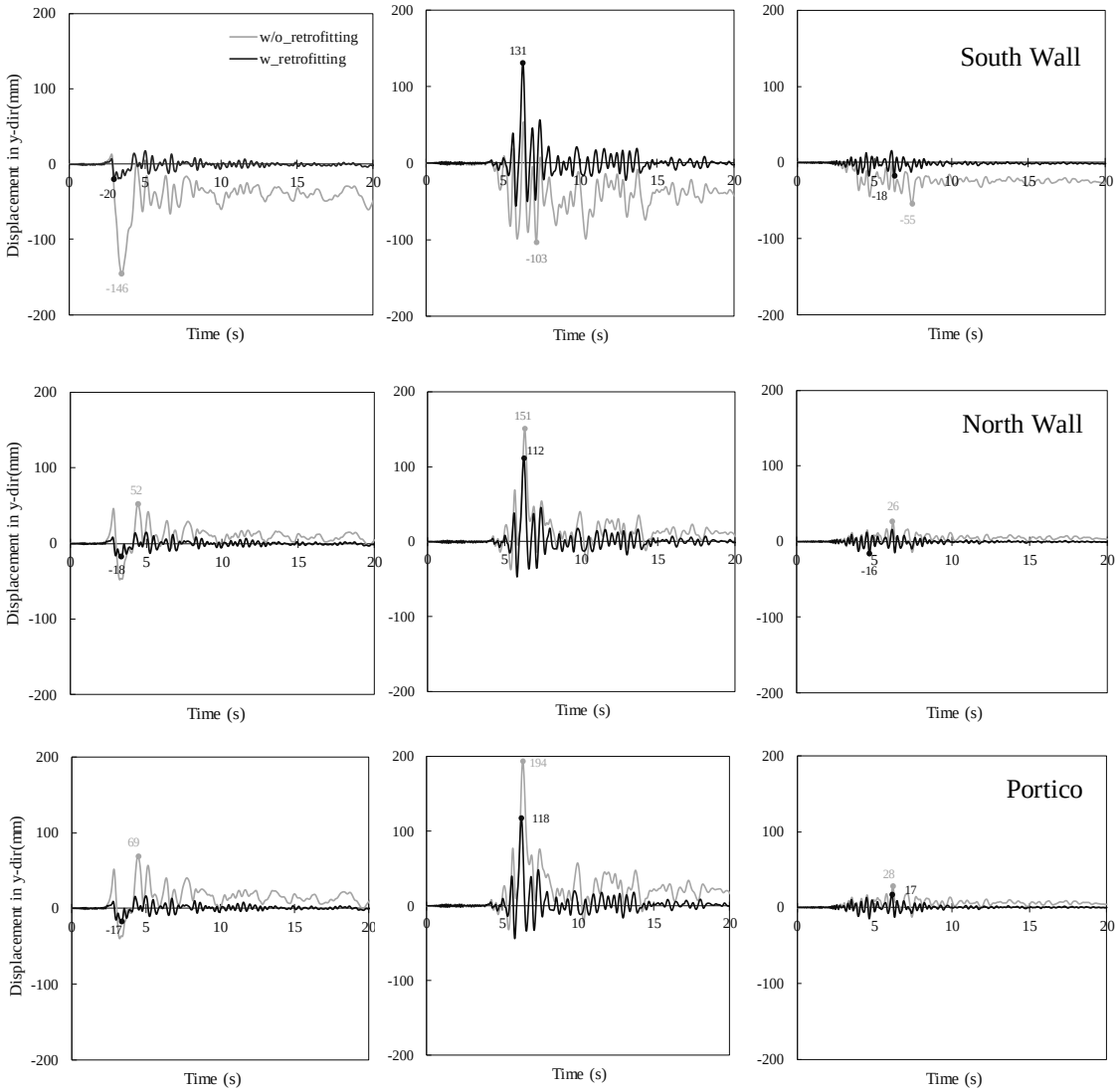

(a) Erzincan *(b) Düzce - Bolu* *(c) Bingöl*

Figure 6.11. *Change in response of control points on South Wall, North Wall and Portico due to retrofitting in terms of out-of-plane displacement*

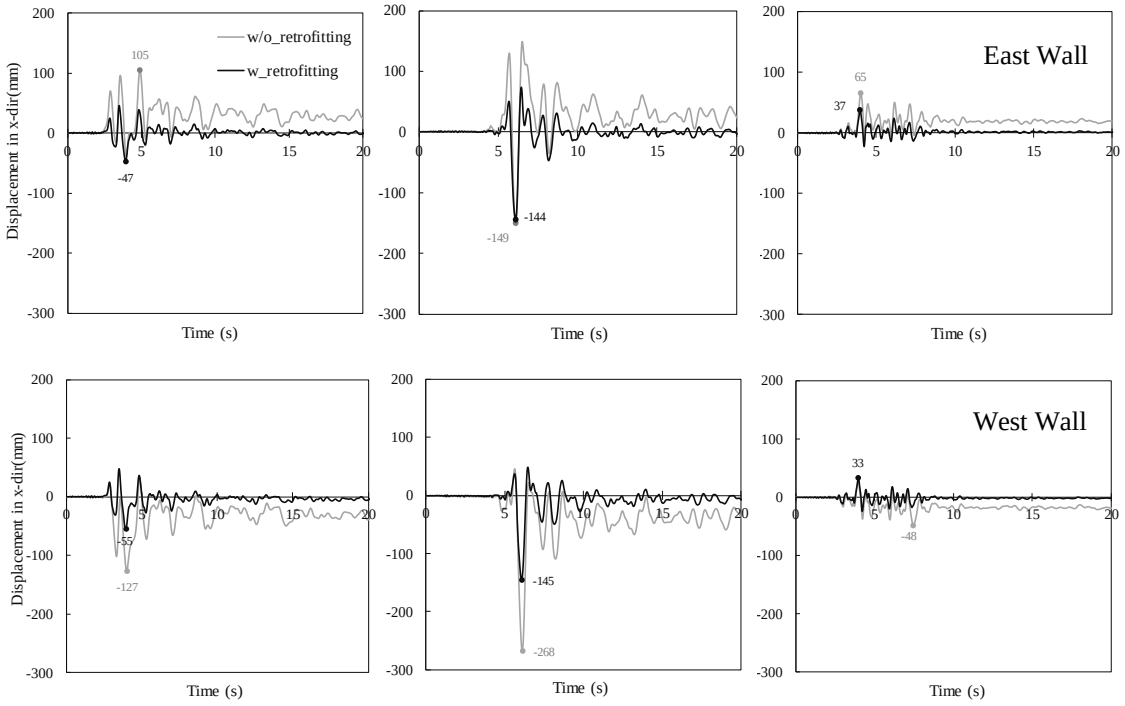

(a) Erzincan *(b) Düzce - Bolu* *(c) Bingöl*

Figure 6.12. *Change in response of control points on East Wall and West Wall due to retrofitting in terms of out-of-plane displacement*

Displacement-time series and peak displacement at each control point at the top level may not be enough to identify the change in response. Therefore, displacement response in the out-of-plane direction along the height of each wall were plotted. In order to plot these curves, time step of the peak displacement response occurred at the control point on the non-retrofitted model, was considered. The vertical section of the mid-length of the wall was considered as the section cut (Figure 6.13(d) and Figure 6.15(d)). On the other hand, the behavior of the edge parts of the portico on each façade are different from the middle section of the main walls, due to the connection with North façade, and, therefore, the description in these parts is given separately. In all plots, the section of curves above 7.8m represents the drum where the dome is constraint. Steel girders were anchored at the bottom and top level of the drum, so this part of the structural component was also examined to see the variation in the response. Due to the fact that two parallel walls do not have maximum out-of-plane displacements at the same time step, both time steps when south or north façade has the maximum displacement were considered which are given in Figure 6.13 and Figure 6.14. The same consideration was made for east and west façade as well in Figure 6.15 and Figure 6.16. Regarding to these figures, it is worth

to mention that implementing steel girders allow reducing the observed out-of-plane displacement of the walls along the height. However, Figure 6.15 and Figure 6.16 show that the retrofitting is not that much effective on the portico walls as on the main walls.

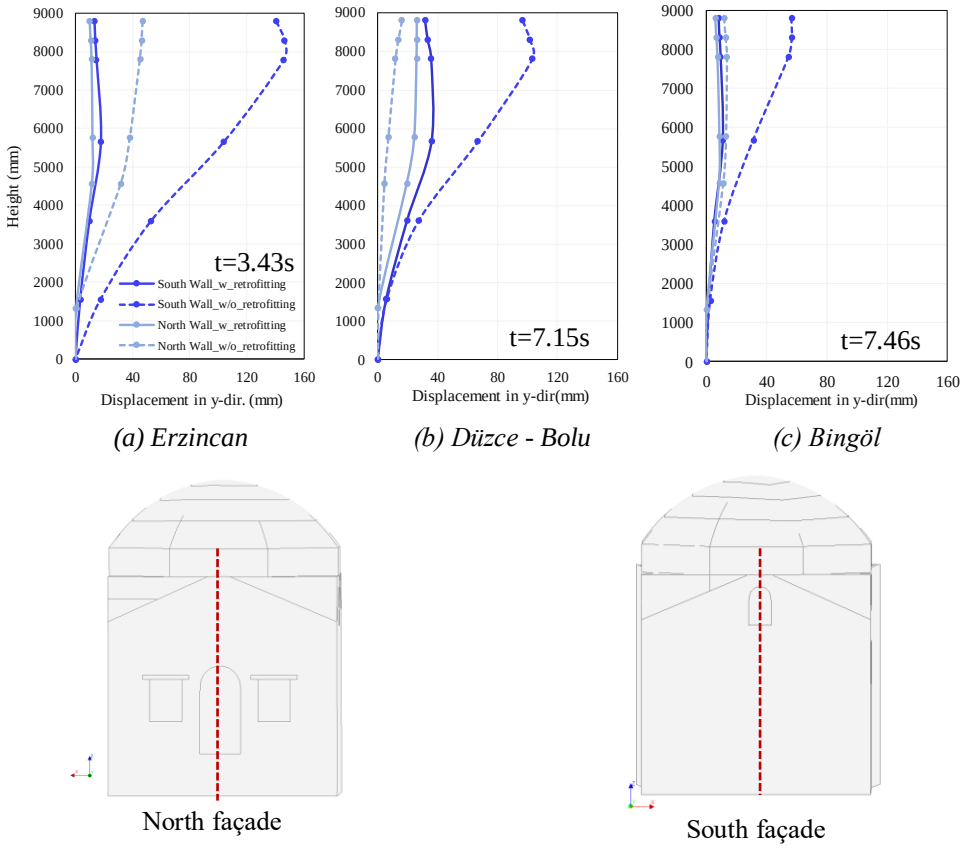

(a) Erzincan *(b) Düzce - Bolu* *(c) Bingöl*

(d) Location of section cuts

Figure 6.13. *Change in out-of-plane behavior at time step when South Wall has peak displacement*

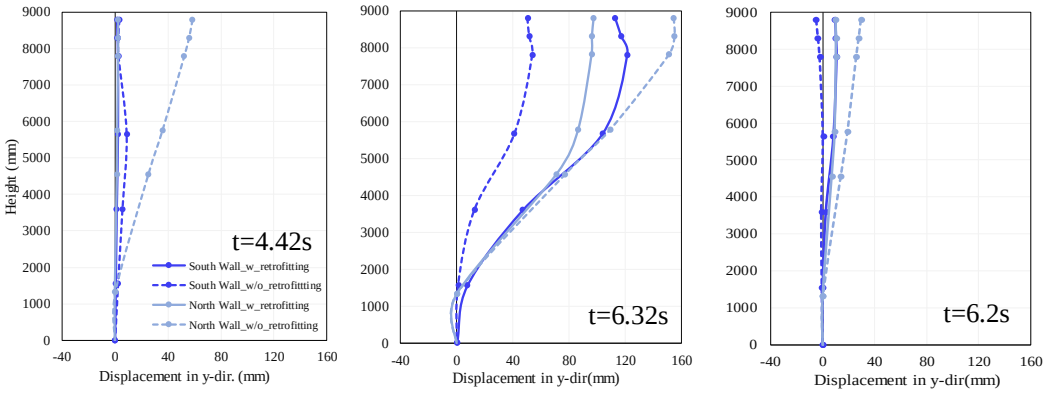

(a) Erzincan *(b) Düzce - Bolu* *(c) Bingöl*

Figure 6.14. *Change in out-of-plane behavior at time step when North Wall has peak displacement*

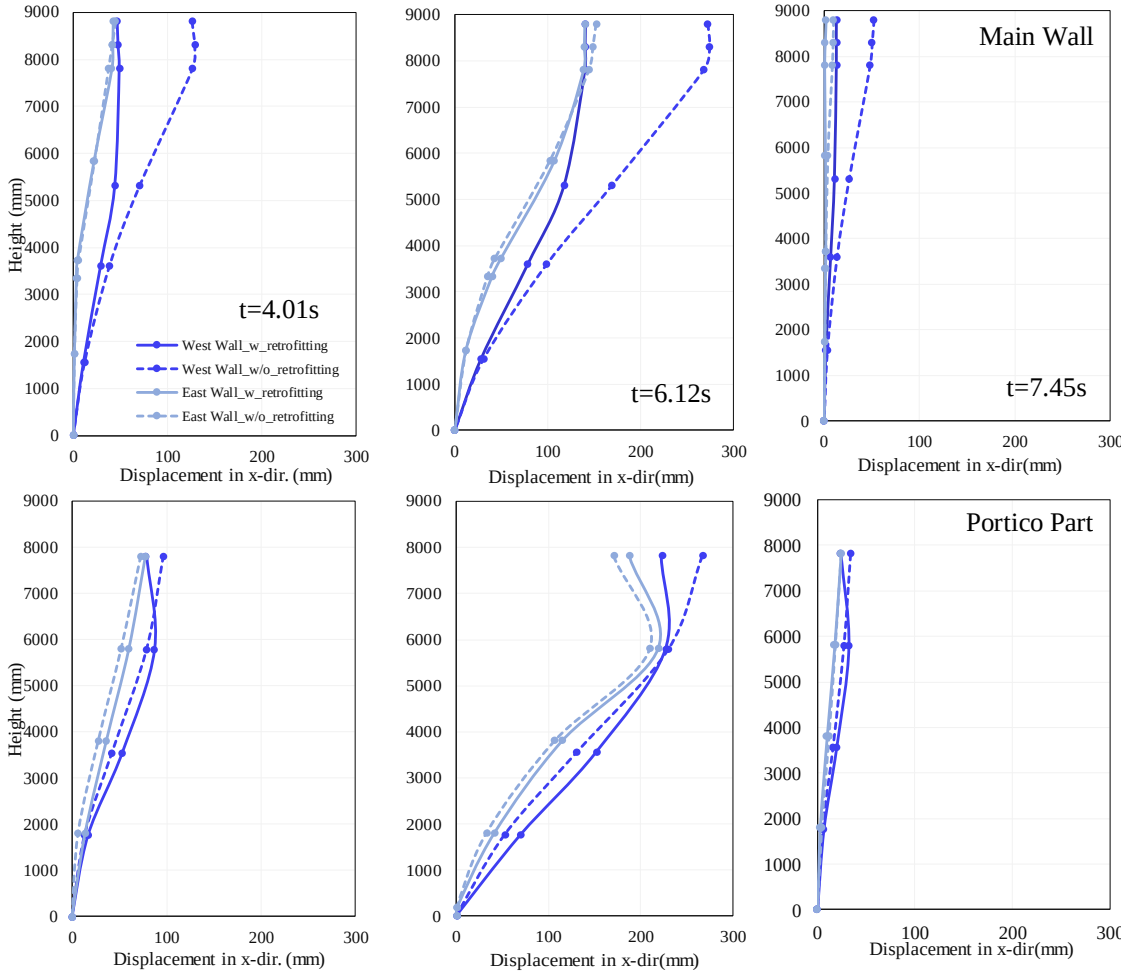

(a) Erzincan *(b) Düzce-Bolu* *(c) Bingöl*

(d) Location of section cuts

Figure 6.15. *Change in out-of-plane behavior in terms of absolute displacement at time step when West Wall has peak displacement*

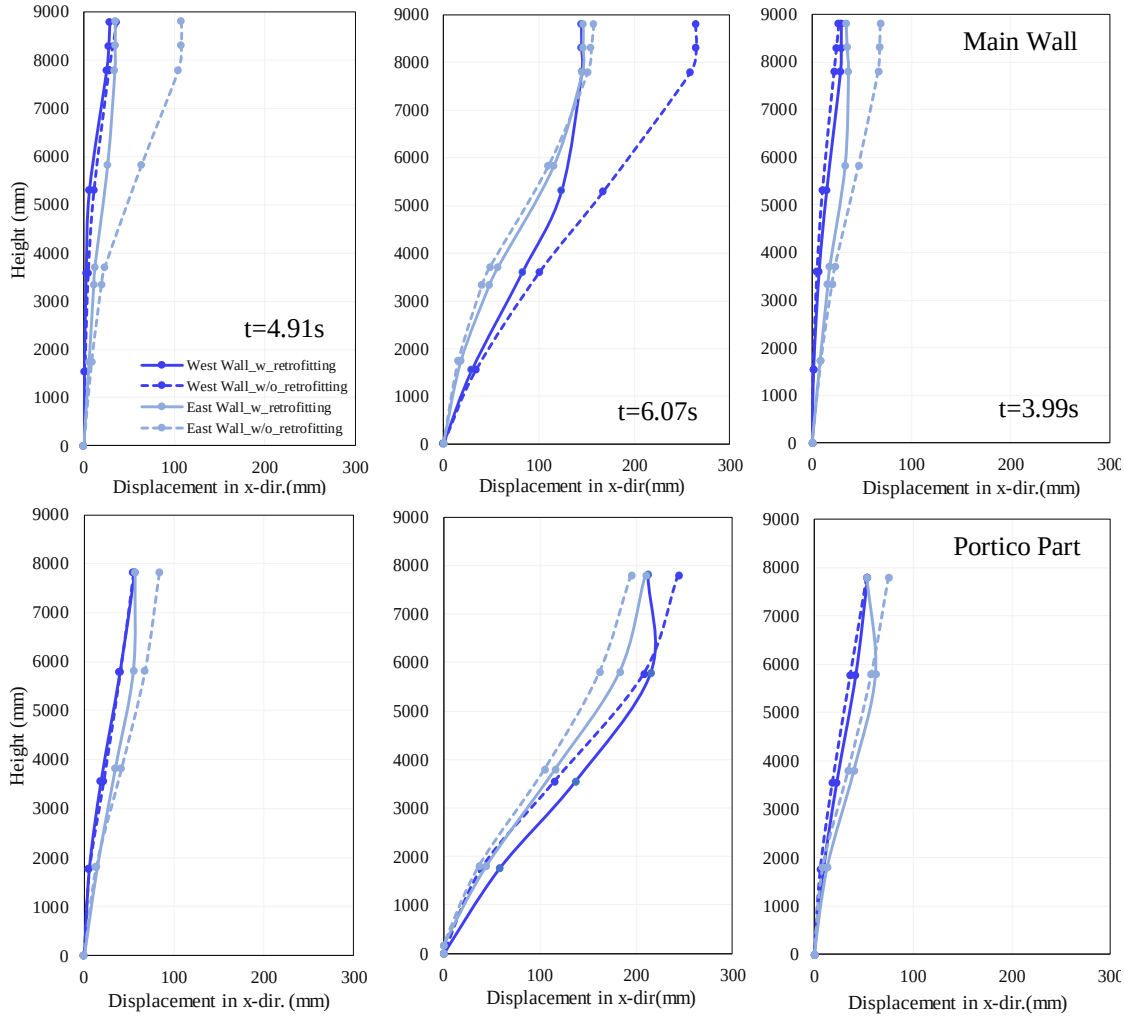

(a) Erzincan *(b) Düzce-Bolu* *(c) Bingöl*

Figure 6.16. *Change in out-of-plane behavior in terms of absolute displacement at time step when East Wall has peak displacement*

6.3.3 Change in relative out-of-plane displacement at the dome supporting walls

The retrofitting action was conducted to provide the box behavior to the structure, by improving the connection between contiguous structural elements. The dome experiences expansion if the integral behavior of its supports, namely the load bearing walls and drum, is not provided. A schematic representation of the dome expansion is given in Figure 6.17 by considering west and east walls. In the non-retrofitted model, different displacements are expected on each parallel wall due to the lack of integrated structural behavior, and, therefore higher relative displacements can be observed (Figure 6.17(b)). Since the residual displacements were observed on the displacement histories for the non-retrofitted case in the previous subsections, relative displacements of the walls were investigated in terms of residual displacements. Once the retrofitted

model achieves box behavior, lower relative residual displacements are expected comparing to the first case (Figure 6.17(c)). Providing that $\Delta res_1 >> \Delta res_2$, severe cracks are expected in the non-retrofitted case.

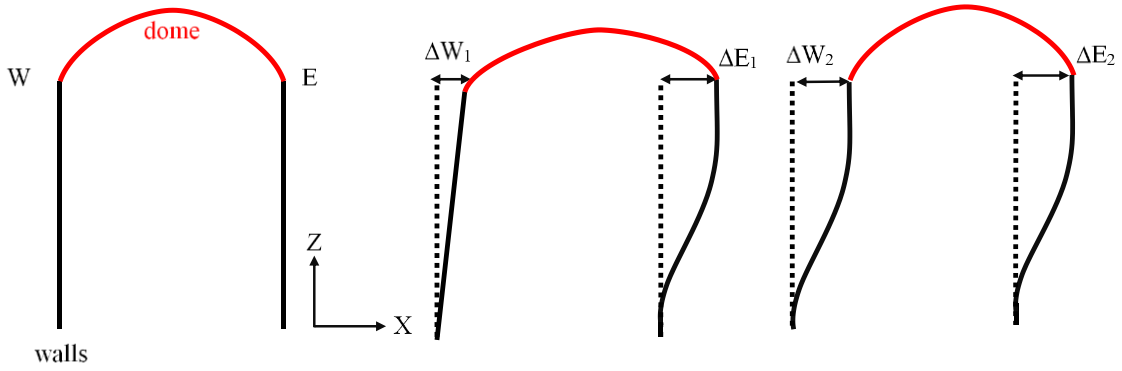

Figure 6.17. *Schematic representation of the residual displacements on the dome supporting walls*

In this sense, the relative out-of-plane movement of the adopted control nodes on the dome supporting walls were investigated. For the transversal direction, the relative displacement was calculated with respect to the west wall (Figure 6.18). In the longitudinal direction, the process was carried by considering the south wall as the reference and difference in displacement-time series of the north and south wall was plotted (Figure 6.19). Response of the both models are given in Figure 6.18 and Figure 6.19 for each ground motion in terms of relative out-of-plane displacement at the dome supporting walls.

Additionally, relative residual displacements have been calculated by taking the average of the time interval after the ground motion reaches almost its 90% energy which corresponds to the time interval between 10 to 20 seconds of each record as shown in Figure 6.4. Relative out-of-plane displacement in the non-retrofitted model is substantially high which lead to expansion of the dome causing high tensile stresses. In fact, severe damage in the form of large cracks is observed on the dome during the site investigations. It is possible to say that the observed damage seems to be resulted due to the high relative displacements in the out-of-plane directions. On the contrary, the retrofitted model presents considerably low relative out-of-plane displacements which

show that the expansion of the dome and severe damage has been limited by introducing the steel retrofitting.

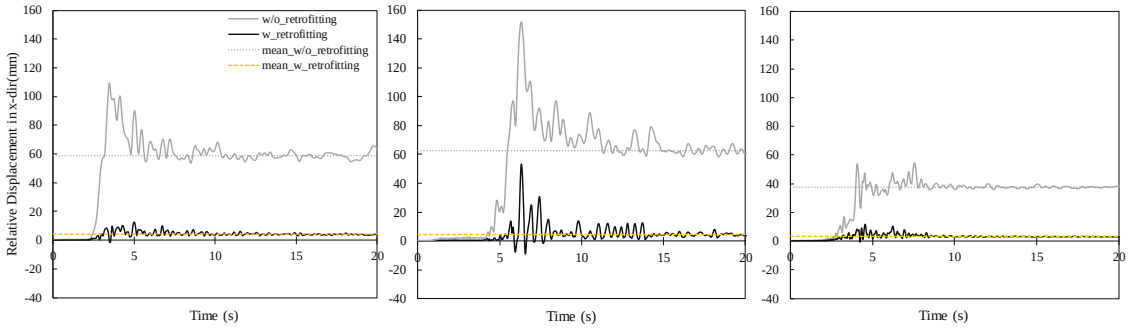

(a)Erzincan *(b) Düzce-Bolu* *(c)Bingöl*

Figure 6.18. *Change in out-of-plane displacement relative to the west wall*

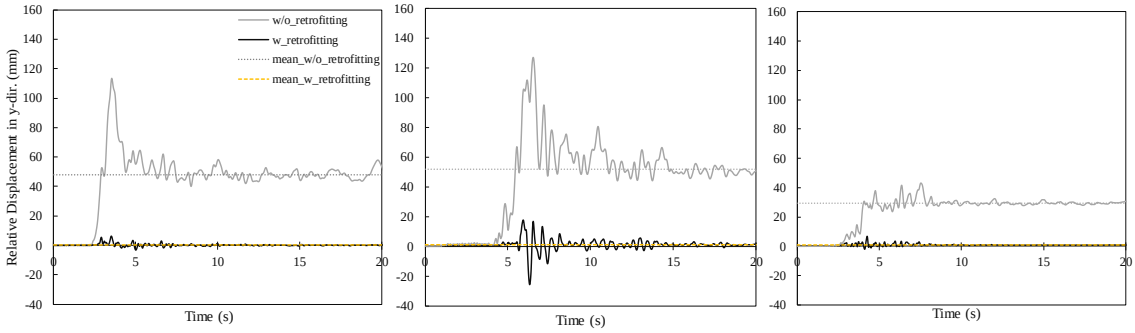

(a)Erzincan *(b) Düzce-Bolu* *(c)Bingöl*

Figure 6.19. *Change in out-of-plane displacement relative to the south wall*

6.3.4 Change in the in-plane displacements

Load bearing walls are considerably stiffer in the in-plane direction when compared to the out-of-plane one. Out-of-plane behavior of the structural components were mitigated due to retrofitting that are shown in the previous sections and variation of in-plane response due to steel girder retrofitting was investigated in this section. In Figure 6.20 and Figure 6.21, displacement response on each control points are given with respect to time. Structural components having in-plane behavior are given according to their longitudinal and transverse orientation, in Figure 6.20 and Figure 6.21, respectively. Larger displacements were imposed by the Bolu Earthquake whereas Bingöl input results in smaller displacements in both retrofitted and non-retrofitted cases. Change in response due to steel girder retrofitting is not noticeable (as in the out-of-plane case) except for the

Bolu Earthquake, see in Figure 6.20(b). Figure 6.22 and Figure 6.23 show the change in displacement-time series of each control points due to steel girder retrofitting with respect to structural components. A slight difference between the two models is visible.

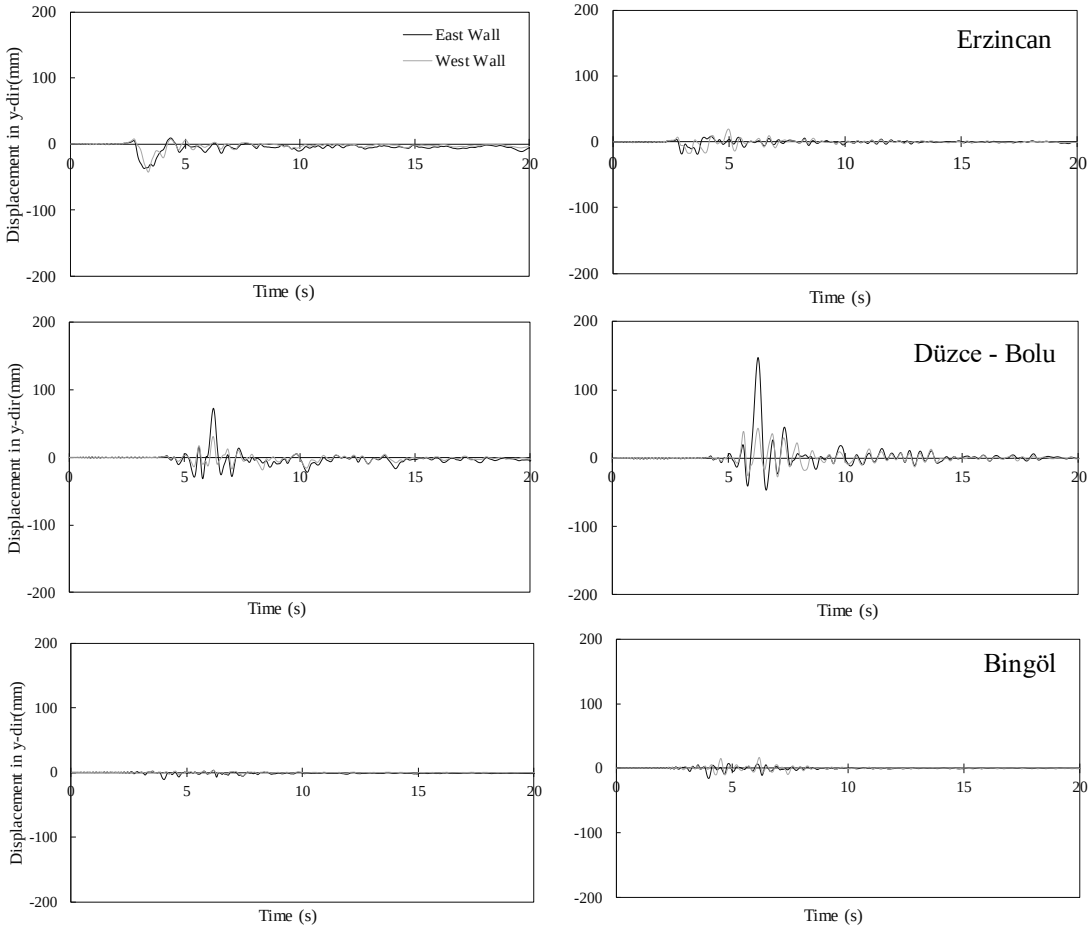

(a)without retrofitting *(b) with retrofitting*

Figure 6.20. *Displacement-time series of control nodes of East and West Walls for 3 ground motions*

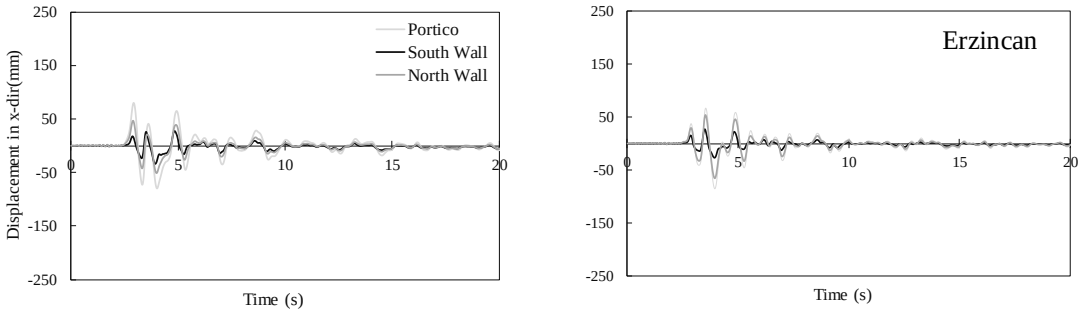

(a)without retrofitting *(b) with retrofitting*

Figure 6.21. *Displacement-time series of control nodes of the north wall, south wall and portico for 3 ground motions*

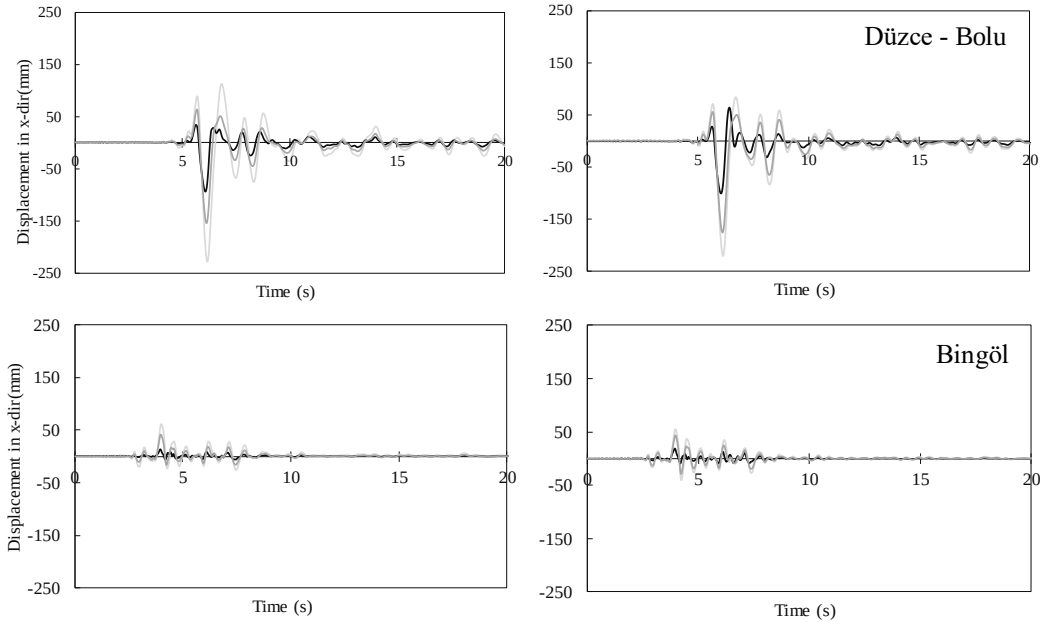

(a)without retrofitting *(b) with retrofitting*

Figure 6.21. (continued) *Displacement-time series of control nodes of the north wall, south wall and portico for 3 ground motions*

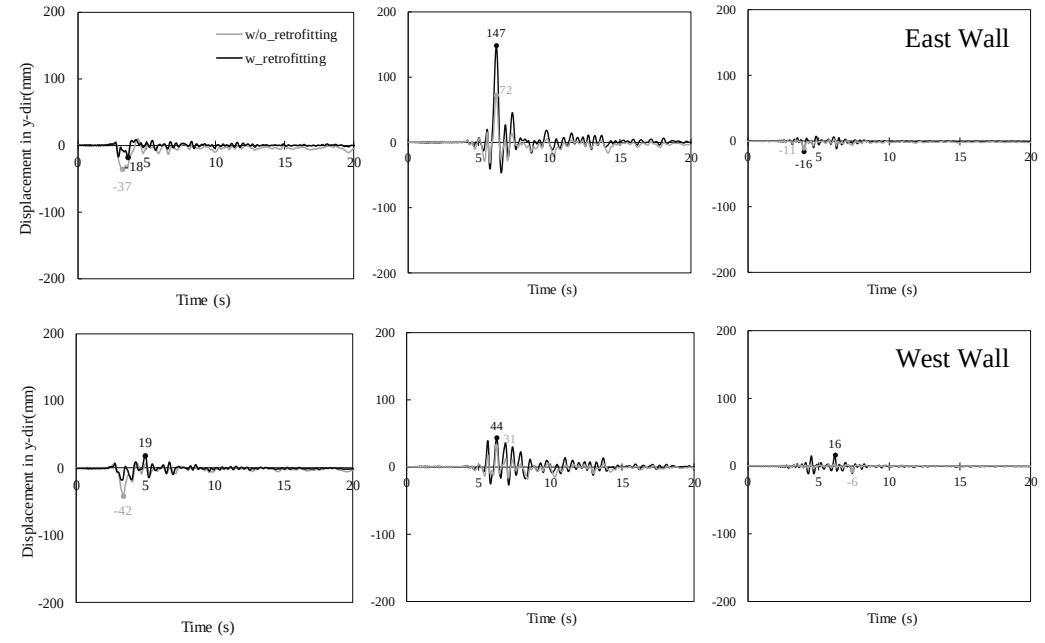

(a) Erzincan *(b) Düzce - Bolu* *(c) Bingöl*

Figure 6.22. *Change in response of control points on the east wall and west wall due to retrofitting in terms of in-plane displacement*

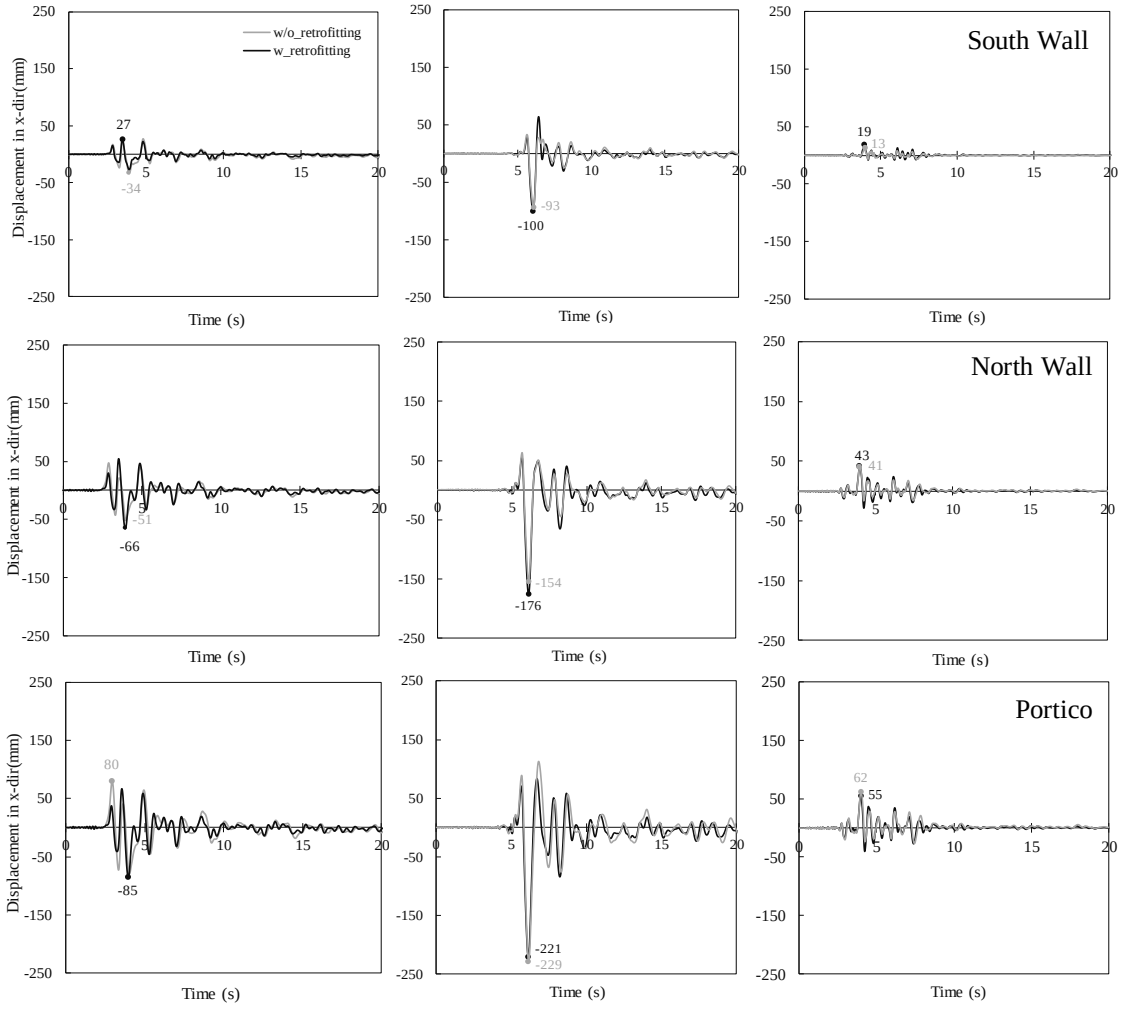

(a) Erzincan *(b) Düzce - Bolu* *(c) Bingöl*

Figure 6.23. *Change in response of control points on South Wall, North Wall and Portico due to retrofitting in terms of in-plane displacement*

According to the results of the in-plane displacements, the parallel walls deforms with different amplitudes in all cases and the retrofitting seem to be ineffective. Within the applied retrofitting scheme, it can be observed that so-called box-behavior was achieved for the investigated mosque by limiting the out-of-plane response of the walls. On the other hand, this behavior imposed additional displacements on the in-plane bearing walls. This outcome can be clearly observed in the in-plane response of the walls under the Düzce-Bolu Earthquake (Figure 6.20).

6.3.5 Change in the absolute acceleration response

Absolute acceleration is another important engineering parameter in terms of seismic forces acted on both structural and non-structural components. Historical

masonry buildings are very stiff structures that respond with high spectral accelerations. Therefore, serviceability of the masonry components should be satisfied. Absolute acceleration response on the both non-retrofitted and retrofitted model was computed at the highest point of the numerical model, i.e. the top point of the dome. Acceleration-time series on the control point are given for non-retrofitted and retrofitted mosque in both transversal and longitudinal directions (Figure 6.24 and Figure 6.25). Increased absolute acceleration values were observed due to steel girder retrofitting in both transversal and longitudinal direction. The response of the control point has similar trend but with higher amplitudes on the retrofitted mosque comparing to the original case. It can be inferred from Figure 6.24 and Figure 6.25 that with the achievement of box-behavior by means of the applied retrofitting scheme, the absolute acceleration demands at the dome is increased. This will certainly increase the inertial forces imposed on the dome.

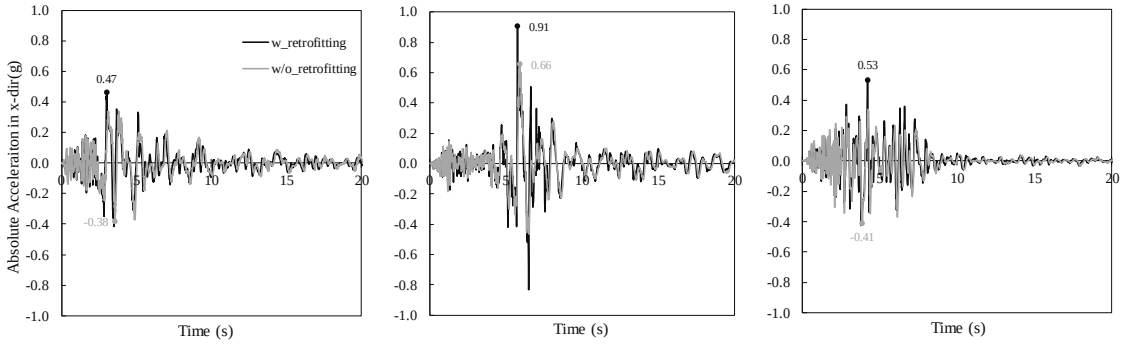

(a) Erzincan *(b) Bolu* *(c) Bingöl*

Figure 6.24. *Change in absolute acceleration demand in transverse direction*

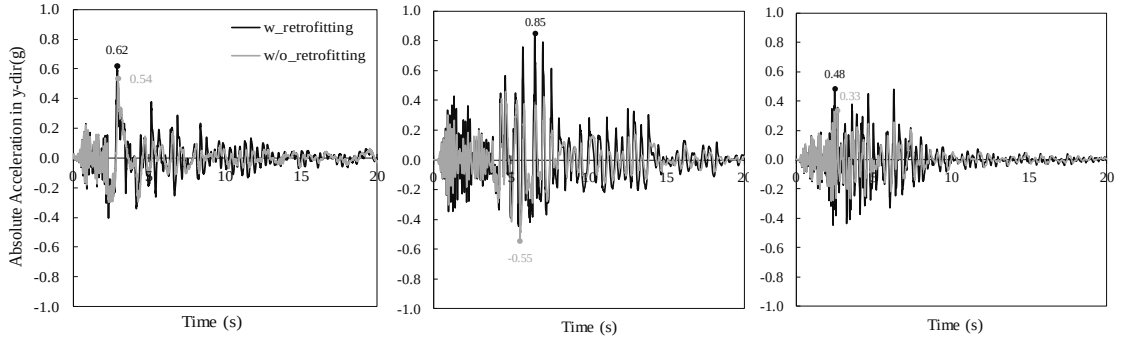

(a) Erzincan *(b) Bolu* *(c) Bingöl*

Figure 6.25. *Change in absolute acceleration demand in longitudinal direction*

6.3.6 Change in the strain distribution

Masonry structures typically have a low tensile strength and as already stated the principal tensile strain distribution is a good qualitative damage indicator. The numerical modelling adopts a fictitious homogenous material and, consequently, the strain values displayed do not correspond to the values which are expected to occur on the real structure. Principal tensile strains are plotted for the time step when each numerical model has its own critical condition. At the time step, when the control point reaches the peak displacement value on each structural component, the principal tensile strain distribution of the global structure was examined and compared with each other. The most critical plot was selected. The plots are given in Figure 6.26 and Figure 6.27 for the most critical case of the Bolu Earthquake, whereas is possible to conclude change in crack pattern when the retrofitting is introduced on the numerical model.

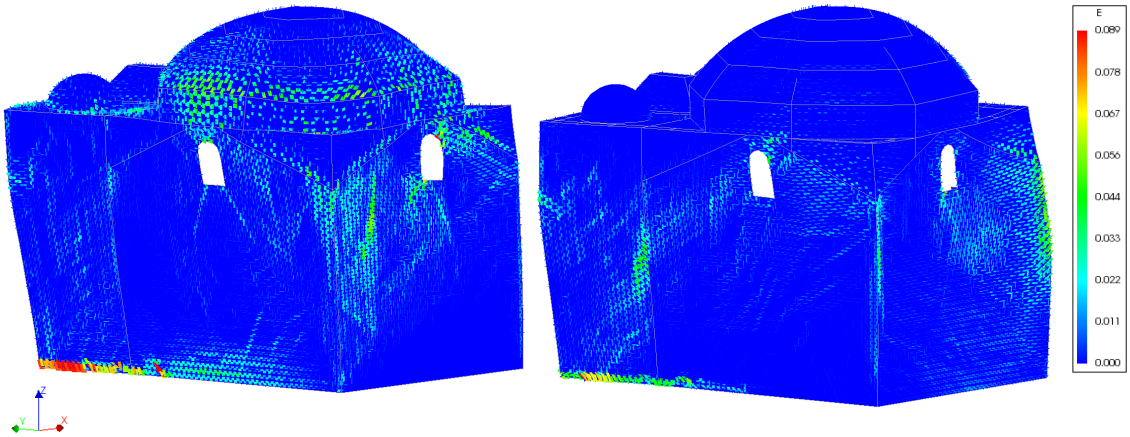

(a) without retrofitting (t=6.12s) *(b) with retrofitting (t=6.28s)*

Figure 6.26. *Principal tensile strains of South-West façade resulted by Bolu record, deformed shape scale factor:5*

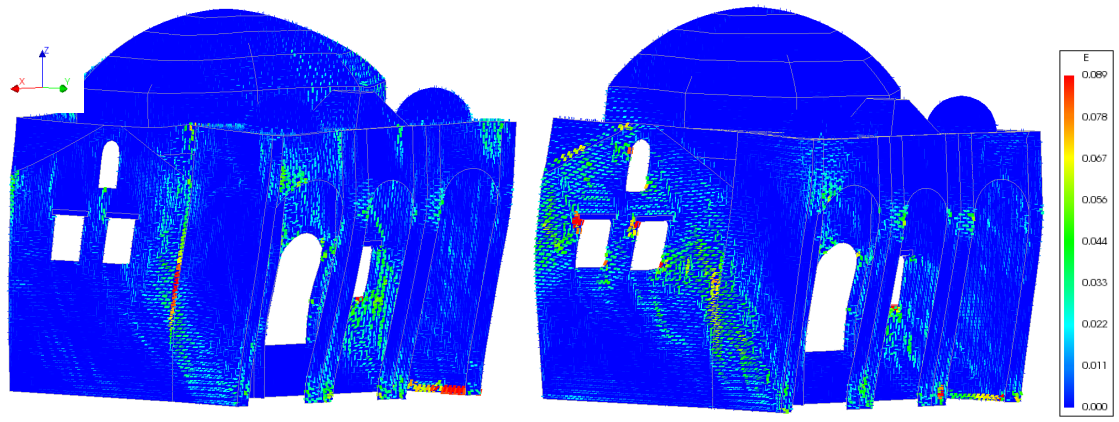

(a) without retrofitting (t=6.12s) *(b) with retrofitting (t=6.28s)*

Figure 6.27. *Principal tensile strains of North-East façade resulted by Bolu record, deformed shape scale factor:5*

For instance, in Figure 6.26(a), it is clear that a tensile strain concentration on the dome which is resulted by the high tensile stress demands on that section. This illustrates that west and south wall were subjected to an out-of-plane behavior which result in an expansion of the western and southern parts of the dome. Moreover, vertical damage is dominant on the walls without retrofitting (Figure 6.26(a) and Figure 6.27(a)). When steel girders were introduced, the damage due to out-of-plane mechanism was reduced. Regarding to Bolu results, the change in failure mechanism can be originated by the retrofitting actions adopted. In Figure 6.27, the vertical damage on the longitudinal wall is dominated by diagonal cracking which is related with the in-plane mechanism. Similar conclusions can be also addressed for the Erzincan and Bingöl earthquakes, which are given in Appendix 2. It can be inferred from this observation that with the application of the retrofitting scheme the damage pattern on the mosque was transformed from the damage associated with the out-of-plane behavior of the walls to the damage due to the in-plane response of the walls.

Still, even with the retrofitting, the structure experiences severe damage under dynamic loading. It is important to mention that out-of-plane behavior is limited and in-plane behavior is dominant which constitutes the type of behavior desired once higher energy dissipation can occur. Referring to subsection 6.3.4, the control point on the east and north wall has higher displacement on the retrofitted model when the Bolu Earthquake was considered (Figure 6.22(b)). For instance, although peak displacement was increased on the north wall, reduction in diagonal crack pattern was observed under severe damage (See Appendix A-2, Figure A2. 9). In addition, regarding to displacement-time series of the east façade point, the peak displacement is almost the twice as much as the non-retrofitted one, but the vertical damage pattern is dominated by diagonal cracks which are related with in-plane behavior.

6.3.7 Change in the hysteretic response

The hysteretic response of a structure presents information about loading and unloading phases of the structure under dynamic loading with respect to its nonlinear capacity. In these graphs, the interaction between base shear force and horizontal displacements in the orthogonal directions of the numerical model are given. The base shear force was calculated by adding up reaction forces on the supports of the numerical model at each time step. In order to understand the effect of the steel girder retrofitting in the nonlinear range, the hysteretic behavior of each control node was plotted and given in transversal and longitudinal direction in Figure 6.28 and Figure 6.29, respectively. More detailed version of the hysteretic curves was given in Figure 6.30 and Figure 6.31.

In Figure 6.28, east and west walls are subjected to out-of-plane displacements. On the other hand, north and south walls experience out-of-plane displacements in Figure 6.29. These graphs illustrate the hysteretic response for both non-retrofitted and retrofitted models. In the nonlinear range, large displacements are visible and, consequently these impose severe damage on the structure. In addition, it is possible to state residual displacements which was mentioned earlier on the displacement-time histories. The structure reaches its capacity in both directions at all control points and the light nonlinear response was observed by the Bingöl Earthquake which is expected due to its lower spectral ordinates (Figure 6.28(c), Figure 6.29(c)). Besides, the hysteretic responses give more information about the evolution of the nonlinear behavior on the structure rather than the change in peak displacements. Refer to the response of east wall in Figure 6.28(b), considerable change in response is observed especially in the positive X direction due to the steel girder retrofitting while the peak displacement value does not change significantly (Table 6.4)

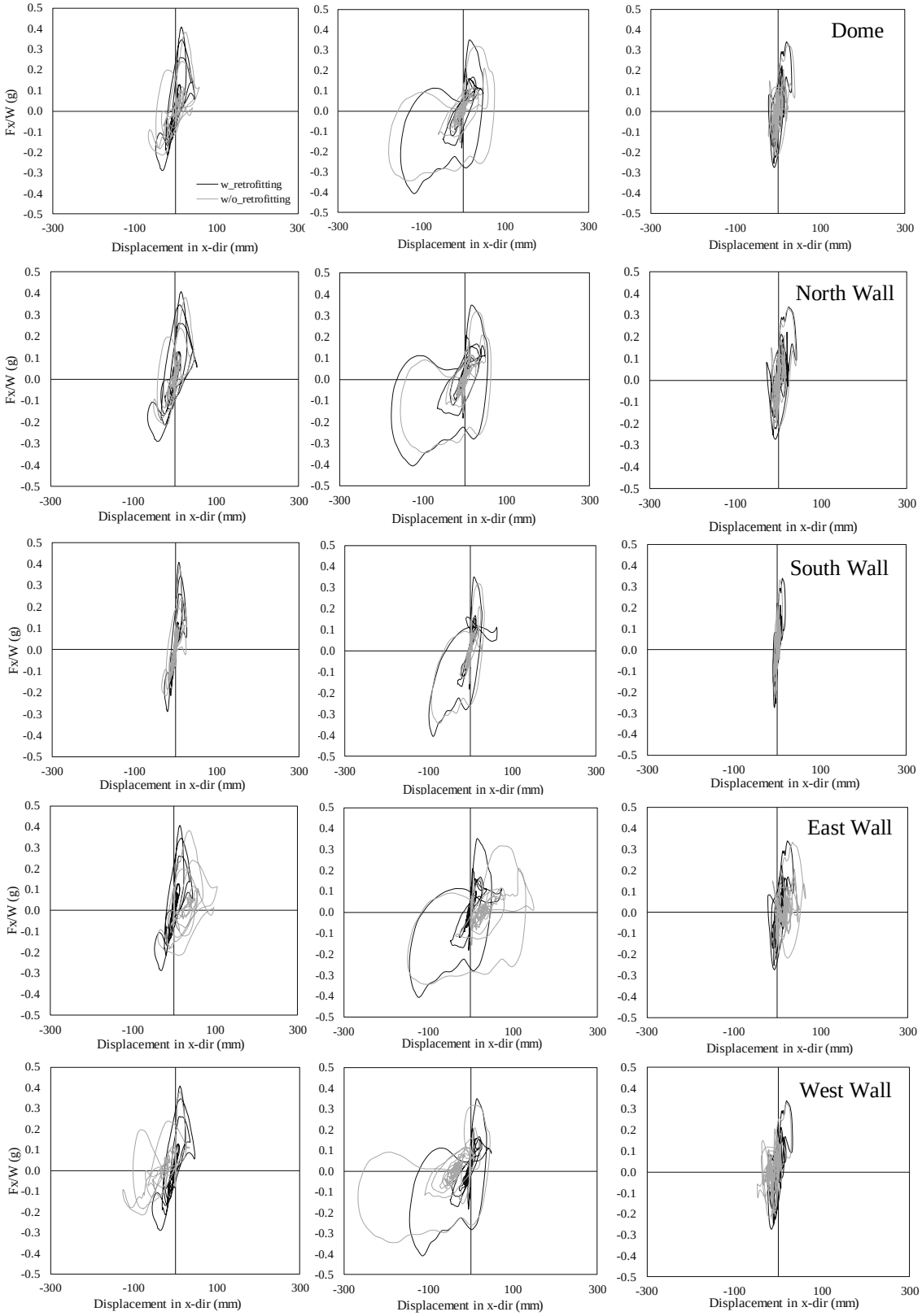

(a) Erzincan *(b) Düzce - Bolu* *(c) Bingöl*

Figure 6.28. *Change in the hysteretic response in the transversal direction*

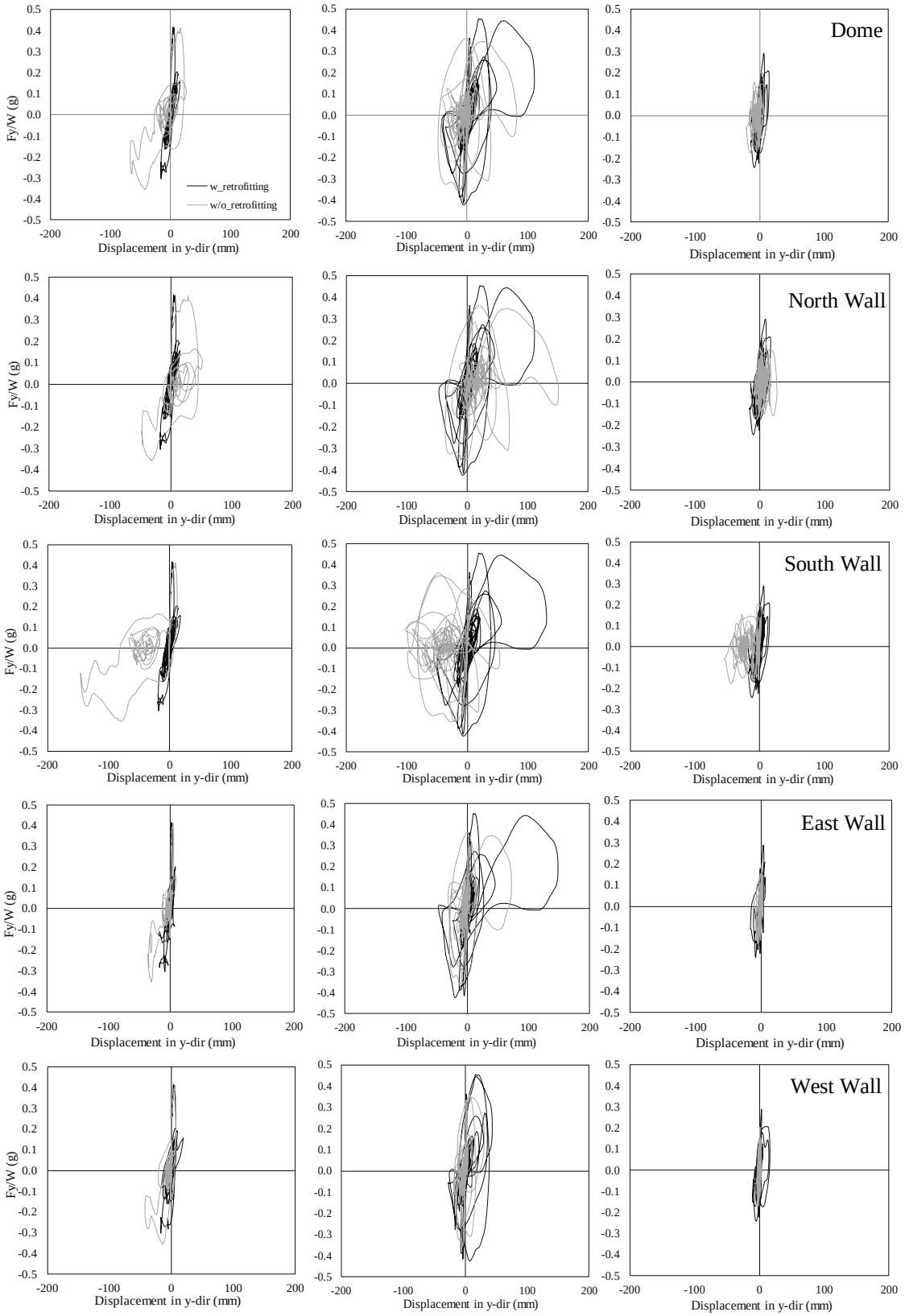

(a) Erzincan *(b) Düzce - Bolu* *(c) Bingöl*

Figure 6.29. *Change in the hysteretic response in the longitudinal direction*

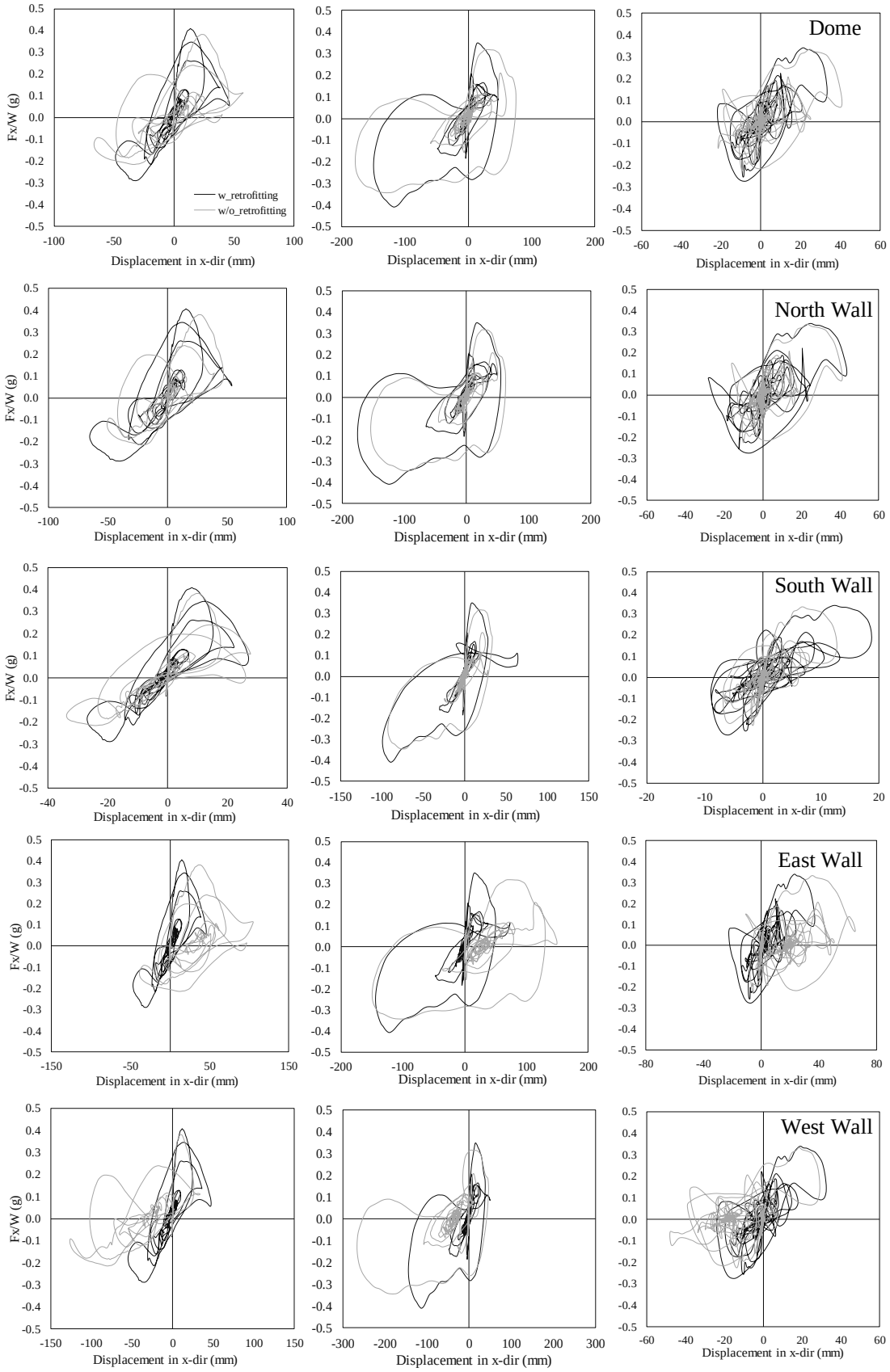

(a) Erzincan *(b) Düzce - Bolu* *(c) Bingöl*

Figure 6.30. *Change in the hysteretic response in the X direction, detailed*

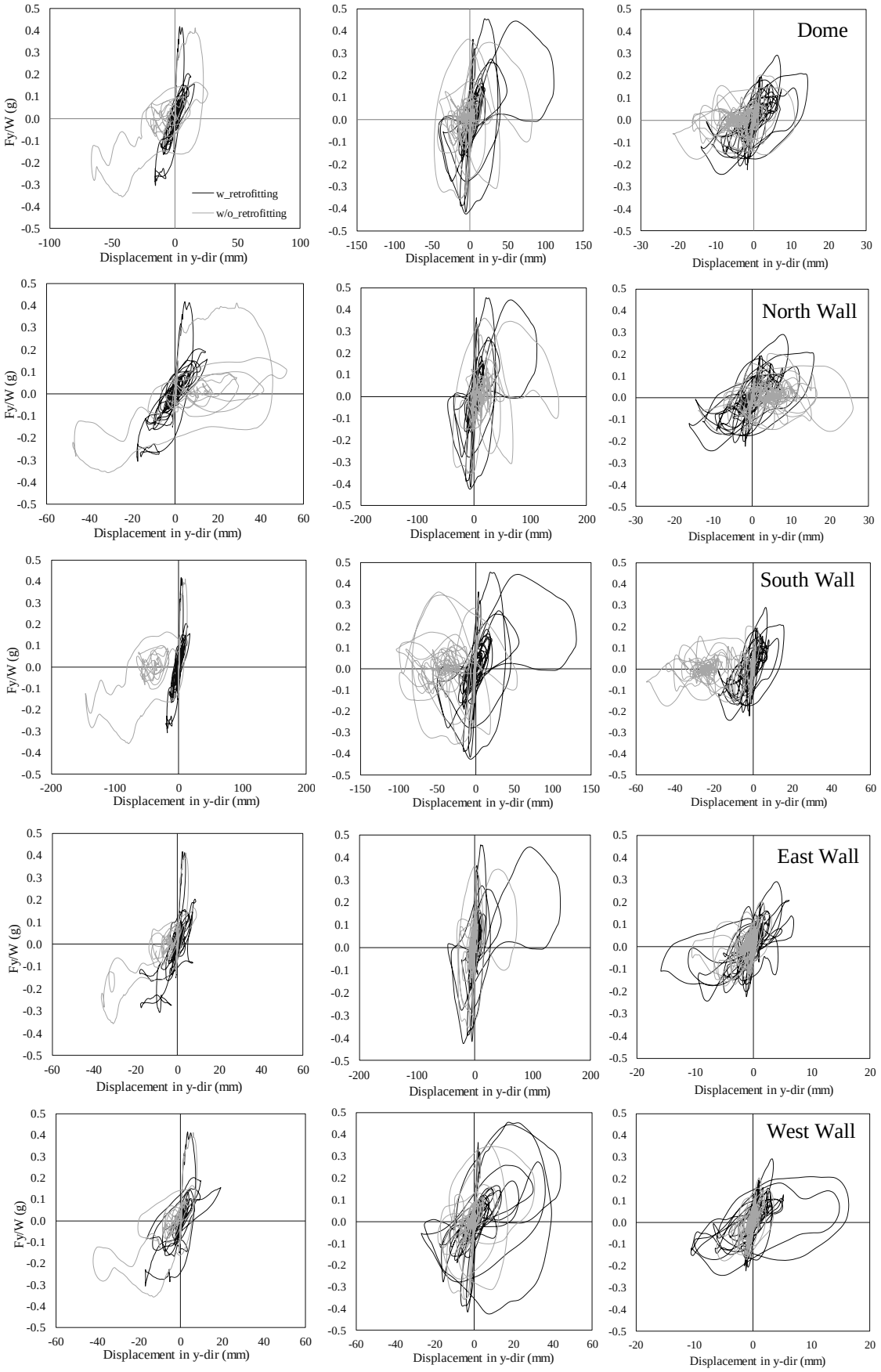

(a) Erzincan *(b) Düzce - Bolu* *(c) Bingöl*

Figure 6.31. *Change in the hysteretic response in the Y direction, detailed*

6.3.8 Correlation of cracks on the non-retrofitted mosque

The nonlinear dynamic analysis of non-retrofitted Kurşunlu Mosque has the ability to validate the nonlinear behavior of the non-retrofitted condition of the real structure. The existing cracks observed on the mosque were satisfactorily reproduced with the conducted nonlinear dynamic analyses. In this section, correlation of the damage pattern obtained by the numerical model with the crack propagation observed during visual inspections was carried out. The investigation was conducted in terms of principal tensile strains. Selection of the plots of principal tensile strains was explained in the previous sub-section 6.3.6. In Figure 6.32, the crack pattern on the South Wall is similar with the numerical model subjected to two different dynamic loading. High tensile stresses lead to severe damage due to the out-of-plane behavior in the perpendicular direction of the wall. On the deformed finite element model, it is possible to say that the dome and drum is subjected to expansion due to the movement along in the out-of-plane direction (Figure 6.32(a)). Therefore, severe damage is observed due to low tensile strength which is not able to resist against high concentration of tensile stresses. Since the similar severe damage was also observed in-situ, validation of the numerical model can be also concluded (Figure 6.32(b)).

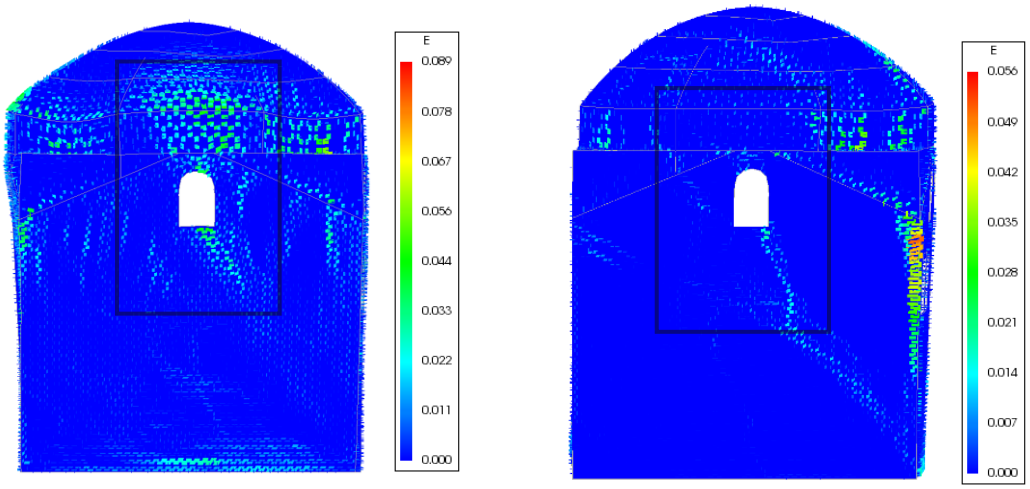

Erzincan (t=3.43 s) *Bingöl (t=3.99 s)*

(a) Total principal tensile strain pattern on the non-retrofitted model

Figure 6.32. *Correlation of cracks observed in-situ and numerical model on the south façade*

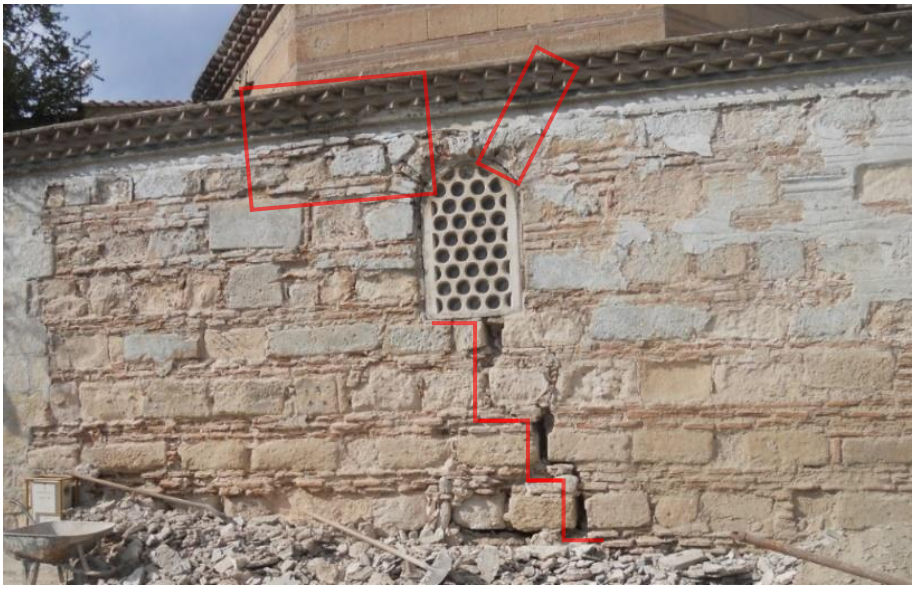

(b) Crack observed on the South façade

Figure 6.32 (continued) *Correlation of cracks observed in-situ and numerical model on the south façade*

A vertical crack was observed on the mosque during the visual inspections on the west façade where the west main load bearing wall intersects with north wall and portico wall (Figure 6.33(a) and Figure 6.33(b)). It is important to mention that the vertical crack is due to the lack of connection between masonry base courses of these structural components. Similar damage pattern was concluded on the finite element model subjected to Bingöl dynamic loading (Figure 6.33(c)). It is clear that these segments try to separate from each other. The dynamic analyses also show that portico and west wall have different displacement response in transverse direction which also result opening along that intersection although full connectivity is assumed (Figure 6.15 and Figure 6.16).

(a) West façade *(b) Closer look to the vertical crack*

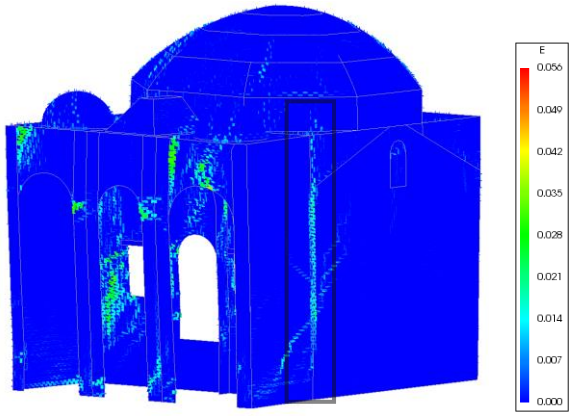

(c) Total principal tensile strain pattern on the non-retrofitted model, Bingöl (t=3.99 s)

Figure 6.33. *Correlation of the vertical crack observed in the numerical model and in-situ*

Additionally, several cracks were reported on the East façade (Figure 6.34). Even though the image of the real mosque is very limited, several conclusions related with the finite element model damage correlation can be done. Vertical damage is located on upper and lower parts of the window opening which is similar with the dynamic analysis resulted by Bingöl loading. Moreover, internal damage is observed on the dome as given in Figure 6.35. Figure 6.35(a) is given in order to show the orientation and location of the

severe damage with respect to load bearing walls. The crack was initiated diagonally to the south and west wall. The orientation of the parallel cracks is compatible with the total principal tensile strain distribution resulted by dynamic loading (Figure 6.35(e)). Since the principal tensile strains propagate on the south and west portion of the dome, damage is expected not only in parallel to the walls but also diagonally orientated to them. Figure 6.35(b) and Figure 6.35(d) depict that both parallel cracks propagate till the drum section which was also observed on the finite element model of non-retrofitted mosque. Although the damage on the dome is not linear and distinct enough on the numerical model, region that the tensile strains propagate are compatible with the location of the observed damage.

Regarding to comparison, the correlation of the in-situ investigations and dynamic analysis results are compatible. Numerical cases are in a good agreement with the real damage and several conclusions were made; the non-retrofitted structure is dominantly subjected to out-of-plane behavior which results high tensile stresses on the significant portion of the structure. Because of this, the mosque subjected to severe damage on the intrados and vertical damage on the load bearing walls. This study also shows that principal tensile strain distribution is a good damage indicator and outcomes of the change in seismic response due to steel girder retrofitting prove the effectiveness of the applied retrofitting scheme.

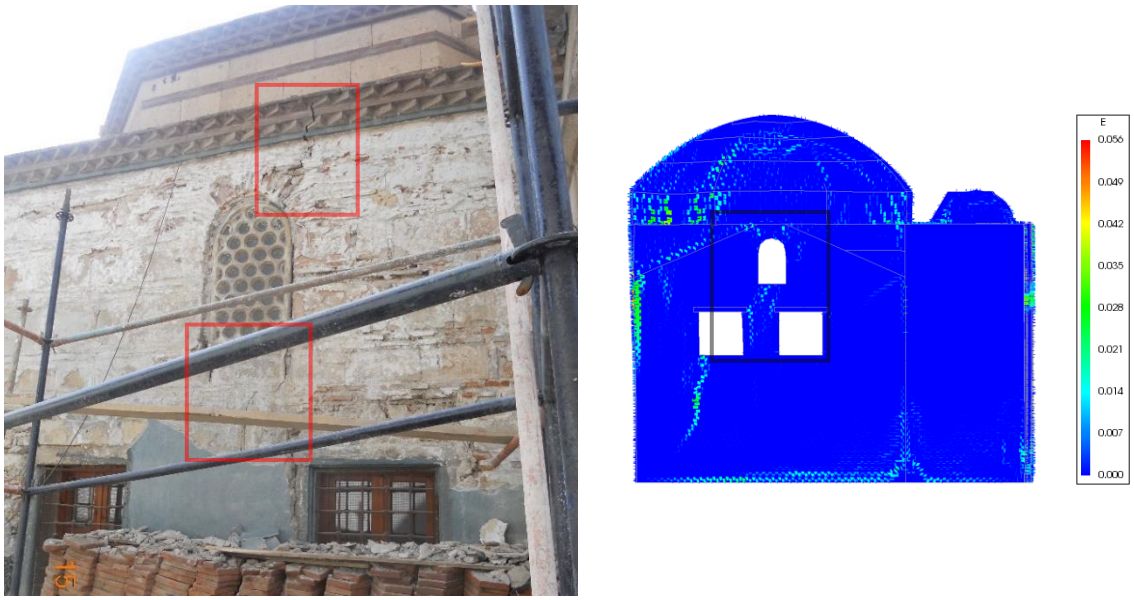

(a) Vertical crack on the East façade

(b) Total tensile principal strains on the East façade, under the Bingöl EQ (t=3.99s)

Figure 6.34. *Correlation of the vertical crack observed on the east façade in the numerical model and in-situ*

(a) Interior face of the south and west wall and intrados

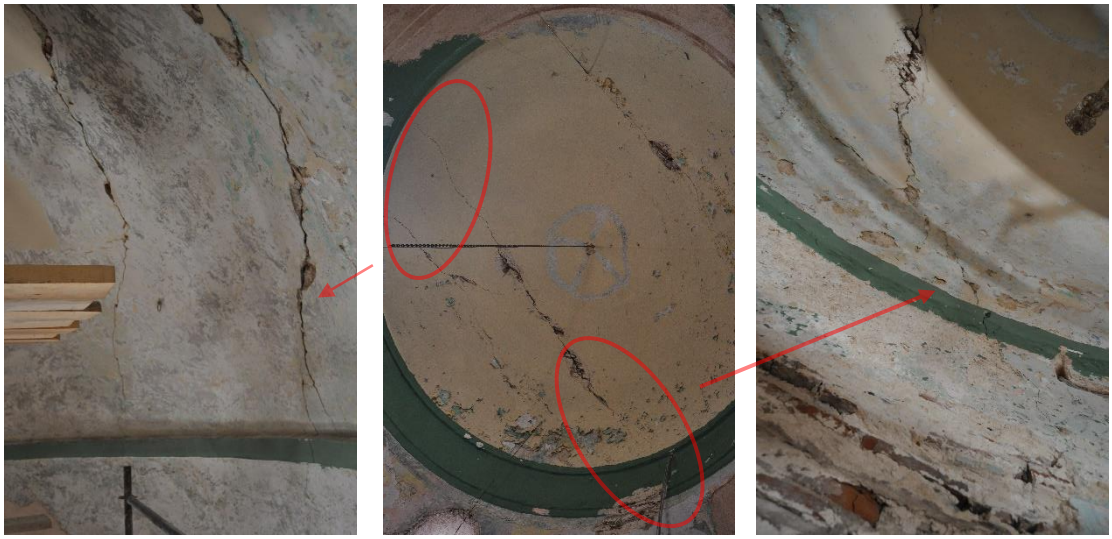

(b) Dome-drum-south wall *(c) Intrados* *(d) Dome-drum-west wall*

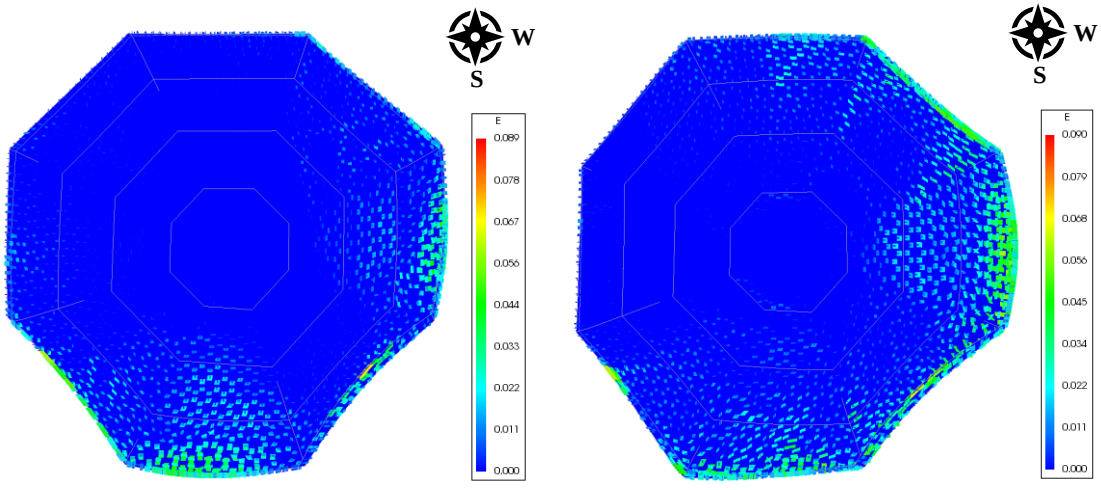

Erzincan (t=3.43s) *Bolu (t=6.12s)*

(e) Total principal tensile strains on the dome, bottom view

Figure 6.35. *Correlation of the crack observed on the dome interior face in the numerical model and in- situ*

6.4 Final Remarks

Three different ground motions were used in order to perform nonlinear dynamic analyses. It is important to mention that a significant number of ground motion is required aiming a representative seismic assessment. Yet, owing the required high computational effort to perform non-linear dynamic analysis on large structures, a limited number of earthquake is usually considered. Here, three ground motions with different seismological features were selected. During the ground motion selection process, the peak ground velocity was also taken as an intensity measure apart from the peak ground acceleration and spectral acceleration of the fundamental mode of the mosque. The Erzincan Earthquake has the maximum PGV and Bingöl has the minimum PGV values. In addition, Bingöl has a higher PGA in the longitudinal direction than the Erzincan input but the response of Erzincan is more critical. This shows that the PGV can be a good intensity measure for historical structures during the selection process.

Several control points were defined to investigate the response of the structure. Different parameters were compared to identify the effectiveness of the steel girder retrofit. The drift ratio values on the selected control points were compared with the limit state values defined according to TYDRYK 2017 Implemented retrofitting actions provided lower drift ratio response for Erzincan and Bingöl earthquake. However, regarding to the guideline suggestions, the non-retrofitted and retrofitted models have high drift ratio, which corresponds to failure state of the structure, under Bolu record excitation.

According to the analyses results, the model without the retrofitting experiences high residual displacements whereas, in the retrofitted model, the imposed residual displacements are limited. Thus, the steel girders are effective to what concerns the out-of-plane behavior providing the so-called box behavior for the historical structure. This can be observed from both time-series of the response, out-of-plane movement profiles and principal tensile strain distributions.

Besides, the effectiveness of the retrofitting action is not that much effective for in-plane movements. Seismic demands along the in-plane direction of the retrofitted walls can be greater compared to the non-retrofitted ones. This can be attributed to the change in the behavior mode of the mosque from the out-of-plane response to the in-plane response in general. Therefore, principal tensile strain distributions were studied and the effectiveness of retrofitting in the in-plane of the load bearing walls was investigated.

The main objective of this study is to present the effectiveness of the steel girders in the out-of-plane direction, especially to avoid the expansion of the dome. Relative residual displacements were calculated on the parallel walls when they are subjected to a seismic load perpendicular to them. The improvement in the response is clear and presented in Figure 6.36. A limited and controllable expansion of the dome in both orthogonal directions can be addressed due to presence of steel girders. As a matter of fact, this is also observed on the deformed shapes and principal tensile strain distributions.

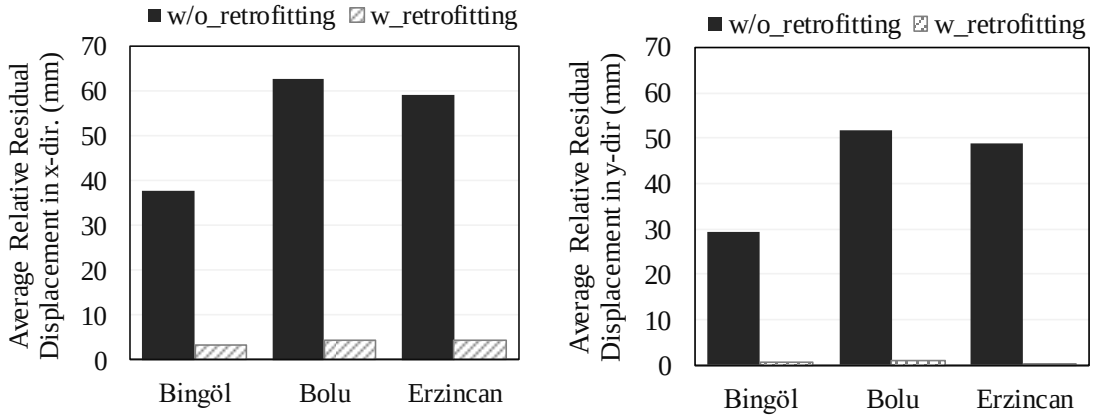

(a)Transversal direction *(b)Longitudinal direction*

Figure 6.36. *Variation in the average relative residual displacement with respect to each ground motion*

Additionally, absolute acceleration response of the models was investigated. Response of both models have similar trends, but higher absolute acceleration values were observed on the retrofitted model. Finally, numerical damage patterns resulted by each earthquake were investigated in order to validate the adopted material behavior as already done for nonlinear static analysis. The analyses results show that total principal tensile strain distributions on the non-retrofitted numerical model present similar damage pattern with the observed damage. Hence, it is important to mention that adopted linear and nonlinear material properties and constitutive material model are in good agreement with the real behavior of the structure.

7. CONCLUSIONS

Historical structures are admitted as architectural heritage and these structures play a vital role on the cultural and social identity in national and diversity in global basis. Therefore, protection and preservation of these constructions has to be provided. As already highlighted in Chapter 1, Turkey is home to an enormous number of architectural heritage throughout the country. However, the legacy of the country is under high seismic risk because of the fact that Turkey is located in the second most seismic active region on the Earth. Therefore, necessary precautions have to be taken in order to protect and maintain the legacy of the history.

In the present study, historical masonry mosque, namely Kütahya Kurşunlu Mosque was investigated. Severe damage was observed on the mosque and several interventions and retrofitting actions were carried out. It is possible to say regarding to the site observations that the severe damage can be attributed to the lack of connections and integrity of the overall system. The masonry structural system of the mosque did not exhibit integrated behavior, so called box-behavior. Within this context, steel girder elements were introduced to structure and anchored at the top of the load bearing walls, and, bottom and top level of the octagonal drum (dome support). In order to study the effectiveness of the introduced retrofitting technique, finite element method was used. Finite element model of the non-retrofitted and retrofitted Kütahya Kurşunlu Mosque was prepared and calibrated according to the dynamic properties obtained from the experimental modal analysis. Next, seismic response of the two models were studied by nonlinear pushover analysis and nonlinear bi-directional dynamic analysis. The nonlinear pushover analysis was performed as proportionally to the mass of the structure in the transversal and longitudinal directions. The nonlinear dynamic analysis was conducted by using three different real ground motions in which both horizontal components of the accelerograms were used.

The final conclusions according to the results obtained from the pushover and dynamic analysis are presented as follows;

- The only difference of the two models was made by introducing the steel elements to the numerical model. In fact, the modal properties are the same which results the same elastic limit state during the pushover analysis. Therefore, it is not possible to conclude the contribution of the steel elements to the structural behavior in the linear range.

- From the pushover analysis, it is found that the stronger direction of the mosque is longitudinal direction (Y) which has a value of lateral force capacity 0.6g and 0.5g for retrofitted and non-retrofitted model.
- The load capacity of the non-retrofitted model decreases considerably in each direction whereas the adopted steel girders contribute to the nonlinear behavior of the structure.
- The last step of the pushover curves does not indicate the total collapse of the structure however, the curves are efficient enough to verify the nonlinear behavior of the structure. The total principal tensile strain distribution presents a numerical damage which is similar with the observed damage on the non-retrofitted mosque. In fact, total principal tensile strain distributions obtained from pushover analysis in +Y and +X direction are representative of the observed damage.
- For nonlinear dynamic analysis, real ground motions of three different destructive earthquakes were selected. During the selection process, spectral acceleration of the fundamental mode, PGA and PGV were considered as intensity measures. Although Bingöl record has higher PGA, the response resulted by the Erzincan Earthquake, which has lower PGA but higher PGV, is more critical.
- Residual displacements resulted in the out-of-plane direction was limited by introducing steel elements. Time series of the out-of-plane movement on the parallel walls show that displacement response is similar and has the same trend. Structural integrity seems to be provided for the upper part of the structure.
- As per TYDRYK (2017), time history analysis of the Bolu Earthquake resulted high drift ratio which corresponds to failure even though the retrofitting actions were performed. However, Bingöl and Erzincan analyses show that the retrofitting is effective in terms of change in damage limit states.
- The retrofit allows to reduce relative displacement of east and west wall in the transversal direction whereas the relative displacement was reduced in the south and north wall in the longitudinal direction. Thus, crack opening and expansion of the dome is limited.
- The validation of the performed analysis can be made by considering non-retrofitted model. Once the damage is known for this case, numerical damage verifies the constituted hypotheses. Therefore, the response of the retrofitted case obtained from numerical analysis is assumed to be as representative for the actual response.

Four main tasks are recommended for the future studies;

I. The first task is to investigate the additional proposed retrofitting technique by the Directorate General of Foundations which is the application of the steel tie rods along the wall length at the mid-height. The seismic response of the different types of retrofitting actions can be compared.
II. The second task is to perform additional dynamic analyses. This aims to improve the different possibilities of the response under various types of seismic effects.
III. The third task considers the effect of the vertical earthquake component on the structural response.
IV. The fourth and final task is to perform kinematic analysis in order to study seismic failure mechanisms of the structural components subjected to out-of-plane movement.

REFERENCES

AFAD. (2018). Seismicity Map of Turkey. Retrieved from https://tdth.afad.gov.tr/

Aguilar, R., Torrealva, D., Ramos, L. F., and Lourenço, P. B. (2012). Operational Modal Analysis Tests on Peruvian Historical Buildings : The Case Study of the 19 th Century Hotel Comercio. In *15th World Conference on Earthquake Engineering, Lisbon Portugal*.

Akkar, S., Sucuoğlu, H., and Yakut, A. (2005). Displacement-based fragility functions for low- And mid-rise ordinary concrete buildings. *Earthquake Spectra*, *21*(4), 901–927.

Akyüz, H. ., Hartleb, R., Barka, A., Altunel, E., Sunal, G., Meyer, B., and Armijo, R. (2002). Surface Rupture and Slip Distribution of the 12 November 1999 Düzce Earthquake (M 7.1), North Anatolian Fault, Bolu, Turkey. *Bulletin of the Seismological Society of America*, *91*(1), 61–66.

Almac, U., Alaboz, M., Bal, I. E., Karahan, O., and Dashti, S. (2016). Structural observations on Macedonian tower, Edirne. *Structural Analysis of Historical Constructions: Anamnesis, Diagnosis, Therapy, Controls - Proceedings of the 10th International Conference on Structural Analysis of Historical Constructions, SAHC 2016*, (October), 1764–1768.

Angelillo, M., Lourenço, P., and Milani, G. (2014). Masonry behavior and modelling. In M. Angelillo (Ed.), *Mechanics of Masonry Structures* (pp. 1–24). Udine: CISM International Centre for Mechanical Sciences, Springer.

ARTeMIS Modal. SVS-Structural Vibration Solutions A/S. Denmark.

AutoCAD. (2016). Autodesk Student License Version.

Avşar, Ö., and Özdemir, G. (2013). Response of Seismic-Isolated Bridges in Relation to Intensity Measures of Ordinary and Pulselike Ground Motions. *Journal of Bridge Engineering*, *18*(3), 250–260.

Boore, D. M., and Bommer, J. J. (2005). Processing of strong-motion accelerograms: Needs, options and consequences. *Soil Dynamics and Earthquake Engineering*, *25*(2), 93–115.

Braga, A. A. B. (2014). *Study of the Armenian Church in Famagusta*. MSc Thesis. Guimarães: University of Minho, Advanced Masters in Structural Analysis of Monuments and Historical Constructions.

Cagnan, Z. (2012). Numerical models for the seismic assessment of St. Nicholas Cathedral, Cyprus. *Soil Dynamics and Earthquake Engineering*, *39*, 50–60.

Can, H., Kubin, J., and Ünay, A. İ. (2012). Seismic Behavior of Historical Masonry Buildings with Irregular Geometry. *Journal of the Faculty of Engineering and Architecture of Gazi University*, *27*(3), 679–686.

CEB-FIP. (1993). *Model Code 90*. UK: Thomas Telford Ltd.

Chopra, A. (2012). *Dynamics of Structures Theory and Application to Earthquake Engineering* (4th ed.). New Jersey: Printince Hall.

Ciocci, M. P., Sharma, S., and Lourenço, P. B. (2018). Engineering simulations of a super-complex cultural heritage building: Ica Cathedral in Peru. *Meccanica*, *53*(7), 1931–1958.

Cunha, A., and Caetano, E. (2005). From input-output to output-only modal identification of civil engineering structures. In *1st International Operational Modal Analysis Conference, IOMAC 2005* (pp. 1–22).

Doebling, S. W., Farrar, C. R., and Cornwell, P. (1997). A Statistical Comparison Of Impact And Ambient Testing Results From The Alamosa Canyon Bridge. *Proceedings of SPIE the International Society for Optical Engineering*, *3089*(505), 264–270.

Doğangün, A., Acar, R., Livaoğlu, R., and Tuluk, Ö. (2006). Performance of masonry minarets against earthquakes and winds in Turkey. In *1st Internatıional Conference on Restoration of Heritage Masonry Structures*. Cairo.

Dogangun, A., Acar, R., Sezen, H., and Livaoglu, R. (2008). Investigation of dynamic response of masonry minaret structures. *Bulletin of Earthquake Engineering*, *6*, 505–517.

Dolatshahi, K. M., Nikoukalam, M. T., and Beyer, K. (2018). Numerical study on factors that influence the in-plane drift capacity of unreinforced masonry walls. *Earthquake Engineering & Structural Dynamics*, 1–20. https://doi.org/10.1002/eqe.3024

EN 1998-2. (2005). Part 2: Bridges. *Eurocode 8 - Design of Structures for Earthquake Resistance*.

Ertuğrul, Z. Ç. (2015). Computer Modelling and Seismic Performance Assessment of a Byzantine Basilica. In I. N. Psycharis, S. J. Pantazopoulou, and M. Papadrakakis (Eds.), *Seismic Assessment, Behavior and Retrofit of Heritage Buildings and Monuments* (Vol. 37, pp. 265–280). Switzerland: Springer International Publishing.

Ewins, D. (2000). *Modal testing: Theory, Practice, and Application*. England: Research Studies Press LTD.

Farrar, C. R., and Worden, K. (2007). An introduction to structural health monitoring. *Philosophical Transactions of the Royal Society A: Mathematical, Physical and Engineering Sciences*, *365*(1851), 303–315.

Friswell, M. I., and Mottershead, J. E. (1995). *Finite element model updating in structural dynamics* (1st ed.). Springer Science+Business Media Dordrecht, Kluwer Academic Publishers.

FX+ for DIANA. (2013). Midas FX+ for DIANA, Customized Pre/Post-processor for DIANA. MIDAS Information Technology Co., Ltd.

Gentile, C., and Saisi, A. (2007). Ambient vibration testing of historic masonry towers for structural identification and damage assessment. *Construction and Building Materials*, *21*(6), 1311–1321.

ICOMOS-TR. (2013). ICOMOS Turkey Architectural Heritage Conservation Charter. Retrieved from http://www.icomos.org.tr/Dosyalar/ICOMOSTR_0623153001387886624.pdf

ICOMOS. (1964). International Charter for the conservation and restoration of monuments and sites (The Venice Charter 1964). *International Congress of Architects and Technicians of Historic Monuments*, 1–4.

ISCARSAH. The International Scientific Committee on the Analysis and Restoration of Structures of Architectural Heritage. Retrieved May 1, 2018, from https://iscarsah.org/

ISCARSAH. (2003). Recommendations for the analysis, conservation and structural restoration of Architectural Heritage. *ICOMOS*, (June).

Italian Code, C. (2009). Technical Standards for Constructions - DM 14/01/2008. In *Gazzetta Ufficiale Serie Generale n.47 del 26/02/2009*. Italy.

Jokilehto, J. (1999). *A History of Architectural Conservation*. Butterworth-Heinemann.

Kalkan, E., and Gülkan, P. (2004). Site-dependent spectra derived from ground motion records in Turkey. *Earthquake Spectra*, *20*(4), 1111–1138. https://doi.org/10.1193/1.1812555

Karanikoloudis, G., and Lourenço, P. B. (2018). Structural assessment and seismic vulnerability of earthen historic structures. Application of sophisticated numerical and simple analytical models. *Engineering Structures*, *160*, 488–509.

Kazaz, İ., and Kocaman, İ. (2018). Seismic load capacity evaluation of stone masonry mosques. *Journal of the Faculty of Engineering and Architecture of Gazi University*. https://doi.org/10.17341/GUMMFD.30784

KOERI. Boğaziçi University Kandilli Observatory and Earthquake Research Institute Regional Earthquake-Tsunami Monitoring Center. Retrieved April 30, 2018, from http://www.koeri.boun.edu.tr/sismo/2/deprem-bilgileri/buyuk-depremler/

Lara, R. (2016). *Structural analysis of the church of the Monastery of São Miguel de Refojos*. MSc Thesis. Guimarães: University of Minho, Advanced Masters in Structural Analysis of Monuments and Historical Constructions.

Lourenço, P. B. (2001). Analysis of historical constructions: From thrust-lines to advanced simulations. In P. B. Lourenço and P. Roca (Eds.), *Historical Constructions* (pp. 91–116). Guimaraes.

Lourenço, P. B. (2002). Computations on historic masonry structures. *Progress in Structural Engineering and Materials*, *4*(3), 301–319. https://doi.org/10.1002/pse.120

Lourenço, P. B., Krakowiak, K. J., Fernandes, F. M., and Ramos, L. F. (2007). Failure analysis of Monastery of Jerónimos, Lisbon: How to learn from sophisticated numerical models. *Engineering Failure Analysis*, *14*(2), 280–300. https://doi.org/10.1016/j.engfailanal.2006.02.002

Lourenço, P. B., Mendes, N., Costa, A. A., and Campos-Costa, A. (2017). Methods and Challenges on the Out-of-Plane Assessment of Existing Masonry Buildings. *International Journal of Architectural Heritage*, *11*(1), 1.

Lourenço, P. B., Mendes, N., Ramos, L. F., and Oliveira, D. V. (2011). Analysis of masonry structures without box behavior. *International Journal of Architectural*

Heritage, *5*(4–5), 369–382. https://doi.org/10.1080/15583058.2010.528824

Lourenço, P. B., Trujillo, A., Mendes, N., and Ramos, L. F. (2012). Seismic performance of the St . George of the Latins church : Lessons learned from studying masonry ruins. *Engineering Structures*, *40*, 501–518.

Mangia, L., Ghiassi, B., Sayın, E., Onat, O., and Lourenço, P. . (2016). Pushover Analysis of Historical Eltihatun Mosque. In *12th International Congress on Advances in Civil Engineering*. İstanbul.

Mendes, N. (2012). *Seismic Assessment of Ancient Masonry Buildings : Shaking Table Tests and Numerical Analysis*. PhD Thesis. Guimarães: University of Minho, Faculty of Engineering.

The Nara Document on Authenticity, ICOMOS, UNESCO, ICCROM (1994). Retrieved from http://whc.unesco.org/uploads/events/documents/event-833-3.pdf

Nohutcu, H., Demir, A., Ercan, E., Hokelekli, E., and Altintas, G. (2015). Investigation of a historic masonry structure by numerical and operational modal analyses, (24), 821–834.

Orbaşlı, A. (2007). *Architectural Conservation: Principles and Practice*. Wiley-Blackwell.

Ozturk, B. (2017). Seismic behavior of two monumental buildings in historical Cappadocia region of Turkey. *Bulletin of Earthquake Engineering*, *15*(7), 3103–3123.

Ramos, L. F. (2007). *Damage identification on masonry structures based on vibration signatures*. PhD Thesis. Guimarães: University of Minho, Faculty of Engineering.

Ramos, L. F., Aguilar, R., and Lourenço, P. B. (2010). Operational modal analysis of historical constructions using commercial wireless platforms. *Structural Health Monitoring*, *10*(5), 511–521.

Ramos, L. F., Marques, L., Lourenço, P. B., Roeck, G. De, Campos-costa, A., and Roque, J. (2010). Monitoring historical masonry structures with operational modal analysis : Two case studies. *Mechanical Systems and Signal Processing*, *24*, 1291–1305.

Roca, P. (2005). Considerations on the significance of history for the structural analysis of acient constructions. In C. Modena, P. . Lourenço, and P. Roca (Eds.), *Structural Analysis of Historical Constructions* (pp. 63–73). London: Taylor & Francis Group.

Roca, P. (2006). The study and restoration of historical structures: From principles to practice. In P. B. Lourenço, P. Roca, C. Modena, and S. Agrawal (Eds.), *Structural Analysis of Historical Constructions* (pp. 9–24). New Delhi.

Roca, P., Cervera, M., Gariup, G., and Pela, L. (2010). Structural analysis of masonry historical constructions. Classical and advanced approaches. *Archives of Computational Methods in Engineering*, *17*(3), 299–325. https://doi.org/10.1007/s11831-010-9046-1

Rockwell, T. (2013). North Anatolian Fault. In P. T. Bobrowsky (Ed.), *Encyclopedia of Natural Hazards* (pp. 738–739). Springer.

SAP2000. Structural Analysis Programme. Berkeley: Computers and Structures Inc.

Version 15.1.0.

SeismoSignal. (2016). SeismoSoft, Student Version.

Şeker, B. Ş., Çakir, F., Doğangün, A., and Durmuş, A. (2015). Investigation of structural behaviour of Historical Erzurum Lala Pasha Mosque using finite element method. *Pamukkale University Journal of Engineering Sciences*, *21*(3), 82–87.

Şeker, B. Ş., Doğangün, A., and Çakır, F. (2013). Structural Anaysis and Assessment of Historical Kara Mustafa Pasha Mosque in Merzifon, Turkey. *Süleyman Demirel University Journal of Technologic Sciences*, *5*(1), 112–120.

Sevim, B., Bayraktar, A., Altunişik, A. C., Atamtürktür, S., and Birinci, F. (2011). Assessment of nonlinear seismic performance of a restored historical arch bridge using ambient vibrations. *Nonlinear Dynamics*, *63*(4), 755–770.

Silva, L. C. (2013). *Analysis of Christchurch Catholic Basilica, New Zealand*. Master of Science Thesis. Guimarães: University of Minho, Faculty of Engineering.

TEC. (2007). Turkish Earthquake Code: Specifications for the Buildings to be Constructured in Disaster Areas. In *Official Newspaper*. Ankara.

TEC. (2019). Turkish Earthquake Code: Specifications for Building Design Under Earthquake Effects.

TNO DIANA. (2017). User's Manual Release 10.2. The Netherlands.

Tomaževič, M. (1999). *Earthquake-Resistant Design of Masonry Building*. London: Imperial College Press.

TR-NSMN. Strong Motion Database. Retrieved from kyhdata.deprem.gov.tr.

Trifunac, M. D., and Brady, A. G. (1975). A study on the duration of strong earthquake ground motion. *Bulletin of the Seismological Society of America*, *65*(3), 581–626.

TYDRYK. (2017). Tarihi Yapılar İçin Deprem Risklerinin Yönetimi Kılavuzu. *Vakıflar Genel Müdürlüğü*.

UNESCO. (a). World Heritage List. Retrieved May 1, 2018, from http://whc.unesco.org/en/list/

UNESCO. (b). UNESCO World Heritage List in Turkey. Retrieved April 30, 2018, from http://whc.unesco.org/en/statesparties/tr

UNESCO. (1954). Hague Convention - The Convention for the Protection of Cultural Property in the Event of Armed Conflict.

UNESCO. (1972). Convention Concerning the Protection of the World Cultural and Natural Heritage. *General Conference Seventeenth Session*, *1*(November), 135–145. https://doi.org/10.1111/j.1468-0033.1973.tb02056.x

Yılmaz, N., and Avşar, Ö. (2013). Structural damages of the May 19, 2011, Kütahya-Simav earthquake in Turkey. *Natural Hazards*, *69*(1), 981–1001. https://doi.org/10.1007/s11069-013-0747-2

Http-1. UNESCO. World Heritage List. Retrieved May 1, 2018, from http://whc.unesco.org/en/list/

Http-2. Cyprus: what was built for war, today symbolizes peace. Retrieved May 2, 2018, from https://medium.com/@UNDP_PFF/cyprus-what-was-built-for-war-today-symbolizes-peace-martinengo-bastion-the-walls-of-ba40a250df92

Http-3. Retrieved May 1, 2018, from http://www.bbc.com/news/world-africa-33587325

Http-4. Retrieved May 13, 2018, from http://www.kulturvarliklari.gov.tr/TR,44798/turkiye-geneli-korunmasi-gerekli-tasinmaz-kultur-varlig-.html

Http-5. Retrieved May 13, 2018, from http://www.kulturvarliklari.gov.tr/TR,44799/illere-gore-korunmasi-gerekli-tasinmaz-kultur-varligi-i-.html

Http-6. UNESCO World Heritage List in Turkey. Retrieved April 30, 2018, from http://whc.unesco.org/en/statesparties/tr

Http-7. Retrieved from https://hometurkey.com/en/attractions/unesco-world-heritage-sites-in-turkey

Http-8. Retrieved May 13, 2018, from https://plus.google.com/photos/photo/105596551663140924133/6492445840149832274

Http-9. Retrieved May 13, 2018, from http://www.mustafacambaz.com/details.php?image_id=7060

APPENDICES

APPENDIX - 1 : ARCHITECTURAL DRAWINGS

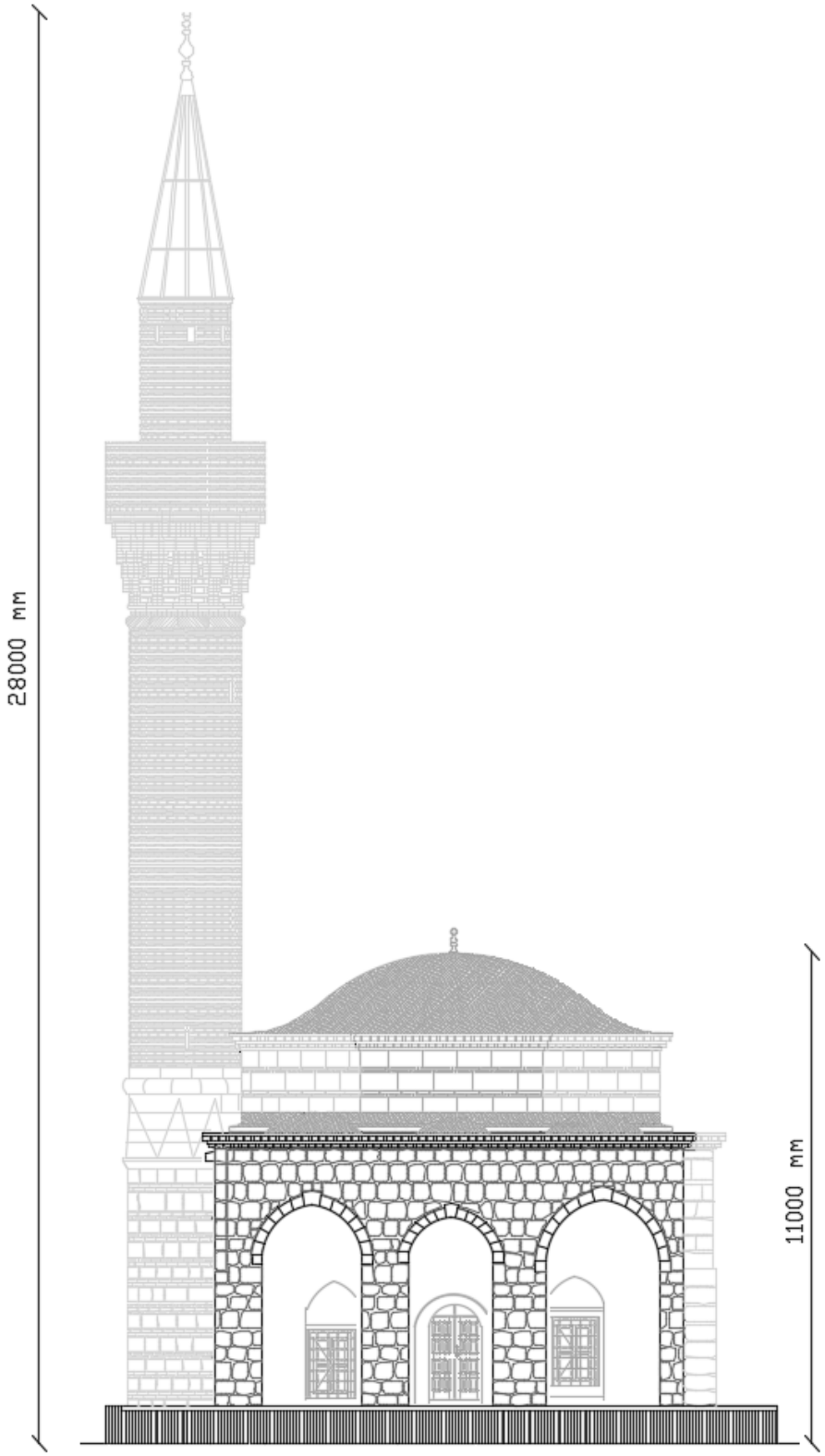

Figure A1. 1. *North façade*

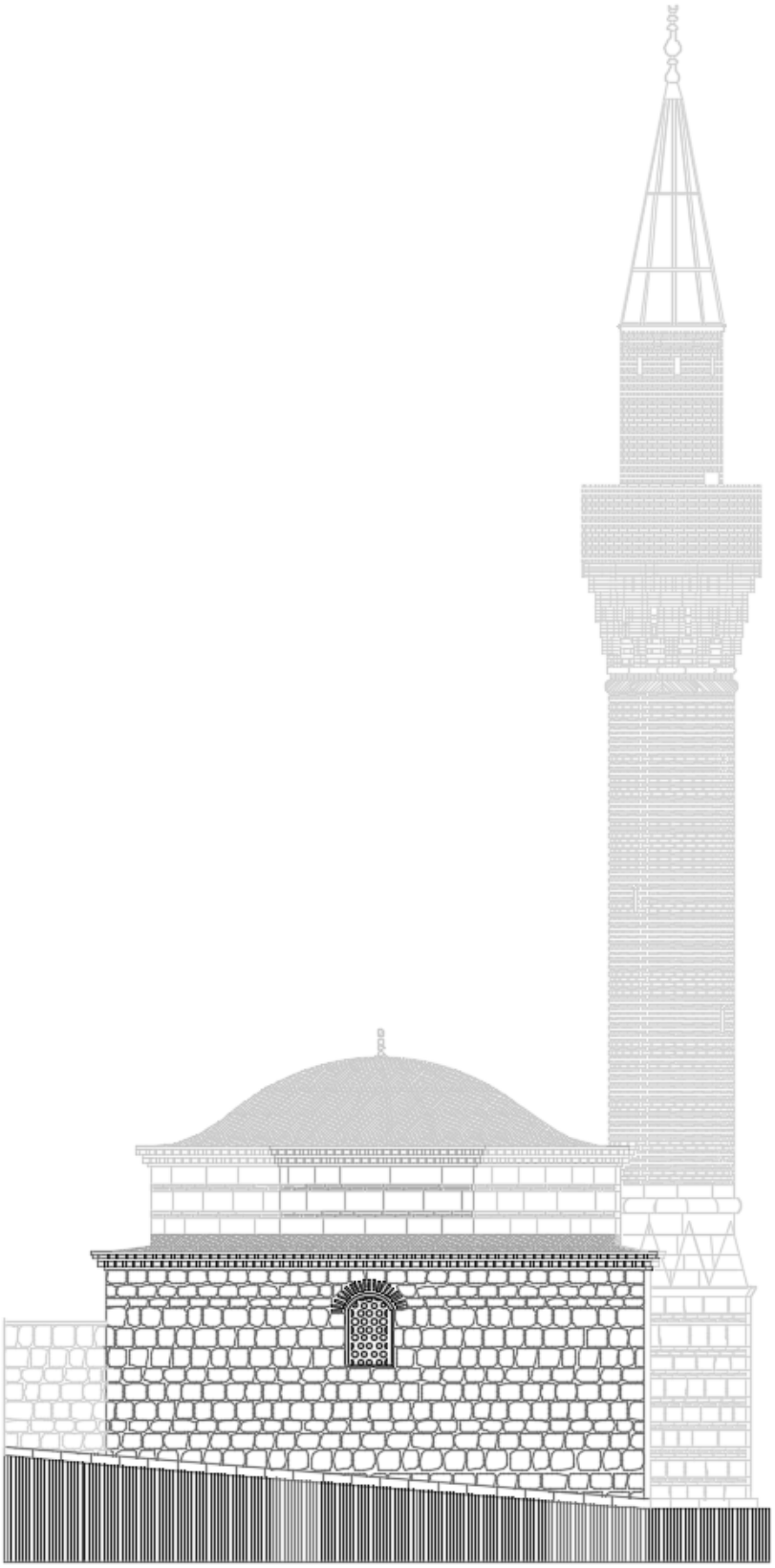

Figure A1. 2. *South façade*

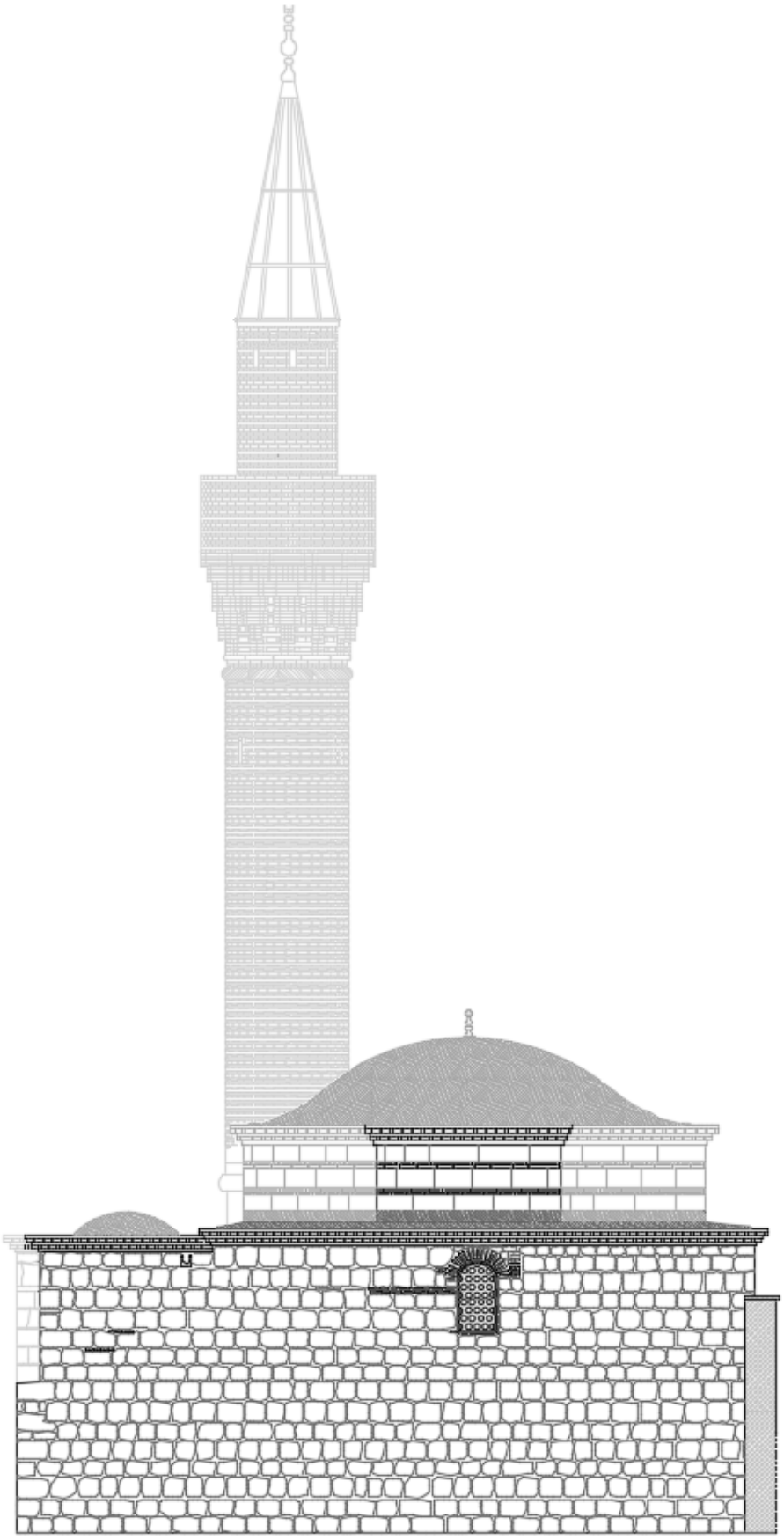

Figure A1. 3. *West façade*

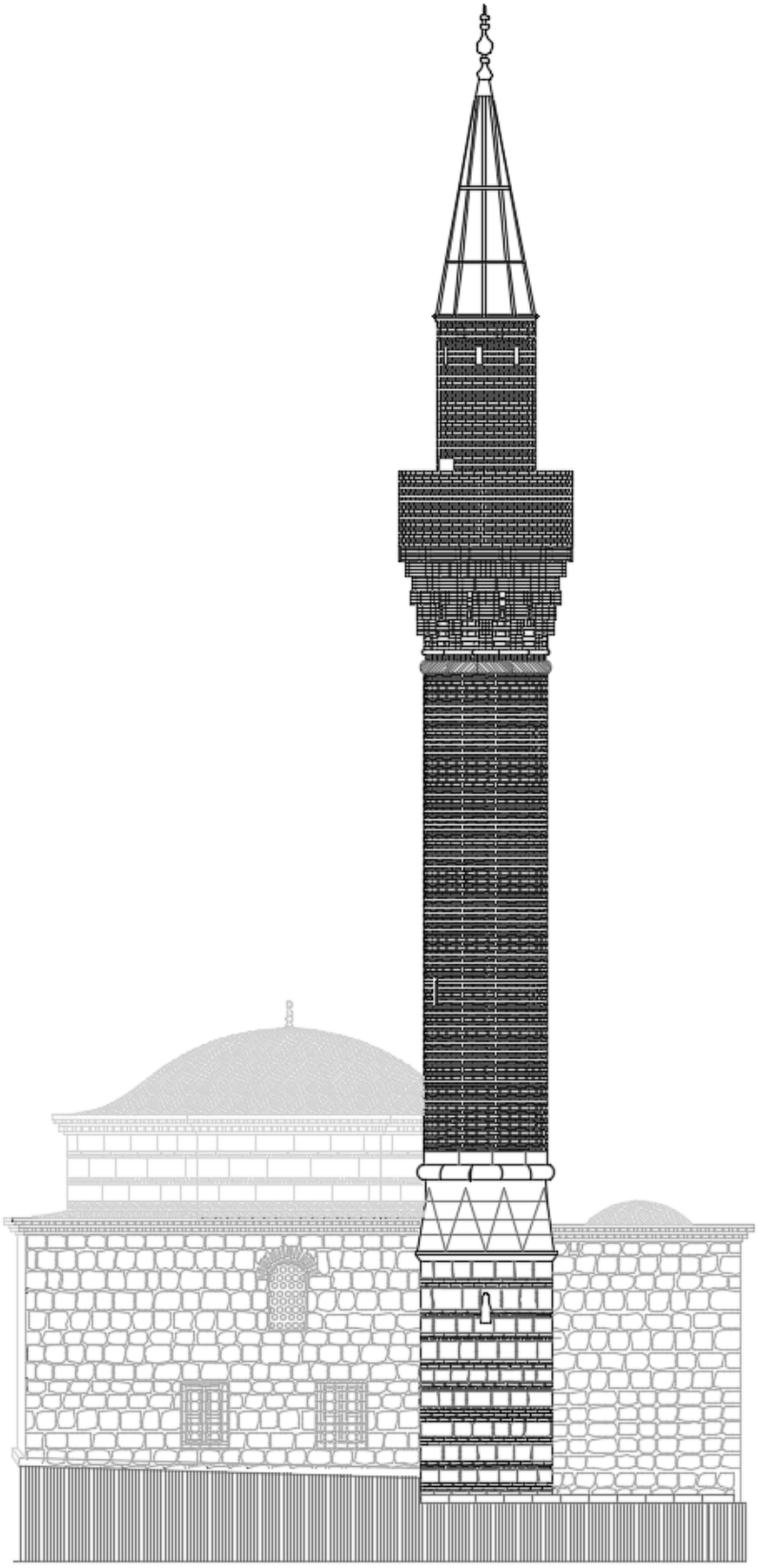

Figure A1. 4. *East façade*

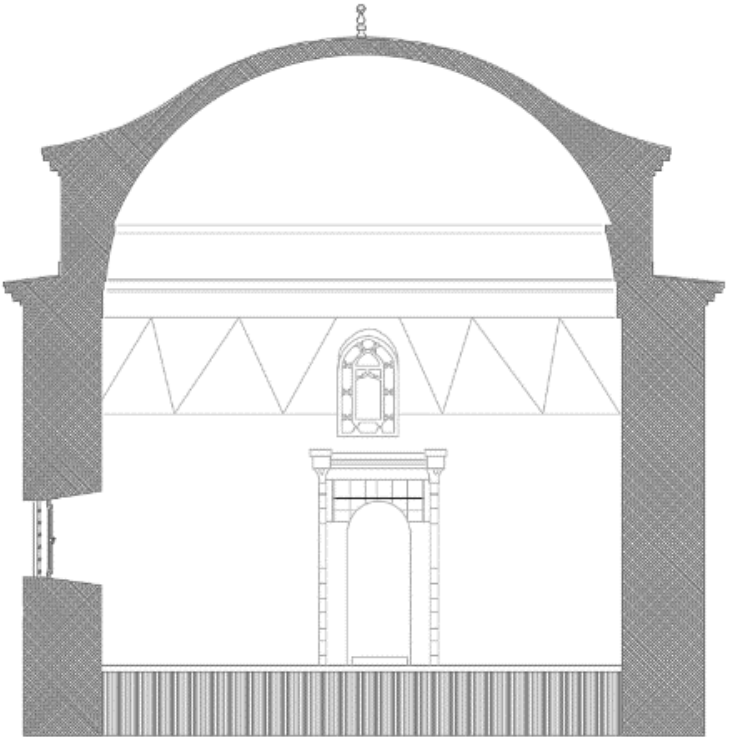

Figure A1. 5. *Section A-A*

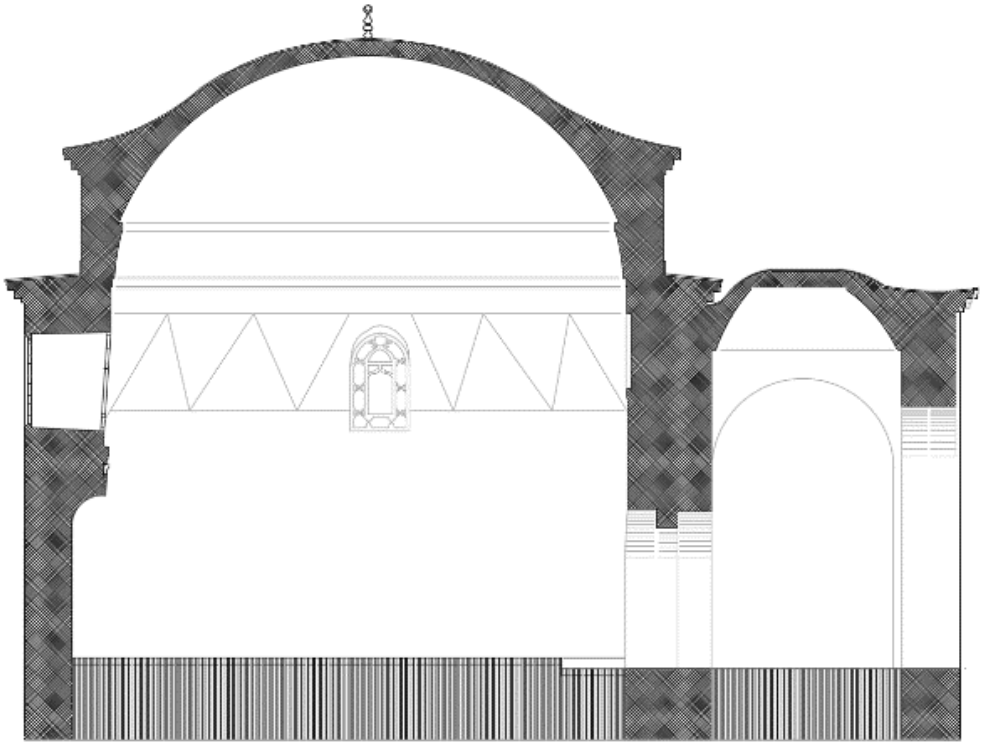

Figure A1. 6. *Section C-C*

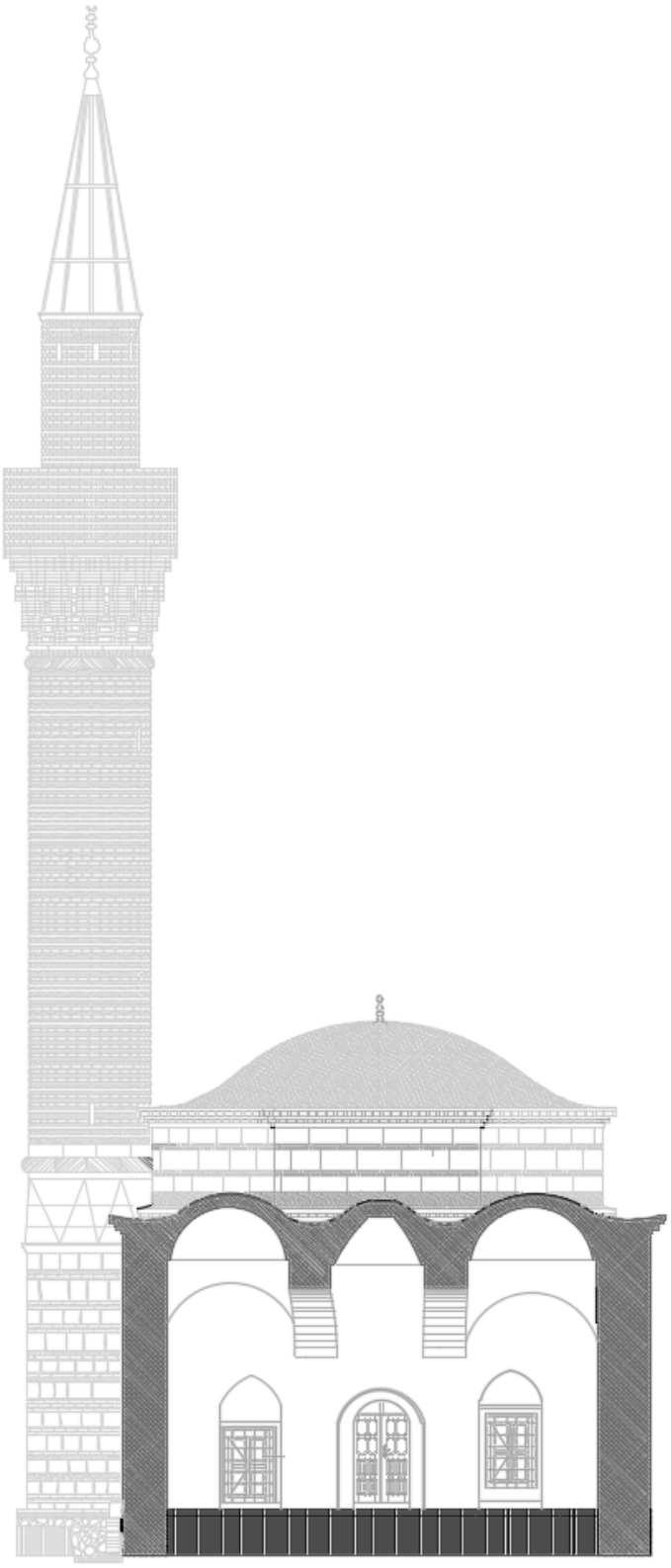

Figure A1. 7. *Section B-B*

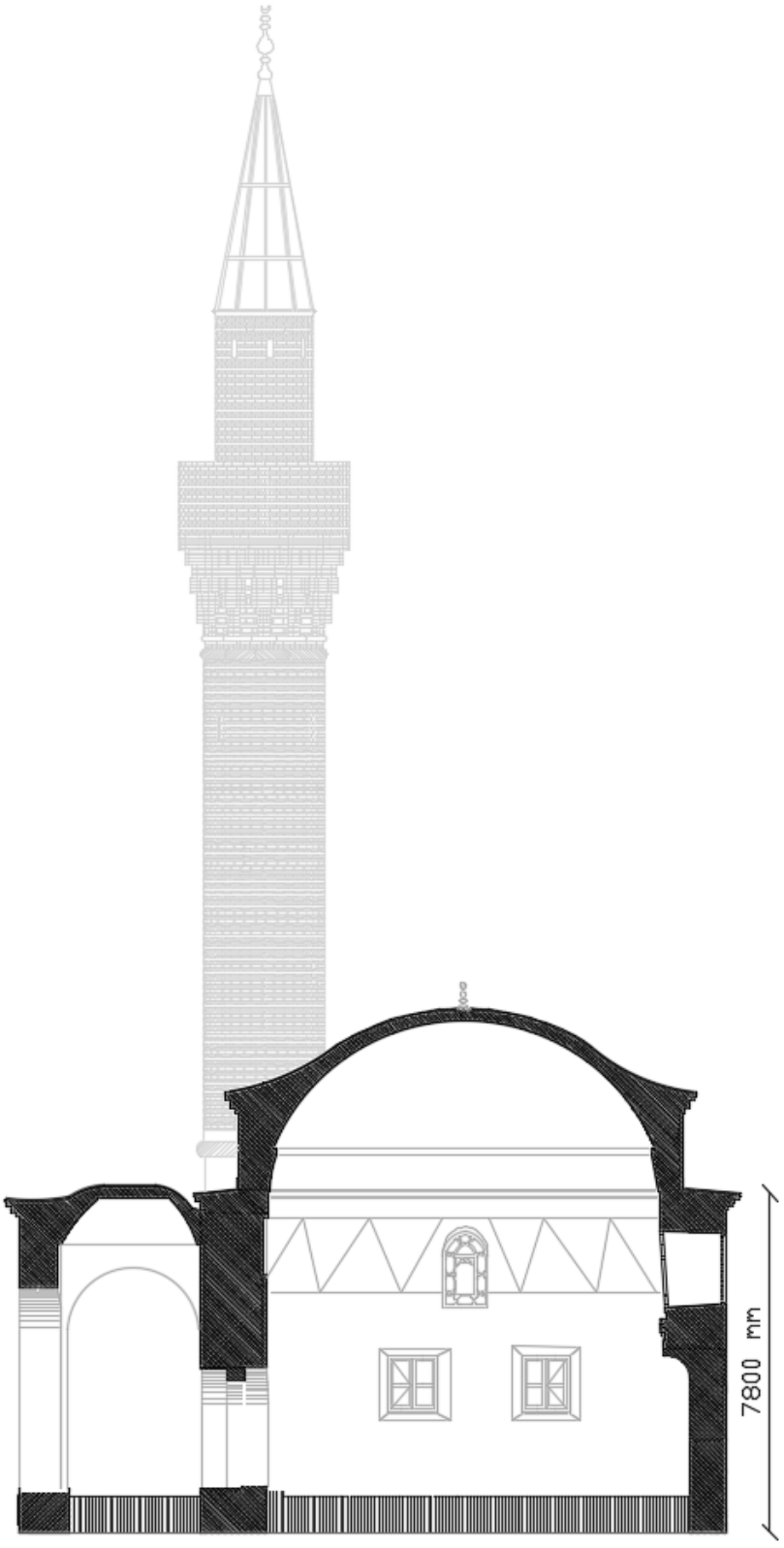

Figure A1. 8. *Section D-D*

APPENDIX - 2 : DAMAGE ASSESSMENT

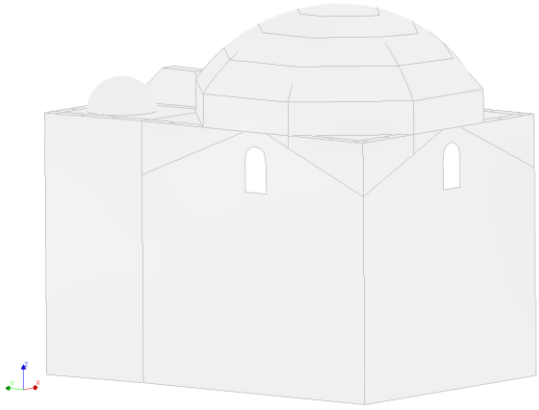

(a) View point A; South-West

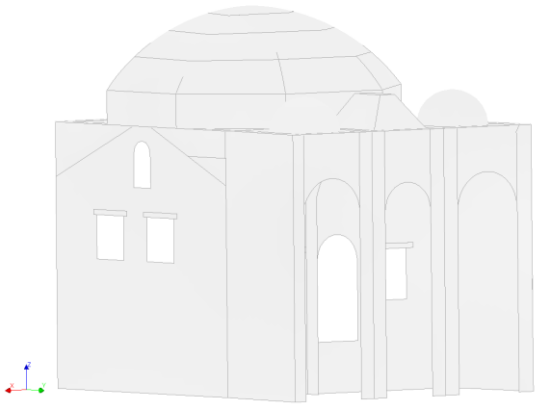

(b) View point B; North-East

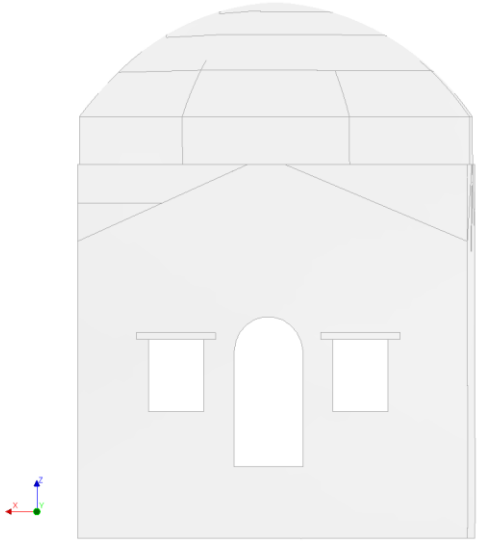

(c) View point C; North Wall

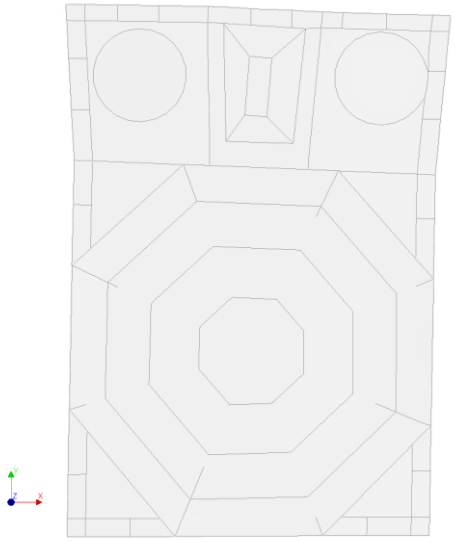

(d) View point D; Top view

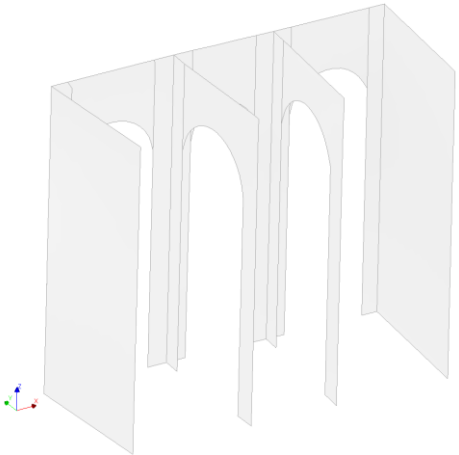

(e) View point E; Portico

Figure A2. 1. *View points on the undeformed model*

Erzincan Earthquake

View point A;

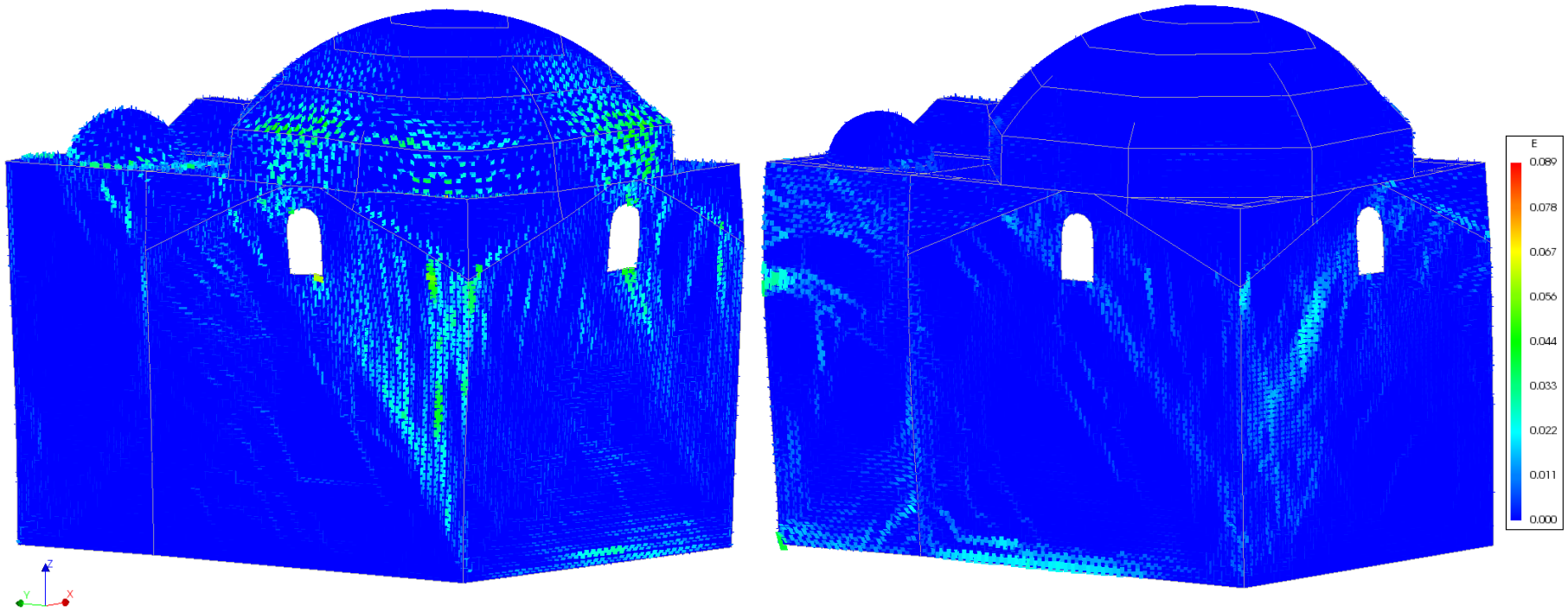

(a) without retrofitting (t=3.43 s) *(b) with retrofitting (t=3.95 s)*

Figure A2. 2. *Principal tensile strains of the South-West façade, deformed shape scale factor:5, the Erzincan Earthquake*

View point B;

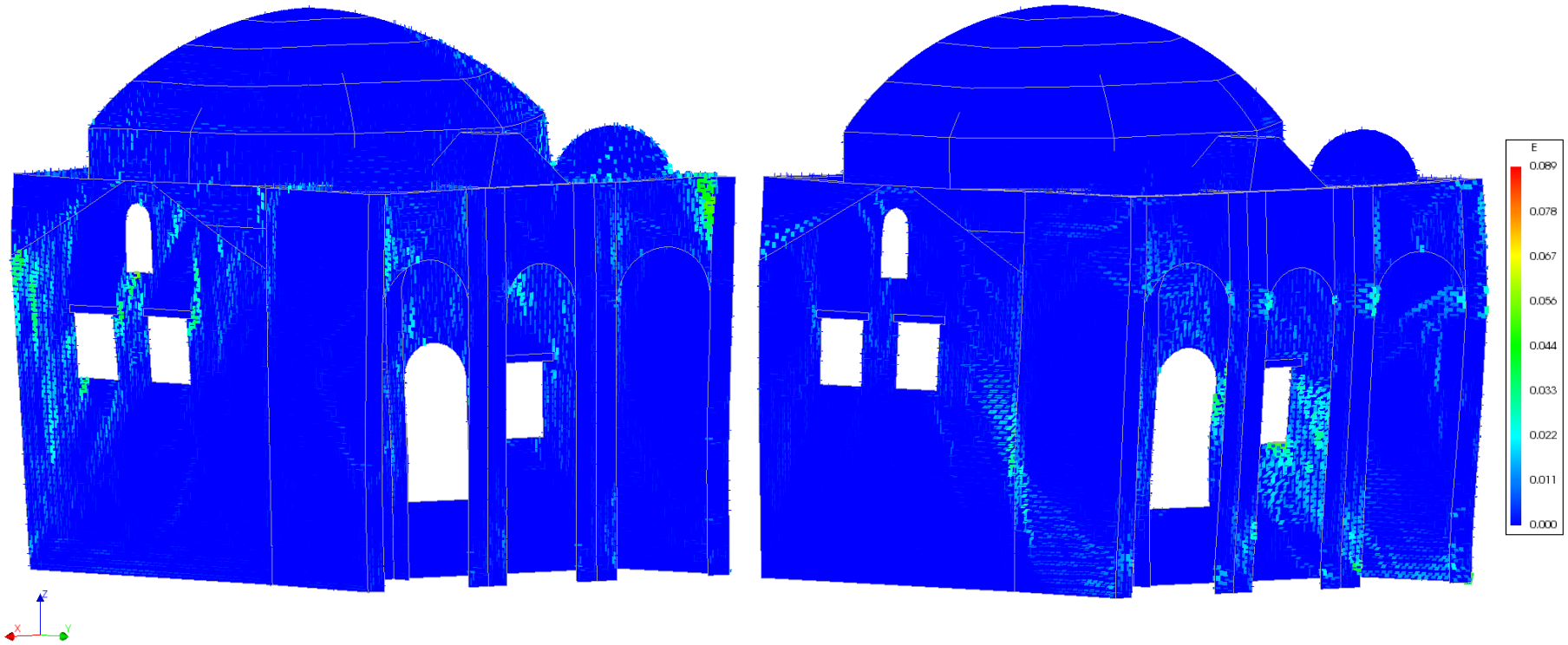

(a) without retrofitting (t=3.43 s) *(b) with retrofitting (t=3.95 s)*

Figure A2. 3 *Principal tensile strains of North-East façade, deformed shape scale factor:5, the Erzincan Earthquake*

View point C;

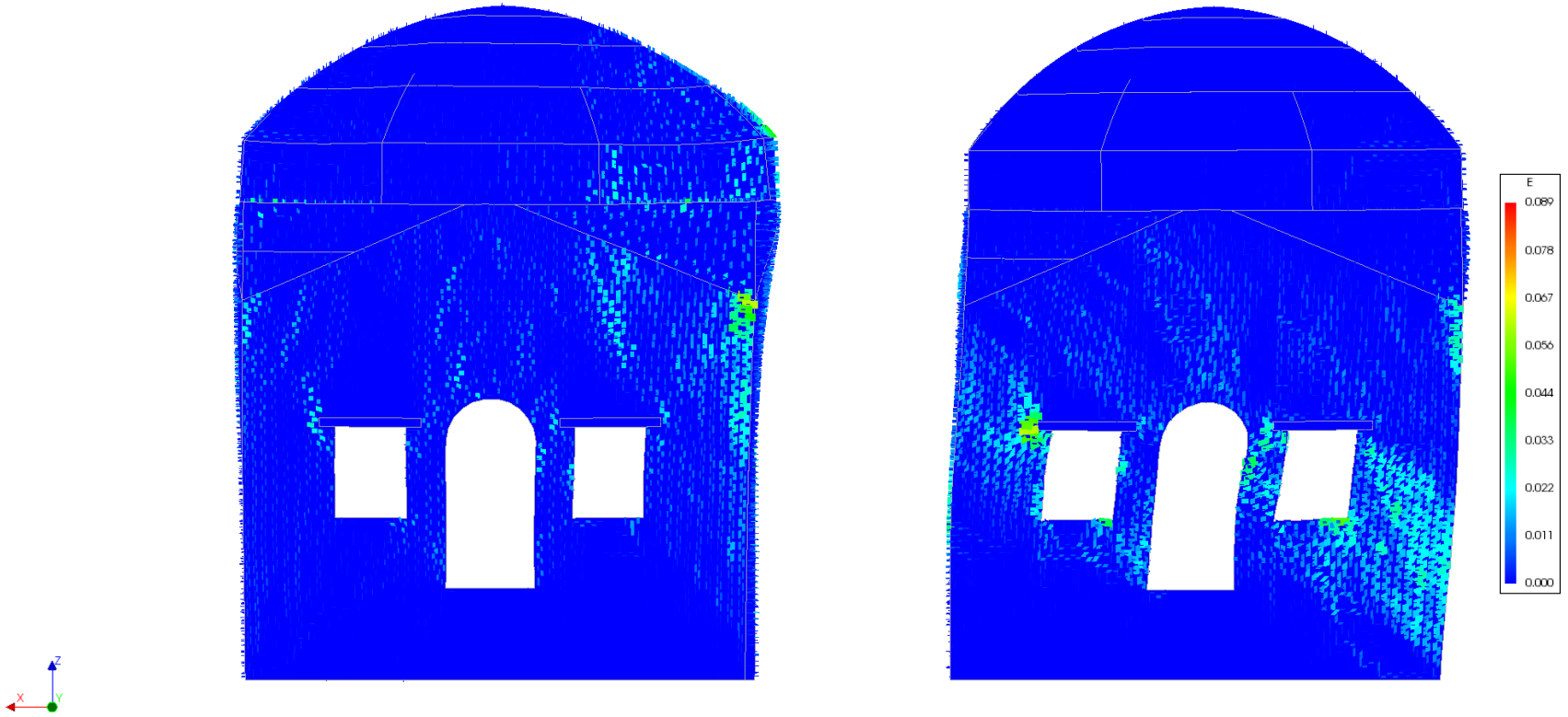

(a) without retrofitting (t=3.43 s) *(b) with retrofitting (t=3.95 s)*

Figure A2. 4. *Principal tensile strains of North Wall without portico, deformed shape scale factor:5, the Erzincan Earthquake*

View point D;

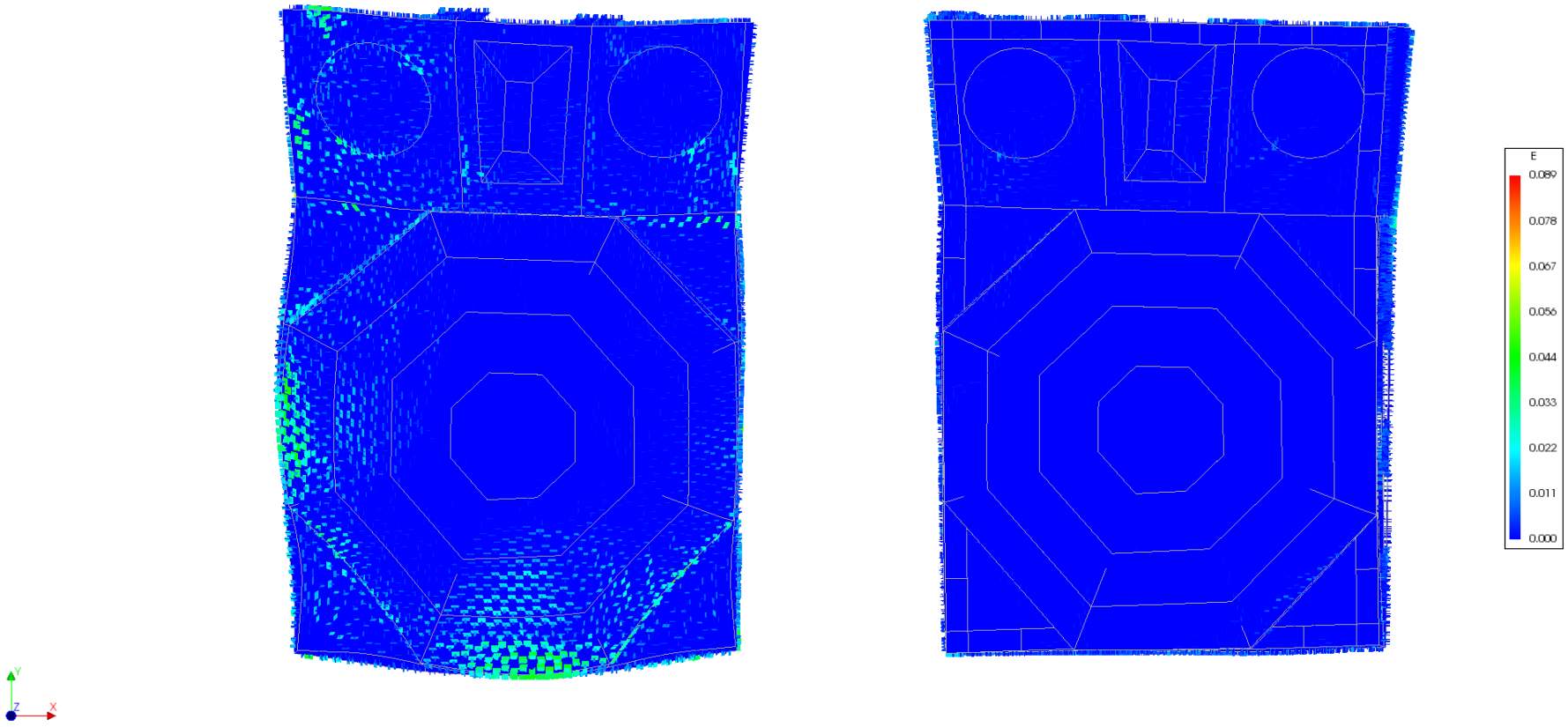

(a) without retrofitting (t=3.43 s) *(b) with retrofitting (t=3.95 s)*

Figure A2. 5. *Principal tensile strains of dome, deformed shape scale factor:5, the Erzincan Earthquake*

View point E;

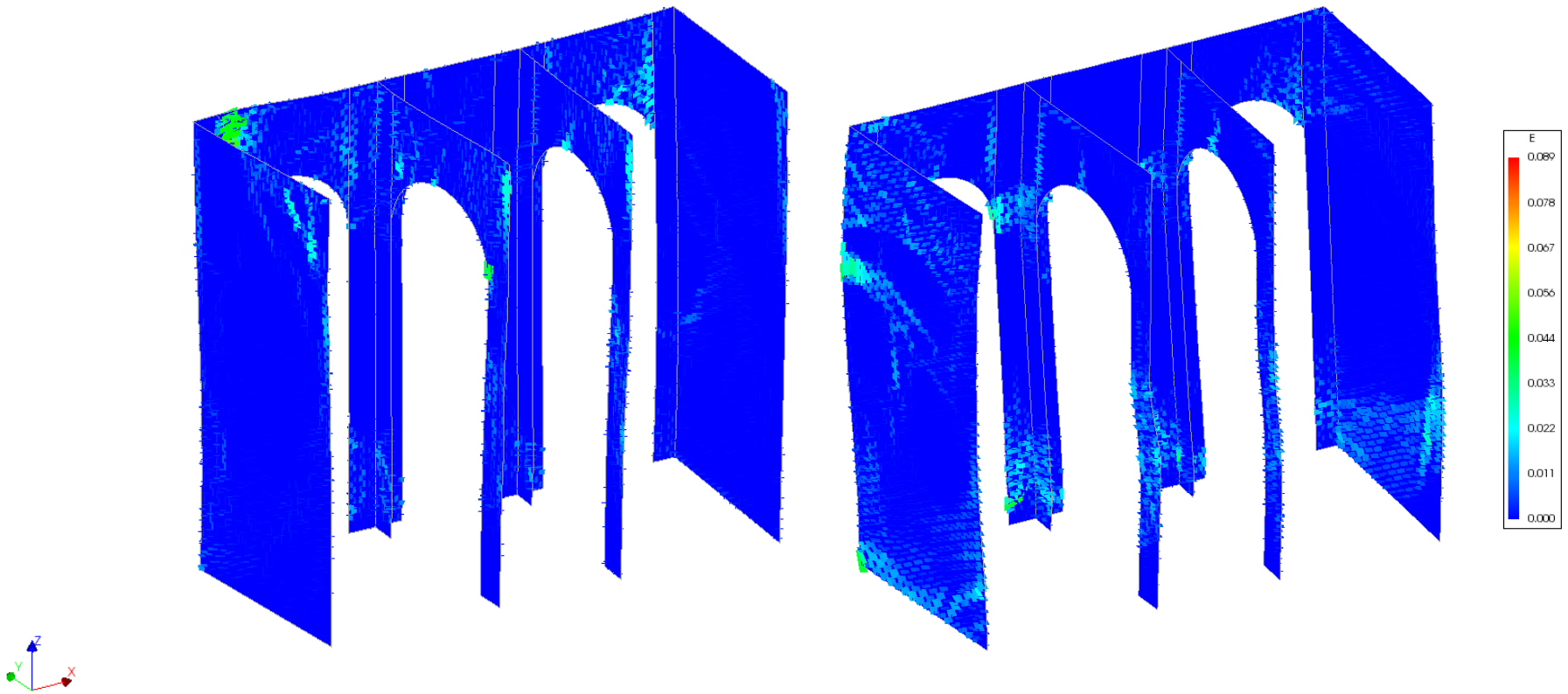

(a) without retrofitting (t=3.43 s) *(b) with retrofitting (t=3.95 s)*

Figure A2. 6. *Principal tensile strains of portico, deformed shape scale factor:5, the Erzincan Earthquake*

Bolu Earthquake

View point A;

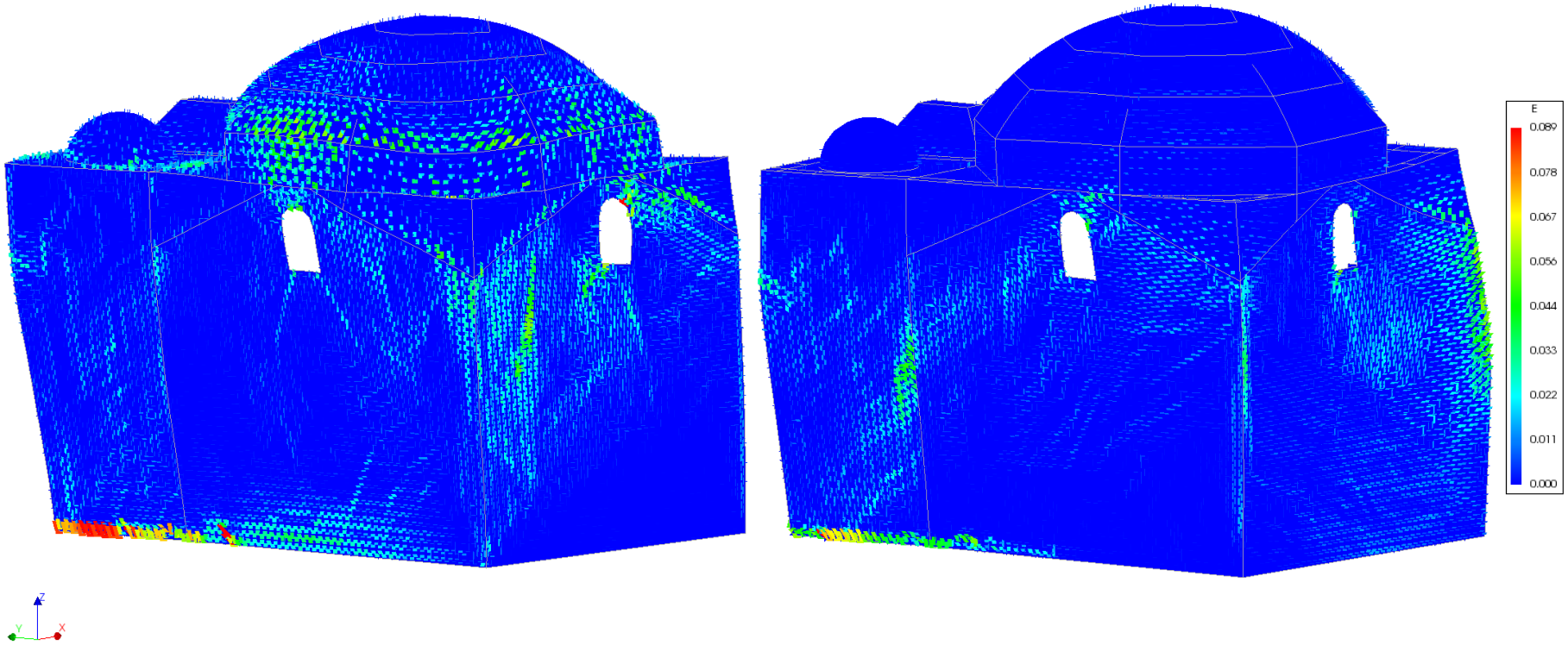

(a) without retrofitting (t=6.12 s) *(b) with retrofitting (t=6.28 s)*

Figure A2. 7. *Principal tensile strains of South-West façade, deformed shape scale factor:5, the Bolu Earthquake*

View point B;

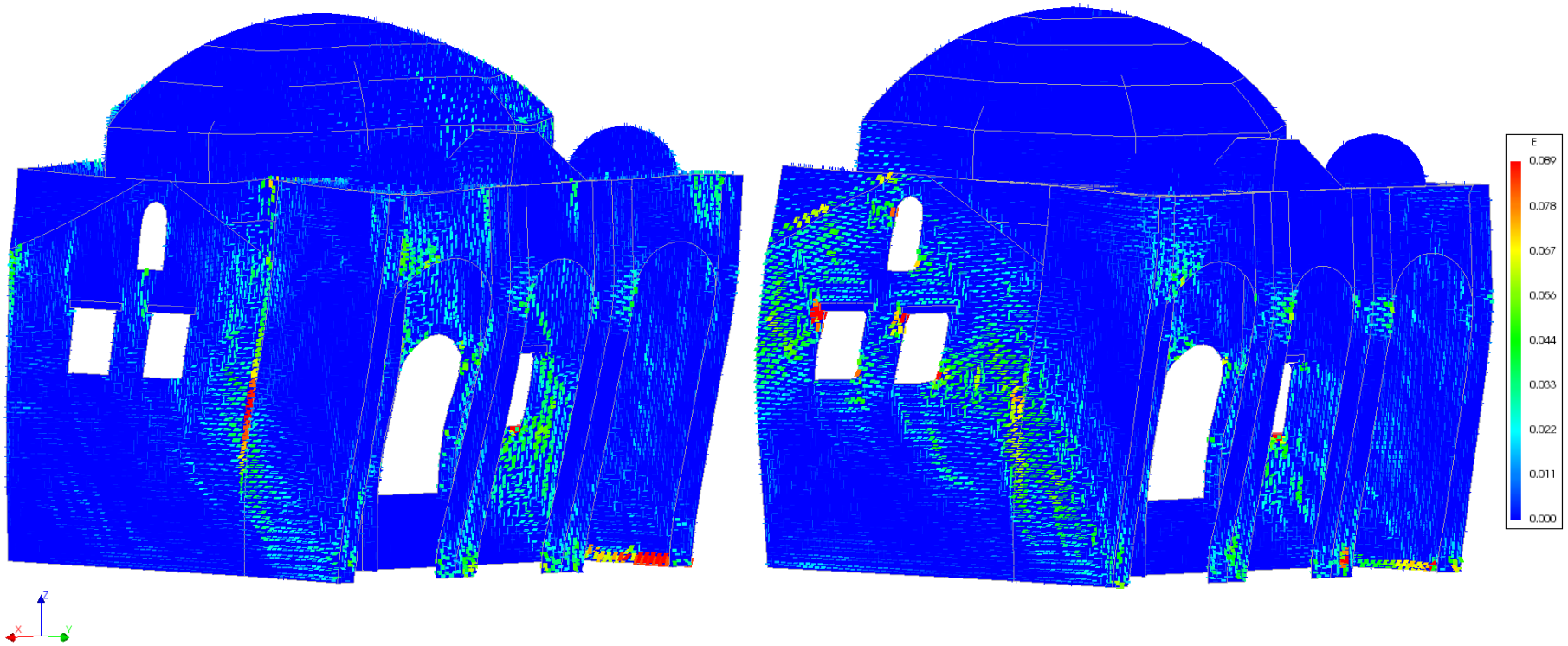

(a) without retrofitting (t=6.12 s) *(b) with retrofitting (t=6.28 s)*

Figure A2. 8. *Principal tensile strains of North-East façade, deformed shape scale factor:5, the Bolu Earthquake*

View point C;

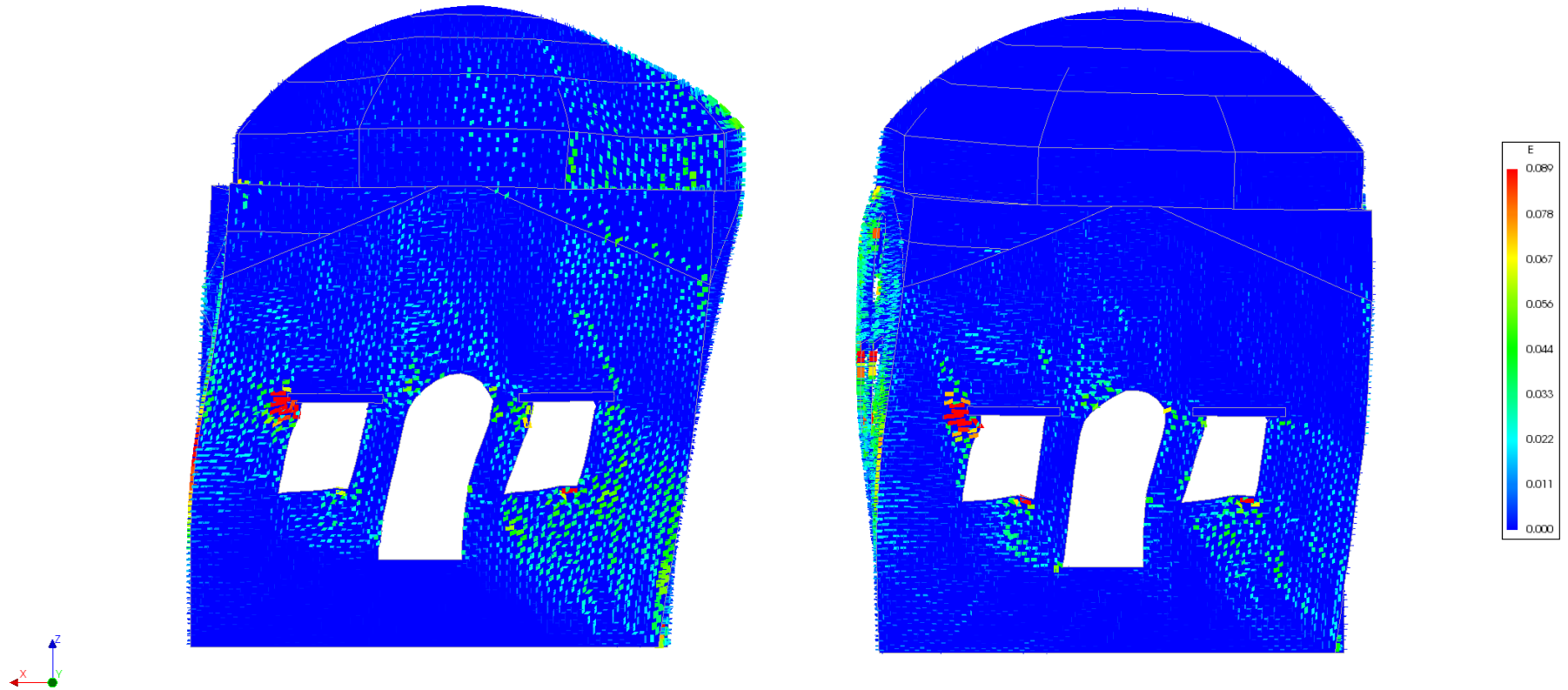

(a) without retrofitting (t=6.12 s) *(b) with retrofitting (t=6.28 s)*

Figure A2. 9. *Principal tensile strains of North Wall without portico, deformed shape scale factor:5, the Bolu Earthquake*

View point D;

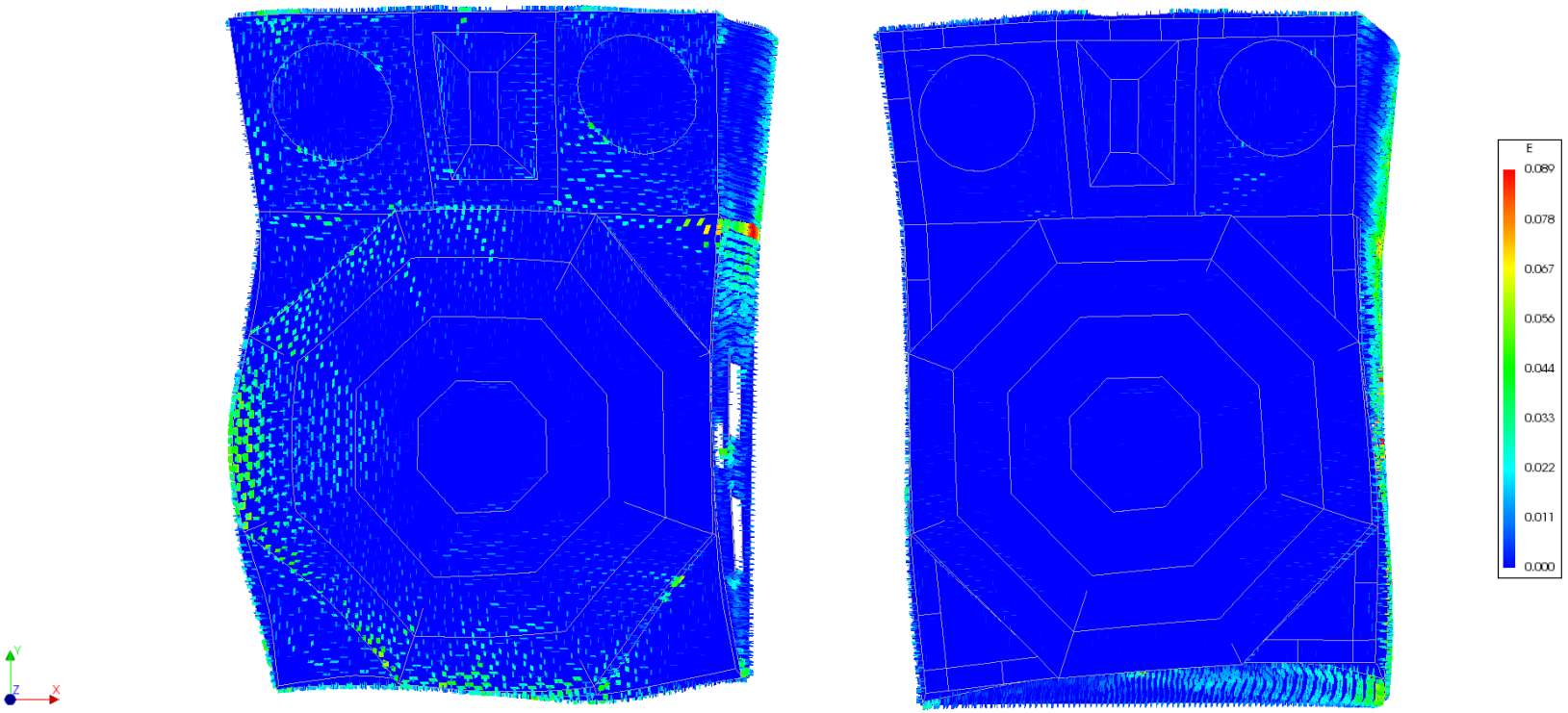

(a) without retrofitting (t=6.12 s) *(b) with retrofitting (t=6.28s)*

Figure A2. 10. *Principal tensile strains of dome, deformed shape scale factor:5, the Bolu Earthquake*

View point E;

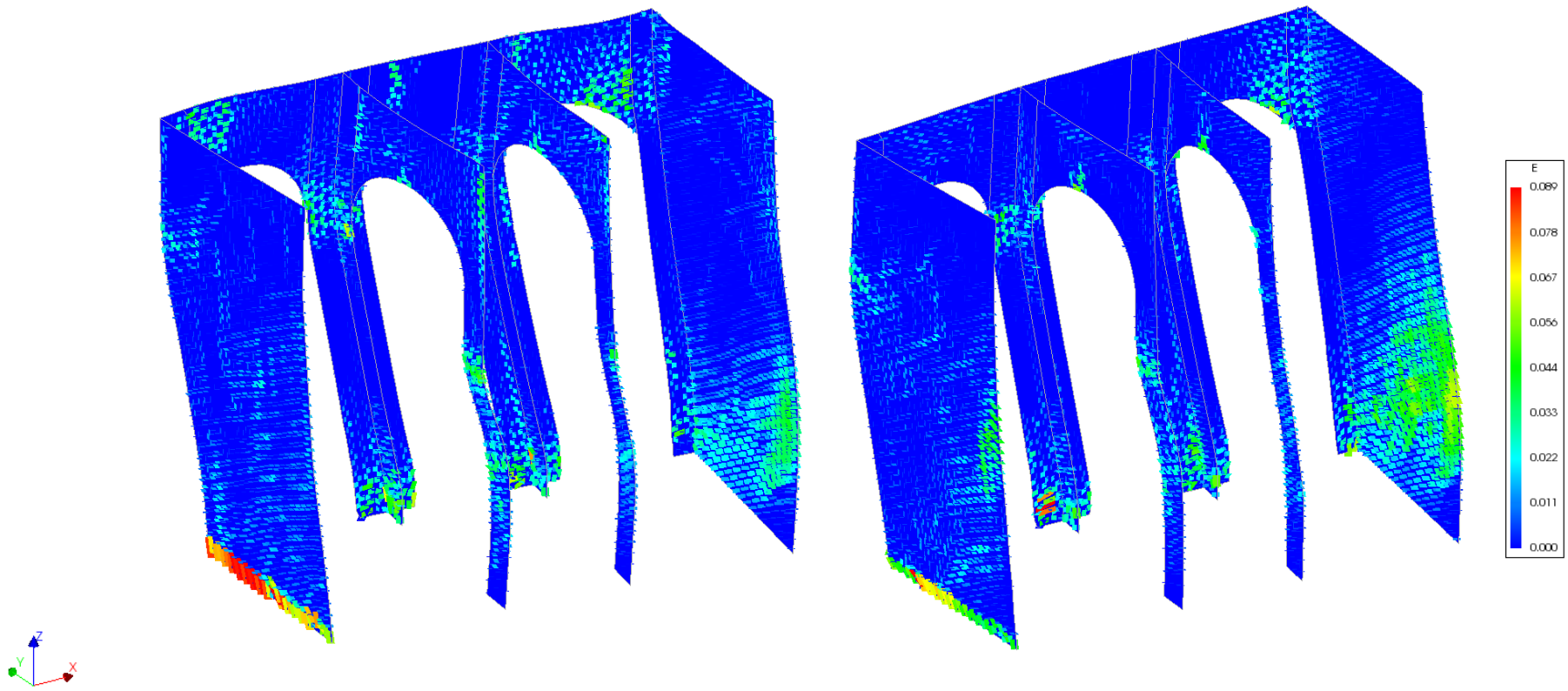

(a) without retrofitting (t=6.12 s) *(b) with retrofitting (t=6.28 s)*

Figure A2. 11. *Principal tensile strains of portico, deformed shape scale factor:5, the Bolu Earthquake*

Bingöl Earthquake

View point A;

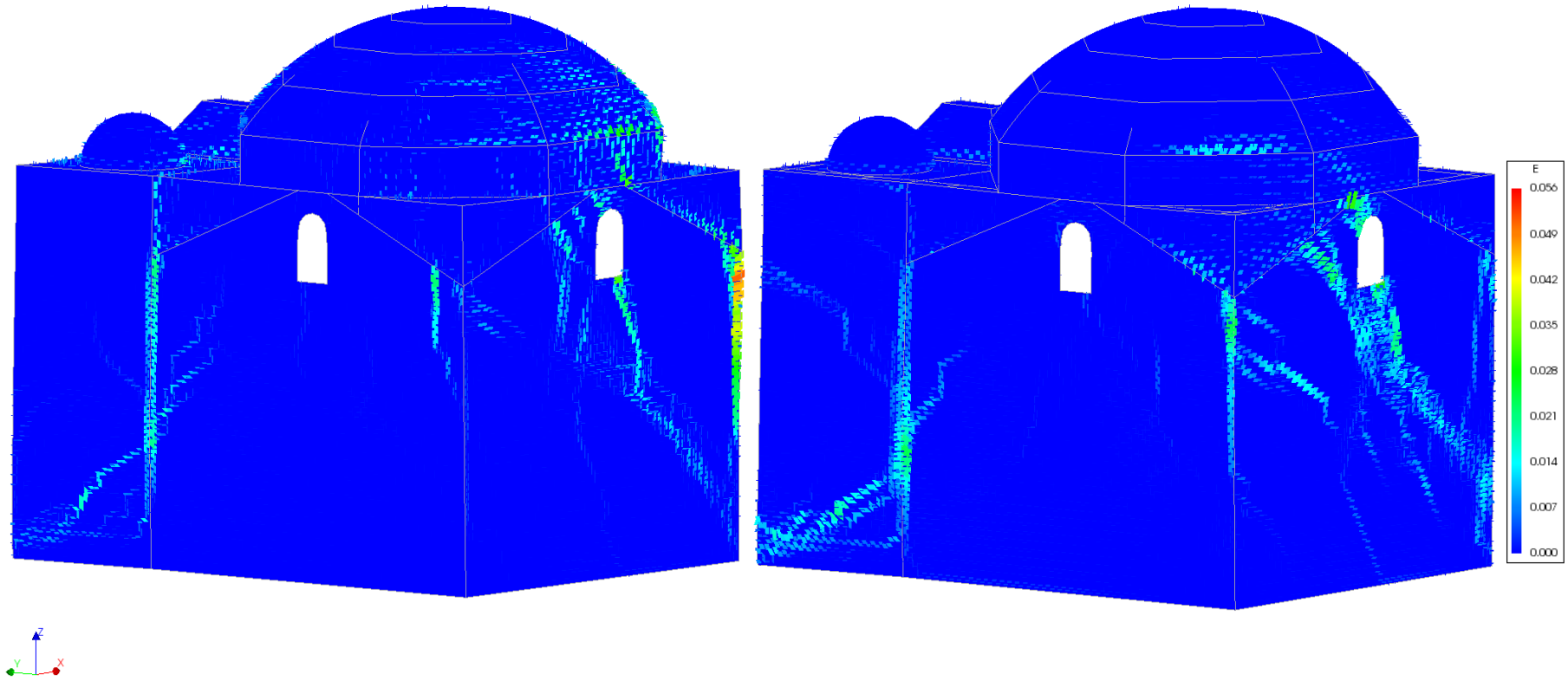

(a) without retrofitting (t=3.99 s) *(b) with retrofitting (t=3.96 s)*

Figure A2. 12. *Principal tensile strains of South-West façade, deformed shape scale factor:5, the Bingöl Earthquake*

View point B;

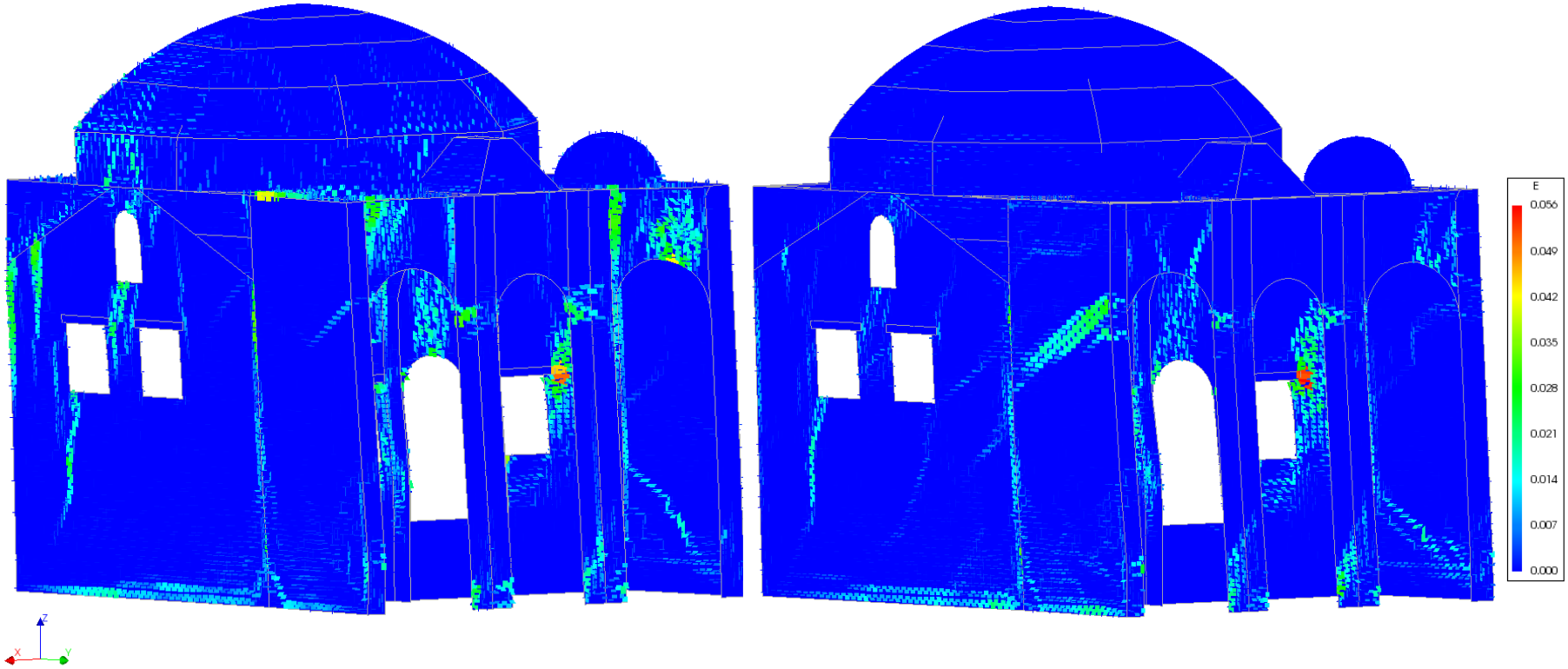

(a) without retrofitting (t=3.99 s) *(b) with retrofitting (t=3.96 s)*

Figure A2. 13. *Principal tensile strains of North-East façade, deformed shape scale factor:5, the Bingöl Earthquake*

View point C;

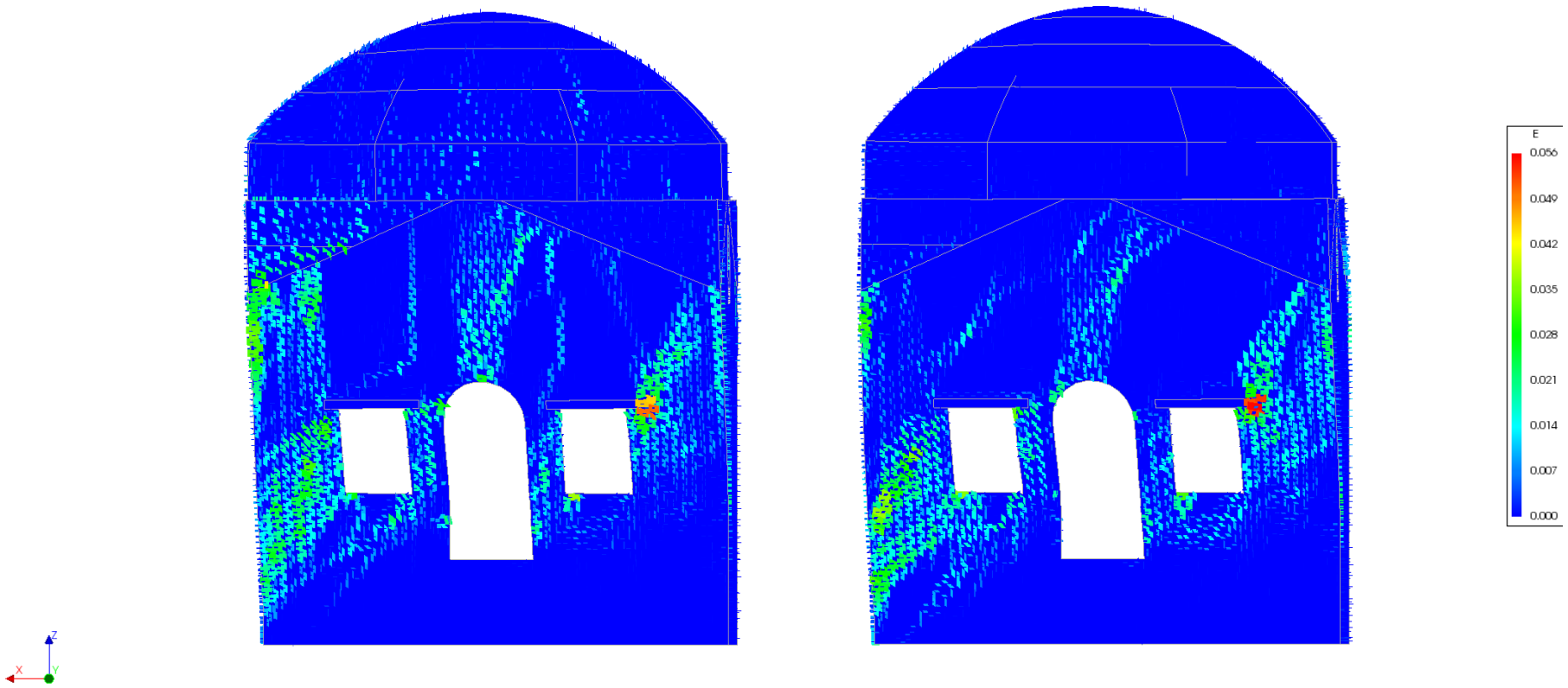

(a) without retrofitting (t=3.99 s) *(b) with retrofitting (t=3.96 s)*

Figure A2. 14. *Principal tensile strains of North Wall without portico, deformed shape scale factor:5, the Bingöl Earthquake*

View point D;

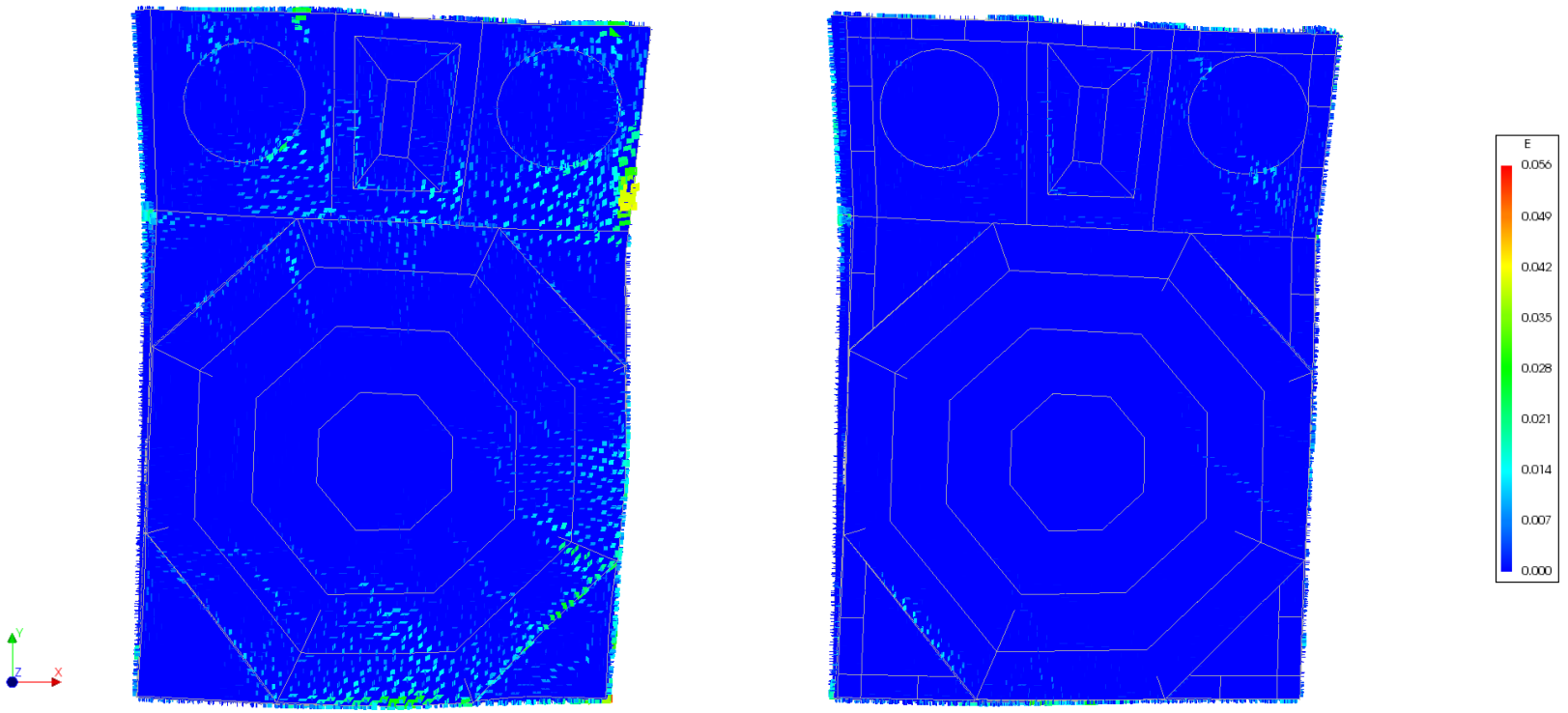

(a) without retrofitting (t=3.99 s) *(b) with retrofitting (t=3.96 s)*

Figure A2. 15. *Principal tensile strains of dome, deformed shape scale factor:5, the Bingöl Earthquake*

View point E;

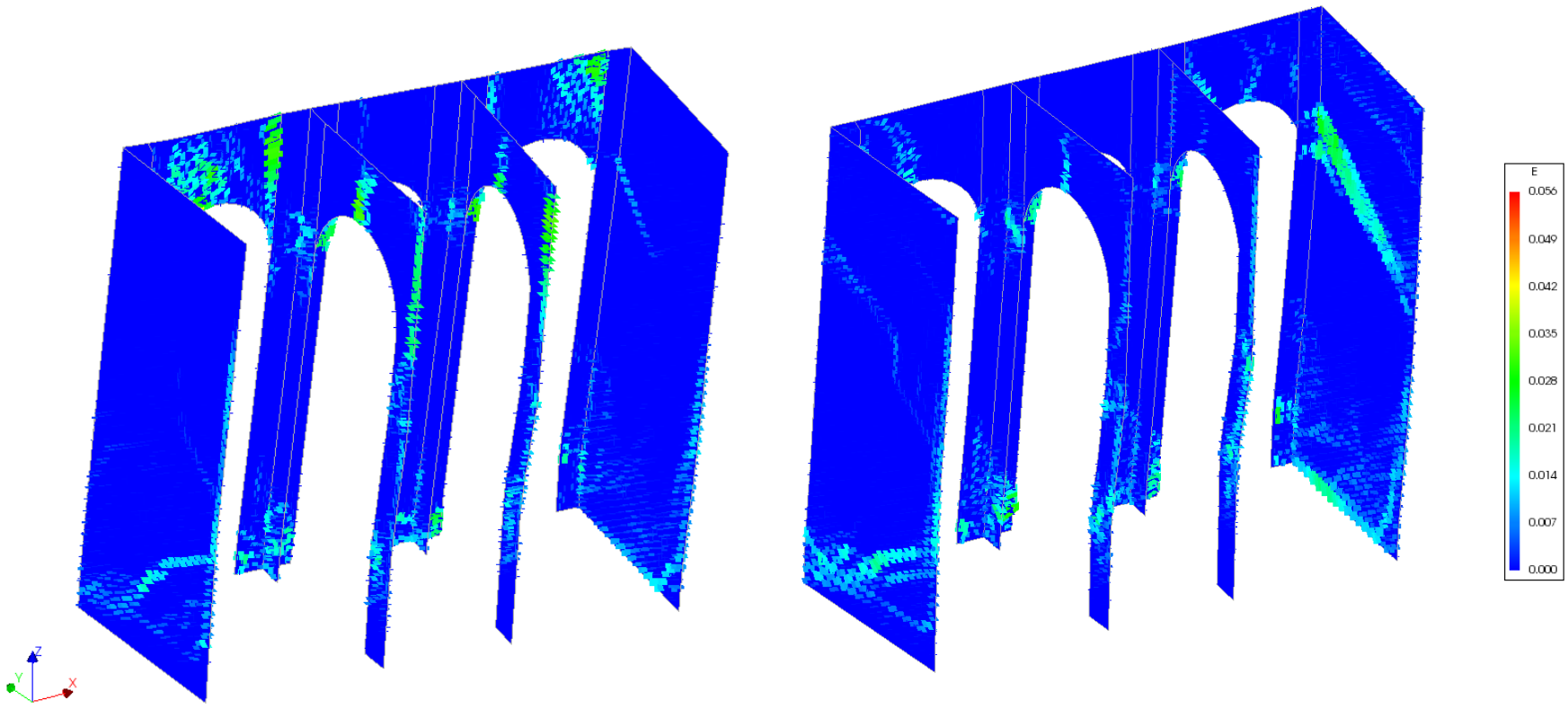

(a) without retrofitting (t=3.99 s) *(b) with retrofitting (t=3.96 s)*

Figure A2. 16. *Principal tensile strains of portico, deformed shape scale factor:5, the Bingöl Earthquake*